ULTRASONIC NON-DESTRUCTIVE TESTING USING PULSE COMPRESSION

BY

FUEI KIT LAM

A DOCTORAL THESIS

Submitted in partial fulfilment of the requirements
for the award of the degree of Doctor of Philosophy
of the Loughborough University of Technology

November, 1975

Supervisor: Dr J Szilard
Department of Electronic and Electrical Engineering

To my wife, Dip.

ACKNOWLEDGEMENTS

Thanks are due to the University of Hong Kong for granting a year's study leave, to the Commonwealth Scholarship Commission for the award of a Commonwealth Academic Staff Scholarship which supported the author's stay in the U.K., and to Alcan Co Ltd (U K), for the free samples of aluminium strips used in this project.

Part of the work was carried out at the Electrical Engineering Department, University of Hong Kong, and part at the Electronic and Electrical Engineering Department, Loughborough University of Technology. The author is grateful to the Departments concerned for the use of their facilities.

The author also wishes to express his appreciation to his supervisor, Dr J Szilard for the varied guidance and discussions throughout the research.

Finally, my thanks go to Mrs M Newman who very patiently carried out the typing of this thesis.

SYNOPSIS

In the testing of highly absorbent materials, it is necessary to use high transmitted power to obtain echoes with an acceptable signal-to-noise ratio from deep defects. However, the maximum peak power which can be used is limited by the construction problems of the probes and the physical properties of the crystal materials. Using longer pulses to transmit more energy could improve the detection, but would reduce the resolution of the system. Pulse compression techniques which overcome the conflict between resolution and pulse duration, provide a possible solution to the above problem. The method involves the transmission of a long coded pulse and the processing of the received echo to obtain a relatively narrow pulse, thus preserving resolution.

After a study of the principles of pulse compression, various practical schemes were investigated, and the linear frequency-modulated pulse compression systems were found to be most economical to implement. Upon being received, the pulse may be compressed by means of a dispersive ultrasonic delay line, and a simple Gaussian shape filter may be employed to reduce the resulting sidelobes.

Theoretical studies on the dispersive modes of propagation of elastic waves in narrow metallic strips were then made, and demonstrated the feasibility of using a metallic strip as the dispersive delay device, provided that equalisers are introduced to compensate for the inherent time delay non-linearities in the strip. Design problems associated with the piezoelectric bar transducers for use with the line were also investigated.

Based on the above studies, a pulse compression testing system consisting of a transmitting unit, a pair of wide-band transmitting and receiving transducers and a receiving unit, has been constructed. The transmitting unit comprises a linear frequency-modulated oscillator and timing circuits; the receiving unit incorporates equalisers, a weighting filter and an aluminium strip delay line. The operating system achieves a time bandwidth product of 80 and a sidelobe level of -25 dB.

Practical tests were carried out and test results are reported. Finally, the power and limitations of the testing system are discussed.

TABLE OF CONTENTS

LIST OF PRINCIPAL SYMBOLS

CHAPTER 2

T	duration of long pulse
t	time delay
f	frequency

CHAPTER 3

$f(t)$	linear FM signal as a function of time
ω	radian frequency
ω_o	centre frequency of FM signal
μ	radian frequency sweep rate
T	duration of FM signal
Φ	phase of FM signal
ω_i	instantaneous signal frequency
$\Delta\omega$	net frequency sweep across the pulse
$F(\omega)$	spectrum of linear FM signal
$C(X), S(X)$	Fresnel integrals
X	argument of Fresnel integrals
$\Phi_1(\omega)$	square law phase term
$\Phi_2(\omega)$	residual phase term
$H_f(\omega)$	transfer function of compression filter
η	a normalised frequency parameter
$T\Delta f$	time bandwidth product
$B_f(\omega)$	phase characteristic of compression filter
t_d	time delay
$f_1(t)$	exponential form of representation of linear FM signal
$F_1(\omega)$	spectrum of $f_1(t)$
$y(t)$	output time function

$Y(\omega)$	output spectrum
$y_1(t)$	matched filter autocorrelation output
$G(\omega)$	complete Gaussian spectrum
K	a constant associated with the Gaussian envelope
$g(t)$	compressed pulse from a complete Gaussian spectrum
D	attenuation in dB at edge frequencies in a truncated Gaussian spectrum.
$G_2(\omega)$	truncated Gaussian spectrum
$g_2(t)$	compressed time output from the truncated Gaussian spectrum
P_N	average output noise power after Gaussian filter
N_o	one-sided spectral density of white noise
S/N	signal-to-noise ratio
$A(\omega)$	amplitude characteristic of a linear system
$B(\omega)$	phase characteristic of a linear system
$H(\omega)$	transfer function of a linear system
J(x)	Bessel function
$e_i(t)$	input signal to the linear system
$E_i(\omega)$	spectrum of $e_i(t)$
$e_o(t)$	output signal from the linear system
B_e	phase error
t_g	group time delay
t_e	time delay error
n	number of cycles of the error component over the signal band
$\hat{t}_e$	peak time delay error
c	$\frac{2\pi}{\Delta\omega} = \frac{1}{\Delta f}$

CHAPTER 4

u,v,w	components of displacement in the X,Y and Z directions
γ	propagation constant
U_s, W_s / U_a, W_a	amplitudes of displacement in the X and Z directions
h	thickness of the plate
V	phase velocity
V_s	bulk shear wave velocity
σ	Poisson's ratio
U	group velocity
D	specific group delay
L	length of delay line
I	bisection interval
z	real variable
P_i	inflexion point
λ	wavelength
$f_r t$	resonant frequency-thickness product
f_r	frequency of resonance
f_a	frequency of anti-resonance
k	electromechanical coupling
t	thickness of bar transducer

CHAPTER 5

Z_x	characteristic acoustic impedance of transducer material
C_o	clamped capacitance
ϕ	Ideal transformer ratio
$\frac{\alpha}{\pi}$	fractional frequency deviation
f_o	open-circuit resonant frequency
A	area of transducer
ρ	density of transducer material
v_t^D	velocity of compressional wave along the thickness axis
ε^s_{33}	clamped dielectric constant
t	thickness of transducer
e	a piezoelectric constant
Z_q	characteristic impedance of load
Z_b	characteristic impedance of backing medium
V_i	input voltage
V_o	output voltage
F	force exerted on transducer face
C_M	capacitance of the series tuned circuit
L_M	inductance of the series tuned circuit
C_N	capacitance of the shunt tuned circuit
L_N	Inductance of the shunt tuned circuit
C_m, L_m, R_m	circuit elements in the simplified transducer equivalent circuit
f_r	measured resonant frequency
a	radius of piston source
λ	wavelength of sound
f'_o	resonant frequency of tuned circuit.

APPENDIX A

$H_1(\omega)$	frequency response function of the matched filter
$h_1(t)$	impulse response of the matched filter
$F^*(\omega)$	complex conjugate of spectrum function $F(\omega)$
$y_1(t)$	matched filter output

APPENDIX D

Z_a		series element of the lattice
Z_b		shunt element of the lattice
R_o		characteristic impedance
s_n	=	$\sigma_n + j\omega_n$ complex frequency
$\bar{\omega}_o$		resonant frequency for Z_a and Z_b branches
ω^2_o		$\bar{\omega}^2_o - \sigma^2_o$
B		phase shift of network
t_d		group time delay

CHAPTER 1

INTRODUCTION

1.1 Review of ultrasonic non-destructive testing methods

Ultrasonics has been employed extensively in non-destructive testing (N.D.T.) for detecting internal anomalies and measuring physical properties. The types of anomalies that can be detected include voids, delaminations, cracks, porosity and inclusions. The detection of these irregularities in the test specimen is based on the fact that ultrasound is responsive to changes in acoustic impedances. The defects being of different acoustic impedances from the surrounding media, will give rise to differential reflections of the incident ultrasonic energy. On the other hand, physical properties, such as elastic moduli, Poisson's ratio etc., may be determined from the velocity of the ultrasonic energy in the material.(1)

The fact that ultrasonic inspection provides quick, on the spot information presents no hazards and lends itself to automation, makes it complementary to radiographic methods as an inspection tool.

The common established methods of ultrasonic testing include the pulse technique and the resonance technique.(2)

To avoid interference between the transmitted and received wave, pulse methods are frequently employed in ultrasonic flaw detection systems. There are three basic inspection techniques: pulse echo, through transmission and 'mirror shadow' techniques. In the pulse echo system short pulses of radio frequency ultrasound are transmitted at regular intervals into the test object. Reflections from the test piece are displayed on an oscilloscope (A-scan presentation). Any discontinuities will appear as indications between the front and back

surface echoes. The time of occurrence and amplitude of these echoes are then related respectively to the location and maghitude of the defects. For convenience, a single transmit and receive transducer is often employed. In the through transmission method two transducers are required. Signals through the test piece from the transmitting transducer are observed for test information. Any discontinuities will cause a proportional decrease in the received signal. Finally, in the 'mirror shadow' method, after passing through the test object, the signals are made to reflect through it again by a reflecting surface. This method is useful on thin parts and can give better definition of defective areas.(3)

The resonance techniques rely upon the setting up of standing wave conditions in the test specimen by changing the applied frequency. These resonance points are then monitored and suitably interpreted in terms of the thickness of the specimen.(4) If the thickness of the specimen is known, the technique can be utilised to detect delaminations, because of the apparent reduction in thickness.(5)

However, in many situations, such as those that exist in nuclear power components and aerospace structures, these basic techniques have proved to be inadequate. Specific testing methods have been devised. These unconventional techniques may be conveniently described under the following headings:-

(a) Impedance technique

(b) Acoustic impact technique

(c) Acoustic emission

(d) Surface and Lamb waves technique

(e) Ultrasonic spectroscopy

(f) Ultrasonic imaging.

In the impedance technique use is made of the changes in either the magnitude or the phase of the acoustic impedance of the test specimen in the presence of a defect, as seen by the transducer.(6) This approach, which can in fact be regarded as a generalisation of the resonance technique, has been widely adopted in testing laminated structures. Utilising the fact that defects located throughout the thickness of the composite would act as an acoustical termination site, Botsco (1966) developed the Sonic Resonator for non-destructive testing of composite structures by monitoring the change in impedance value.(7) Lopilato and Carter (1966) exploited the sharp change in the phase of the impedance in the defective zone and outlined an ultrasonic phase sensitive procedure for the inspection of adhesively bonded structures.(8)

The acoustic impact technique is based upon the concept that an anomaly changes the mechanical impedance of a structure or part, and consequently affects the vibrational response of the structure in the area of the defect. Such a technique has been employed by Schroeer, Rowand and Kamm (1970) in detecting cracks concealed under fastener heads.(9) An acoustic pulse is applied to the specimen and the 'time-to-damp' of the vibrations within the material serves as an indication of the presence or absence of anomalies. This decrement testing has also been applied by Harris-Maddox (1964) to the testing of steel-rubber bond in the casing of solid-fuel rocket motors, though the decay of multiple echoes in the outer steel casing is monitored in this case.(10)

Testing methods based on acoustic emission differ from other methods in that no probing ultrasonic beam is introduced in the test object, the deformations registering their own presence and magnitude by characteristic emissions. The acoustic emission technique relies on the release of elastic energy held locally in the strained material during

a deformation process. These resulting elastic waves or 'noises' are detected through the use of highly sensitive transducers or listening devices. Schofield (1963) established the detection of acoustic emission as a technique for studying material deformation processes.[11] The potentialities and limitations of the method are discussed by Pollock (1971).[12] By providing a detailed time account of the occurrence of deformation in the interior of the specimen, this method is a powerful extractor of information about the dynamic behaviour of flaws. At the present time, its main application is the monitoring of the growth of cracks and flaws in pressure vessels[13] and welded structures, but it has great potential in predicting incipient failures in many structures.

Various modes of wave propagation are also utilised in ultrasonic testing. Surface elastic waves that propagate along the boundary surface of solids are useful for inspecting materials for surface and sub-surface cracks and voids. They have been applied, for example, in the inspection in situ of turbine blades for fatigue cracks towards the root.[14] More recently, Hudgell et al (1974) attempted to apply the surface wave mode-conversions to the measurement of depth of surface-breaking cracks.[15] However, Lamb waves represent the most widely used mode by far, especially in the inspection of thin plates. Lamb waves in a plate can be generated by allowing plane ultrasonic waves to travel through a water coupling to strike the surface at an angle of incidence. Depending on this angle of incidence, frequency, plate thickness and the material of the plate, particular modes of Lamb waves are excited. If the plate has defects (laminations, inclusions or cracks), then the propagation of Lamb waves is interrupted and a reflection takes place. This sensitivity to small defects renders them useful in the examination of thin walled parts such as thin walled long tubings.[16]

Lamb waves have also been employed in thickness measurements. Frederick and Worlton (1962) demonstrated the usefulness of Lamb wave modes in measuring tubing wall thicknesses.[17] Recently, Davey and Aldridge (1969), making use of Lamb wave propagating effects, developed ultrasonic micrometers for accurate measurements of plate thicknesses.[18]

Gericke showed in 1963 that useful information concerning the microstructure of materials or geometries of small defects, can be obtained from ultrasonic inspection by transmitting broadband pulses and analysing the received spectrum.[19] His work has led to the development of ultrasonic spectroscopy, which makes use of frequency dependence of reflection, diffraction and attenuation in the test materials. Later research[20] confirmed that this technique allows more information to be extracted about flaw sizes and shapes. Whaley et al (1972) extended this method of spectral analysis to give improved resolution both for thickness measurements and near-surface flaws.[21] Morgan (1974) introduced surface wave spectroscopy,[22] which offers great promise in the assessment of the depth of surface-opening cracks. The main limitations in applying spectroscopy lie in the difficulties of producing transducers having uniform broadband characteristics, and in the extra complexity required in data processing.

Ultrasonic imaging techniques provide an ability to display position, shape or orientation of defects not otherwise visible. By showing the relationship between the flaws and the boundaries of the test piece, they may be used as an efficient form of N.D.T. They could give greater speed and accuracy of interpretation of ultrasonic data. The more familiar types of pictorial presentation of flaws are the B-scan and C-scan display. A-scan is essentially a one-dimensional display. In B-scan a cross-sectional view through the

test material is provided. Though commonly employed in medical diagnostic fields, B-scan methods have not gained wide acceptance in N.D.T., as they require accurately linked mechanical scanning arrangements and, in some cases, an inconveniently long time to build up a picture. C-scan systems present a plan view of defects without indicating their depth. They are obviously most suitable for laminar flaws within a pre-determined range. The current direction of development being taken in B- and C- scanning methods is towards automation.(23)

It is, however, more common to employ an imaging device in ultrasonic visualisation, whereby the test specimen is insonified with an ultrasonic beam and the imaging device is positioned behind the specimen as a 'receiver'. Various methods have been suggested for transposing the acoustic energy into a visual image.(24) The most direct method is the Sokolov camera, which is analogous to a T.V. camera with piezo-sensitive material replacing the photo-sensitive element. Other techniques inlcude the use of Pohlman cell, the liquid levitation method, the photo-elastic and Schlieren methods, liquid crystals, photographic methods and holographic methods. The Pohlman cell makes use of the effects of ultrasonic radiation pressure, which causes a preferential alignment of small aluminium flakes suspended in a fluid. The same radiation pressure effects are employed in the liquid levitation method. The beam from an ultrasonic source, after interacting with a specimen to be examined, is allowed to strike a liquid-to-air interface from below. The sound image then appears as a relief image on the fluid surface, as the fluid surface rises in dependence upon the impinging acoustic intensity. The photo-elastic and Schlieren methods both depend on the change in the refractive index of a transparent medium, which results from the stress associated with an ultrasonic wave.

The liquid crystal and photographic presentations are based upon thermal and chemical effects. In general, all these methods suffer from poor sensitivity. In the holographic technique,[25] a recording of the diffraction pattern of an object 'illuminated' with coherent ultrasound is made. Through the use of another coherent reference wave, both amplitude and phase information are recorded. The object wavefront can then be reconstructed optically. This method dispenses with lenses or mirrors and provides a three-dimensional display of the defect. Though it has shown considerable promise in laboratory studies, it is still difficult to apply the technique in practical test situations.

The above survey gives a brief résumé of the principles and phenomena now being used for non-destructive testing, or which have shown potential possibilities. This enumeration of methods is by no means exhaustive, as each application calls for different test requirements and hence has its own specific solution. In practice, the conventional pulse-echo technique is by far the simplest and most widely adopted method. However, for the testing of highly absorbent materials it has proved to be inadequate. This inadequacy is discussed in the following Section, where a method to overcome it is proposed.

1.2 Purpose of the project

A simple pulse-echo flaw detector is limited in resolution by the pulse width and in range by the average power (energy) radiated.

Range resolution is the ability of a system to distinguish between two sequential echoes whose reflectors lie at different distances on, and normal to, the axis of the sound field. The limit beyond which two sequential echoes are too close together to be separated, is known as the resolving power of the system, which can be expressed in terms

of a time increment or as a minimum resolvable thickness for a material of known sound velocity. It is determined by the transmitted pulse width. Figure 1a shows two defects to be resolved by a pulse-echo system; they are separated in range by a distance ΔR. The difference in time Δt, between the echoes received from the defects is:

$$\Delta t = \frac{2\Delta R}{v} \qquad (1.1)$$

where R = distance to the first defect

$R + \Delta R$ = distance to the second defect

v = velocity of sound in the material.

The two defects are resolved by the system when:

$$T < \frac{2\Delta R}{v} \qquad (1.2)$$

where T = width of the transmitted pulse.

Figure 1b illustrates the case where the reflected pulses overlap and the targets are not resolved. Figure 1c illustrates resolution. Therefore, a good resolution demands a narrow transmitted pulse in pulse-echo systems.

The range of an echo-location system is related to its sensitivity. The sensitivity denotes the smallest defect that can be detected throughout the testing range. For a given sensitivity the range depth capability could only be extended by increasing the average power radiated. The average power radiated depends upon:

(i) The peak power radiated

(ii) The repetition rate

(iii) The width of the transmitted pulse

(iv) The shape of the output pulse - the optimum shape being rectangular, as only a rectangular shape results in a peak power radiation throughout the entire pulse duration.

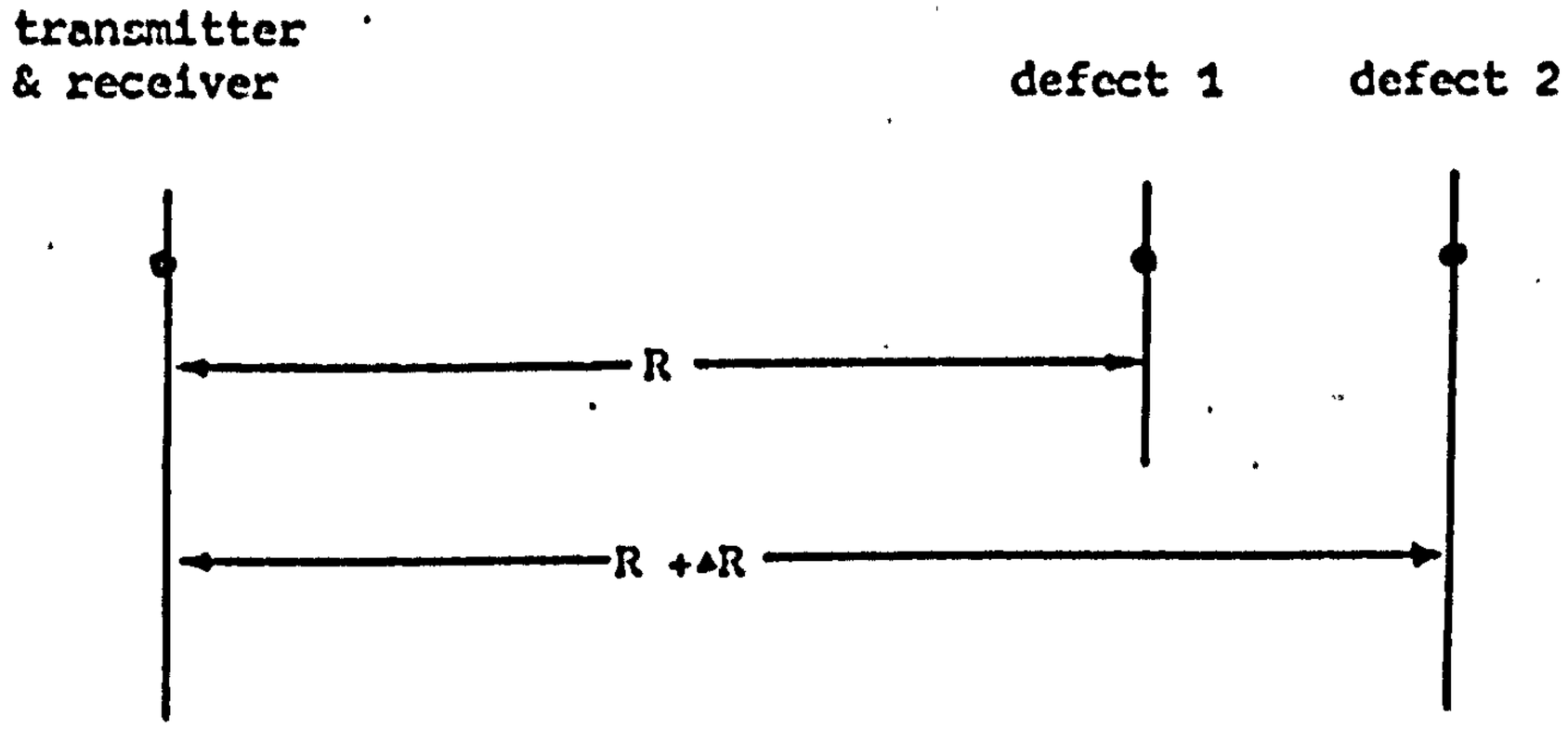

1a Two defects to be resolved

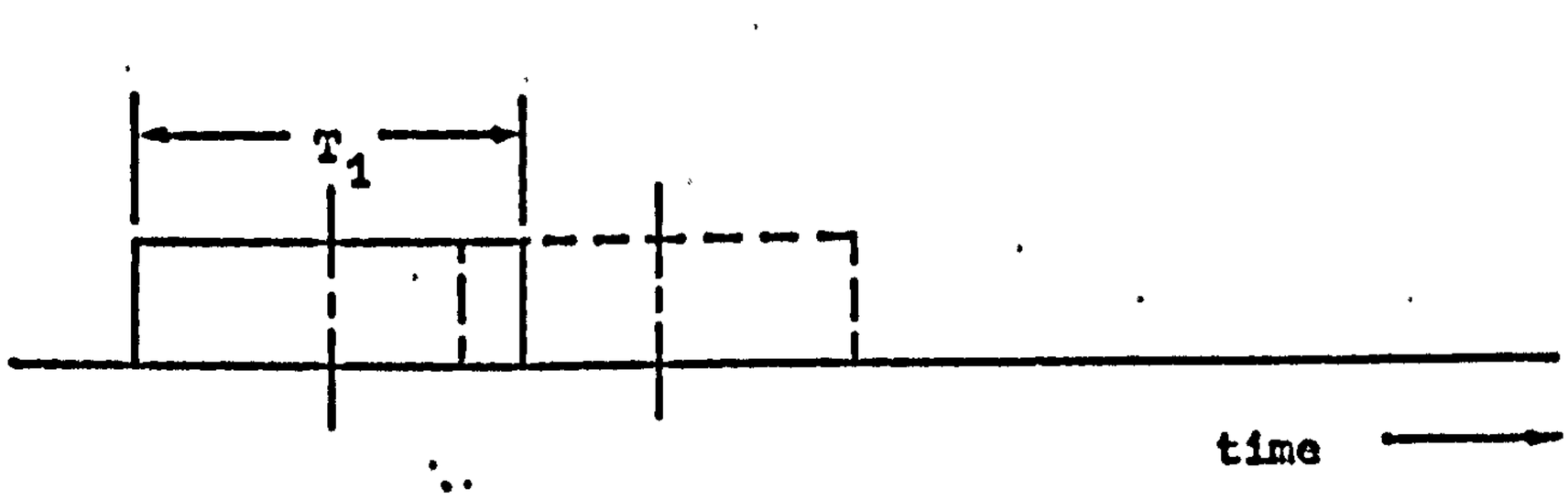

1b Two echoes that overlap

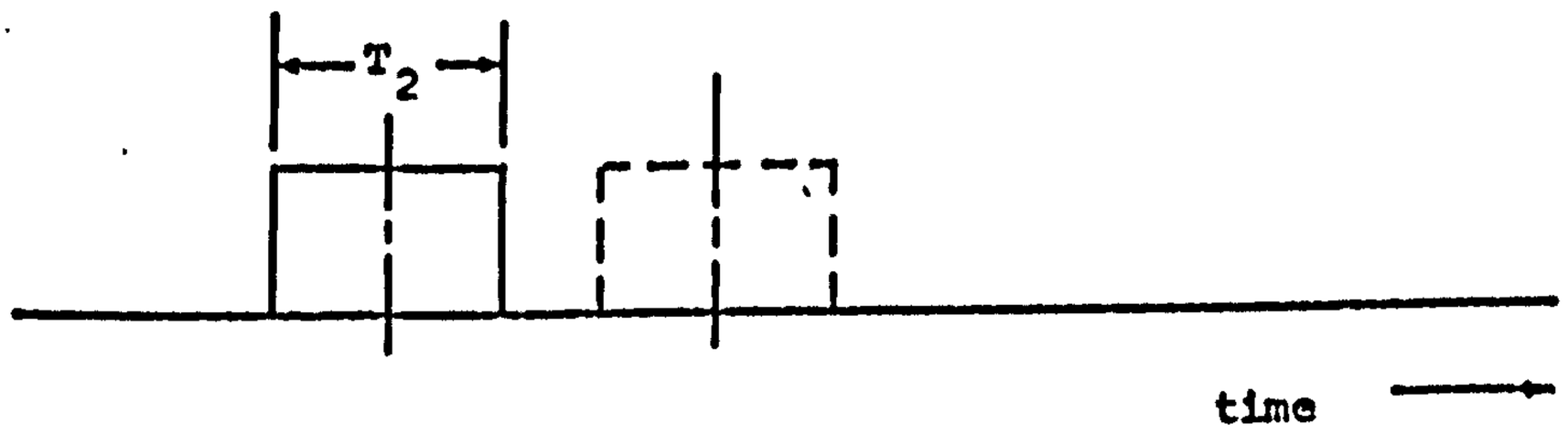

1c Resolution

Figure 1.1 Resolution of a simple pulsed detection system

Normally the pulse repetition rate of the system is specified through the range ambiguity and reverberation considerations, that is, it is necessary to wait until the echo from the most distant reflector has returned or reverberations in the specimen have died away, before another pulse can be sent. Thus, there is a limit on the shortest repetition period that can be used in the ranging system.

Once the repetition rate is fixed, the power radiated can be controlled by varying either the peak power or the width of the transmitted pulse. However, for a required resolution, the average power and hence the range of detection, can only be extended by increasing the peak power radiated.

In the non-destructive testing of metals which have low attenuation characteristics, little problem exists in applying this simple pulse-echo system, since a moderate amount of peak power would give a sufficient range depth.[2] However, when used for the testing of highly absorbent materials, this simple system would require an extremely large peak power because in these cases, in order to effect returning echoes from a reasonable depth with magnitudes larger than the receiver noise, it demands large average transmitted power. For example, in the testing of plastics, which may typically have an attenuation of the order of 0,1 dB/mm at 2 MHz, returning echoes from a depth of 50 mm would suffer an attenuation of 100 dB from the transmission path alone. Problems then arise when the peak power limitation of the system is reached. The maximum peak power which can be used, is normally limited by the construction problems of the probes or the physical properties of the transducer materials. When quartz is used as the transducer material, it has been found that the maximum radiated power is limited by the dielectric breakdown of the insulating medium at the transducer edges,[26] whilst if barium titanate is used, the maximum power handling capacity of the radiating

transducer is restricted by its effective heat dissipating ability and mechanical fatigue problems.[27] Heating effects are more serious in the latter case because barium titanates have high dielectric loss, which increases with the level of the impressed electric field. Consequently, practical testing of highly absorbent materials is usually carried out at low carrier frequencies (1 MHz or below) or with longer transmitted pulses at the expense of resolution.

As ultrasonics has now found increasing applications in the testing of such absorbent materials as plastics, rubber, concrete, ceramics and wood, there is an obvious need to extend the applicability of the pulse-echo system to these situations. This is the aim of the present project. It is proposed to overcome the apparent dilemma between energy (range) and resolution consideration by building a system using pulse compression. The technique involves the transmission of a long coded pulse and the processing of the received echo to obtain a relatively narrow pulse. This reconstitution of a short pulse from a long transmitted one would enable the system to possess the increased detection capability of a long-pulse system, while retaining the resolution capability of a narrow-pulse system. Thus a more efficient use of the average-power capability of the transducer is permitted.

The test frequency of the system will be chosen in the region of 2 MHz, which represents a suitable compromise between attenuation and resolution in the testing situations. For high transmitted energy a long pulse, say of the order of 400 μs, will be employed. The bandwidth of the system would be designed to be 10-15% of the centre frequency. At this percentage bandwidth, practical fabrication of the radiating transducers should be feasible. With these design parameters the pulse compression system will have an output pulse duration of about 5 μs

and a time-bandwidth product of around 80, which is a figure of merit for pulse compression systems (Section 3.2). It will be noted that a 400 μs pulse would require a long coupling delay (approximately equivalent to 300 mm of water column) for single transducer operation, and a two transducer arrangement is thus envisaged. Before proceeding to the detailed design of the system, an investigation into the principles of pulse compression will be made. This will be the subject of the next chapter.

CHAPTER 2

PULSE COMPRESSION TECHNIQUES

2.1 Introduction

The concept of pulse compression came about towards the close of the Second World War, when radar designers were confronted with the problem of extending the range of radar under the constraints of peak power limitations in the transmitters being used. As a straightforward increase in the duration of the transmitted pulse would result in loss of resolution, this solution was not acceptable. The method of pulse compression was then introduced by a number of applied scientists, (Hüttmann[28] 1940, Sproule and Hughes[29] 1944, Dicke[30] 1945, Darlington[31] 1949, and Cauer[32] 1950). Meanwhile the independent theoretical work of North, Shannon, Gabor, Woodward and others resulted in the formulation of the statistical theory of communication, which placed pulse compression techniques on a firm theoretical foundation. Since then pulse compression techniques have been employed in various sonar and seismic surveying as well as in radar systems. Relevant references on early work in pulse compression radar are Cook[33] 1960, Klauder et al[34] 1960, Ohman[35] 1960, Ramp and Wingrove[36] 1961, Tiberio[37] 1961 and Lohrmann[38] 1962. Early works in pulse-compressive sonar and seismic exploration include Stewart and Westerfields[39] 1959, Remley[40] 1963, and Goupillaud and Lee[41] 1963.

2.2 A heuristic development of the pulse compression concept

The pulse compression principle may be visualised most easily by referring to Figure 2.1 which shows a long signal of duration T (Figure 2.1 a) with its frequency linearly swept (Figure 2.1 b). After transmission, reflection and reception, this long pulse is applied to a device having a time delay versus frequency characteristic given in Figure 2.1 c; the time delay in the device is a linear function of frequency such that the highest significant frequency in the pulse is delayed a greater amount t_1, while the lowest significant frequency is delayed a small amount t_2, and such that $t_1 - t_2 = T$.
The front of the received pulse is therefore constrained to 'wait' for the later parts, and a time compression of the pulse results, (Figure 2.1 d). If energy is preserved during compression, the output narrow pulse will have a large increase in amplitude. If the duration of the narrow pulse represents the desired resolution, it can be seen that this technique permits the use of a much longer transmitted pulse of width T with the consequent increase in the final echo-to-noise ratio.

2.3 Comments on pulse compression technique from communication theory viewpoint

Although the basic principles of pulse compression were formulated long before communication theory was applied to the design of echo ranging systems, a discussion on the operation of pulse compression systems in terms of communication theory will be instructive in appreciating the limits of the concept.

Two basic principles of signal theory are of relevance in this discussion:

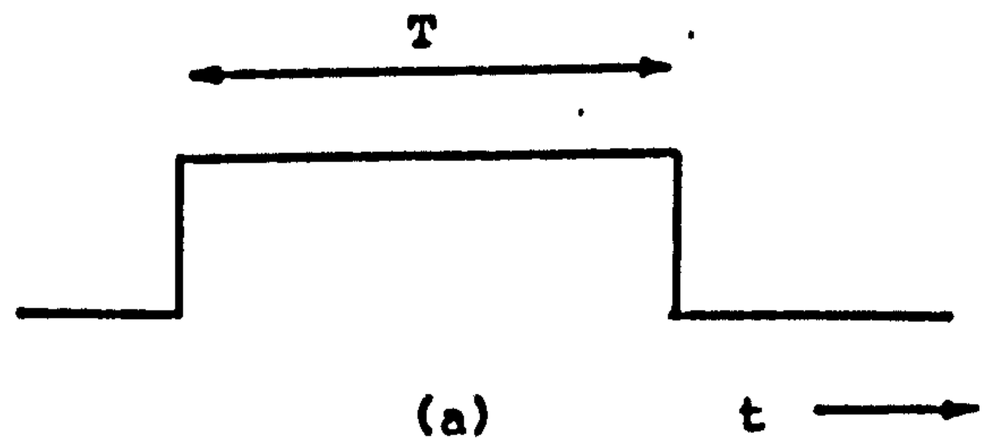

(a)

Wide-pulse envelope

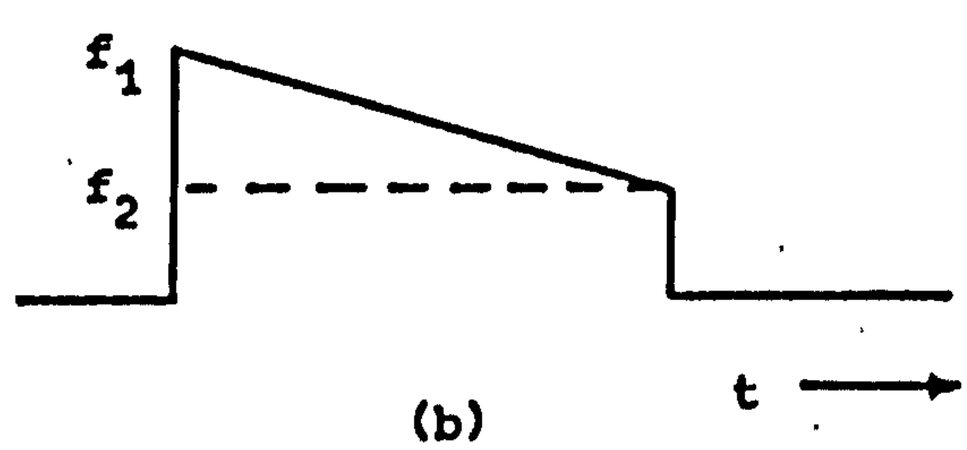

(b)

Carrier-frequency modulation

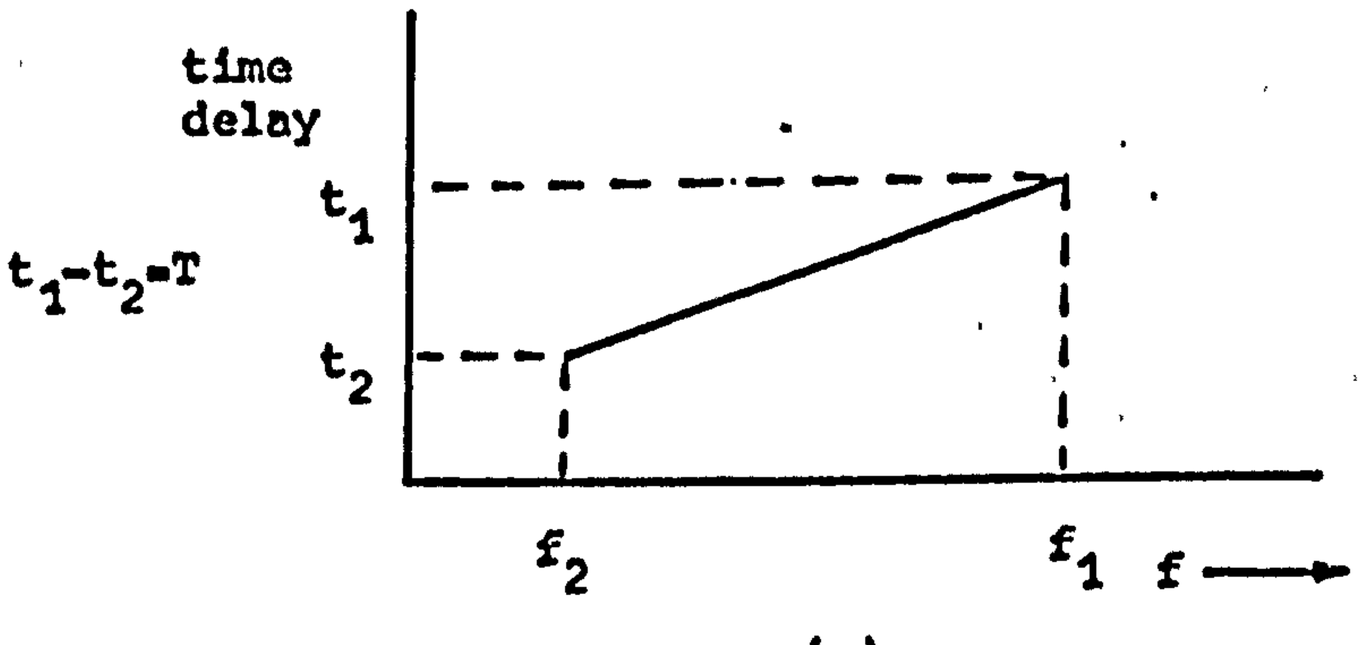

(c)

Filter time delay characteristics

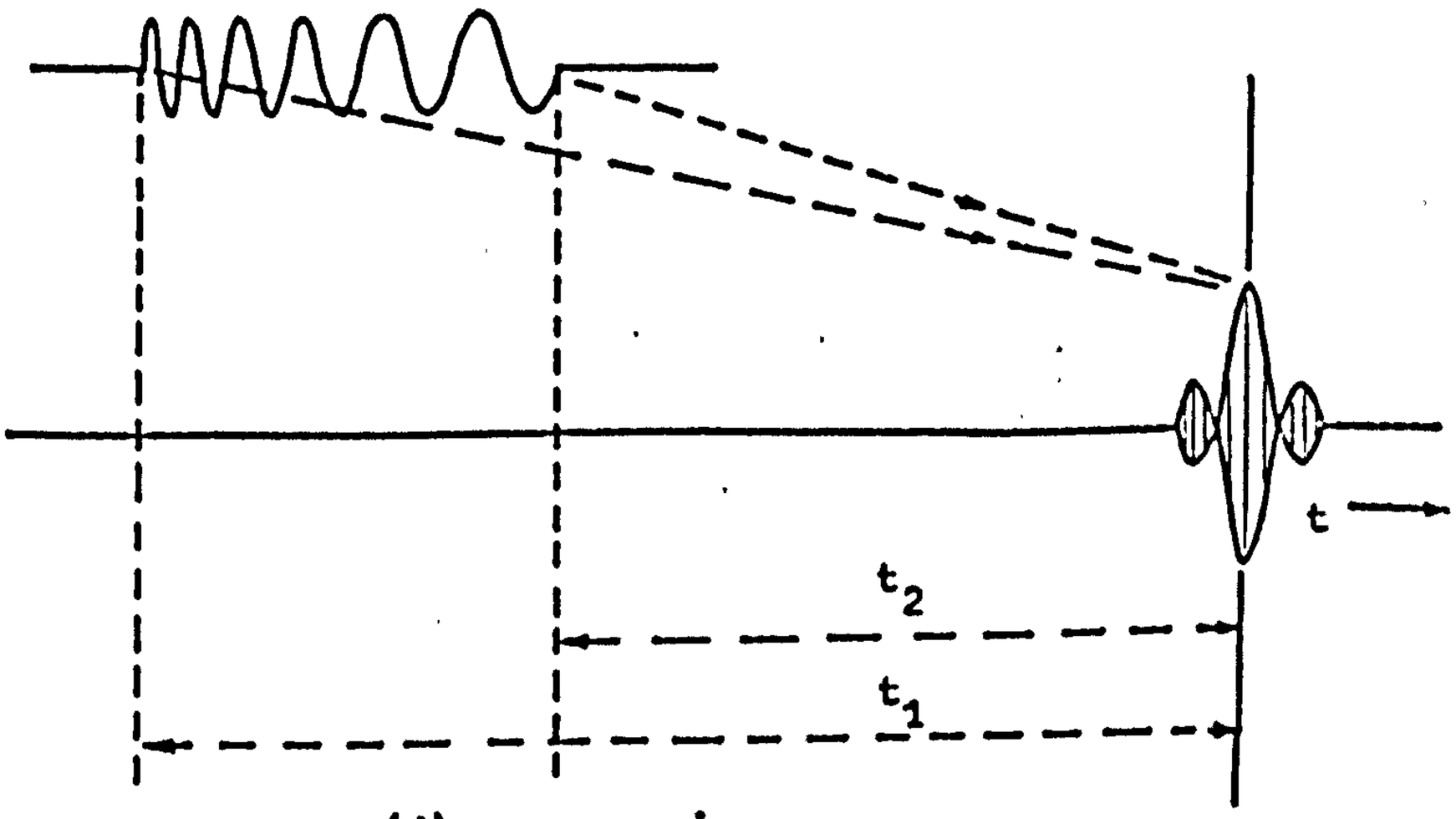

(d)

Time compression of the long pulse

Figure 2.1 Principles of Pulse Compression

(a) The Energy Principle which states that with matched-filter reception the detectability of a signal, when perturbed by white Gaussian noise, is governed solely by its energy.[42,43]

(b) The Uncertainty Relation which states that the product of the effective bandwidth occupied by a signal waveform and its effective time duration must be greater than or equal to a constant.[44]

The first principle was an outcome of matched filtering or correlation theory. It follows that the shape of the transmitted waveform is of no importance for detection, except that it influences the ability of implementing the matched filter, which will produce the maximum output signal-to-noise ratio. The latter ratio depends entirely upon the energy in the waveform. A longer duration pulse will consequently give a better signal-to-noise ratio. The Uncertainty Relation defines the effective time duration of a pulse achievable with a given effective bandwidth. Thus, the ultimate resolution obtainable with a certain transmitted signal is a function not necessarily of its duration, but of its bandwidth.

Pulse compression recognises these facts. An increase in detection range is sought through an increase in the transmitted signal, which possesses high energy. To yield good resolution, the long duration pulse must be modulated to increase the bandwidth of the signal, which may then be compressed in time.

The process of time compression can best be explained in terms of the phase distribution of the spectral components in the pulse. In an orthodox short pulse, its spectrum consists of a continuous range of frequency components, all of which come into phase at the centre of the pulse. In the long transmitted pulse in pulse compression, the

spectral components are not all in phase together at any time due to the modulation in the carrier. This phase dispersion in the latter results in a much longer pulse envelope (i.e. time duration), even though it may possess an identical amplitude spectrum (i.e. the same bandwidth) as the former short pulse. If the phase dispersion in the long pulse is removed, the pulse will be shortened in duration. It will, in fact, be compressed into a short pulse having equal bandwidth. Obviously, the relation between phase and frequency (phase dispersion) in the transmitted spectrum need not be restricted to a particular law. Provided the receiver phase response is designed in a complementary manner, so that it will bring the widely distributed Fourier components into phase at one particular instant (which will be the centre of the compressed pulse), pulse compression will be effected.

From the previous Section, a direct way of realising a pulse compression system will be as shown in Figure 2.2 a. When compared with a conventional echo-ranging system (Figure 2.2 b), the items of difference will be identified as the device for generating the swept frequency long pulse and that for compressing it. It is also clear from the above discussion that the long FM pulse may be generated 'passively' from a short pulse, through rearrangements of the phases of the latter. Thus, the sweep generator in Figure 2.2 a may be replaced by a short pulse driving a pulse stretching network, which possesses a phase characteristic opposite to those of the pulse compressor. Under these circumstances, the isolated items of difference between conventional and pulse-compressive echo-ranging systems become as shown in Figure 2.2 c. The equivalence of the resolution capability of the two systems is evident; the pulse compression system achieves its higher transmitted average power through the use of complicated pulse

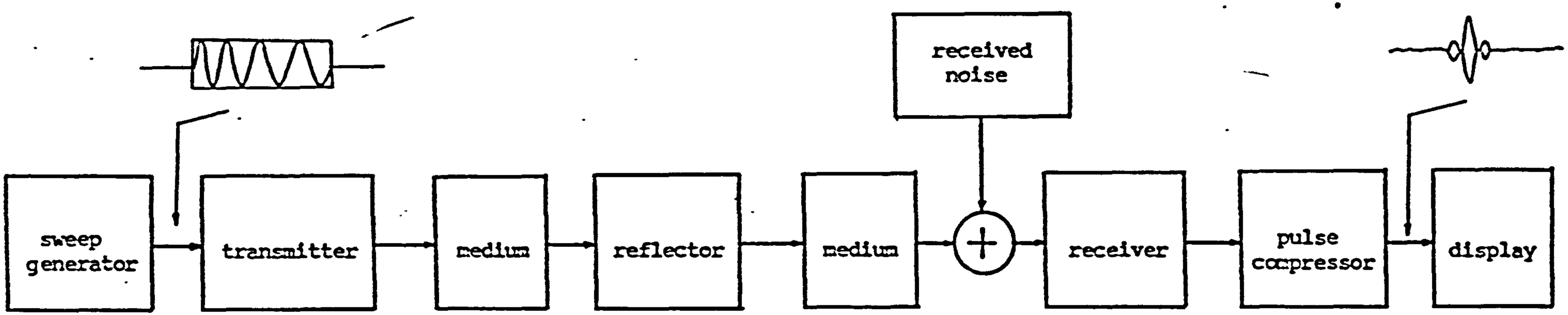

Figure 2.2a A simple pulse-compression echo ranging system

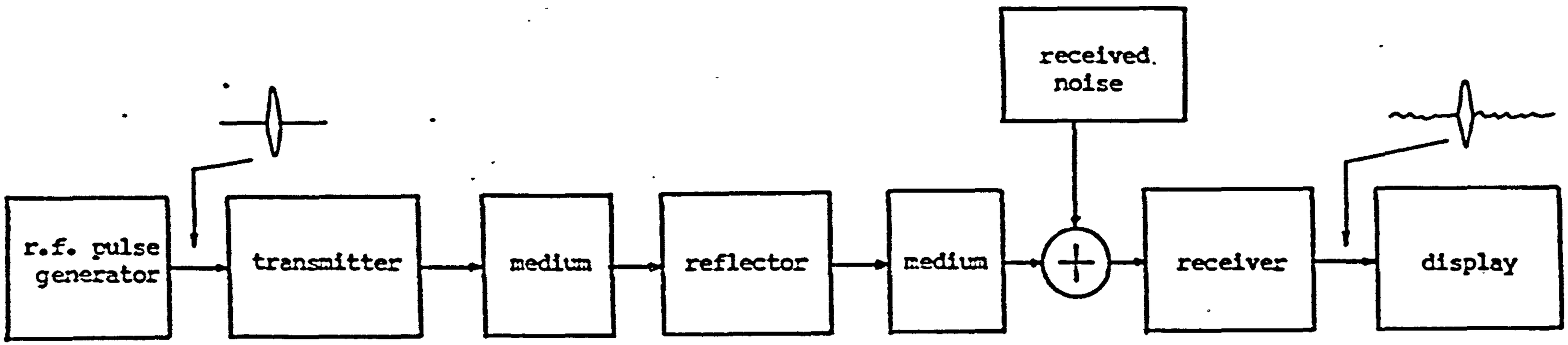

Figure 2.2b A conventional echo ranging system

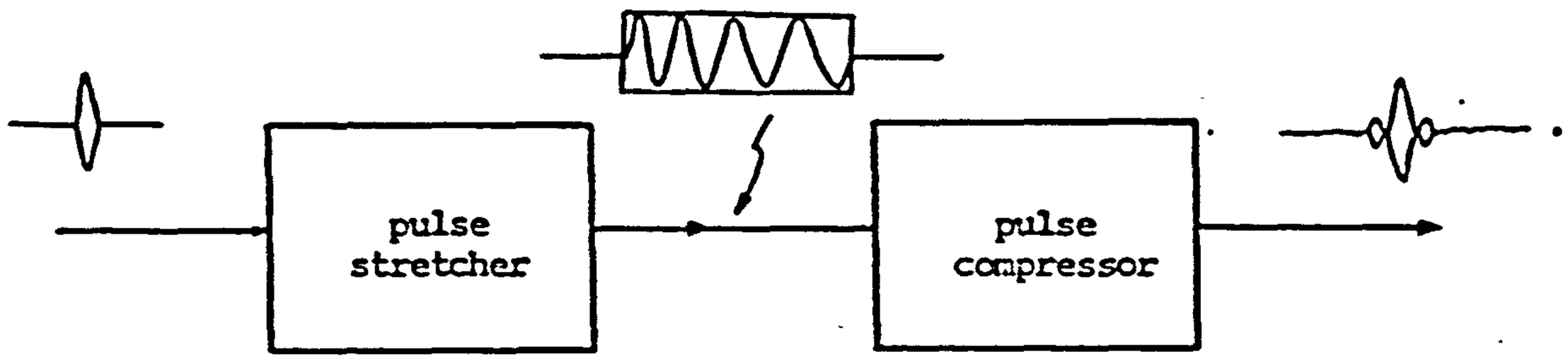

Figure 2.2c The additional elements in a pulse compression system —— the pulse stretcher and its complementary pulse compressor

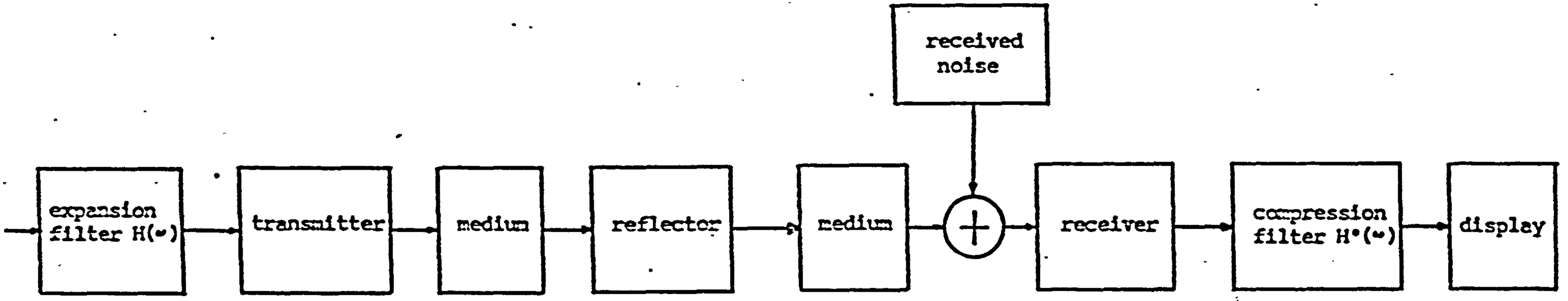

Figure 2.2d Pulse compression using conjugate filters

Figure 2.2 Comparisons between pulse compression and conventional echo ranging systems.

stretching and compressing networks. The injection of a short pulse into the first network produces a long duration pulse between the networks, but a short pulse again at the output. The processes of pulse compression and expansion are therefore seen to be reversible and linear processes.[45] In fact, a general way of representing the pulse compression technique would be as shown in Figure 2.2 d, where the expansion and compression filters are indicated as conjugates (matched) to each other. This representation illustrates clearly that pulse compression is but a practical implementation of a matched filter system.

2.4 Various schemes of implementing pulse compression

From the discussion in the foregoing paragraph, it can be seen that there are two distinct ways of implementing a pulse compression system: the active generation scheme, where the transmitted waveform is generated through an active circuit, and the passive generation scheme where a pulse stretching network is utilised to produce the long duration pulse. However, the particular type of active circuit, pulse stretching and pulse compression networks employed, will depend upon the choice of the type of waveform transmitted. Thus, pulse compression systems are generally classified according to their transmitted waveforms. Three general groupings may be formed and they are briefly described in the following:-

(a) Linear FM[46]

The linear FM, or chirp, waveform is the easiest to generate. Devices for generating and processing it have received much research interest. These mainly fall into two broad classes:

(i) Electrical devices that use the dispersive characteristics of an electrical network,

and

(ii) ultrasonic devices in which an input electrical signal is converted into an acoustic wave, propagates through a medium and is then converted back to an electrical signal at the output.

The implementation of the linear FM is shown in Figure 2.3. In the active generation scheme (Figure 2.3 a), the linear swept signal is generated using a voltage-controlled oscillator and is then compressed by a linear dispersive delay line. However, in the passive generation scheme (Figure 2.3 b), the swept signal is produced by the application of a short r.f. pulse to the linear dispersive delay line. Upon being received, the signal is then time inverted so that the same line may be utilised for compression. Its major disadvantage is that the output compressed pulse possesses undesirable range sidelobes and that weighting is required to reduce these sidelobes to an acceptable level. This weighting would cause a 1 or 2 dB loss in signal-to-noise ratio.

(b) Non-linear FM[47]

Theoretically, the undesirable sidelobes in the compressed linear FM waveform could be eliminated through the use of non-linear FM waveforms which can be designed to provide an amplitude spectrum that will dispose of the need for a shaping (weighting) filter to suppress the sidelobes. Of course, the pulse compressor must then be designed to match this transmitted waveform. However, the specific modulation law to give the desired amplitude spectrum together with a given time envelope, is normally theoretically tedious to derive and practically difficult to implement. Moreover, the synthesis of a compressing device having a given non-linear frequency law is not a straightforward procedure and this inevitably results in greater system complexity.

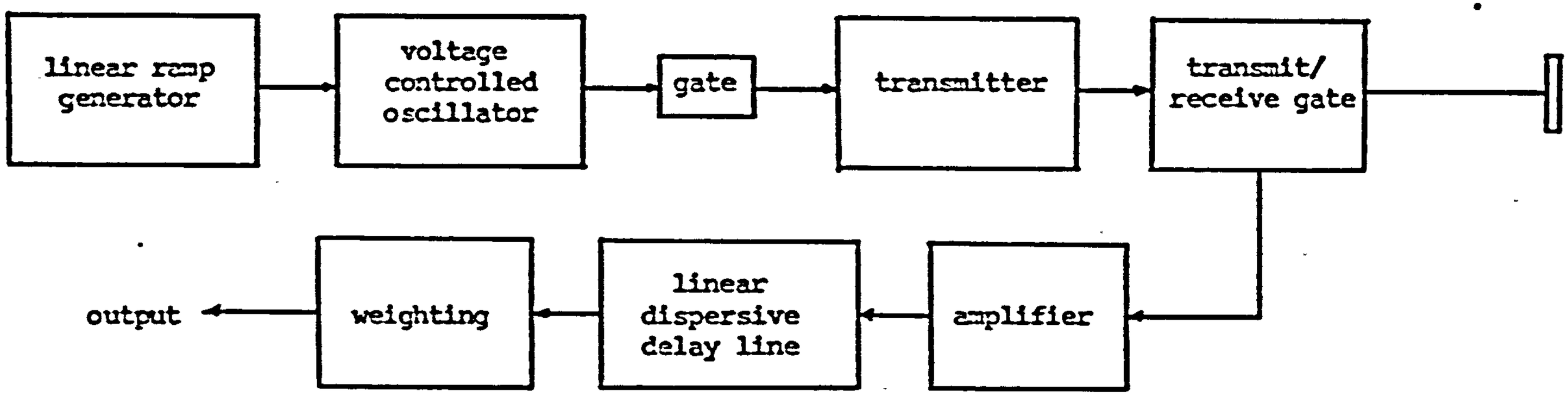

(a) Active generation scheme

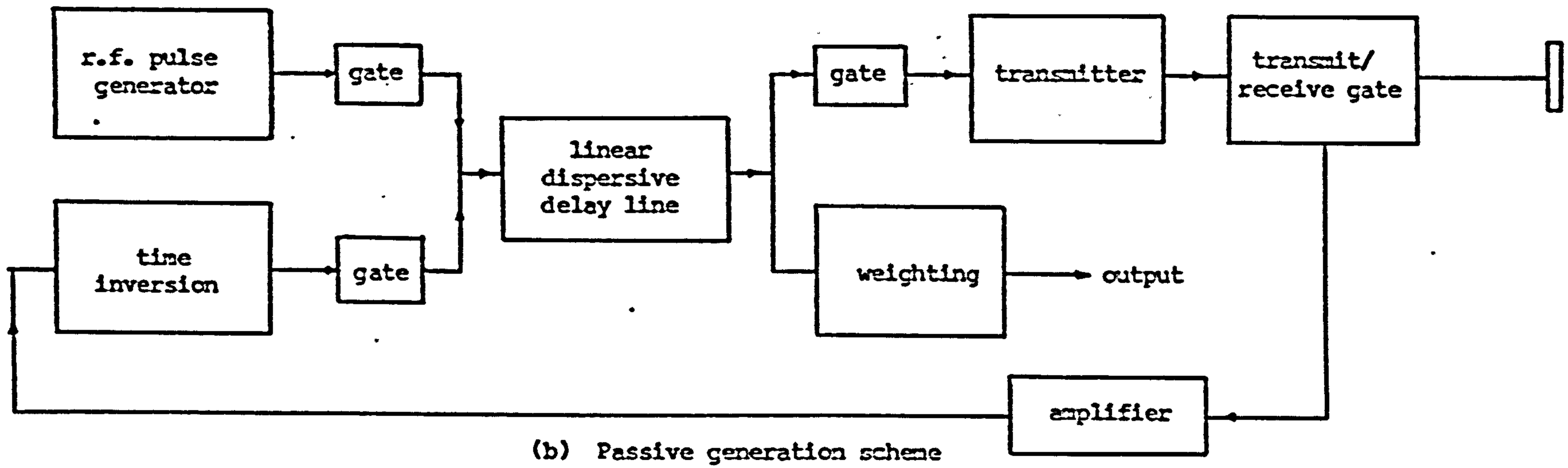

(b) Passive generation scheme

Figure 2.3 Linear FM pulse compression implementation

(c) Discrete coded waveform[46]

Instead of employing continuous frequency modulation, the modulation could also be carried out in a number of discrete steps. The stepped FM waveform is a typical example. The required frequency law is quantised in a number of steps. The long pulse is sub-divided into a number of shorter subpulses, each of equal duration. Each subpulse is then transmitted with a particular frequency which corresponds to each step in the quantised frequency law. In general, these stepped FM waveforms require a parallel filter bank in the receiver. The individual filters are matched to each subpulse, and they are followed by a coherent summation network. Because of this implementation complexity, stepped FM waveforms are not widely used except in extremely large time bandwidth product systems.

If instead of varying the frequency of each individual subpulse, the phase of each subpulse is selected in accordance with a phase code, a phase coded waveform results. Both the binary phase codes and the poly-phase codes have been employed. In the former, the phases of the transmitted subpulses alternate between zero and π, while in the latter, the phases alternate among several values rather than just zero and π. The discrete nature of these signals makes it possible to utilise tapped delay lines for matched-filter implementation as well as for signal generation. A general tapped delay line matched filter configuration is shown in Figure 2.4. The taps are spaced at intervals of the subpulse width, and the correct phase conjugation and matching amplitude weighting are placed in each tapped output lead of the delay line. This implementation using tapped delay line, although flexible, is expensive especially when the number of tapping points becomes large. The line must also be correctly terminated both at the end and at all its tapping points.

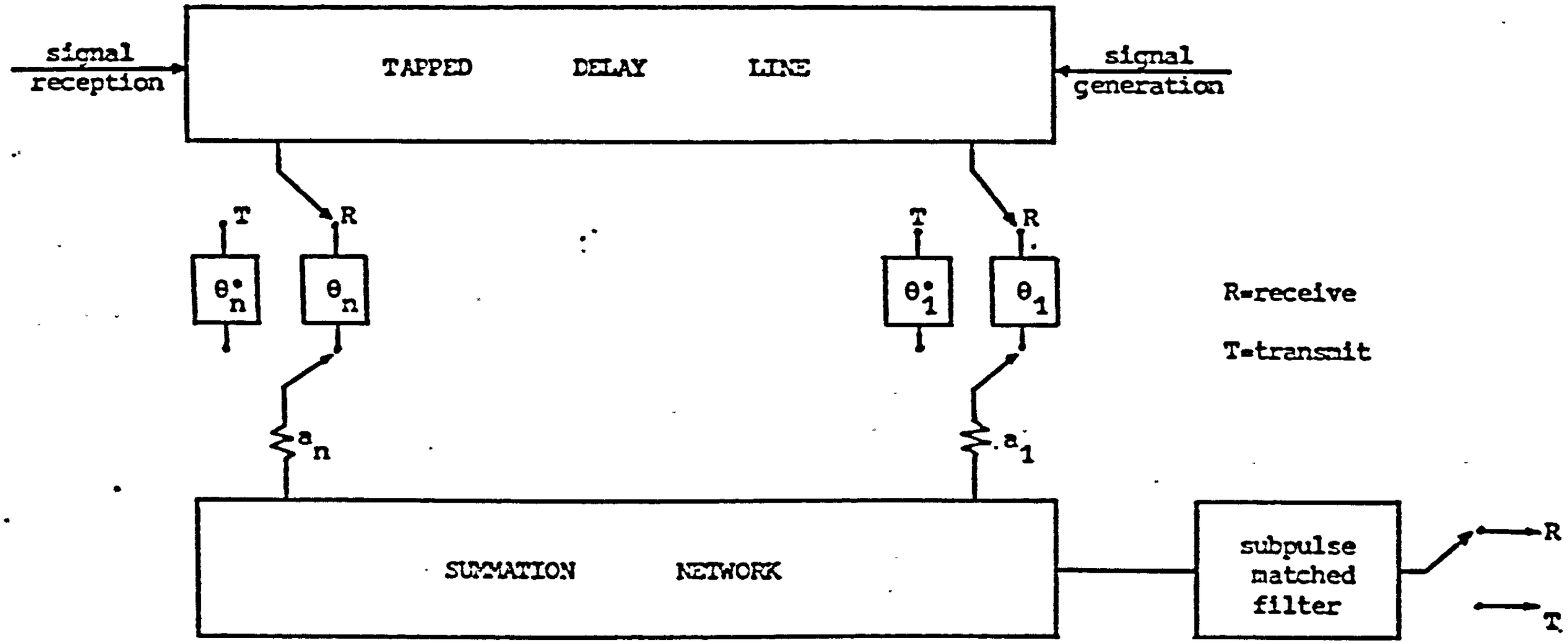

Figure 2.4 Matched-filter configuration with conjugate phase shifters for signal generation and signal processing for phase coded waveforms

From this discussion on pulse compression systems, the linear FM system stands out as being the simplest and most economical to implement for the project. At the required test frequency and pulse duration it is feasible to use an ultrasonic strip line as the dispersive delay device. This line could be economically fabricated.

As mentioned previously, two implementations are possible - an active scheme or a passive scheme. However, if the latter is employed, reception of the reflected echo must wait after transmission is completed, since the same dispersive delay line is being utilised in both transmit and receive channels. For a transmitted signal of around 400 μs duration this will involve the use of inconveniently long delay medium in the ultrasonic NDT system implementation. In addition to this, the passive scheme is also more difficult to implement from an electronic point of view. To obtain a reasonably good signal-to-noise ratio in the long transmitted signal, a large driving-pulse must be applied to the delay line, which normally has a quite high insertion loss, and to effect time inversion, heterodyne and filtering circuits must be employed. In contrast, the active generation scheme does not require long delay medium if separate transmitting and receiving transducers are used. At 2 MHz the linear FM waveform is easily generated using a multivibrator type of voltage-to-frequency convertor. The transmitted waveform could be designed to provide flexibility as well, by having adjustable pulse duration, delay slope and sweep rate.

Thus, a linearly FM pulse compression system implemented 'actively' will be the most appropriate for the project at hand.

2.5 Sidelobe suppression and choice of weighting function

The envelope of the compressed pulse in a linear FM pulse compression system is of sin (x)/x form, with a large central peak and subsidiary peaks either side of it (Section 3.2). These subsidiary peaks are known, by analogy with aerial theory, as range or time sidelobes. The first and largest of these sidelobes is only 13.2 dB below the peak of the compressed pulse and the near sidelobes fall off at approximately 4 dB per sidelobe interval, with the sidelobe null points being spaced $1/\Delta f$ seconds apart, (Δf being the nominal spectrum bandwidth). These range sidelobes degrade the multiple-target resolution capability of the detection system, since the sidelobes of a larger response pip can bury the main pip of a smaller response located nearby. The problem of reducing spatial sidelobes has already been tackled by the aerial designers, by tapering the energy distribution across the aerial aperture. In pulse compression systems the range sidelobes are reduced by tapering the signal energy across the frequency spectrum. This can be achieved either by weighting, or shaping the spectrum by frequency domain filtering or time domain envelope shaping. This weighting procedure alters the amplitude of the spectral components in the compressed pulse, such that they will give rise to a time waveform with acceptable sidelobes.

Much work has been done on choosing the best type of weighting filter, and in all cases this reduction of sidelobe levels is accompanied by a broadening of the main compressed pulse and a reduction in signal-to-noise ratio below the theoretical optimum value. Some of the possible weighting functions are Taylor weighting, Hamming, cosine-power, triplet and Gaussian. The choice of a weighting function is not clear cut, as it involves the different possible trade-offs

between sidelobe broadening, loss in signal-to-noise ratio, sidelobe suppression and sidelobe decay rate. A detailed comparison of the characteristics of the various weighting functions in terms of these factors, has been given by Temes.[48]

The Taylor weighting, Hamming and Gaussian functions are the common ones employed in practical pulse compression systems. The Taylor weighted type and the simpler Hamming functions are approximations to the unrealisable Dolph-Tchebycheff function which is optimum in having the lowest sidelobes for a given widening of the compressed pulse. The Gaussian shape weighting does not give as low a sidelobe suppression as the other two. It is, however, better than a Hamming function as far as loss in signal-to-noise ratio is concerned, and the pulse widening is very similar.[49] The Gaussian weighting is by far the easiest to implement. The Taylor or Hamming weightings are normally introduced in the time domain by amplitude weighting the envelope of the FM signal or, if frequency weighting is desired, are introduced in the form of transversal filters, and these implementations are quite involved. In contrast, the Gaussian shaped frequency filtering can be realised easily with a network of inductors, capacitors and resistors. It also has the advantage that its response shape being Gaussian, the phase characteristic of the filter is smooth and relatively linear, and its effect on the phase characteristic of the receiving system is minimal. On account of these practical considerations, Gaussian weighting will be employed for sidelobe suppression in the proposed system.

CHAPTER 3

MATHEMATICAL TREATMENT OF A LINEAR FM PULSE COMPRESSION SYSTEM

In this chapter an analytical treatment of pulse compression with linear FM will be presented. The effects of amplitude and phase distortions as well as Gaussian weighting on the output waveform, are also analysed.

3.1 Spectrum of a linear FM signal[33]

The rectangular envelope linear FM signal as shown in Figure 3.1 can be represented as:

$$f(t) = A \cos (\omega_o t + \tfrac{1}{2} \mu t^2) \qquad -\frac{T}{2} \leq t \leq \frac{T}{2} \tag{3.1}$$

where A = constant envelope function and can be taken to be unity.

$\omega_o = 2\pi f_o$ = centre frequency of the signal.

μ = radian frequency sweep rate across the pulse.

With the phase of Equation (3.1) represented by $\phi = \omega_o t + \tfrac{1}{2} \mu t^2$, the instantaneous signal frequency is defined by:

$$\omega_i = \frac{d}{dt} \{\phi(t)\} = \omega_o + \mu t \tag{3.2}$$

Thus, during the T-second interval of the pulse, the instantaneous frequency changes in a linear fashion from $\omega_o - \frac{\mu T}{2}$ to $\omega_o + \frac{\mu T}{2}$, and the sign of μ determines whether the slope of the sweep is positive or negative. The net frequency sweep, $\Delta\omega$, is then the difference of these two values, or μT.

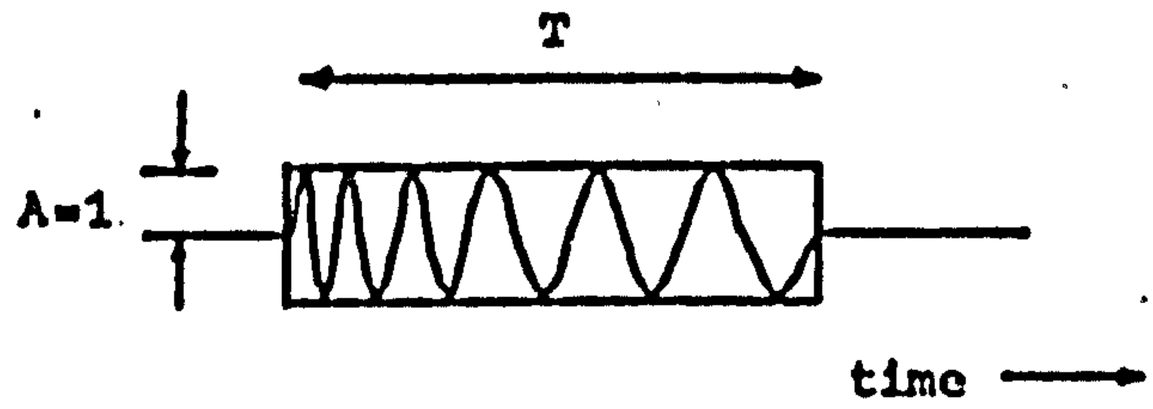

Figure 3.1 A linear FM signal

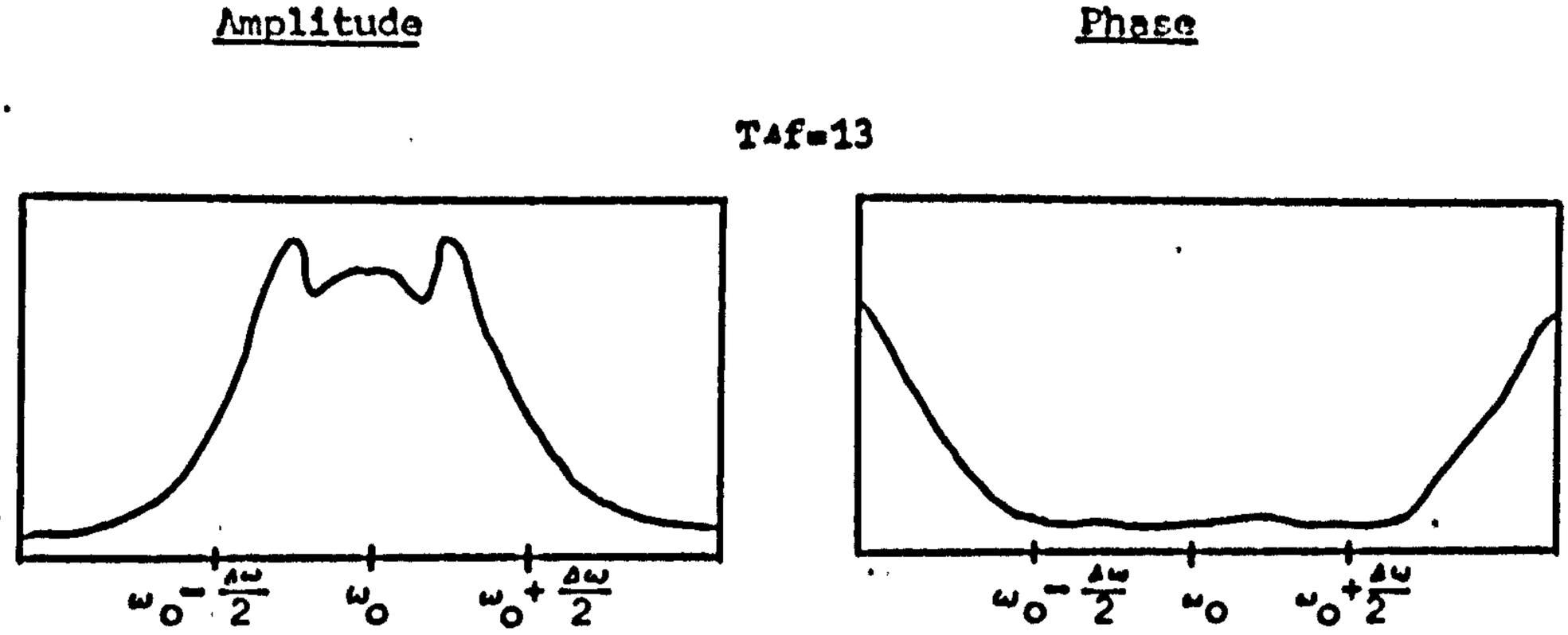

Figure 3.2 Post-compression amplitude and phase spectra for various compression ratios (from Chin & Cook)

The spectrum of the signal, $F(\omega)$, may be found from the Fourier Transform of $f(t)$.

$$F(\omega) = \int_{-\infty}^{\infty} f(t)\, e^{-j\omega t}\, dt$$

$$= \int_{-\frac{T}{2}}^{\frac{T}{2}} \cos\left(\omega_o t + \tfrac{1}{2}\mu t^2\right) e^{-j\omega t}\, dt$$

$$= \tfrac{1}{2}\int_{-\frac{T}{2}}^{\frac{T}{2}} \left\{\exp j\left\{(\omega_o - \omega)\, t + \tfrac{1}{2}\mu t^2\right\}\right\} dt$$

$$+ \tfrac{1}{2}\int_{-\frac{T}{2}}^{\frac{T}{2}} \left\{\exp -j\left\{(\omega_o + \omega)\, t + \tfrac{1}{2}\mu t^2\right\}\right\} dt \qquad (3.3)$$

The second integral essentially defines the spectrum at negative frequencies and has a negligible contribution at positive frequencies, provided that the ratio of $\frac{\omega_o}{\Delta\omega}$ or $\frac{f_o}{\Delta f}$ is sufficiently large, which would be the case in the practical implementation.

By completing the square of the bracketed term in Equation 3.3, the following spectrum expression is obtained:

$$F(\omega) = \tfrac{1}{2} \exp\left\{-j\left[\frac{(\omega - \omega_o)^2}{2\mu}\right]\right\} \int_{-\frac{T}{2}}^{\frac{T}{2}} \exp\left[j\,\frac{\mu}{2}\left(t - \frac{\omega - \omega_o}{\mu}\right)^2\right] dt \qquad (3.4)$$

Letting $\sqrt{\mu}\left(t - \frac{\omega - \omega_o}{\mu}\right) = \sqrt{\pi}\, x$,

the expression becomes after a change of variable,

$$F(\omega) = \tfrac{1}{2}\sqrt{\frac{\pi}{\mu}} \exp\left\{-j\left[\frac{(\omega - \omega_o)^2}{2\mu}\right]\right\} \int_{-X_1}^{X_2} \exp\left[j\,\frac{\pi x^2}{2}\right] dx \qquad (3.5)$$

where $X_1 = \dfrac{\mu T}{2} + (\omega - \omega_o)$,

$$X_2 = \frac{\frac{\mu T}{2} - (\omega - \omega_o)}{\sqrt{\pi\mu}} .$$

This integral yields

$$F(\omega) = \tfrac{1}{2}\sqrt{\frac{\pi}{\mu}}\, e^{-j(\omega - \omega_o)^2/2\mu} \left[C(X_1) + C(X_2) + jS(X_1) + jS(X_2) \right] \tag{3.6}$$

where

$$C(X) = \int_0^X \cos \frac{\pi y^2}{2}\, dy \quad \text{and} \quad S(X) = \int_0^X \sin \frac{\pi y^2}{2}\, dy$$

are the Fresnel integrals.

From Equation (3.6), the spectrum is seen to have three components:

Amplitude term

$$|F(\omega)| = \tfrac{1}{2}\sqrt{\frac{\pi}{\mu}} \left\{ \left[C(X_1) + C(X_2) \right]^2 + \left[S(X_1) + S(X_2) \right]^2 \right\}^{\frac{1}{2}} \tag{3.7}$$

Square-Law Phase term

$$\Phi_1(\omega) = \frac{(\omega - \omega_o)^2}{2\mu} \tag{3.8}$$

Residual Phase term

$$\Phi_2(\omega) = \tan^{-1} \left[\frac{S(X_1) + S(X_2)}{C(X_1) + C(X_2)} \right] \tag{3.9}$$

On being received, the square-law phase term will be cancelled by the compression filter, which has a complementary phase characteristic, of the form:

$$H_f(\omega) = \exp\left[j \frac{(\omega - \omega_o)^2}{2\mu} \right] \qquad (3.10)$$

For large $T\Delta f$ ratio, the ratio

$$\frac{S(X_1) + S(X_2)}{C(X_1) + C(X_2)} \doteq 1$$

over the significant interval of ω_o to $\omega_o \pm \frac{\Delta\omega}{2}$, and

$\phi_2(\omega)$ approximates a constant phase angle, $\pi/4$, in this region.

By making the substitution

$$\mu = \frac{\Delta\omega}{T},$$

and $\omega - \omega_o = \frac{\eta\Delta\omega}{2}$, where η is a normalised frequency parameter, the argument of the Fresnel integral becomes

$$X = \sqrt{T\Delta f}\ \left(\frac{1 \pm \eta}{\sqrt{2}}\right) \qquad (3.11)$$

The post-compression amplitude and phase spectra are thus functions of $T\Delta f$, the time bandwidth product or the compression ratio (Section 3.2), and independent of any particular value of centre frequency and bandwidth.

Figure 3.2 illustrates the shape of the spectrum components for values of compression ratio of 13, 52 and 130. Qualitatively, these curves show that, as the compression ratio is increased, the spectrum shape becomes more nearly rectangular, with a total bandwidth approaching $\Delta\omega$. These spectral distributions suggest that the compressed waveform might be of a $(\sin x)/x$ form.

3.2 Compressed pulse time waveform

As mentioned earlier, a square-law phase characteristic filter will be employed to compress the transmitted pulse. The transfer function of the filter is, from Equation 3.10:

$$H_f(\omega) = |H_f(\omega)| e^{jB_f(\omega)} = \exp\left(j\frac{(\omega - \omega_o)^2}{2\mu}\right)$$

Its phase characteristic $B_f(\omega)$ is

$$B_f(\omega) = \frac{(\omega - \omega_o)^2}{2\mu} \tag{3.11}$$

and the associated time delay is

$$t_d = -\frac{dB_f(\omega)}{d\omega} = -\frac{(\omega - \omega_o)}{\mu} \tag{3.12}$$

It should be noted that this characteristic is physically unrealisable, since it yields negative time delays over half the frequency band. For realisability, a sufficiently large constant delay must be added so that the filter time-delay is positive at all frequencies of interest. For analytical convenience this constant delay term will not be included in the analysis.

3.2.1 Derivation of the compressed pulse waveform[50]

In this analysis it is more expedient to use the exponential form of notation to represent the input signal, which may be described by:

$$f_1(t) = \exp\left\{j\left(\omega_o t + \tfrac{1}{2}\mu t^2\right)\right\} \qquad -\frac{T}{2} \leq t \leq \frac{T}{2}$$

$$f_1(t) = 0 \qquad |t| > \frac{T}{2} \tag{3.13}$$

This pulse spectrum is:

$$F_1(\omega) = \int_{-\infty}^{\infty} f_1(t)\, e^{-j\omega t}\, dt$$

$$= \int_{-\frac{T}{2}}^{\frac{T}{2}} \exp\left\{ j \left[(\omega_o - \omega)\, t + \tfrac{1}{2}\, \mu t^2 \right] \right\} dt \qquad (3.14)$$

The output spectrum after passing through the compression filter is:

$$Y(\omega) = F_1(\omega)\, H(\omega)$$

$$= \exp\left(j \frac{(\omega_o - \omega)^2}{2\mu} \right) \int_{-\frac{T}{2}}^{\frac{T}{2}} \exp\left\{ j \left[(\omega_o - \omega)\, t + \tfrac{1}{2}\, \mu t^2 \right] \right\} dt \qquad (3.15)$$

The output time function y(t) is the inverse Fourier Transform of this spectrum:

$$y(t) = \frac{1}{2\pi} \int_{-\infty}^{\infty} \left\{ \exp\left(j \frac{(\omega_o - \omega)^2}{2\mu} \right) \right.$$

$$\left. \int_{-\frac{T}{2}}^{\frac{T}{2}} \exp\left(j\, (\omega_o - \omega) t_1 + j \frac{\mu t_1^2}{2} \right) dt_1 \right\} e^{j\omega t}\, d\omega$$

$$= \frac{1}{2\pi} \int_{-\frac{T}{2}}^{\frac{T}{2}} \left\{ e^{j\left\{ \frac{1}{2}\mu t_1^2 + \omega_o t_1 + \frac{\omega_o^2}{2\mu} - \left(\frac{\omega_o + \mu t_1 - \mu t}{2\mu} \right)^2 \right\}} \right\}$$

$$\left\{ \int_{-\infty}^{\infty} e^{\frac{j}{2\mu} \{\omega - (\omega_o + \mu t_1 - \mu t)\}^2}\, d\omega \right\} dt_1 \qquad (3.16)$$

Letting

$$x = \left(\frac{\omega - (\omega_o + \mu t_1 - \mu t)}{\sqrt{2\mu}} \right)$$

then

$$\int_{-\infty}^{\infty} e^{-\frac{j}{2\mu}\{\omega - (\omega_o + \mu t_1 - \mu t)\}^2} d\omega$$

$$= \sqrt{2\mu} \int_{-\infty}^{\infty} e^{j x^2} dx$$

$$= \sqrt{2\mu} \left(\sqrt{\pi}\, e^{j\frac{\pi}{4}} \right)$$

Therefore, Equation 3.16 reduces to:

$$y(t) = \sqrt{\frac{\mu}{2\pi}} \int_{-\frac{T}{2}}^{\frac{T}{2}} \left\{ e^{j\left[\frac{1}{2}\mu t_1^2 + \omega_o t_1 + \frac{\omega_o^2}{2\mu} - \frac{(\omega_o + \mu t_1 - \mu t)^2}{2\mu}\right]} \right\} (e^{j\frac{\pi}{4}})\, dt_1$$

$$= \sqrt{\frac{\mu}{2\pi}}\, e^{j(\omega_o t - \frac{1}{2}\mu t^2 + \frac{\pi}{4})} \int_{-\frac{T}{2}}^{\frac{T}{2}} e^{j\mu t\, t_1}\, dt_1$$

$$= \sqrt{\frac{\mu T^2}{2\pi}}\, \frac{\sin\frac{\mu t T}{2}}{\frac{\mu t T}{2}}\, \exp\left[j(\omega_o t - \tfrac{1}{2}\mu t^2 + \tfrac{\pi}{4})\right] \qquad (3.17)$$

Putting $\mu T = \Delta\omega = 2\pi\Delta f$

$$y(t) = \sqrt{T\Delta f}\, \frac{\sin\frac{\mu t T}{2}}{\frac{\mu t T}{2}}\, \exp\left[j(\omega_o t - \tfrac{1}{2}\mu t^2 + \tfrac{\pi}{4})\right] \qquad (3.18)$$

The envelope of Equation 3.18 is plotted in Figure 3.3. It is seen that the collapsed pulse has an amplitude increase of $\sqrt{T\Delta f}$ over the input pulse, giving an output to input peak power ratio of $T\Delta f$. If the output pulse width is measured at the points $t = \pm \frac{1}{2}\Delta f$ (which correspond approximately to the 4 dB points), the long pulse can be seen to have been narrowed by a factor of $\frac{1}{T\Delta f}$.

It is of interest to note that the output pulse has a "residual" FM, with its carrier being frequency swept at the same rate as the input pulse but in the opposite direction. Moreover, it has an envelope of $\frac{\sin x}{x}$ form, whereas the input pulse has a rectangular envelope. This apparent Fourier-transform relation between the time envelopes of the input pulse and the compressed one can, in fact, be established as a general rule for the linear FM situation.(34)

3.2.2 Comparison with the matched filter output waveform

The output waveform bears great similarity to that obtained when the rectangular linear FM signal is passed through its own matched filter. From Equation A.7 in Appendix A, the matched filter autocorrelation output is:

$$y_1(t) = \sqrt{T\Delta f}\ \frac{\sin\left[\frac{\mu t}{2}(T - |t|)\right]}{\frac{\mu t T}{2}}\ \cos \omega_o t \qquad -T < t < T \qquad (3.19)$$

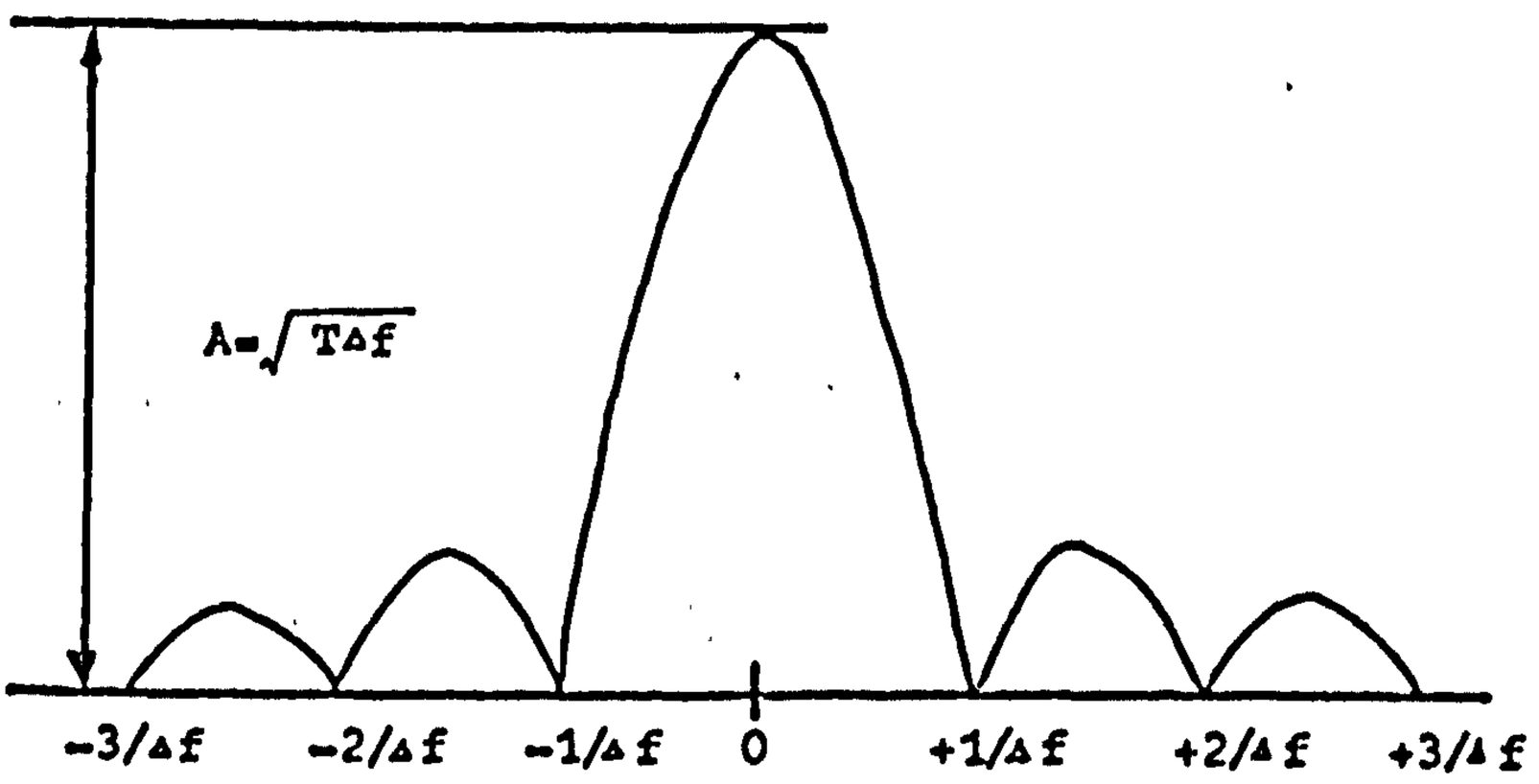

Figure 3.3 Envelope of the compressed pulse

Functionally, Equations 3.18 and 3.19 become more nearly alike in their envelope terms as the product $T.\mu T = T\Delta f$ increases. The similarity between the output signals does not mean that they have similar values of signal-to-noise ratio, for the ideal linear delay filter is an all-pass network and allows infinite noise energy passing through. The similarity between the signals does suggest, however, that a large signal-to-noise ratio may be obtained in the linear delay filter case by incorporating a band-pass network that will limit the noise but will transmit nearly all the signal frequencies. Since this is exactly what happens in a practical implementation, where both the dispersive delay line and the weighting filter are band-pass devices and suppress the noise outside the signal band, it can be appreciated that the proposed linear FM pulse compression system provides an easy realisation of a matched filtering process. In fact, Price et al[34] have mathematically demonstrated that the degradation in signal-to-noise ratio from the ideal maximum (i.e. the matched filter reception), when the linear FM signal passes through a lossless linear delay filter, followed by a sharp cut-off filter of bandwidth Δf, is within 0.5 dB for $T\Delta f$ products greater than 20, and is of the order of 0.2 dB for a $T\Delta f$ product of 80. It must also be pointed out that the exact matched filter characteristics for the input signal are extremely difficult to synthesise. Its amplitude characteristics, for example, would have to resemble one of the spectra shown in Figure 3.2.

The result in this Section clearly shows that $T\Delta f$, the time bandwidth product, which determines the magnitude of the amplitude increase as well as the resolution in the output pulse, is a parameter of fundamental significance in the system design. This parameter

is also known as the compression ratio, since it is the factor by which the long pulse has been compressed. Obviously, it is desirable for a system to have a time bandwidth product as large as possible, but the parameter is directly related to the complexity of the system.(51)

3.3 The compressed pulse with Gaussian weighting(52)

To derive the form of the compressed pulse with Gaussian weighting introduced, the system in Figure 3.4 will be studied. It will be noted that two assumptions have been made:

(a) The Gaussian weighting is introduced before the linear dispersive delay network.

(b) The input spectrum has a perfectly rectangular distribution, truncating at edge frequencies of $(\omega_o - \frac{\Delta\omega}{2})$ and $(\omega_o + \frac{\Delta\omega}{2})$ respectively.

As the system is linear, assumption (a) does not entail any approximations. Assumption (b) is equivalent to ignoring the effects of truncating, in time, the linear FM signal. As illustrated in Figure 3.2, this approximation is quite accurate for large $T\Delta f$ products where the spectrum of the linear FM signal tends to be rectangular.

Referring to Figure 3.4, the rectangular spectrum of the long duration pulse, after passing through the Gaussian weighting network, takes up a Gaussian distribution with the spectrum truncated at $(\omega_o - \frac{\Delta\omega}{2})$ and $(\omega_o + \frac{\Delta\omega}{2})$ respectively. Because of the truncation of this Gaussian spectrum, the compressed pulse output after the dispersive delay line will consist of unwanted sidelobes, which have to be estimated in the system design.

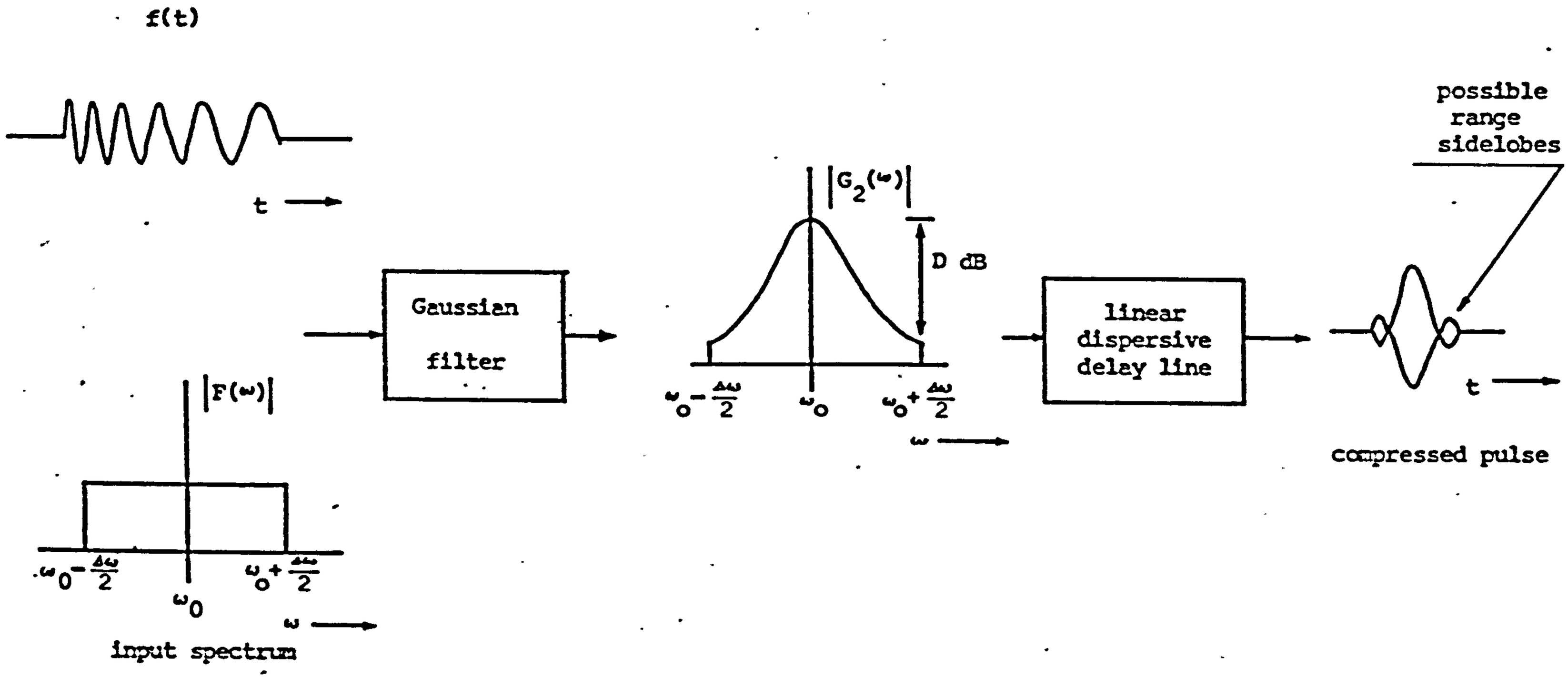

Figure 3.4 Pulse compression with Gaussian weighting

The approach will be to consider the spectrum after weighting, as composed of three parts; firstly, one of unlimited bandwidth and secondly, the part of the same Gaussian spectrum lying below the lower edge frequency $(\omega_o - \frac{\Delta\omega}{2})$ of the original input spectrum and finally, the part of the same Gaussian spectrum lying above the higher edge frequency $(\omega_o + \frac{\Delta\omega}{2})$ of the original input spectrum. The dispersor will be assumed to bring the components of the complete spectrum all into phase at a particular time. Hence, this will produce a compressed pulse with a Gaussian shaped envelope, while the missing parts of the complete Gaussian spectrum will produce range sidelobes on the ideal compressed pulse.

3.3.1 Output pulse from a complete Gaussian spectrum

Let the complete Gaussian spectrum, $G(\omega)$, be represented by:

$$G(\omega) = \exp\left\{ - K \left[(\omega - \omega_o) / \Delta\omega \right]^2 \right\} \qquad (3.20)$$

where K is a constant associated with the Gaussian envelope.

The compressed pulse $g(t)$ is given by:

$$g(t) = \frac{1}{2\pi} \int_{-\infty}^{\infty} \exp\left\{ -K \left[(\omega - \omega_o)/\Delta\omega\right]^2 \right\} e^{j\omega t} \, d\omega$$

$$= \frac{1}{2\pi} \exp\left[- \frac{(\Delta\omega)^2 t^2}{4K} \right] \exp(j\omega_o t) \int_{-\infty}^{\infty} e^{\frac{-K}{\Delta\omega^2}\left\{\left[\omega-\omega_o-j\left(\frac{\Delta\omega}{2K}\right)^2 t\right]^2\right\}} d\omega \qquad (3.21)$$

Using $\int_{-\infty}^{\infty} e^{-x^2} dx = \sqrt{\pi}$, $g(t)$ can be evaluated:

$$\therefore g(t) = \sqrt{\frac{\pi}{K}} \frac{\Delta\omega}{2\pi} \exp\left[- (\Delta\omega)^2 t^2 / 4K \right] \exp(j\omega_o t) \qquad (3.22)$$

3.3.2 Sidelobes due to spectrum truncation

With the truncated spectrum, the output will consist of a complete Gaussian pulse plus the pulse signals produced by the minus missing spectral components. These pulse signals are given by:

$$-\frac{1}{2\pi}\int_{\omega_o+\frac{\Delta\omega}{2}}^{\infty} \exp\left\{-K\left[(\omega-\omega_o)/\Delta\omega\right]^2\right\} e^{j\omega t}\, d\omega$$

$$-\frac{1}{2\pi}\int_{-\infty}^{\omega_o-\frac{\Delta\omega}{2}} \exp\left\{-K\left[(\omega-\omega_o)/\Delta\omega\right]^2\right\} e^{j\omega t}\, d\omega$$

$$= -\frac{1}{2\pi}\exp(j\omega_o t)\left\{\int_{\frac{\Delta\omega}{2}}^{\infty} \exp\left(-\frac{K\omega_1^2}{(\Delta\omega)^2}\right) e^{j\omega_1 t}\, d\omega_1 + \int_{-\infty}^{-\frac{\Delta\omega}{2}} \exp\left(-\frac{K\omega_1^2}{(\Delta\omega)^2}\right) e^{j\omega_1 t}\, d\omega_1\right\} \qquad (3.23)$$

Noting that

$$\int_{\frac{\Delta\omega}{2}}^{\infty} \exp\left(-\frac{K\omega_1^2}{(\Delta\omega)^2}\right) e^{j\omega_1 t}\, d\omega_1 = \int_{\frac{\Delta\omega}{2}}^{\infty} G_1(\omega_1)\, e^{j\omega_1 t}\, d\omega_1$$

$$= \frac{1}{jt}\left[G_1(\omega_1)\exp(j\omega_1 t)\right]_{\omega_1=\frac{\Delta\omega}{2}}^{\infty} - \frac{1}{jt}\int_{\frac{\Delta\omega}{2}}^{\infty} G_1'(\omega_1)\, e^{j\omega_1 t}\, d\omega_1$$

$$= - (jt)^{-1} G_1(\tfrac{\Delta\omega}{2}) \exp (j \tfrac{\Delta\omega}{2} t)$$

$$- \frac{1}{jt} \left\{ \frac{1}{jt} \left[G_1' (\omega_1) \exp (j\omega_1 t) \right]_{\omega_1=\frac{\Delta\omega}{2}}^{\infty} - \frac{1}{jt} \int_{\frac{\Delta\omega}{2}}^{\infty} G_1''(\omega_1) e^{j\omega_1 t} \, d\omega_1 \right\}$$

$$= - (jt)^{-1} G_1(\tfrac{\Delta\omega}{2}) \exp (j \tfrac{\Delta\omega}{2} t) + (jt)^{-2} G_1'(\tfrac{\Delta\omega}{2}) \exp (j \tfrac{\Delta\omega}{2} t)$$

$$- (jt)^{-3} G_1''(\tfrac{\Delta\omega}{2}) \exp (j \tfrac{\Delta\omega}{2} t) + \ldots\ldots\ldots \qquad (3.24)$$

which, for large t is asymptotic to:

$$- (jt)^{-1} G_1(\tfrac{\Delta\omega}{2}) \exp (j \tfrac{\Delta\omega}{2} t) \qquad (3.25)$$

similarly, for large t

$\int_{-\infty}^{-\frac{\Delta\omega}{2}} G_1(\omega_1) e^{j\omega_1 t} \, d\omega_1$ is asymptotic to:

$$\vdots$$

$$+ (jt)^{-1} G_1(-\tfrac{\Delta\omega}{2}) \exp (-j \tfrac{\Delta\omega}{2} t) \qquad (3.26)$$

Therefore for large t, the pulse signals given by Equation 3.23 can be represented as:

$$(j2\pi t)^{-1} \exp (j\omega_o t) \left\{ \exp (-\tfrac{K}{4}) \exp (j \tfrac{\Delta\omega}{2} t) - \exp (-\tfrac{K}{4}) \exp (-j \tfrac{\Delta\omega}{2} t) \right\}$$

$$= (\tfrac{\Delta\omega}{2\pi}) \exp (-\tfrac{K}{4}) \frac{\sin \frac{\Delta\omega t}{2}}{\frac{\Delta\omega t}{2}} \exp (j\omega_o t) \qquad (3.27)$$

The envelope of Equation 3.27 is:

$$(\pi t)^{-1} \exp\ (-\frac{K}{4})$$

which, relative to the peak of the pulse from untruncated spectrum (Equation 3.22) is:

$$\frac{(\pi t)^{-1} \exp\ (-\frac{K}{4})}{\sqrt{\frac{\pi}{K}}\ \frac{\Delta\omega}{2\pi}}$$

$$= \frac{\sqrt{K}\ \exp\ (-\frac{K}{4})}{\pi^{\frac{3}{2}}\ \Delta f t} \qquad (3.28)$$

Defining the attenuation in dB at the edge frequencies in the truncation spectrum to be D, then D and K are related by:

$$D = 20 \log\ (\frac{1}{e^{-K/4}})$$

$$= 5K \log e$$

Thus $K = 0.46\ D$

or $D = 2.1715\ K \qquad (3.29)$

The expression in Equation 3.28 can then be expressed in terms of D. The envelope of the sidelobes is down on the peak value of the compressed pulse by:

$$= D - 10 \log D + 19.34 + 20 \log (\Delta f\ t)\ dB$$

for large t (3.30)

Equation 3.30 provides a design criterion for a Gaussian weighted pulse compression system with a specified sidelobe level. Taking the first three terms, Equation 3.30 gives:

For D = 12 18 24 30 36 42 dB

D - 10 log D + 19.34 = 20.5 24.8 29.5 34.6 39.8 45.1 dB

Then 20 $\log_{10}$ (Δft) has to be added to obtain asymptotic value for any large value of (Δft).

3.4 Degradation of signal-to-noise ratio and pulse widening after weighting[47]

To find the loss in signal-to-noise ratio due to weighting, the output signal-to-noise ratio in the system, as represented by Figure 3.4, will first be evaluated, and is then compared with that obtained in a matched system.

From Figure 3.4 the output time function is given by:

$$\varepsilon_2(t) = 2\left\{\frac{1}{2\pi}\int_{\omega_o-\frac{\Delta\omega}{2}}^{\omega_o+\frac{\Delta\omega}{2}} |F(\omega)|G(\omega)\, e^{j\omega t}\, d\omega\right\}$$

$$= \frac{1}{\pi}\int_{\omega_o-\frac{\Delta\omega}{2}}^{\omega_o+\frac{\Delta\omega}{2}} \sqrt{\frac{\pi}{2\mu}}\, \exp\left\{-K\{(\omega-\omega_o)/\Delta\omega\}^2\right\} e^{j\omega t}\, d\omega \qquad (3.31)$$

where $|F(\omega)|$, the amplitude of the assumed rectangular spectrum, is taken to be $\sqrt{\frac{\pi}{2\mu}}$ for a normalised unit amplitude received long FM pulse, (this is from Equation 3.7). At $\omega = \omega_o$ the combination of Fresnal integrals approximately equals $\sqrt{2}$, and $|F(\omega_o)| = \sqrt{\frac{\pi}{2\mu}}$);

and $G(\omega)$, the weighting function, is represented as

$$\exp\left\{ -K \{(\omega-\omega_o)/\Delta\omega\}^2 \right\} \text{ as before.}$$

Only the amplitude spectrum is used here, as all components will be assumed to have been brought into phase by the dispersive network.

Equation 3.31 may be written as:

$$g_2(t) = \frac{1}{\pi} \int_{-\frac{\Delta\omega}{2}}^{\frac{\Delta\omega}{2}} \sqrt{\frac{\pi}{2\mu}} \exp\left\{ - K \frac{\omega_1^2}{(\Delta\omega)^2} \right\} e^{j\omega_o t} e^{j\omega_1 t} d\omega_1$$

$$= \sqrt{\frac{1}{2\pi\mu}} e^{j\omega_o t} \int_{-\frac{\Delta\omega}{2}}^{\frac{\Delta\omega}{2}} \exp\left\{ - K \frac{\omega_1^2}{(\Delta\omega)^2} \right\} e^{j\omega_1 t} d\omega_1$$

(3.32)

By making a further change of variable,

$$m = \frac{\omega_1}{\Delta\omega}$$

the peak output voltage is:

$$g_2(0) = g_2(t)_{max} = \sqrt{\frac{1}{2\pi\mu}} \Delta\omega \int_{-\frac{1}{2}}^{\frac{1}{2}} e^{-Km^2} dm \qquad (3.33)$$

The average output noise power from the system is:

$$P_N = \frac{N_o}{2\pi} \int_{-\frac{\Delta\omega}{2}}^{\frac{\Delta\omega}{2}} e^{-2K\left(\frac{\omega}{\Delta\omega}\right)^2} d\omega$$

$$= \frac{N_o}{2\pi} \Delta\omega \int_{-\frac{1}{2}}^{\frac{1}{2}} e^{-2Km^2} dm \qquad (3.34)$$

where N_o = one-sided spectral density of the white noise.

Thus, the output signal-to-noise ratio, defined by

$$\left(\frac{S}{N}\right)_W = \frac{\{g_2(t)_{max}\}^2}{P_N}$$

is

$$\frac{\frac{1}{2\pi\mu} (\Delta\omega)^2 \left[\int_{-\frac{1}{2}}^{\frac{1}{2}} e^{-Km^2} dm \right]^2}{\frac{N_o}{2\pi} \Delta\omega \int_{-\frac{1}{2}}^{\frac{1}{2}} e^{-2Km^2} dm}$$

$$= \frac{T}{N_o} \frac{\left[\int_{-\frac{1}{2}}^{\frac{1}{2}} e^{-Km^2} dm \right]^2}{\int_{-\frac{1}{2}}^{\frac{1}{2}} e^{-2Km^2} dm} \qquad (3.35)$$

The output signal-to-noise ratio for the matched-filter system is:

$$\left(\frac{S}{N}\right)_M = \frac{T\Delta f}{N_o \Delta f} = \frac{T}{N_o} \qquad (3.36)$$

The degradation, or mismatch loss, that results from receiver weighting is then:

$$\frac{\left(\frac{S}{N}\right)_W}{\left(\frac{S}{N}\right)_M} = \frac{\left[\int_{-\frac{1}{2}}^{\frac{1}{2}} e^{-Km^2}\,dm\right]^2}{\int_{-\frac{1}{2}}^{\frac{1}{2}} e^{-2Km^2}\,dm} \qquad (3.37)$$

This mismatch loss is plotted as a function of the attenuation D at the edge frequencies in Figure 3.5. It can be seen that the reduction in signal-to-noise ratio is within 2 dB up to values of D=35.

The corresponding pulse widening ratio can be approximately estimated through Equations 3.18 and 3.22, by evaluating the 3 dB pulse width in the envelope of the unweighted compressed pulse and that of the weighted Gaussian compressed pulse with different values of K (or D). The results are plotted in Figure 3.6.

It can be seen that as the loss introduced at the band edge by the Gaussian network is increased in order to achieve an increase in sidelobe discrimination, there is a corresponding increase in mismatch loss and pulse widening. But the marked increase in sidelobe discrimination (see Equation 3.30) is well worth the pulse-width increase and the small cost in signal-to-noise ratio.

3.5 Effects of amplitude and phase distortion

In the foregoing sections the linear FM pulse compression system performance was analysed, but this analysis was based upon an ideal distortionless system. Since in a practical implementation both amplitude and phase distortions will inevitably be present in the system, it is of importance to determine the effects of such distortions upon the resultant output signal. In particular, it is desirable to be able to calculate the deterioration in system performance contributed by the principal sources of distortion in order that distortion tolerances may

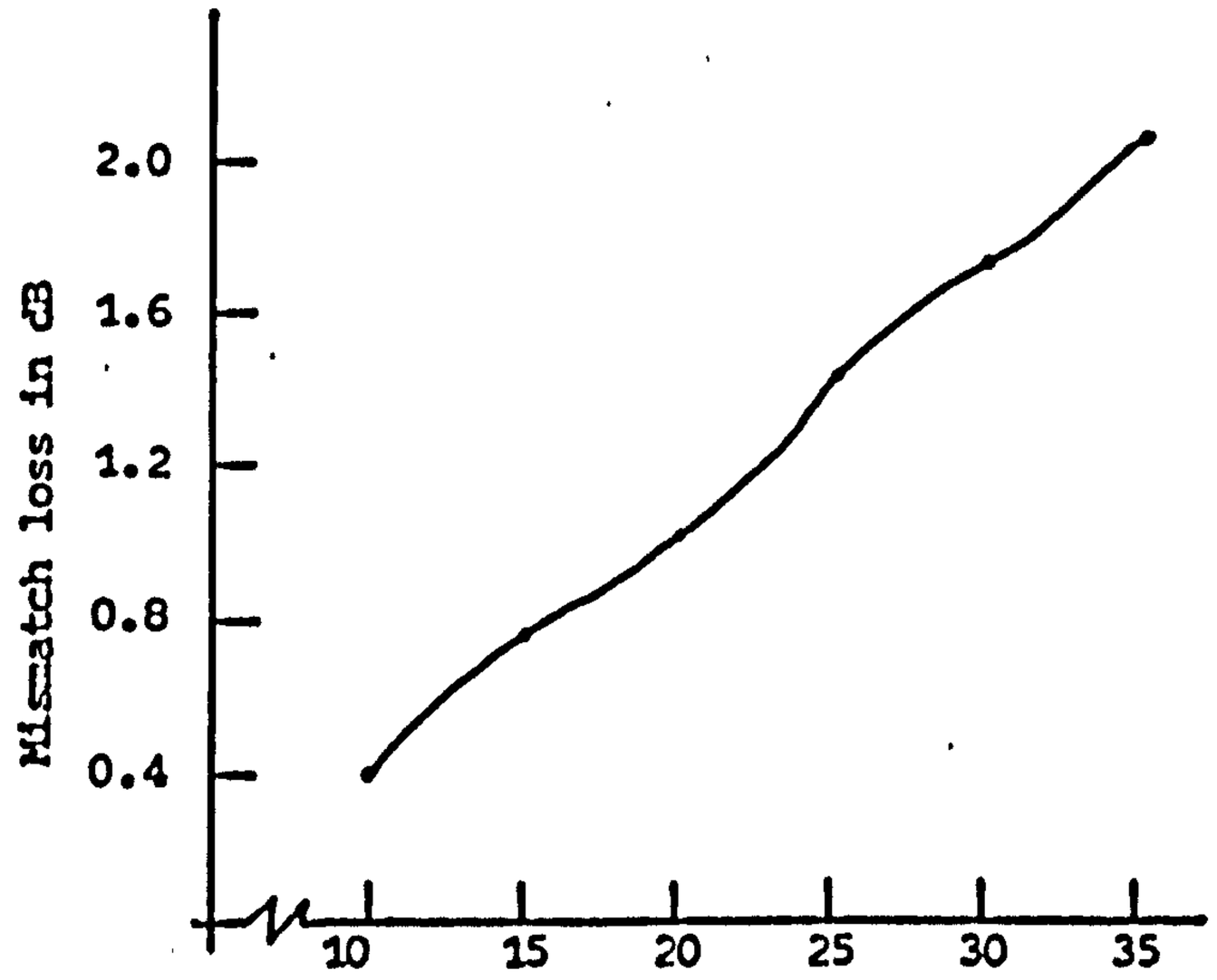

Figure 3.5 Degradation in S/N from the ideal maximum with Gaussian weighting introduced

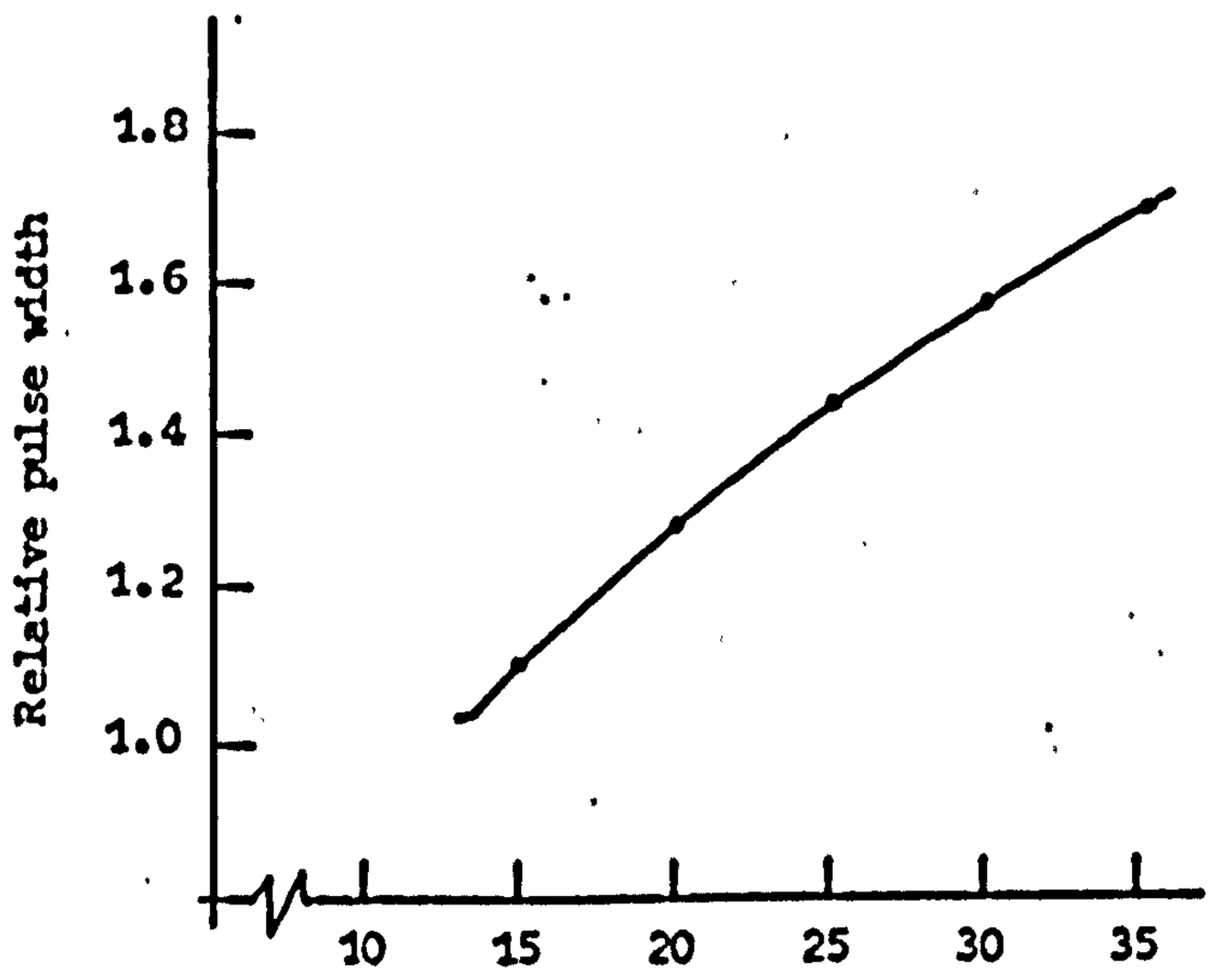

Figure 3.6 Compressed pulse-width increase due to Gaussian weighting

be specified. In this Section, effects of deviations from the ideal system behaviour will be studied. These deviations will normally be those introduced by the delay non-linearities and the non-uniform insertion loss in the strip dispersive delay line, as well as those introduced by the unevenness in the transmitting and receiving transducer responses.

3.5.1 Paired-echo distortion analysis[53]

The effect of departures from the ideal system amplitude and phase characteristics can best be studied in terms of the paired-echo theory. The method is fundamentally an adaptation of the Fourier integral and is particularly useful in getting a first approximation of the resulting distortions without any laborious computations.

If the steady-state amplitude and phase characteristics of an ideal linear system are:

$$A(\omega) = a_o \tag{3.38}$$

$$B(\omega) = b_o\omega \tag{3.39}$$

then a physical system with departures from this characteristic may be written as:

$$A(\omega) = a_o + \sum_n a_n \cos nc\omega \tag{3.40}$$

$$B(\omega) = -b_o\omega + \sum_n b_n \sin nc\omega \tag{3.41}$$

where the departures from the ideal characteristic are given by a Fourier expansion about the frequency band of interest, Δf, and $c = \frac{2\pi}{\Delta\omega} = \frac{1}{\Delta f}$. The corresponding transfer function is:

$$H(\omega) = A(\omega)\, e^{jB(\omega)} \tag{3.42}$$

Taking only one term in the Fourier expansion the steady-state amplitude and phase characteristic is given by:

$$A(\omega) = a_o + a_1 \cos c\omega \tag{3.43}$$

$$B(\omega) = -b_o\omega + b_1 \sin c\omega \tag{3.44}$$

This corresponds to a transfer function:

$$H(\omega) = (a_o + a_1 \cos c\omega)\, e^{j\{-b_o\omega + b_1 \sin c\omega\}}$$

$$= \{a_o + \frac{a_1}{2}(e^{jc\omega} + e^{-jc\omega})\}\{e^{-jb_o\omega} \sum_{k=-\infty}^{\infty} J_k(b_1)\, e^{jkc\omega}\} \tag{3.45}$$

where $J_k(b_1)$ is the usual Bessel function. The distortion components of $H(\omega)$ are illustrated in Figure 3.7.

To evaluate the output signal, $e_o(t)$, corresponding to an input signal, $e_i(t)$, to a system having the characteristics given in Equations 3.43 and 3.44, the following Fourier integrals are written for the input and output signals.

$$e_i(t) = \frac{1}{2\pi} \int_{-\infty}^{\infty} E_i(\omega)\, e^{j\omega t}\, d\omega \tag{3.46}$$

and

$$e_o(t) = \frac{1}{2\pi} \int_{-\infty}^{\infty} H(\omega)\, E_i(\omega)\, e^{j\omega t}\, d\omega \tag{3.47}$$

where $E_i(\omega)$ is the spectrum of the input signal.

Substituting Equation 3.45 into Equation 3.47, the following expression for the output signal is obtained:

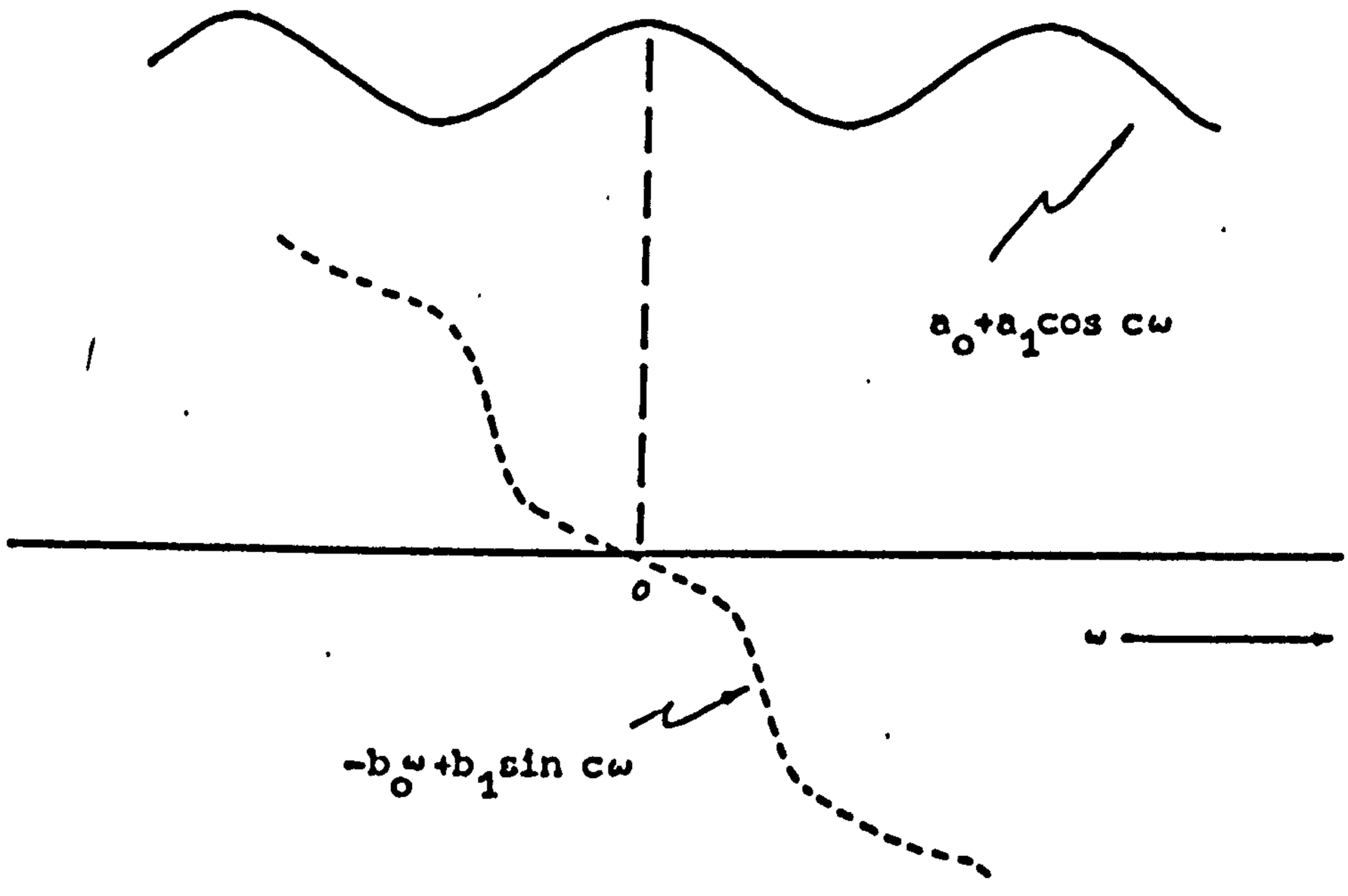

Figure 3.7 Sinusoidal distortion components of $H(\omega)$

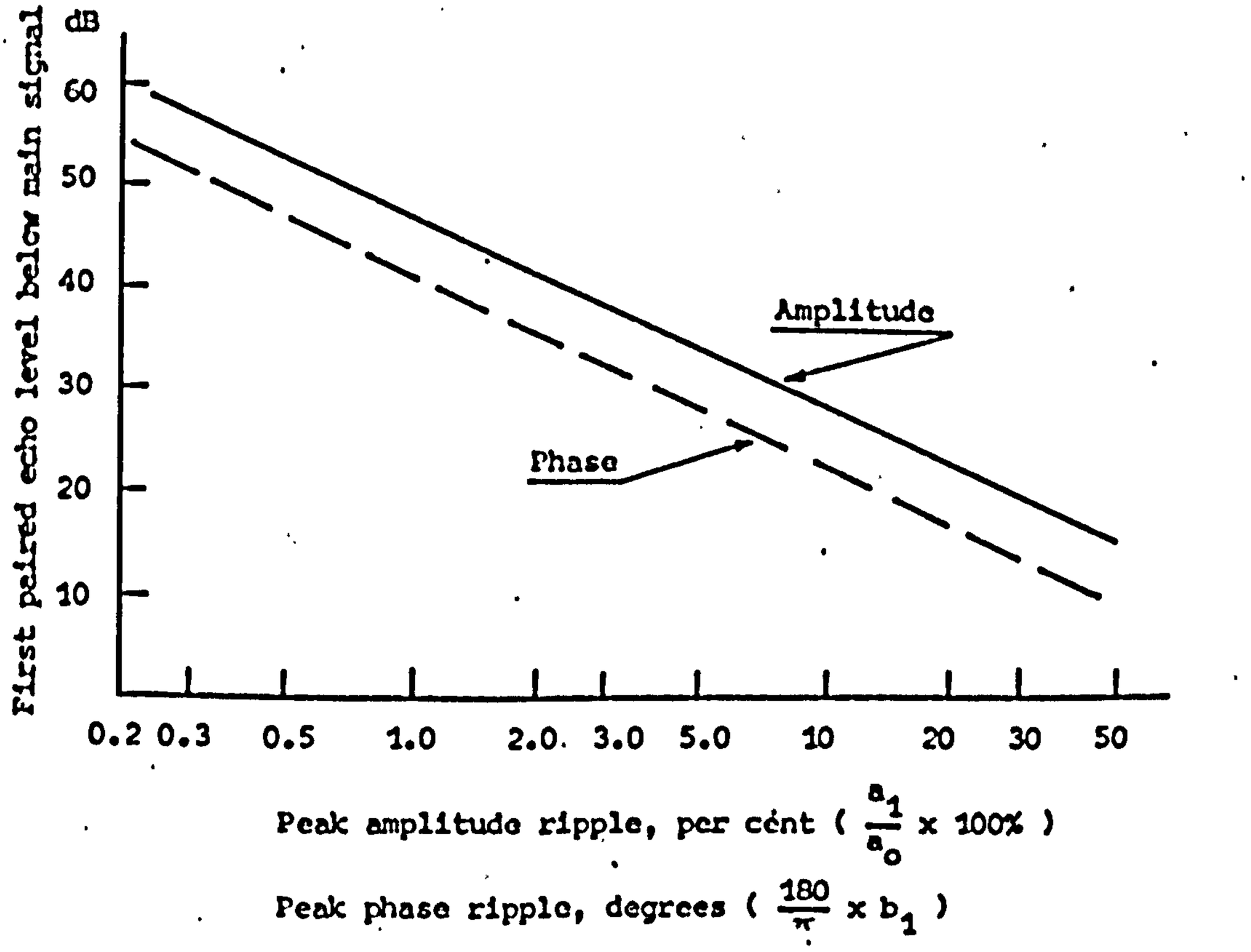

Figure 3.8 Paired-echo distortions due to amplitude and phase errors

$$e_o(t) = \frac{1}{2\pi} \int_{-\infty}^{\infty} a_o\, e^{-jb_o\omega} \left(\sum_{k=-\infty}^{\infty} J_k\,(b_1)\, e^{jkc\omega} \right) E_i\,(\omega)\, e^{j\omega t}\, d\omega$$

$$+ \frac{1}{2\pi} \int_{-\infty}^{\infty} \frac{a_1}{2}\, e^{-jb_o\omega} \left(\sum_{k=-\infty}^{\infty} J_k\,(b_1)\, e^{j(k+1)c\omega} \right) E_i\,(\omega)\, e^{j\omega t}\, d\omega$$

$$+ \frac{1}{2\pi} \int_{-\infty}^{\infty} \frac{a_1}{2}\, e^{-jb_o\omega} \left(\sum_{k=-\infty}^{\infty} J_k\,(b_1)\, e^{j(k-1)c\omega} \right) E_i\,(\omega)\, e^{j\omega t}\, d\omega \qquad (3.48)$$

By using the time shift properties of the Fourier transform and noting that:

$$J_{m-1}\,(x) + J_{m+1}\,(x) = \frac{2m}{x}\, J_m\,(x) \qquad (3.49)$$

and

$$J_{-m}\,(x) = (-1)^m\, J_m\,(x) \qquad (3.50)$$

the output signal can be expressed as:

$$e_o(t) = a_o J_o\,(b_1)\, e_i\,(t - b_o)$$

$$+ J_1\,(b_1) \left[\left(a_o + \frac{a_1}{b_1}\right) e_i(t - b_o + c) - \left(a_o - \frac{a_1}{b_1}\right) e_i\,(t - b_o - c) \right]$$

$$+ J_2\,(b_1) \left[\left(a_o + \frac{2a_1}{b_1}\right) e_i\,(t - b_o + 2c) + \left(a_o - \frac{2a_1}{b_1}\right) e_i\,(t - b_o - 2c) \right]$$

$$+ J_3\,(b_1) \left[\left(a_o + \frac{3a_1}{b_1}\right) e_i\,(t - b_o + 3c) - \left(a_o - \frac{3a_1}{b_1}\right) e_i\,(t - b_o - 3c) \right]$$

$$+ \ldots\ldots \qquad (3.51)$$

From the above equation, the output is seen to have a main component which is a delayed replica of the input signal weighted by the factor $a_o J_o(b_1)$. Flanking this principal component, there exists an

infinite set of distortion signals. These "echoes" that occur in pairs - one preceding and one lagging the principal response - have amplitudes diminishing according to the Bessel function coefficients and time separation from the principal response given by c, 2c, 3c .....seconds respectively.

In the proposed pulse compression system, the coefficients a_1 and b_1 would be small (since compensating techniques would be employed), and the following approximations can be made:

for $b_1 < 0.4$ radians

$$J_o(b_1) = 1 \tag{3.52}$$

$$J_1(b_1) = \tfrac{1}{2} b_1 \tag{3.53}$$

$$J_n(b_1) = 0, \qquad n > 1 \tag{3.54}$$

Equation 3.51 reduces to:

$$e_o(t) = a_o \left[e_i(t - b_o) + \tfrac{1}{2} \left(\frac{a_1}{a_o} + b_1 \right) e_i(t - b_o + c) \right.$$

$$\left. + \tfrac{1}{2} \left(\frac{a_1}{a_o} - b_1 \right) e_i(t - b_o - c) \right] \tag{3.55}$$

Thus it can be seen that a small sinusoidal distortion term produces a single pair of echoes. The amplitude of these paired echoes depends on the magnitude of the phase and amplitude errors, while their time separation from the main echo depends upon the periodicity of the errors across the frequency band. The effects of amplitude and phase distortion can be isolated: the even distortion function in the

amplitude $A(\omega)$ gives echoes of the same polarity and the odd phase function gives echoes of opposite polarity.

The above results can readily be extended to the complex distortion function represented by Equations 3.40 and 3.41. For the amplitude case, the individual components of the distortion function will contribute independent sets of paired echoes. For the phase distortion terms the combined effect is that of a multiplication of imaginary exponential sine functions, which corresponds to a multiplication of Bessel function expansions.[54] However, for small phase errors (less than 0.4 radian), the effects of the various phase error terms can be treated as being essentially independent.

A graph showing the magnitudes of the effects as given by Equation 3.55 is shown in Figure 3.8. This gives a guideline on the permissible levels of distortion magnitudes in both amplitude and phase characteristics throughout the system, for a specified distortion level in the output signal. If -25 dB range sidelobes are aimed at in the proposed system, the paired-echo distortions must necessarily be kept to below this level, say to -30 dB. With this design objective, the amount of tolerable peak amplitude and phase ripples can be read from Figure 3.8 and are of 7% (0.6 dB) and 3 degrees respectively. It is obvious that practical distortion compensation techniques have to be introduced into the system to achieve these low levels of distortion.

3.5.2 Relationship between phase distortion and delay distortion

The previous section specified the amount of phase errors permitted in the system. However, the most convenient practical measurements in evaluating the phase behaviour of the dispersive delay line or the complete system, are those of the group time delay characteristics. It is thus necessary to relate the phase distortion error to the time delay error, so that the latter may be employed as a design criterion.

If tg is the group time delay, and $B(\omega)$ the phase shift function, then:

$$tg = - \frac{dB(\omega)}{d\omega} \qquad (3.56)$$

For a phase shift function, $B(\omega) = (- b_o\omega + b_1 \sin c\omega)$, the group time delay will be:

$$tg = b_o - b_1 \, c \cos c\omega \qquad (3.57)$$

It can be seen that a phase error $B_e = b_1 \sin c\omega$ will associate with a time delay error:

$$t_e = b_1 \, c \cos c\omega$$

Following the above reasoning, a given delay error curve can be related to the phase errors by first expressing it as a combination of a number of sinusoidal components. If each component has a time delay error of the form:

$$(t_e)_n = b_n \, nc \cos n \, c\omega \qquad (3.58)$$

then its associated phase error component will be:

$$(B_e)_n = b_n \sin nc\omega \qquad (3.59)$$

where n = the number of cycles of the error component over the signal band, $\Delta\omega$,

and $c = \frac{2\pi}{\Delta\omega} = \frac{1}{\Delta f}$ as before.

From Equation 3.58, the peak time delay error is:

$$(\hat{t}_e)_n = b_n nc \qquad (3.60)$$

This gives the allowable peak time delay error for a specified peak phase error b_n. For the previous -30dB paired echo specification, the peak time delay error must be less than

$$\hat{t}_e = b_1 c$$

$$= \left(\frac{3}{180} \times \pi\right) \times \frac{1}{200} \qquad = 0.26\ \mu s$$

for a single sinusoidal cycle of delay error over the 200 KHz band. This result demonstrates the stringent requirement that must be imposed upon the linearity of the delay characteristics in the dispersive delay line.

In using the group delay error curve as a design criterion, it must be noted that b_n is the critical factor in determining the paired-echo magnitude. The time delay error correction would be most effective if it could reduce the peak delay error while simultaneously increasing the number of error cycles. This is because for a fixed peak delay error the peak phase error b_n is inversely related to the number of cycles of of the delay error function over the band Δf.

CHAPTER 4

DISPERSIVE DELAY LINE

In the proposed linear FM pulse compression system, the linearly dispersive delay device is the key element. In this chapter, an account of the fabrication of this delay device will be given.

4.1 Types and Selection of linearly dispersive delay devices

From the tentative specification of the system parameters, the main objectives in designing and selecting the required dispersive device can be listed as:

(a) A constant-amplitude characteristic over a bandwidth of at least 200 KHz centred at 2 MHz;

(b) A linear delay slope with a differential delay of 400 μs across the above bandwidth;

(c) Minimum spurious response;

and (d) A low insertion loss.

As mentioned in Section 2.4, for the processing of a linear FM waveform, both ultrasonic devices and lumped constant networks may be employed. The common types of ultrasonic devices are :

(i) guided wave delay lines, (ii) surface acoustic wave devices, (iii) perpendicular diffraction delay lines, (iv) wedge-type delay lines, and (v) YIG (yttrium-iron-garnet) crystals.

However, out of these, only the guided wave delay lines are suitable for the present project. The other devices operate at much higher centre frequencies than the proposed 2 MHz and their dispersion times seldom exceed 100 μs.[46][55] The problem of selecting the type of dispersive

device is then reduced to that of choosing between the ultrasonic guided wave delay lines and the lumped constant network.

In the lumped constant network approach, the composite dispersive delay characteristic is obtained by staggering a number of iterative bridged-T all-pass time-delay networks at different centre frequencies. This technique is well established and detailed approximation synthesis procedures for designing a linear-slope delay filter over a given frequency range, have been outlined by O'Meara's[56] as well as Brandon's[57] papers. However, there are a number of practical problems associated with this filter realisation: The losses involved in the finite Q inductors and the difficulties of achieving the required precision in the network elements are the major ones. A preliminary calculation based on O'Meara's synthesis procedure indicated that over 150 bridged-T sections are required for the proposed linear FM signal. An implementation based on this design involving so many T networks, would require great care in controlling the errors introduced by the inexactitude of the design approximation, the effects of component tolerances, mismatch of impedances and the alignment procedure. In fact, it was reported that for a -30 dB sidelobe level at a time bandwidth product of 80, high quality components with tolerances well within one percent must be used.[49] Obviously, this would be prohibitively expensive and rule out the possibility of employing such a delay filter for the project.

In the guided wave ultrasonic delay line approach, the dispersive delay property is obtained by utilising some of the many possible modes of wave propagation in bounded solids, which have their phase velocities

varying as a function of frequency. With suitable design of transducers and choice of cross-sectional dimensions of the delay medium, a given mode could be preferentially excited and its dispersive delay utilised. In particular, the first longitudinal mode in cylinders and strips has a nearly linear delay-versus-frequency characteristic. Ultrasonic delay lines using this mode have been reported.[58][59] These lines operate up to several megahertz, and have a nominal bandwidth of around 10%. The amount of dispersive delay could be designed by choosing the correct line length and could be of the order of hundreds of microseconds. Their major realisation problems lie in the design of the terminating transducers and the suppression of unwanted responses. Despite these difficulties, it is felt that this guided-wave ultrasonic delay line approach offers a more promising and economical solution to the present problem of fabricating the linear-slope delay line. A delay line using the first longitudinal mode in a narrow strip would be preferable, since it gives better discrimination against unwanted signals than the wire delay line.[60]

4.2 Dispersive delay characteristics of longitudinal modes in strips

To investigate the feasibility of employing the dispersive delay characteristics of the first longitudinal mode in a strip for implementing the compression filter in the proposed system, the longitudinal modes of propagation of elastic waves in thin strips will be studied.

4.2.1 Theory of the propagation of elastic waves in strips

A first approximation to the theory of the propagation of elastic waves in strips should be given by the theory for the infinite plate. If end effects are neglected the results for the strip would approach those predicted for the infinite plate as the width and length of the

strip increase. Plate waves were first investigated by Lamb,[61] who outlined the basic theories for the existence of such waves in a solid plate with free boundaries, for which displacements occur both in the direction of wave propagation and perpendicularly to the plane of the plate. His theory describes the motion of the plate as a combination of pure compressional waves and pure shear waves inside the plate, in accordance with the basic theory of travelling waves in a solid, and in essence, states that up to an infinite number of modes of vibration may exist in a plate, depending upon the material and thickness of the plate and the frequency of the wave. Each mode propagates with a unique phase velocity that is related to the product of frequency times the plate thickness. All these modes - the symmetric (longitudinal) and asymmetric (flexural)- are the roots of two frequency equations, the graphical solution of which yields a set of dispersive curves. In these symmetric modes the boundaries of the plate will move in the opposite direction, giving a sausage-like deformation; while in the asymmetric modes the boundaries move together, giving a wriggling type of deformation. A physical interpretation of these various modes has been given by Redwood[62] who treated the plates as an acoustic waveguide. More thorough presentation of the theory of guided wave propagation can be found in Meeker and Meitzler's work.[63]

Lamb's solution to elastic wave propagation in a plate is obtained by solving the elastic wave equation with the appropriate boundary condition. In order to define the co-ordinate axes used here, the form of the symmetric and asymmetric displacements is shown in Figure 4.1a and Figure 4.1b. The displacements for the symmetrical or longitudinal modes can be written as:

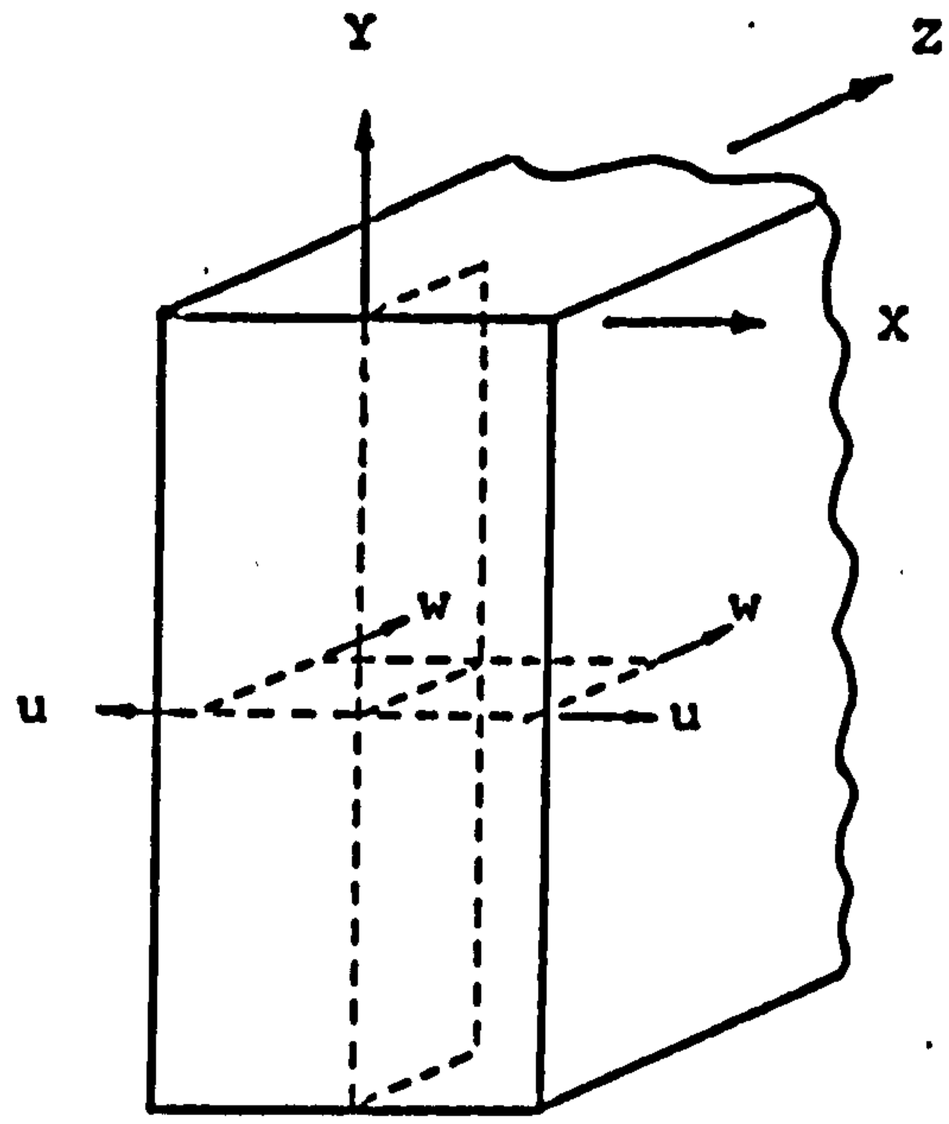

Direction of propagation is in the Z axis

Figure 4.1a Longitudinal mode displacements

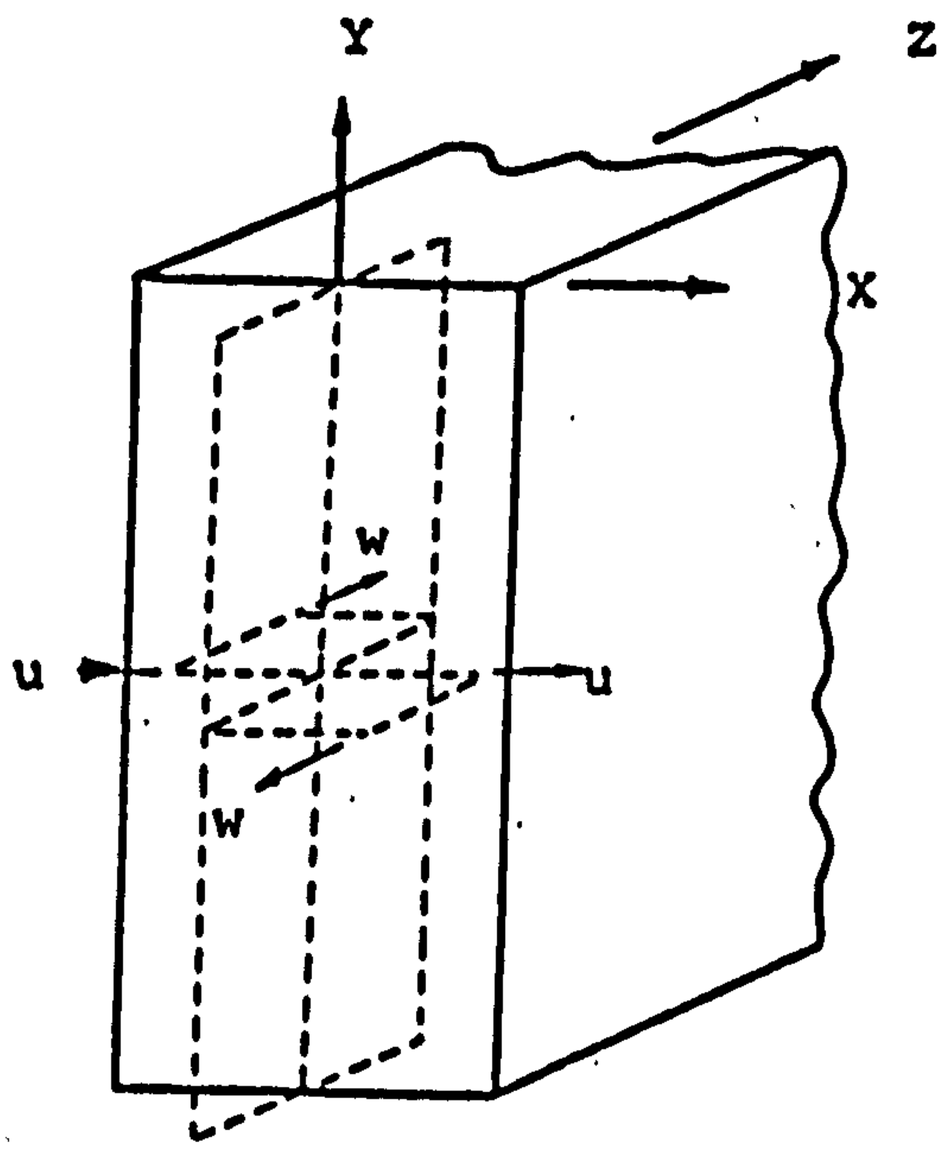

Direction of propagation is in the Z axis

Figure 4.1b Flexural mode displacements

Figure 4.1 Displacement components for longitudinal and flexural elastic wave motions in the infinite plate

$$\left.\begin{aligned} u_s &= U_s(X)\, e^{i(\omega t - \gamma_s Z)} \\ v_s &= 0 \\ w_s &= W_s(X)\, e^{i(\omega t - \gamma_s Z)} \end{aligned}\right\} \qquad (4.1)$$

while those for the asymmetric, or flexural modes, can be written as:

$$\left.\begin{aligned} u_a &= U_a(X)\, e^{i(\omega t - \gamma_a Z)} \\ v_a &= 0 \\ w_a &= W_a(X)\, e^{i(\omega t - \gamma_a Z)} \end{aligned}\right\} \qquad (4.2)$$

In these equations u,v,w are the components of the displacement in the X,Y and Z directions of the plate, U_s and W_a are odd functions of X alone and U_a and W_s are even functions of X alone; ω is the angular frequency and γ is the propagation constant. The plate is defined by the two planes $X = \pm \frac{h}{2}$, so that h is the thickness of the plate. The modes are propagated in the Z direction. The boundary conditions are those of zero stress at $X = +\frac{h}{2}$ and $X = -\frac{h}{2}$. The frequency equation so obtained for longitudinal modes is:

$$\frac{\tan\left\{\frac{\omega h}{2V_s}\left(1 - \frac{V_s^2}{V^2}\right)^{\frac{1}{2}}\right\}}{\tan\left\{\frac{\omega h}{2V_p}\left(1 - \frac{V_p^2}{V^2}\right)^{\frac{1}{2}}\right\}} = -\frac{4\left(\frac{V}{V_p}\right)\left(\frac{V}{V_s}\right)\left(1 - \frac{V_p^2}{V^2}\right)^{\frac{1}{2}}\left(1 - \frac{V_s^2}{V^2}\right)^{\frac{1}{2}}}{\left(2 - \frac{V^2}{V_s^2}\right)^2} \qquad (4.3)$$

and the frequency equation for the flexural modes is:

$$\frac{\tan\left\{\frac{\omega h}{2V_s}\left(1-\frac{V_s^2}{V^2}\right)^{\frac{1}{2}}\right\}}{\tan\left\{\frac{\omega h}{2V_p}\left(1-\frac{V_p^2}{V^2}\right)^{\frac{1}{2}}\right\}} = -\frac{\left(2-\frac{V^2}{V_s^2}\right)^2}{4\left(\frac{V}{V_p}\right)\left(\frac{V}{V_s}\right)\left(1-\frac{V_p^2}{V^2}\right)^{\frac{1}{2}}\left(1-\frac{V_s^2}{V^2}\right)^{\frac{1}{2}}} \qquad (4.4)$$

where $V_p = V_s \sqrt{\frac{2-2\sigma}{1-2\sigma}}$ and $V = \frac{\omega}{\gamma}$.

In these equations V is the phase velocity, V_s is the bulk shear wave velocity, and σ is the Poisson's ratio.

4.2.2 Numerical solution of the frequency equation for the first longitudinal mode

Since it is proposed to utilise the delay characteristics of the first longitudinal mode, the frequency equation in Equation 4.3 has to be solved. As the equation is a transcendental one, numerical methods have to be employed in its solution. On examining Equation 4.3, it is seen that it represents the dependence of $\frac{V}{V_s}$ on $\frac{\omega h}{V_s}$ and σ.

For a given value of σ the dependence of $\frac{V}{V_s}$ on $\frac{\omega h}{V_s}$ for the possible modes could be obtained by determining the various combinations of $\frac{V}{V_s}$ and $\frac{\omega h}{V_s}$ satisfying the equation. Then, the dependence of the group velocity, U, defined by:

$$U = \frac{d\omega}{d\gamma} = \frac{V}{\left(1-\frac{\omega}{V}\frac{dV}{d\omega}\right)} . \qquad (4.5)$$

on the frequency can be determined. As in the design of the delay line, the specific group delay rather than the group velocity, is the more important parameter, Equation 4.5 is written as:

$$\frac{V_s}{U} = \frac{DV_s}{L} = \frac{1 - \frac{\left(\frac{\omega h}{V_s}\right) \; d\left(\frac{V}{V_s}\right)}{\left(\frac{V}{V_s}\right) \; d\left(\frac{\omega h}{V_s}\right)}}{\frac{V}{V_s}} \qquad (4.6)$$

where the specific group delay D is defined as $\frac{L}{U}$, L is the length of the path of propagation and $\frac{DV_s}{L}$ is a dimensionless specific group delay. Based on Equation 4.6 the dependence of $\frac{DV_s}{L}$ on $\frac{\omega h}{V_s}$ for the first longitudinal mode can be calculated.

In solving the frequency equation the method of bisection was employed. It can be briefly described as follows:
Consider a continuous real-valued function f(z) of a real variable z. If f(z) = 0 has a root in the interval I (a, b), where $a \leq z \leq b$, then the sign of f(a) is opposite to that of f(b). If a sequence of intervals I_o, I_1, I_2, ... I_n is produced such that each of these intervals is smaller than its predecessor and each contains the root, the end points of each interval will have a different sign and the mid-points of the intervals furnish a sequence of estimates which converge to the root of f(z). The simplest method of obtaining this sequence is to bisect the intervals. Thus I_1 is obtained from I_o by bisecting I_o and choosing that half at the end points of which f(z) has different signs.

Other intervals of the sequence I_2, I_3, ... I_n are obtained in a similar manner. The procedure is illustrated in Figure 4.2. This procedure is repeated until the required accuracy is obtained.

To find the specific group delay, the discrete set of ordered pairs $\left(\frac{\omega h}{V_s} , \frac{V}{V_s} \right)$ obtained from the previous solution of the frequency equation is substituted into Equation 4.6. In determining the derivative $\frac{d \left(\frac{V}{V_s} \right)}{d \left(\frac{\omega h}{V_s} \right)}$ the Lagrangian differentiation formula was employed. The programming details are given in Appendix B1. The results of the calculation of the dependence of specific delay on the frequency-thickness product for the first longitudinal mode around its linear region, are plotted in Figures 4.3a and 4.3b. An aluminium strip was to be utilised in the implementation, so this curve was obtained with a Poisson's ratio, σ, of 0.350 and a bulk shear wave velocity, V_s, of 3.2 mm/μs. It can be seen that the delay characteristic undoubtedly exhibits a nearly linear variation of delay with frequency, and that it possesses an inflexion point (P_i). Since the magnitudes of deviations from linearity are approximately symmetrical about this inflextion point, this point (at $\frac{fh}{V_s} \doteq 0.69$ for $\sigma = 0.35$) would be chosen as the operating point. Further computations confirm that the maximum delay deviations from linearity are within 0.6% of mid-band delay for frequency ranges up to at least 10% of the mid-band frequency.

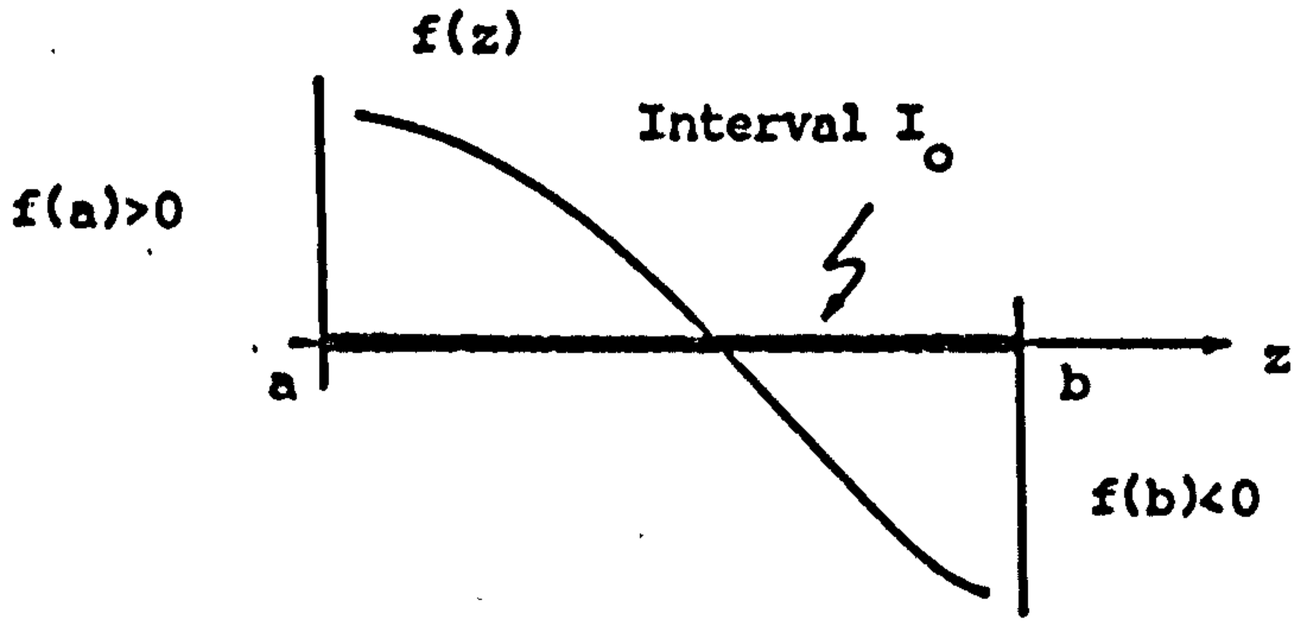

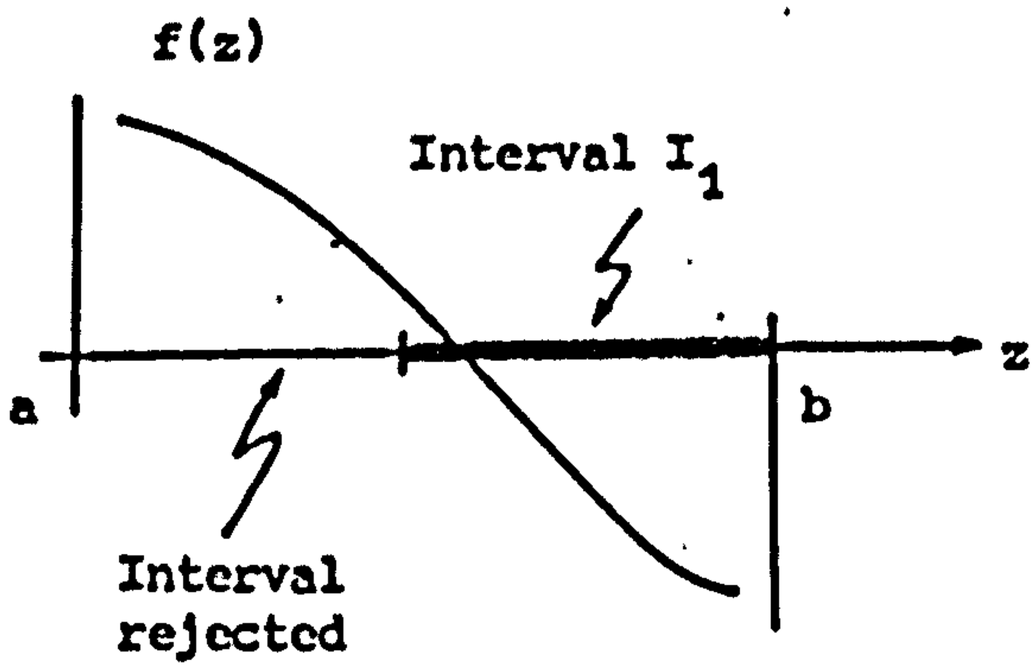

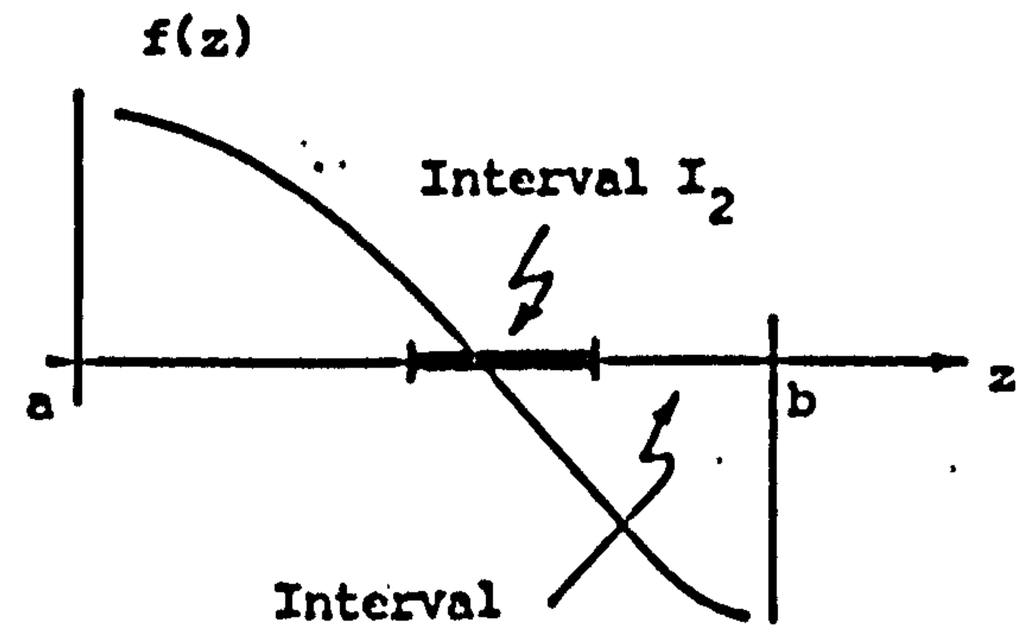

Figure 4.2 Successive steps of the Bisection Method in finding the root of f(z)

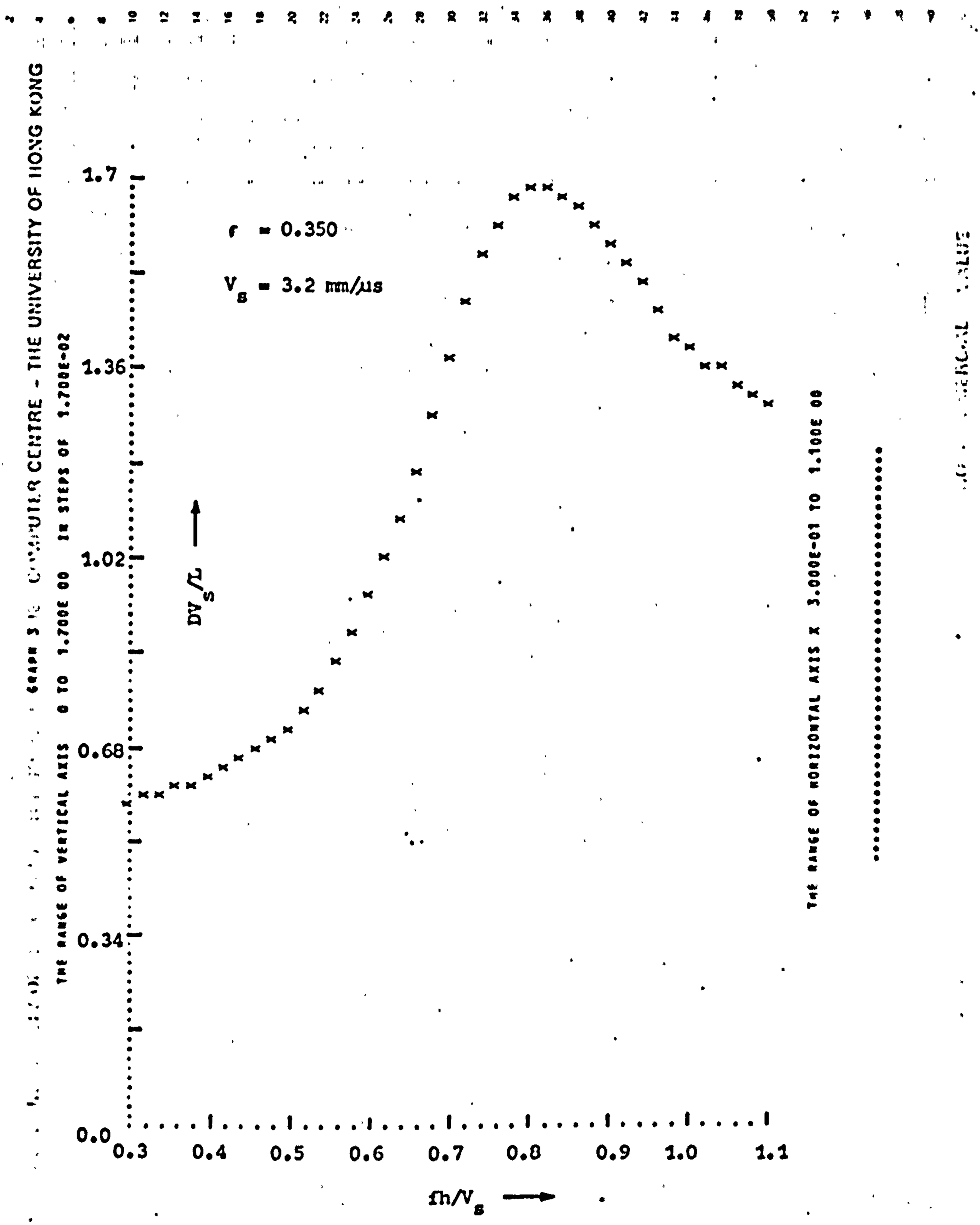

Figure 4.3a Theoretical group delays for the first longitudinal mode in a strip delay line

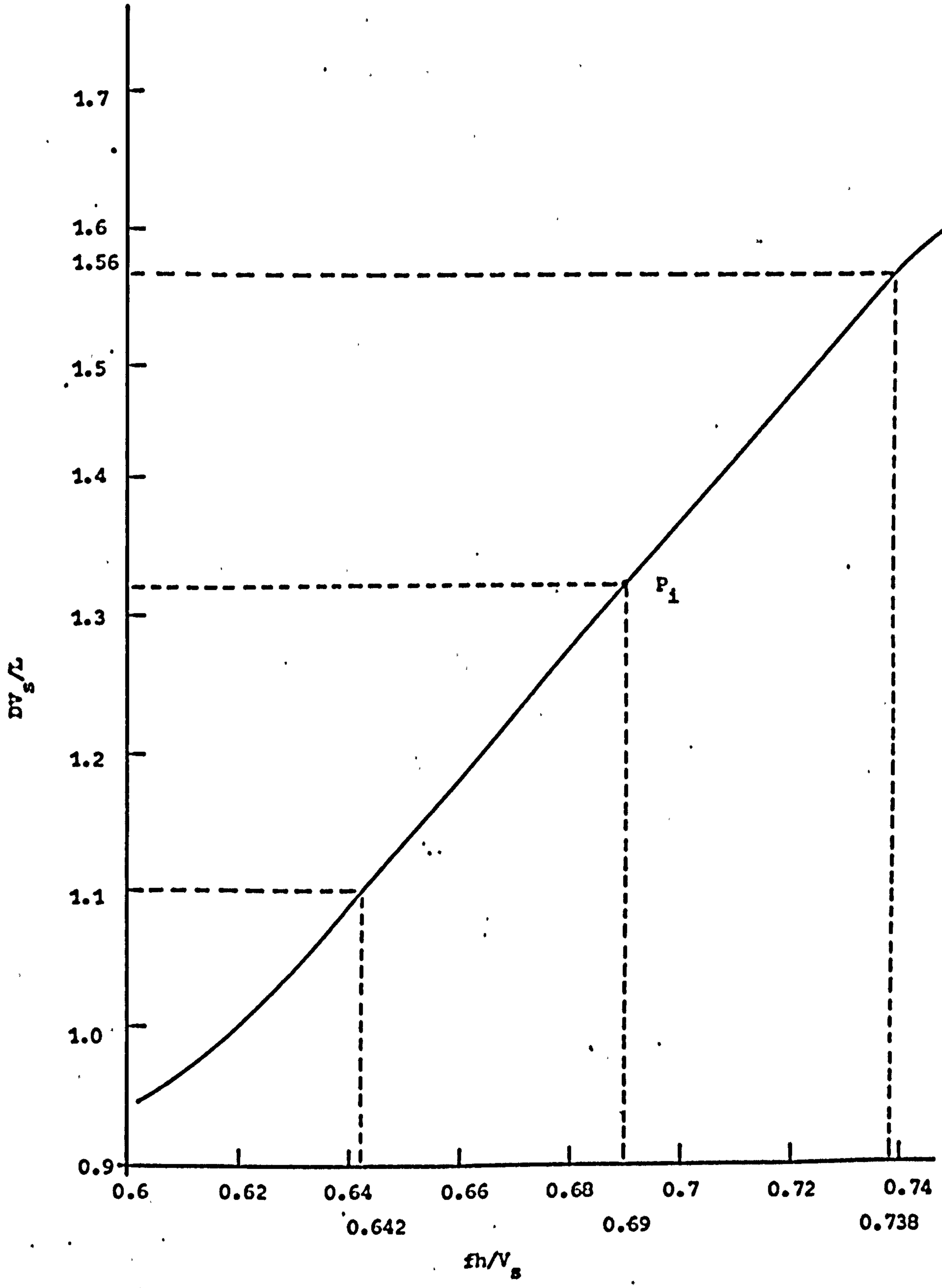

Figure 4.3b Expanded plot around the linear region

4.3 Implementation of the ultrasonic dispersive strip line

4.3.1 Choice of delay medium and dimensions for the line

Having established the feasibility of using a narrow strip as the dispersive delay element, it is then necessary to decide upon the type of delay medium for the line. Ideally, the delay medium should be of low attenuation characteristics, insensitive to temperature changes and capable of being coiled up into a compact shape. For the purpose of the project the polycrystalline aluminium alloy type AA (Aluminium Association) 5052-H32 with a reported loss as low as 0.00055 dB/cm/MHz in the lower megahertz region and a reasonably small temperature coefficient of delay (approximately 300 ppm per degree centigrade) is well suited.[60] The thickness and the length of the line required could be calculated from the curve in Figure 4.3b and also the tentatively specified requirements, namely:

1. Midband frequency = 2MHz
2. Frequency range = at least ± 100 kHz
3. Delay dispersion = 400 μs

Choosing the inflexion point as the operating point, where $\frac{fh}{V_s} = 0.69$, the value of the thickness h would be:

$$h = 0.69 \times \frac{V_s}{f} = 0.69 \times \frac{3.2 \text{ mm}/\mu s}{2 \times 10^6}$$

$$= 1.10 \text{ mm (or } 0.0434 \text{ in.)}$$

The linear operating region extends from $\frac{fh}{V_s} = 0.642$ to $\frac{fh}{V_s} = 0.738$, (representing a bandwidth of 13% around centre frequency); the

corresponding change in specific delay is (1.56-1.1) = 0.46.

Thus the length of line needed to give a dispersion delay of 400μs is given as:

$$\frac{\Delta DV_s}{L} = 0.46$$

$$\therefore \quad L = 2780 \text{ mm (or 109 in.)}$$

Provided that the width of the strip is above 10 wavelengths where the transducer length is adequate to produce a well-collimated beam, the choice of the width dimension is not critical.[64] A strip width of 50.8 mm (or 2 in.), (about 20 wavelengths wide), represents a suitable compromise between the terminating transducer directivity and compactness in the fabricated line.

Samples of M57 SH3 (Alcan's equivalence of AA 5052-H32) aluminium strips, having dimensions of 1.10 × 50.8 × 3048 mm, were requested from Alcan Co Ltd (UK). The length requested was increased to 3048 mm (10 ft.) in order to compensate for any inaccuracies in the computations. Two free samples were given; the strips measuring 1.19 × 50.8 × 3048 were cut from Alcan's standard gauge sheet. With a thickness of 1.19 mm, the operating midband frequency of the system will be at 1.8 MHz instead.

4.3.2 Bar transducers for the line

To excite dispersive longitudinal wave motions in the strip, the lowest thickness-longitudinal mode of vibration in ceramic rectangular bar transducers are employed. A careful design procedure for these transducers is of prime importance as they are one of the controlling factors on the discrimination of unwanted signals in the line. Two principal analytical techniques have been developed by Mason[65]

and Tiersten[66] respectively, to describe the properties of thickness mode piezoelectric transducers, but their results are applicable only to the large area piezoelectric plate, for which no physical quantities may depend on the lateral co-ordinates.[67] In the project, in order to favour the excitation of the first longitudinal mode near the inflexion point, transducers with widths less than the strip thickness are required, ($\frac{h}{\lambda} \doteq 0.50$ in the line). These transducers, having small width to thickness ratio, cannot be designed through these techniques. Theoretical studies of the modes of vibration in infinitely long elastic bars with rectangular cross-section have been made by Mindlin and Fox.[68] The solution involved coupled dilatational and equivoluminal waves, and was restricted to certain frequencies and allowable ratios of width to thickness of the cross-section. In view of these theoretical difficulties, an experimental approach was adopted.

The method employed here followed that of Fabian.[69] A frequency spectrum for the lowest thickness-longitudinal mode of the ceramic material to be used was first plotted in the form of resonant frequency-thickness product, $f_r t$, as a function of width-to-thickness ratio. For this purpose, slabs of PZT 5A of 20mm × 10mm, with standard thicknesses ranging from 0.94mm to 0.68mm (37 to 27 Mil) and poled in the thickness direction, were obtained from Vernitron Ltd (Brush Clevite), and bar transducers of 20mm in length but with varying widths, were sliced off them. After filing to flatness, their width as well as their thickness dimensions were determined with a micrometer. Measurements of electrical resonances of these bar transducers were then made with a Wayne Kerr r.f. admittance bridge. A light spring contact was utilised to facilitate handling and loading of these delicate transducers.

The frequencies at which the effective parallel bridge capacitance was zero, were identified as the resonant and anti-resonant frequencies, respectively. The resonant frequency-thickness products, $f_r t$, were formed and plotted against the width-to-thickness ratio in order to provide a frequency spectrum for PZT 5A (Figure 4.4). The circles in Figure 4.4 denote measured points and the size of circle denotes the relative magnitude of an electromechanical coupling k. The value of k was determined from the approximate expression.[70]

$$k^2 = A \left(\frac{f_a - f_r}{f_r} \right)$$

where A = a constant

f_a = frequency of anti-resonance

f_r = frequency of resonance

Figure 4.4 could be used as a guideline for designing the dimensions for the bar transducers. Since a larger coupling corresponds to a wider bandwidth, the range of the resonant frequency-thickness products, $f_r t$, to be employed, would be between 1.2 to 1.58 MHz-mm. With a centre frequency of 1.8 MHz, the range of thicknesses that could be selected would therefore lie between 0.67 to 0.88 mm. Any particular value of thickness within this range could be chosen; the width could be filed down to yield a width-to-thickness ratio that would give a centre frequency of 1.8 MHz.

Strictly speaking, this design is limited to freely vibrating transducers, but it was found that it could be used to good approximation for bonded transducer design. Typical admittance plots of a bar transducer before and after bonding to the aluminium strip, are as those shown in Figures 4.9a and 4.9b in Section 4.4. It can be seen that the observed

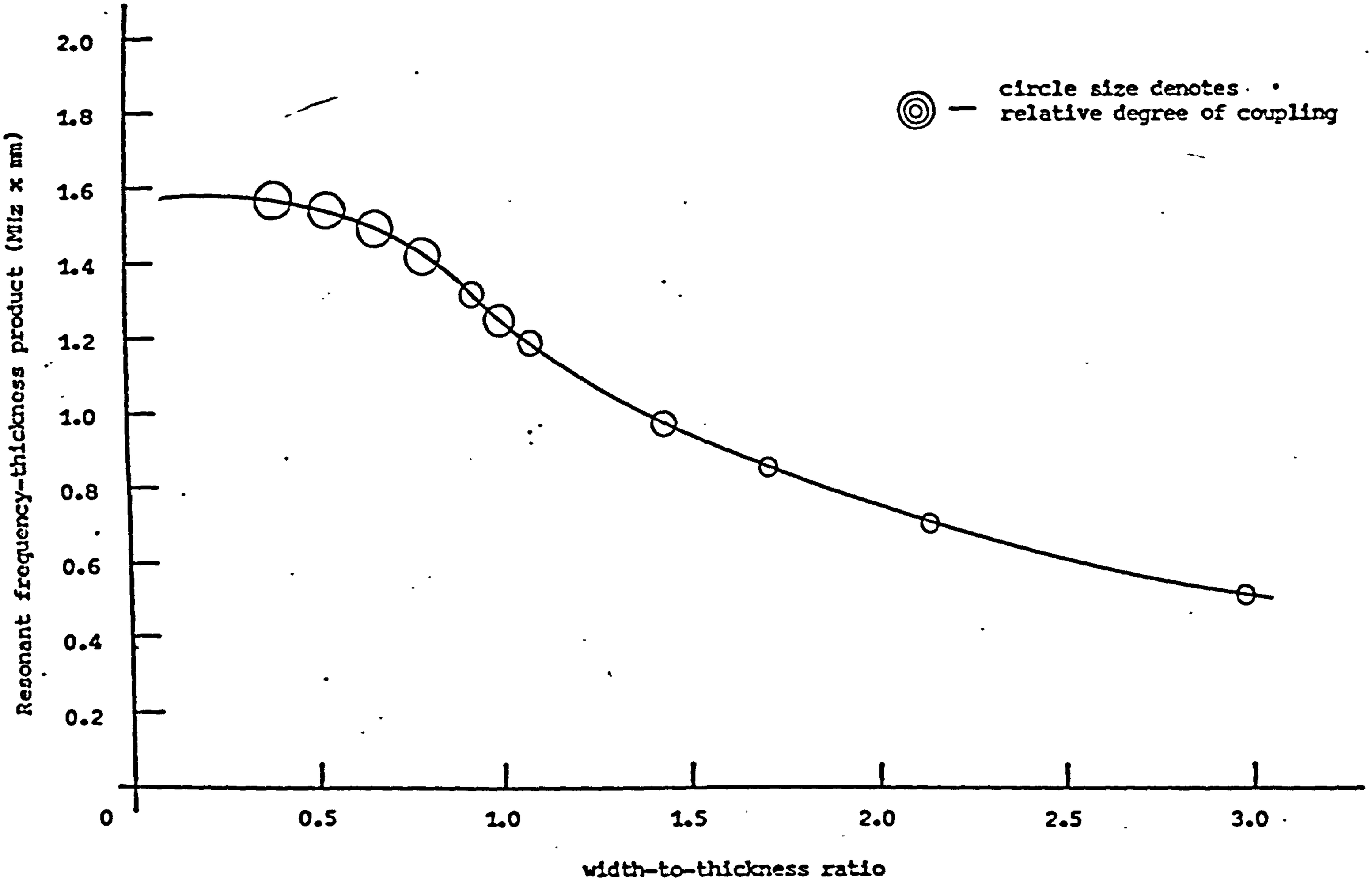

Figure 4.4 Observed frequency spectrum for the first thickness-longitudinal mode in PZT 5A

shift in the frequency of resonance was small.

Based on the above procedure, several pairs of PZT 5A bar transducers for use with the delay line were produced. The final pair used in the assembled delay line has the following dimensions:

Thickness	=	0.80 mm
Width	=	0.57 mm
Length	=	20 mm
Width-to-Thickness Ratio	=	0.71

Its measured resonant frequency was at 1.85 MHz.

4.3.3 Fabrication of the line

The line contains 2743 mm (108 in.) of the previously mentioned aluminium strip and is coiled on to a 285 mm square perspex plate, which is of 6 mm in thickness and has a helical groove 3160 mm long, 2.5 mm wide and 3 mm deep, machined into it. The strip is then inserted with one of its minor edges into the groove and held in position by its own springy force. To give a more secure structure, another 285 mm square perspex plate is placed on top of the other minor edge; and the strip is clamped between the two plates. This assembly is housed in an aluminium box of 440 mm × 350 mm × 80 mm. Apart from providing an effective screening against interferences, the box also contains the necessary terminal posts for mounting of the matching networks, and the input and output BNC connectors. The whole arrangement is shown in Figure 4.5.

Figure 4.6 illustrates the transducer arrangement on the line. The bar transducers were bonded on to the line with the poling direction

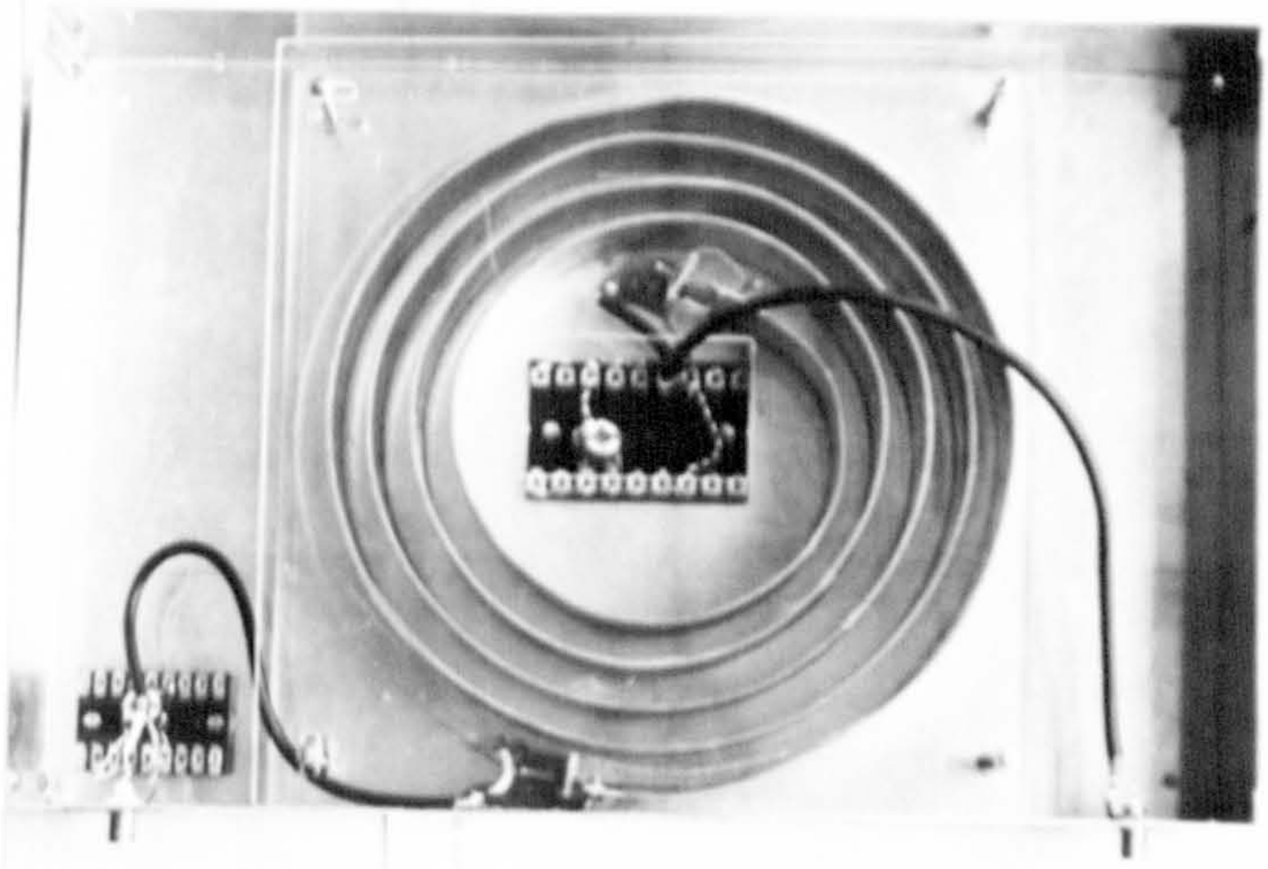

Figure 4.5 The delay line

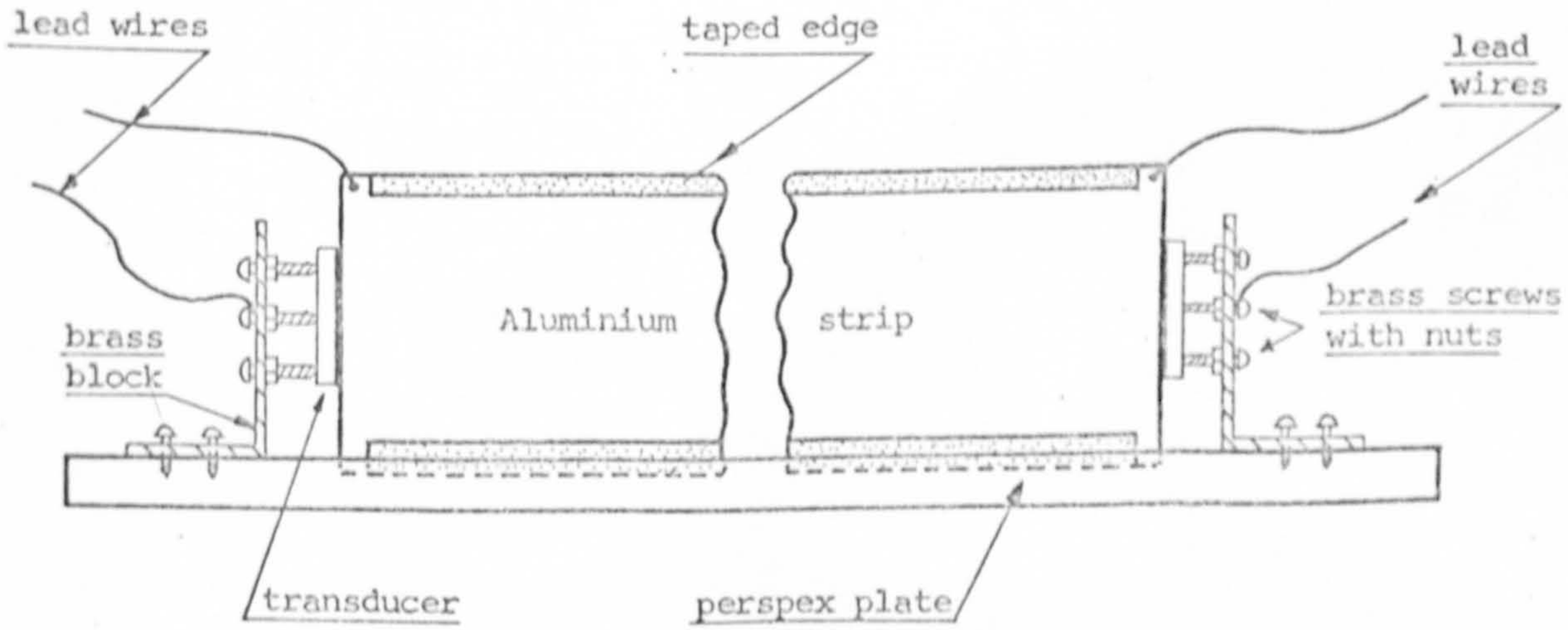

Figure 4.6 Transducer arrangement on the line

parallel to the length of the strip. Conductive resin loaded with silver particles (DAG 915) was used as the bonding medium, and hence the strip could be taken as the earth terminal. Electrical contact on the other electrode of the transducer was made by means of brass screws, which also served to hold the transducer firmly against the end of the strip. After the preliminary adjustments and measurements, which confirmed the satisfactory performance of the line, were completed, a thin aradite (CIBA AY 103 mixed with hardener AY 951 in a ratio of 10:1 by weight) was allowed to run between the transducer and the strip. The transducer was thus permanently set in position.

4.3.4 Notes on the fabrication of the line

Some general remarks on the precautions taken and difficulties encountered in fabricating the line will be given.

(a) It must be emphasised that the design procedure for the bar transducers outlined in Section 4.3.2 is only an approximate approach. The final design relies heavily upon experimental measurements. Ideally, the transducers should be sliced and lapped to the specified dimensions, before plating and polarisation are applied.[71] In the present case, the bars were cut from selected commercial, standard thickness plates with a small pen-knife. They were then filed to the correct width by sandwiching them between feeler gauges. To avoid de-poling of the material as a result of heating and mechanical agitation as well as chipping and cracking of the brittle transducer material during the slicing and filing stages, the processes

must be carefully carried out. This crude method, although tedious, achieved an accuracy in flatness to within 0.01 mm.

(b) From the theoretical studies in Section 4.2.1, it is evident that many other modes exist in the plate. In fact, by solving the frequency equation for flexural modes in Equation 4.4, it will be seen that within the operating frequency band the first two flexural modes could also be excited. Figure 4.7 plots the theoretical group delay curves for the first two longitudinal modes and the first two flexural modes. As good suppression of unwanted modes is desired, the geometry of the strip and the transducers must be such that no energy should be coupled into the flexural modes. From the discussion in Section 4.2.1 it is obvious that anything that destroys the symmetry of the arrangement with respect to the median plane of the strip, would favour flexural modes. Asymmetric transducer arrangements, non-uniform bonding layers, tilted end faces or even non-uniform poling of transducers, could then be causes of unwanted mode generation.[72] Figure 4.8 demonstrates the possible excitation of the first flexural mode in the strip. The photographs were taken during the initial fabrication stage of the line, and the mode was identified through the non-dispersive nature of its time delay.

In the project, conductive resin loaded with silver particles was employed as the bonding medium. This facilitated experimentation as the transducers could then be released easily and re-positioned until a satisfactory line response was obtained. A thin bonding layer was aimed at in order to minimise complications in response because of it.[73] The whole process of bonding the transducers to the line was necessarily a time-consuming one.

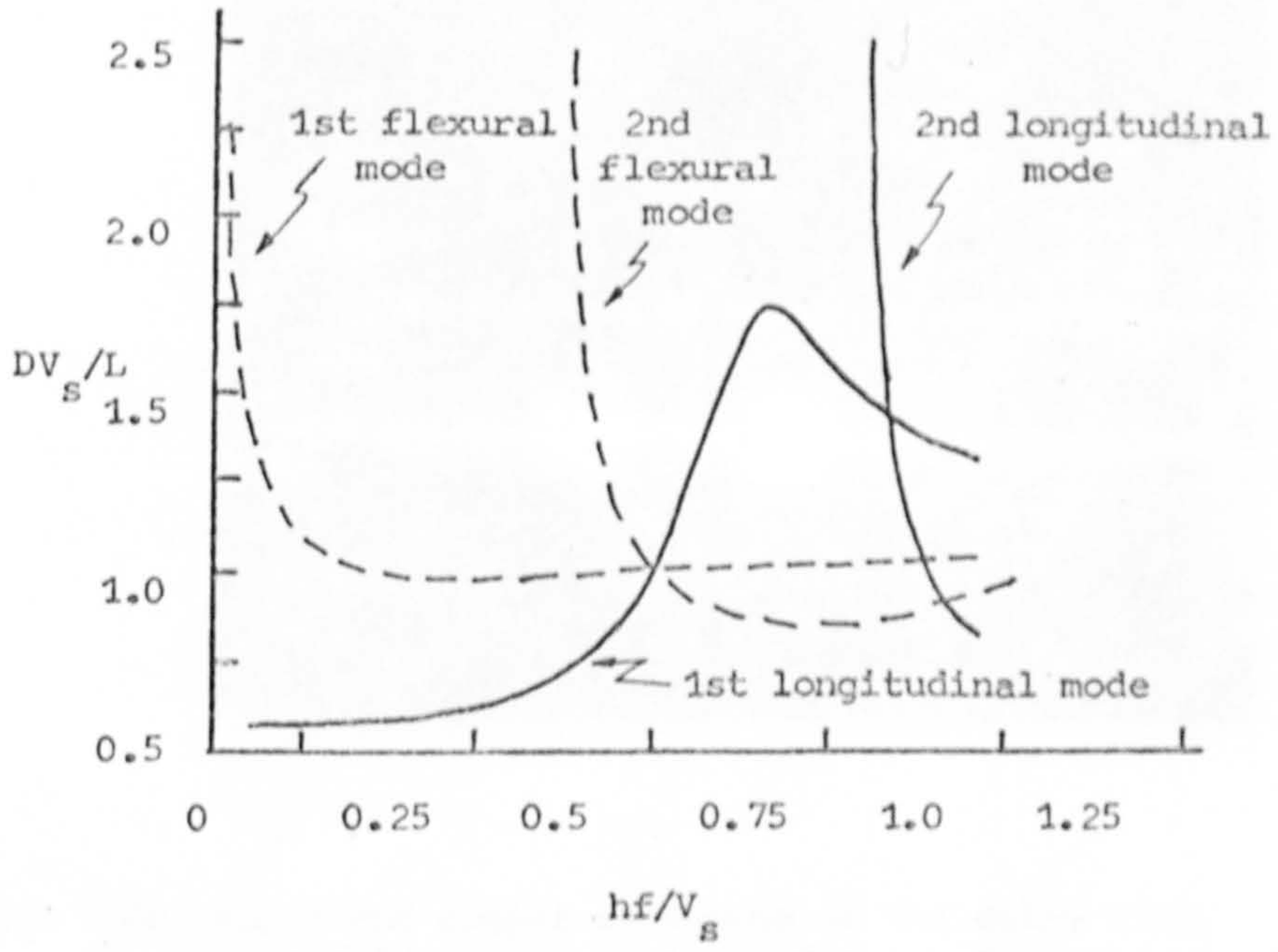

Figure 4.7 Theoretical group delays of elastic modes in a strip delay line (after Meeker)

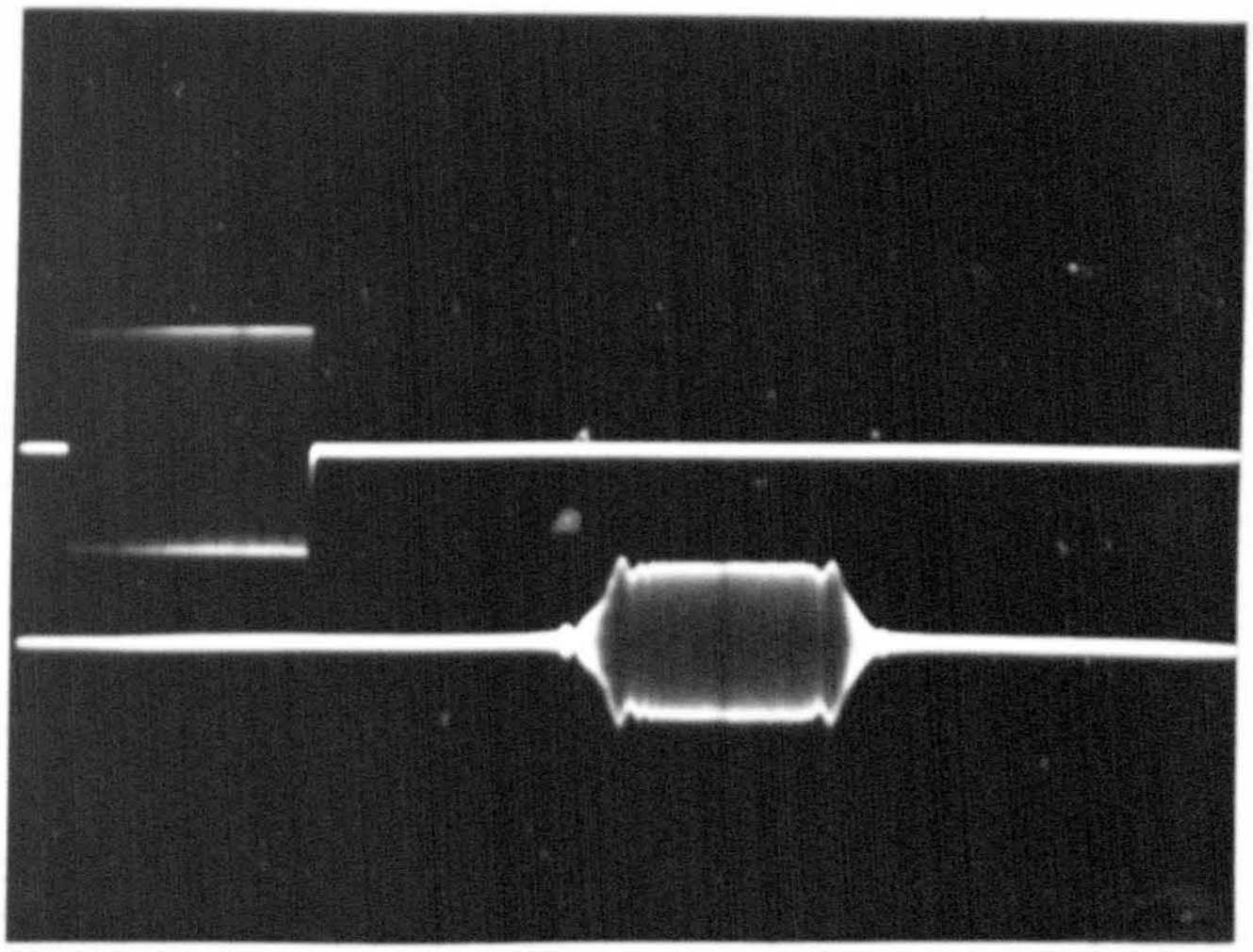

Figure 4.8a Input and output waveforms of the delay line. No flexural mode is excited. Carrier frequency=1.7 MHz. Time scale=0.1 ms/cm.

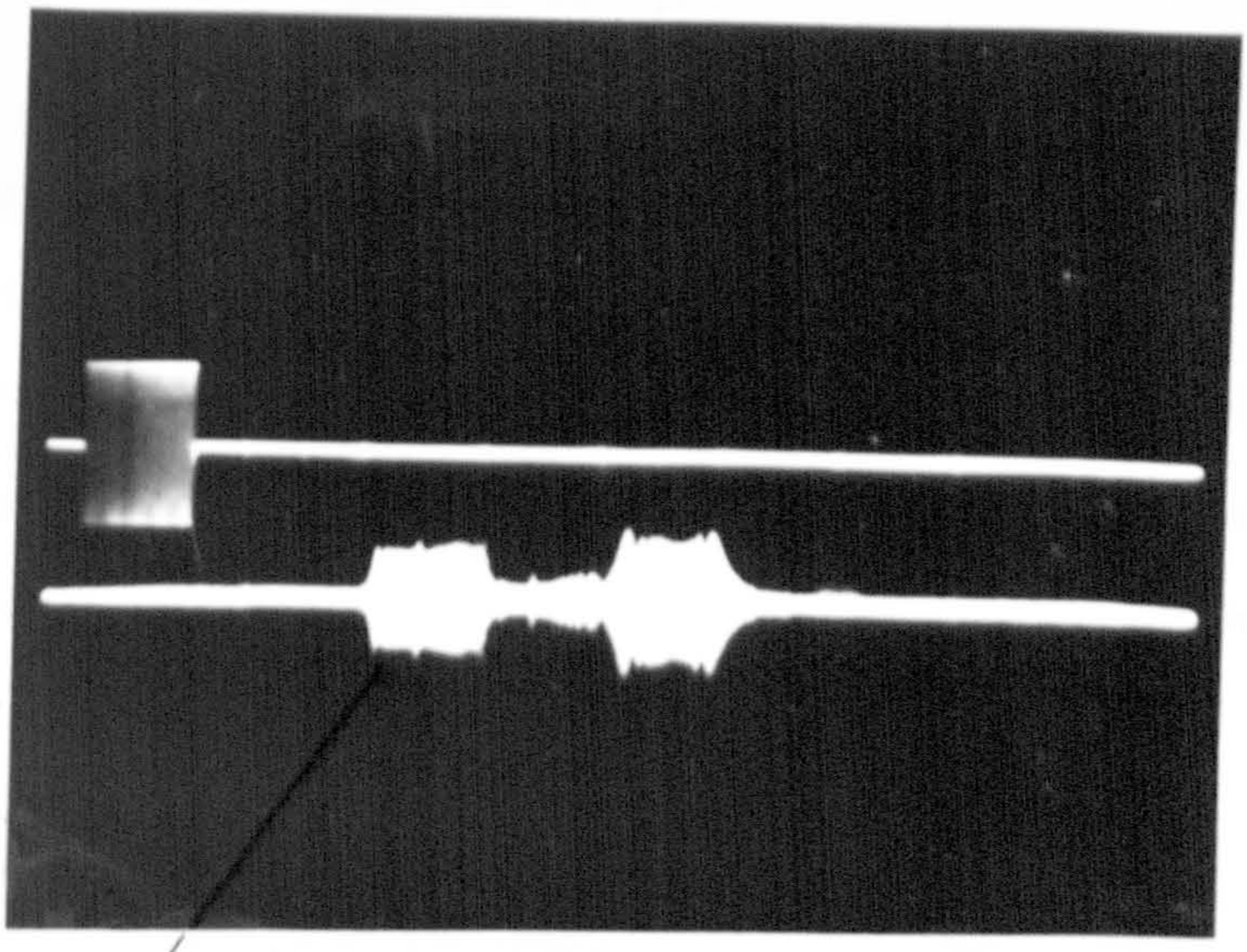

Figure 4.8b Input and output waveforms of the delay line.
/Flexural mode is excited. Carrier frequency=1.9MHz.
Time scale=0.2 ms/cm.

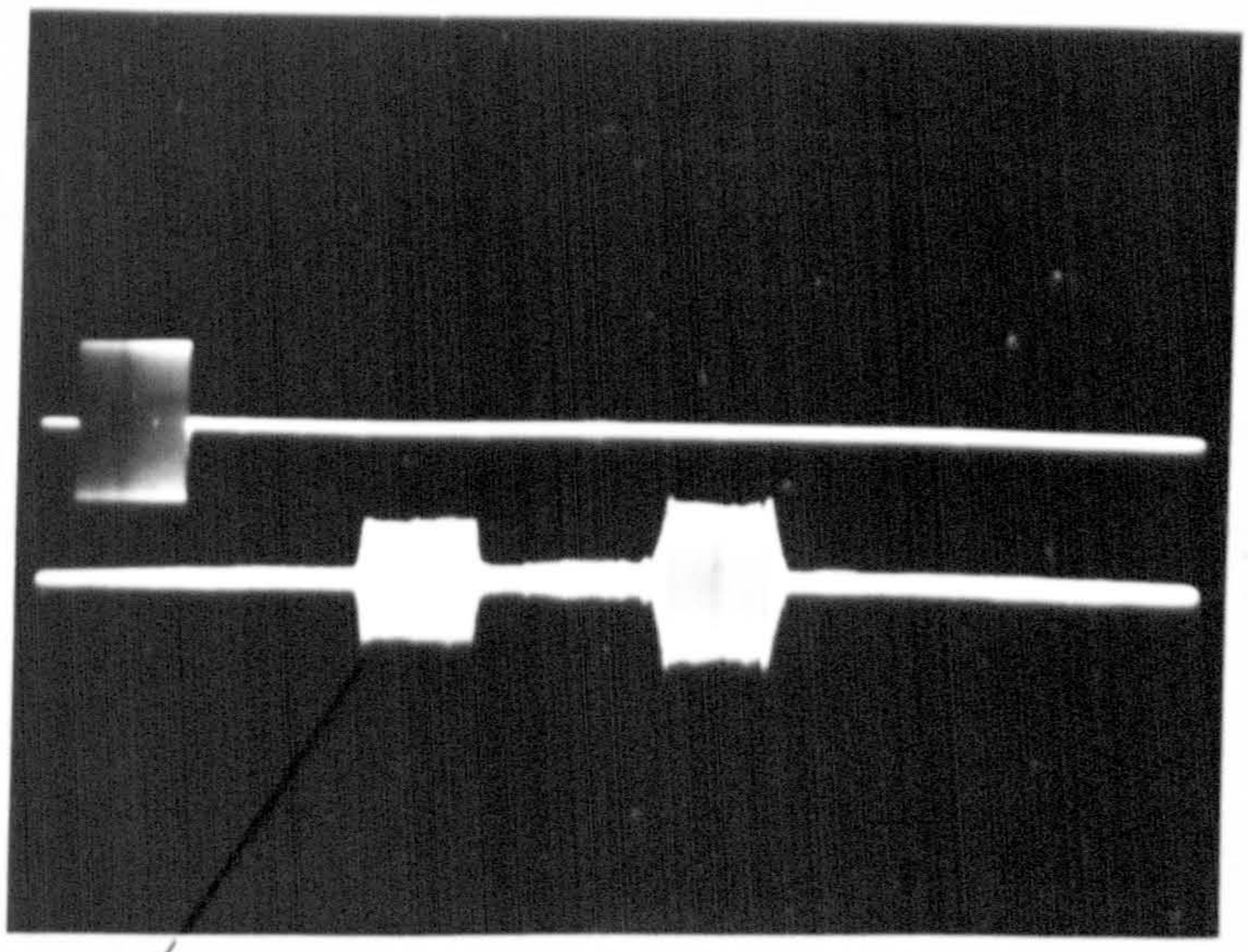

Figure 4.8c Input and output waveforms of the delay line.
/Flexural mode is excited. Carrier frequency=2.0MHz.
Time scale=0.2 ms/cm.

Figure 4.8 Excitation of the first flexural mode in the strip line

(c) It was found that improved discrimination to unwanted responses and a smooth band-pass characteristic were obtained by applying an absorber in the form of an adhesive tape to both minor surfaces of the strip. The tape overlapped a small portion (5 mm) of both major surfaces (Figure 4.6). This arrangement suppressed the interference signals due to multiple reflections from the minor surfaces.

4.4 Measurements on the line and its specifications

The following measurements were made on the assembled line to characterise its performance. The line has a symmetrical transducer arrangement.

(i) Input and output impedances: The transducer is represented in terms of a parallel combination of resistive function $R_E(f)$ and capacitive function $C_E(f)$. These admittance functions, before and after bonding, were determined with a Wayne Kerr r.f. admittance bridge and plotted in Figures 4.9a and 4.9b. The minimum of the resistance curve in Figure 4.9b is of 105 Ω. This point gives the mechanical, or series,resonant frequency of the bonded transducer, which is at 1.85 MHz. The shunt capacitance of the transducer at this series resonant frequency was measured to be 304 pF. For matching purposes, a parallel combination of a 500 Ω variable resistor and an adjustable inductor of approximately 30 μH was connected across both the input and output transducers. The inductor tunes out the static shunt capacitance and shapes the response; while the resistor provides a maximum power transfer and suppresses the 'triple travel' (third-time through signals).

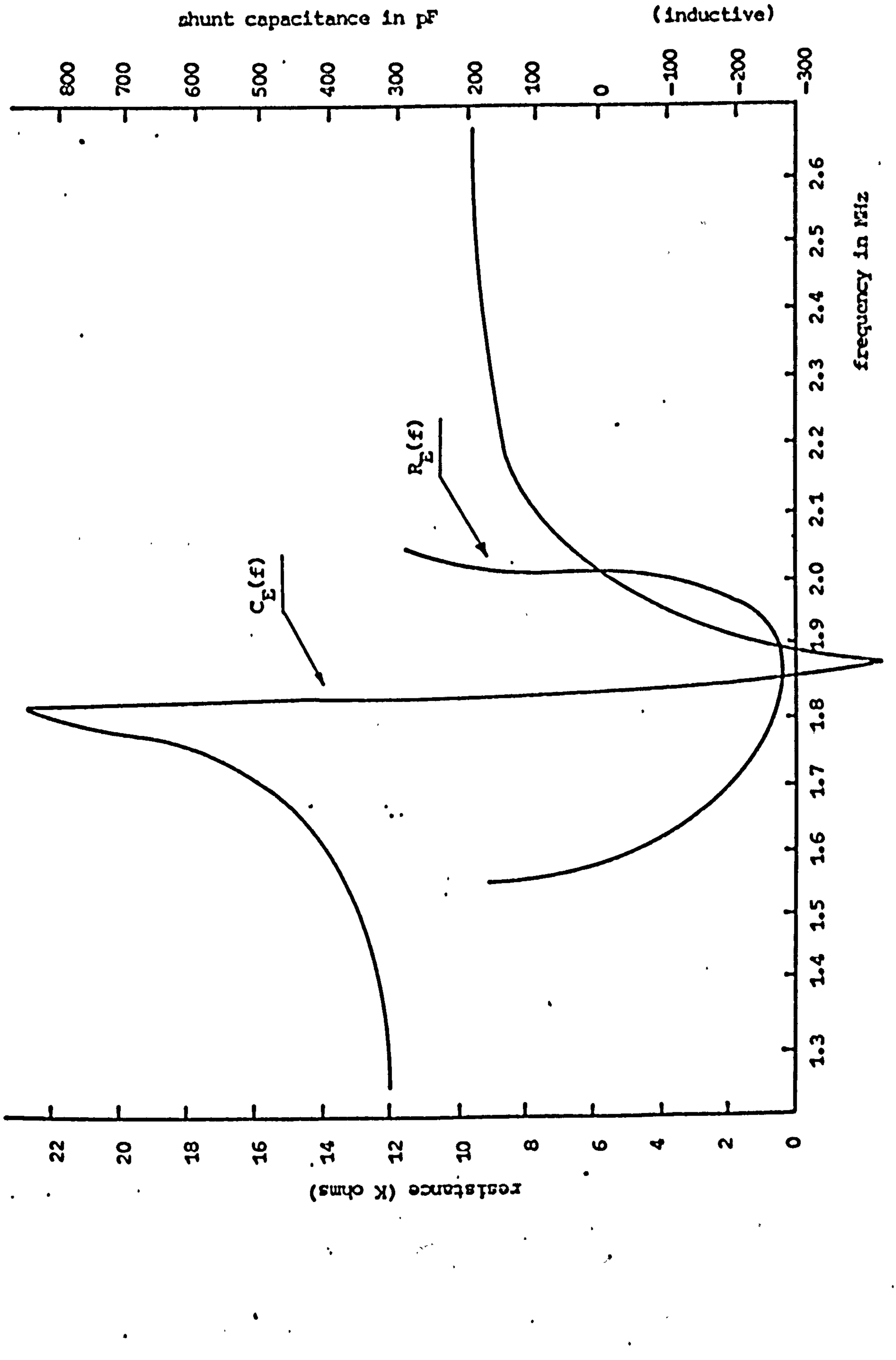

Figure 4.9a Bar transducer admittance plot before loading to the line

Figure 4.9b Bar transducer admittance plot after bonding to the line

(ii) Time delay measurements: Preliminary time delay measurements were made using the set-up as shown in Figure 4.10. A 200 μs rectangular r.f. pulse was impressed upon the properly terminated line. The delay time of the pulse on passing through the line was measured with a dual trace Tektronix type 545A oscilloscope using its calibrated delay time multiplier. The resultant experimental delay versus frequency curve (Figure 4.11) showed close agreement with theoretical predictions based upon the properties of the first longitudinal mode of an infinitely wide strip, and the delay non-linearities were found to be within ± 0.7% across the frequency band of 1.7-1.9 MHz, which was then chosen as the operating bandwidth. It must, however, be pointed out that this simple method is limited in accuracy. This is mainly because the input r.f. pulse being rectangular in its envelope, possesses an infinite bandwidth (of (sin x)/x form), and its passage through the bandlimited line will always produce a distorted output waveform, having variable rise-times at different carrier frequencies. The difficulty of defining the precise arrival times of the output pulse restricted the accuracy of the method to ± 1 μs and a more sophisticated set-up had to be employed in obtaining the delay error curve (See Section 7.1).

(iii) Level of spurious signals: Unwanted signals from the delay line fall into three broad categories: (a) non-dispersive spurious, (b) dispersive spurious and (c) feedthrough signals.

The non-dispersive spurious signals consist of unwanted signals whose delay is relatively constant and which have their origins in the excitation of flexural modes, while the major dispersive spurious signal is the triple travel. Feedthrough occurs when a

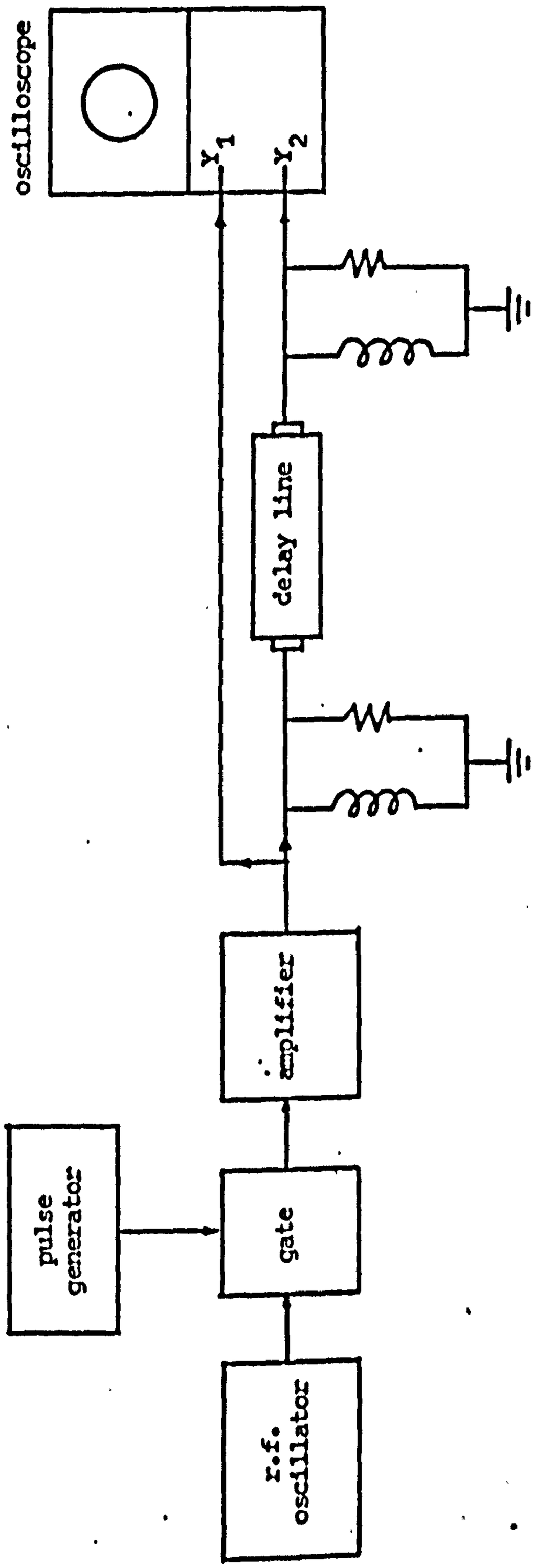

Figure 4.10 Time-delay and insertion loss measurement set-up

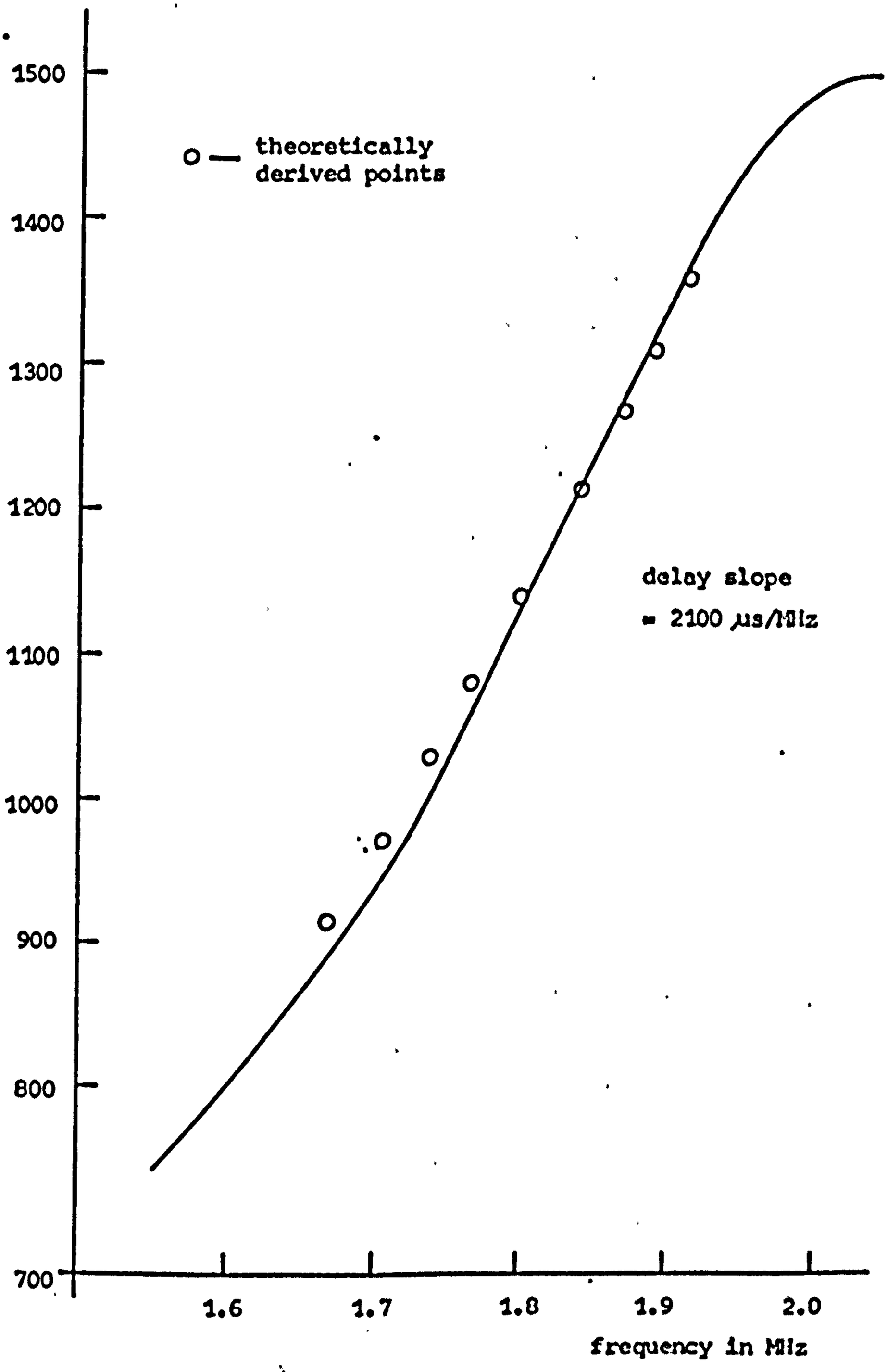

Figure 4.11 Experimental delay curve for the delay line

portion of the input signal appears undelayed at the output of the delay line. Observations on these unwanted signals were made using the experimental set-up as in the previous time delay measurements. The strongest unwanted signal was found to be the triple travel. However, by choosing the correct terminating resistances for the line, this signal could be reduced to 25 dB or more below the main signal over the operating band. The other unwanted signals were of the order of -30 dB. Since when the delay line is used as a compressor all spurious signals will not generally be compressed as in the case of the main signal, there is an additional improvement of spurious signal suppression equal to 10 log. C.R. (approximately 19 dB in the present case), where C.R. represents the compression ratio. The above levels of spurious signals were thus regarded as acceptable.

(iv) Insertion loss: The insertion loss of the delay line was taken with the same circuit arrangement as was used for time delay measurements. The insertion loss curve in Figure 4.12 was obtained by tuning the terminating inductors to the best flat response with the variable resistors set at values which would give minimum triple travel signals.

The characteristics of the line were best summarised through the following specifications:

Centre frequency (f_o)	1.8 MHz
Dispersive bandwidth (Δf)	200 kHz
Delay dispersion	420 μs

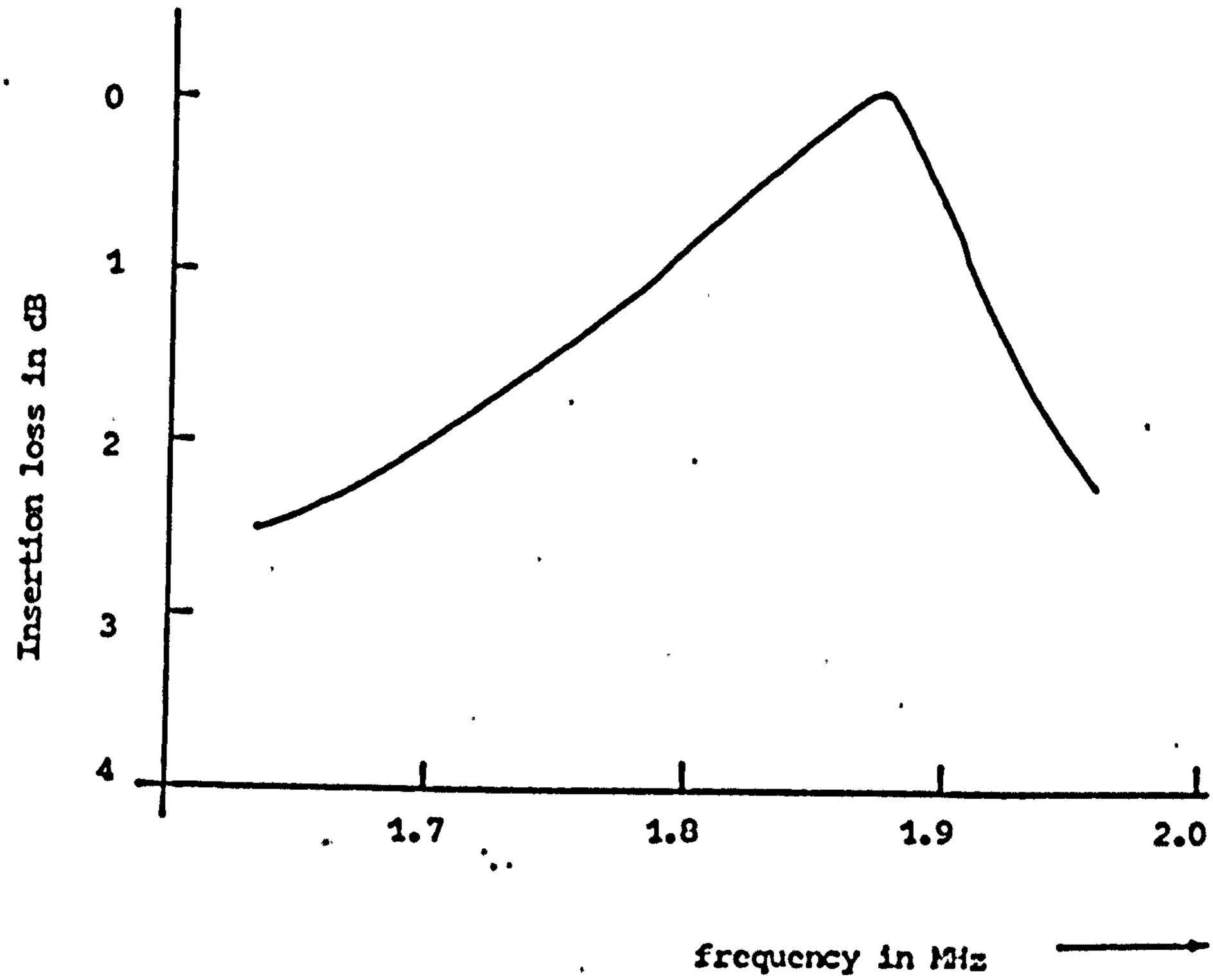

Figure 4.12 Insertion loss curve for the delay line

Centre frequency delay	1133 μs
Delay slopes	2100 μs/MHz
Delay non-linearity	± 7 μs
Compression ratio (C.R.)	84
Insertion loss (worst point)	20 dB
Insertion loss change (across Δf)	2 dB
Spurious signals across Δf - pulse test method	
Non-dispersive spurious	- 30 dB
Dispersive spurious	- 30 dB
Triple Travel	- 25 dB
Feedthrough	- 30 dB
Input and output resistance	105 Ω
Input and output capacitance	304 pF
Length × width × thickness	2743 mm × 50.8 mm × 1.19 mm

4.5 General Comments

1. From the theoretical studies in Section 4.2, it is obvious that by selecting delay media having different values of Poisson's ratio, σ, a possible range of slopes and various curvatures in the delay characteristics can be obtained. Over the range of σ = 0.20 to σ = 0.40, the maximum slope at the inflexion point decreases by a factor of 3; but for a given bandwidth, larger values of σ will give smaller deviations from linearity.[64] In general, the choice of the delay medium is governed by fabrication and attenuation considerations.

2. The particular method of coiling and holding the aluminium strip produced no appreciable change in its characteristics and showed the relatively inactive conditions of the minor surface of the strip.

3. The present line has a delay non-linearity of approximately ± 0.7% over the total linear delay range. This is apparently a rather small error. However, as was shown in Section 3.5.2, the tolerable delay error is based on an absolute deviation from the linear delay and not on a percentage deviation. It can be seen that this delay error sets a limit on the length as well as on the percentage bandwidth of the line.

4. The economic aspect of this implementation is worth noting. In the initial stage of the project (1970), a quotation was requested from Anderson Laboratories, U.S.A., on one of its unweighted strip dispersive delay lines (Type 4201-D), which is centred at 5 MHz, having a dispersive bandwidth of 210 kHz and a delay dispersion of 354 μs per pair with with an insertion loss of about 40 dB. (Appendix C). The quotation price was as high as U.S.$ 5,000.

CHAPTER 5

TRANSMITTING AND RECEIVING TRANSDUCERS

System specifications dictate that these transducers should be capable of operating over a reasonably wide band (say, a 3 dB bandwidth at ± 10% of centre frequency). Consequently, lead backing was employed to increase their bandwidth.

5.1 Effects of backing on the performance of piezoelectric ceramic transducers.[74]

The feasibility of employing backing techniques to produce the required bandwidth in the thickness mode piezoelectric transducer was first studied. Mason's equivalent circuit (Figure 5.1), which describes the thickness mode transducer in terms of its impedance and transfer properties, is well suited for the purpose.[65]
In the equivalent circuit the transducer is considered as a six-terminal device, one pair representing the electrical terminals, the other two pairs the mechanical loading on the flat faces of the transducer. The symbols in Figure 5.1 have the following meanings:-

Z_x	=	$A\rho v_t^D$	characteristic acoustic impedance of the transducer
C_o	=	Ae_{33}^S/t	clamped capacitance
ϕ	=	Ae_{33}/t	ideal transformer ratio
$\frac{\alpha}{\pi}$	=	f/f_o	fractional frequency deviation
f_o	=	$v_t^D/2t$	open-circuit resonant frequency
A	=		area of transducer
ρ	=		density of transducer material

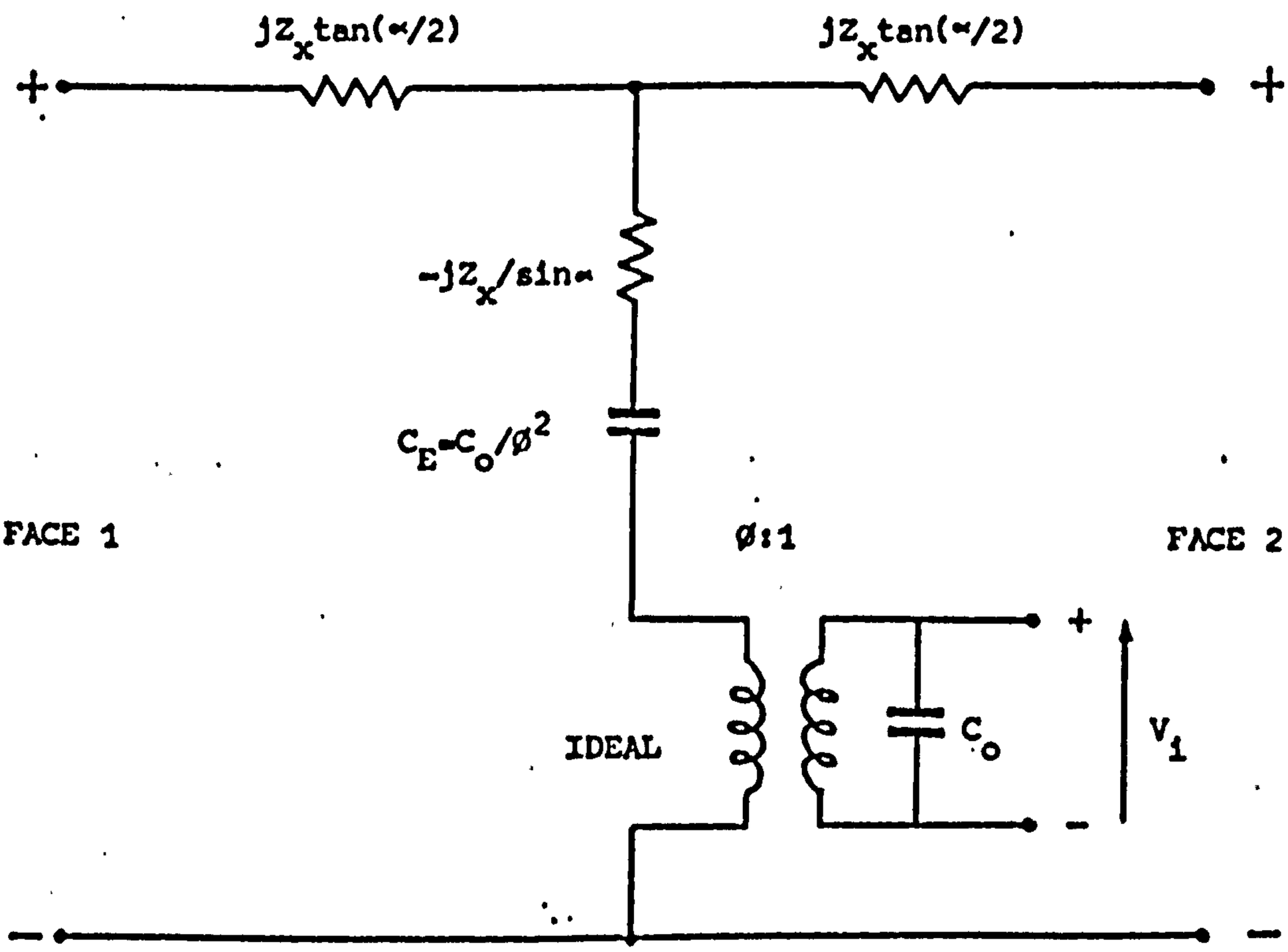

Figure 5.1 Mason's equivalent circuit representation of a thickness mode piezoelectric transducer

v_t^D = velocity of compressional wave along the thickness axis

ε_{33}^s = clamped dielectric constant

t = thickness of transducer

e_{33} = a piezoelectric constant (stress/electric field at constant strain)

When the transducer is loaded on both sides by impedances Z_q and Z_b, the load and backing impedances respectively, the equivalent circuit may be re-drawn as shown in Figure 5.2a. This circuit has a series element (the term $jZ_x \tan(\alpha/2)$) with infinite value at the half-wave resonant frequency. Following Mason, the circuit may be transformed into the equivalent form shown in Figure 5.2c through the use of a network identity due originally to Norton.(75) (Figure 5.2b). The circuit can now be analysed.

The transducer, when working as a transmitter, is generally driven by a low impedance source. In this case the input clamped capacitance, C_o, may be neglected, and the equivalent circuit reduces to the form of Figure 5.3. If the transducer is used as a receiver, the corresponding equivalent circuit is as shown in Figure 5.4. Thus, the voltage transfer functions, F_1/V_i and V_o/F_2, of the transmitting and receiving transducers with various backing and loading materials, can be obtained using standard circuit techniques and their frequency responses plotted. Figures 5.5 and 5.6 show such response plots, in decibels, for the cases of air, lead and brass backings, respectively. In these results, the transducer is assumed to radiate into a water load and the bonding thickness has been neglected. The calculations were performed for a 12 mm diameter PZT 5A transducer with a resonant thickness frequency of

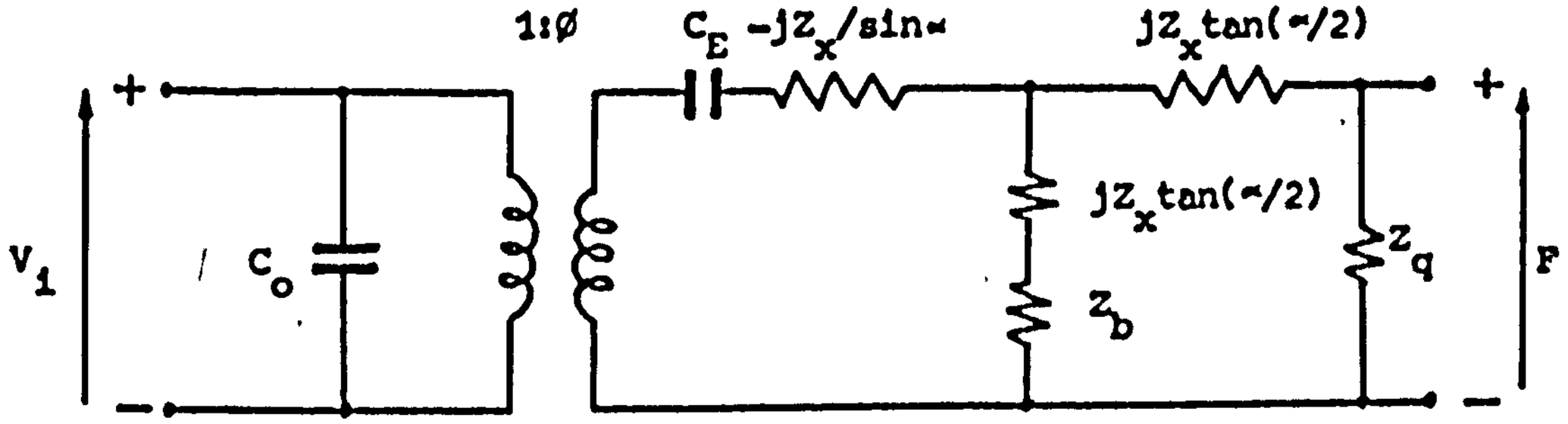

Figure 5.2a Equivalent circuit for transducer loaded on both faces

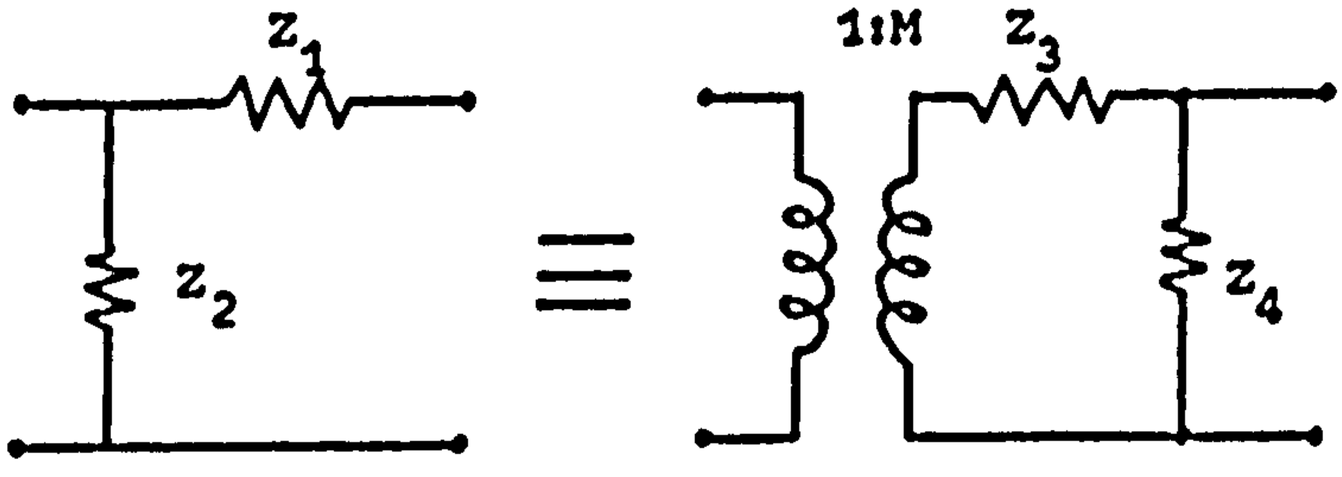

Norton's Network Identity

$M=(Z_1+Z_2)/Z_2$; $Z_3=Z_1(Z_1+Z_2)/Z_2$; $Z_4=Z_1+Z_2$

Figure 5.2b The transformed circuit in figure 5.2c is obtained by equating $Z_3=(1/j\omega C_E - jZ_x/\sin\alpha)$ and $Z_4=jZ_x\tan(\alpha/2) + Z_b$ in the above network identity.

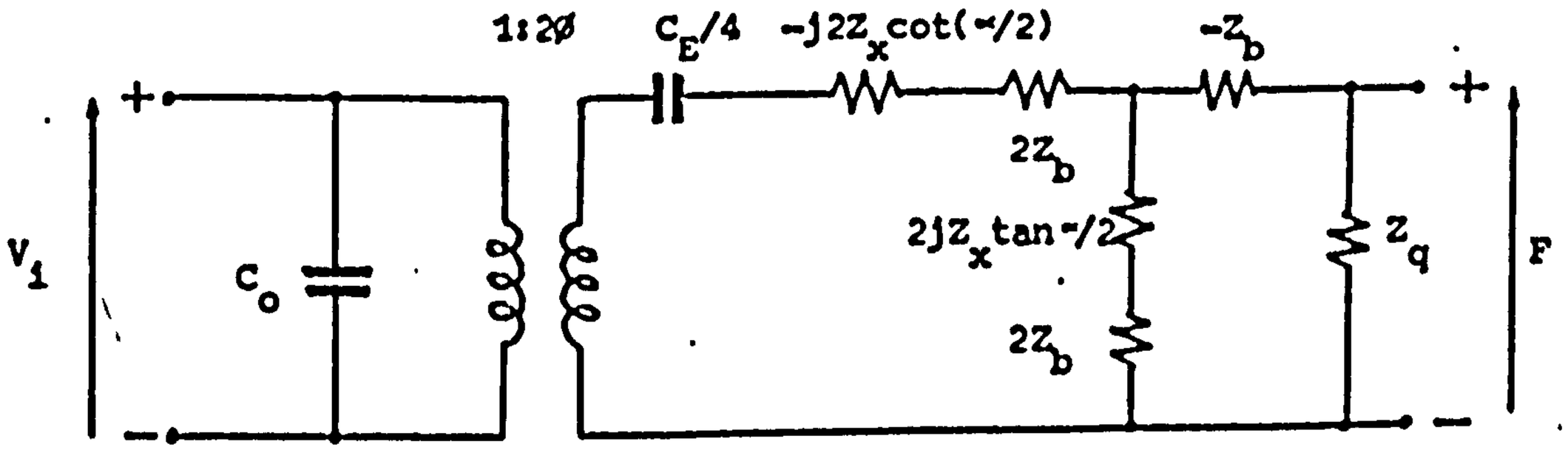

Figure 5.2c The final equivalent circuit

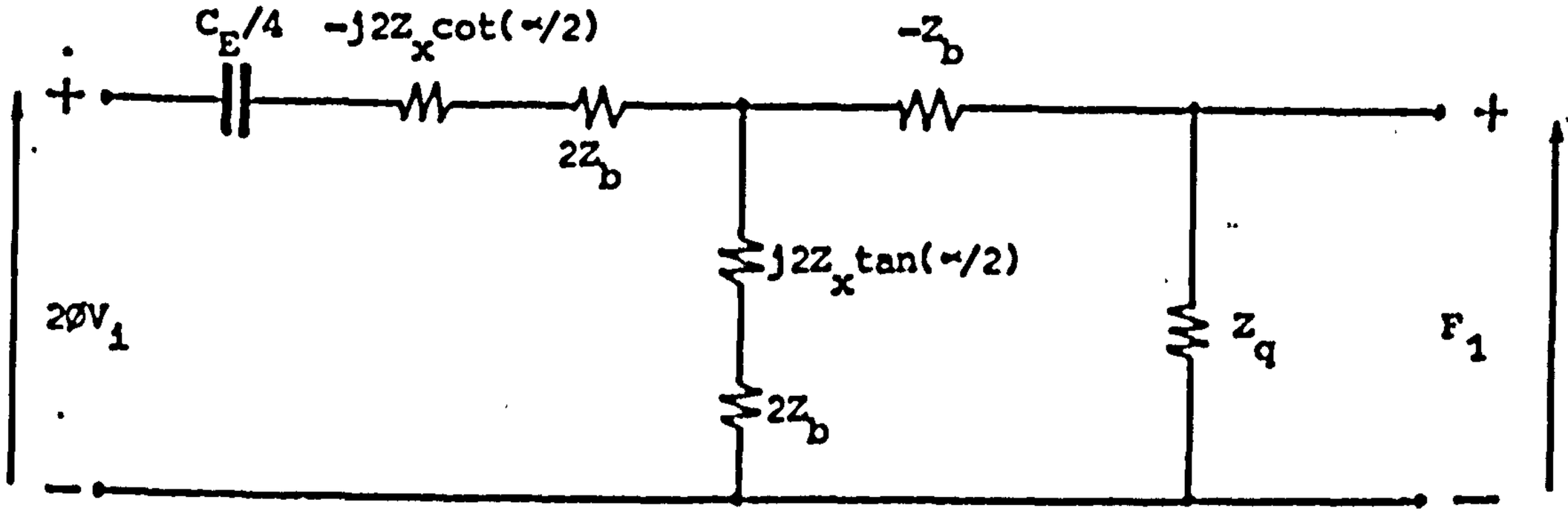

Figure 5.3 Equivalent transmitting transducer circuit

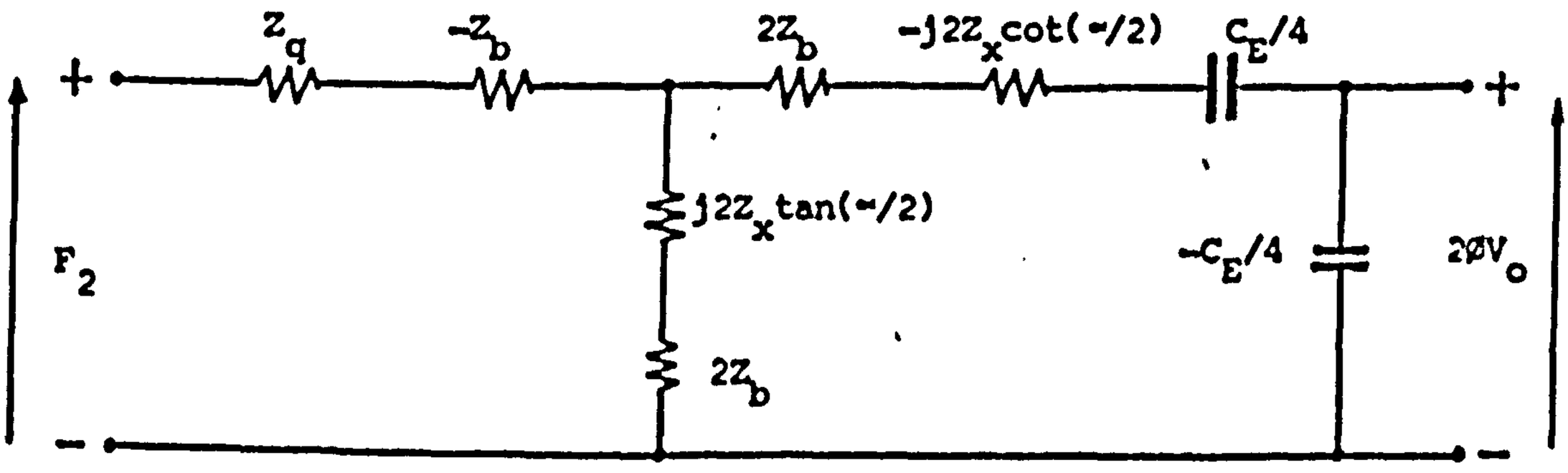

Figure 5.4 Equivalent receiving transducer circuit

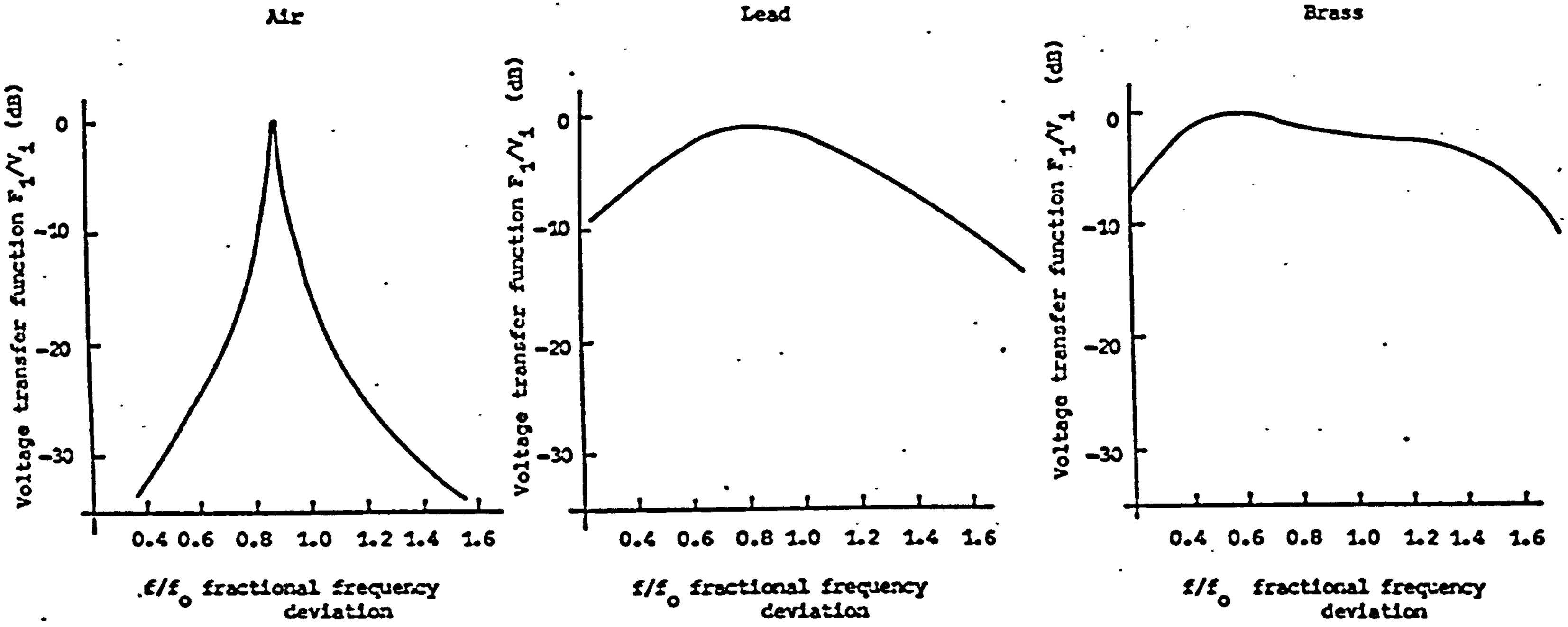

Figure 5.5 Voltage transfer function of transmitting transducer for various backing media

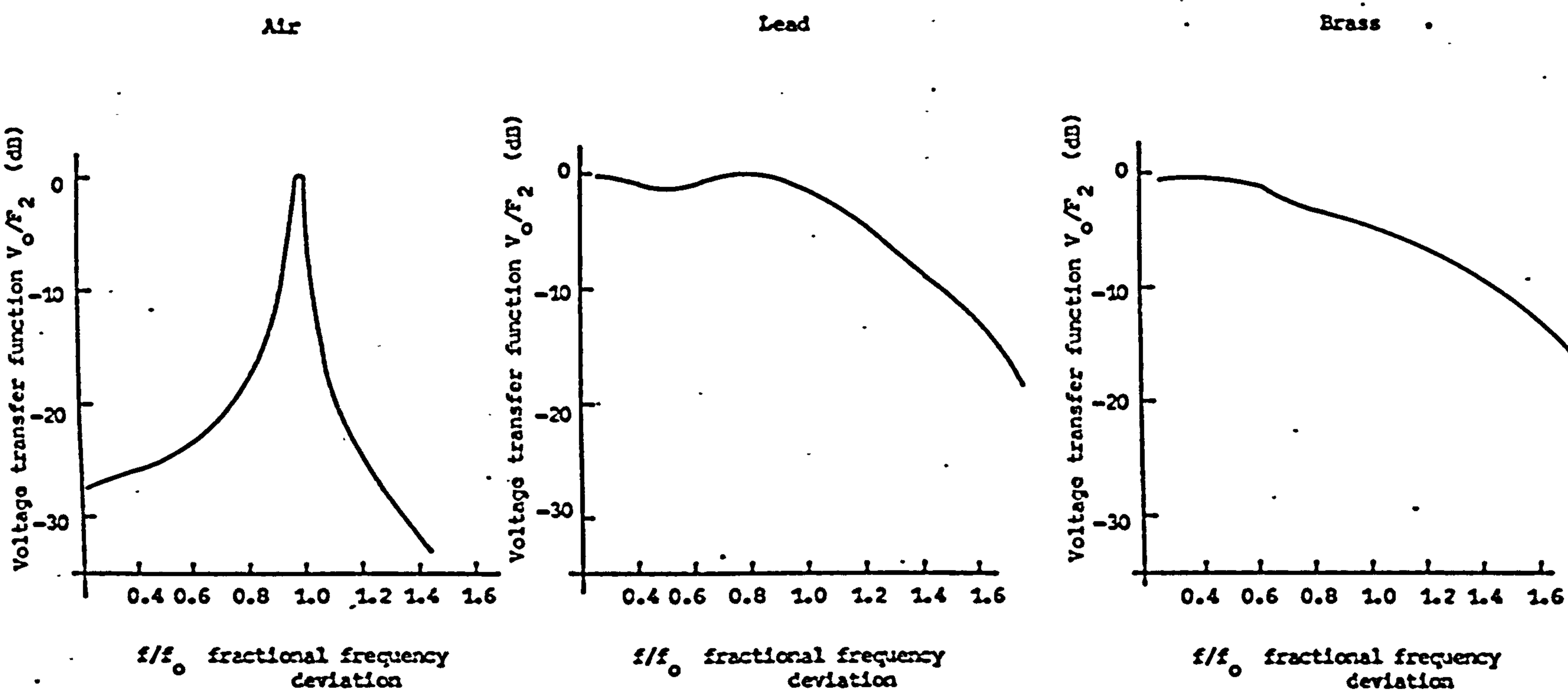

Figure 5.6 Voltage transfer function of receiving transducer for various backing media

2 MHz, as this is the nearest available standard frequency to the centre frequency of the dispersive delay line, which is at 1.8 MHz. The constants used in the computations are listed in Table 5.1 and manufacturers' data has been used in deriving the circuit values.(76) The computer program written for these calculations is given in Appendix B.2. If identical transmitting and receiving transducers are employed, the overall frequency response of the system would be given by the sum of the curves in Figures 5.5 and 5.6. The resultant plot is shown in Figure 5.7. In all the plots the maximum output conditions were taken as the zero decibel reference level. These results indicate that both brass and lead backings increase the bandwidth considerably and ripples within the pass-band region are small. Thus, it was affirmed that a sufficiently wide-band transducer for the project could conveniently be produced with an appropriate backing. In order to avoid multiple reflections within the backing medium, an absorbent backing material is desired. Lead, being relatively lossy, will be chosen as the backing material.

5.2 Construction and Mountings

Two piezoelectric ceramic (PZT 5A) transducers, A and B, of 12 mm diameter, were employed in the probe units. These transducers were standard frequency discs having nominal resonant frequency of 2 MHz (frequency tolerances ±7%), and were supplied by Vernitron (Brush Clevite) Ltd. Lead was used to provide the heavy damping and hence the required bandwidth. A schematic diagram of the mounting arrangement is shown in Figure 5.8. The ceramic disc was bonded to a 35 mm long lead rod, having the same diameter as the disc but tapering towards the other end. A very thin layer of electrically

Parameters	Symbol	Unit	Values
Area of transducer	A	m^2	1.131×10^{-4}
Thickness of transducer	t	m	0.945×10^{-3}
Density of transducer material	ρ	kg/m^3	7.75×10^3
Velocity in transducer material	v_t^D	m/s	4.35×10^3
Clamped dielectric constant	$\epsilon_{33}^S/\epsilon_o$	-	830
Clamped capacitance	C_o	pF	859
Acoustic impedance of transducer	Z_x	ohms	3.813×10^3
Ideal transformer ratio	Φ	newt/volt	1.847
Acoustic impedance of backing medium	Z_b	ohms	3.076×10^3 for lead 4.185×10^3 for brass 4.524×10^{-2} for air
Acoustic impedance of loading medium	Z_q	ohms	1.674×10^2 for water
Open-circuit resonant frequency	f_o	MHz	2.3

Table 5.1 Constants and circuit values of a 12 mm diameter 2MHz resonant (f_o') PZT 5A transducer

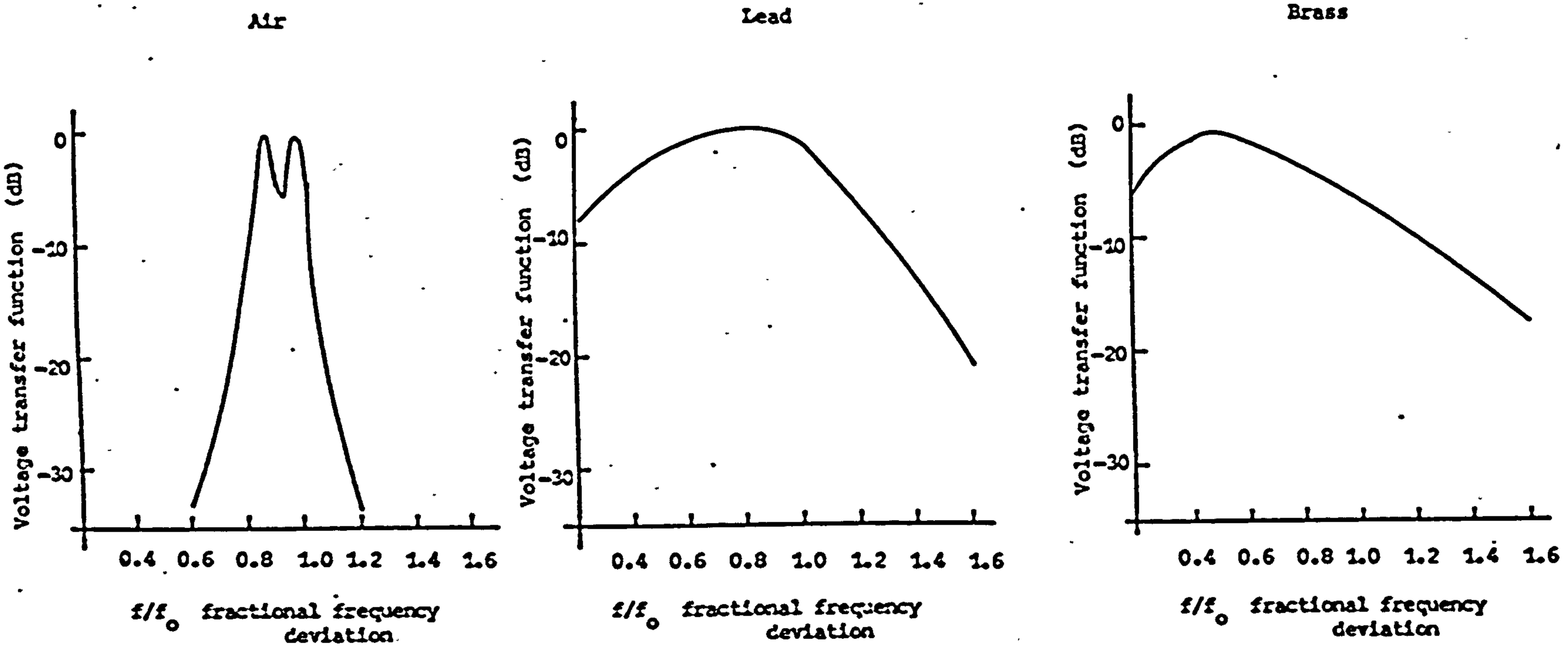

Figure 5.7 Overall transfer characteristics for the transducers

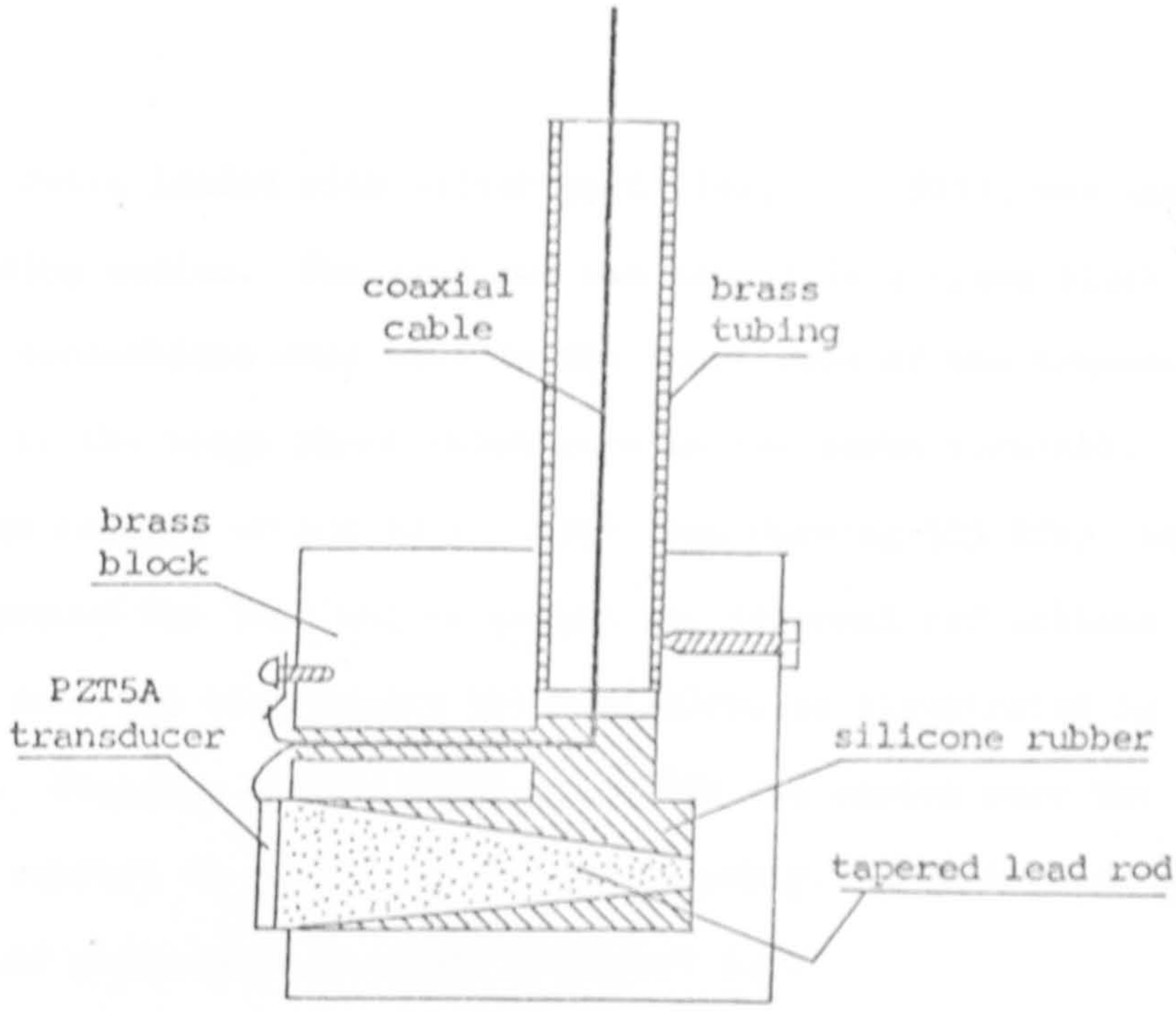

Figure 5.8 Schematic diagram of the probe unit

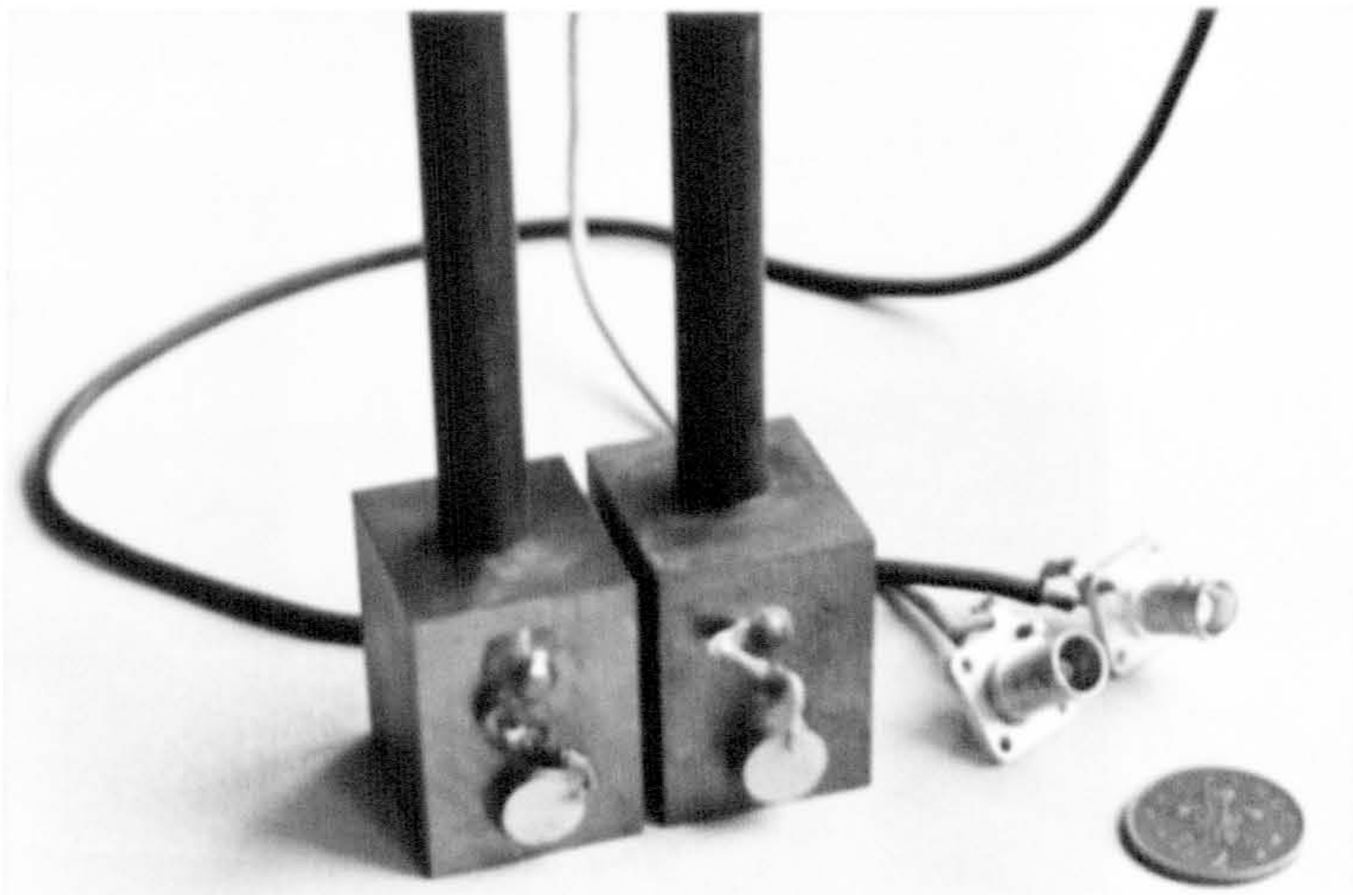

Figure 5.9 Assembled probe units

conducting resin loaded with silver particles, (DAG 915), was used as the bonding medium. The lead rod was housed in a brass block. Electrical connections were made to the front face of the transducer as well as to the brass block which acts as the earth terminal. An absorbent coating of silicone rubber (Dow Corning 583 RTV) was then cast around the lead rod to absorb any internal reflections inside the rod, and also around the lead wire, as illustrated in the Figure. Finally, a thin layer of Bostik was coated over the transducer surface to give a waterproof assembly. A photograph of the assembled probe unit is shown in Figure 5.9.

5.3 Measurements on the Transducers

In order to assess the actual performance of the assembled transducers some measurements, based on a simplified form of the above equivalent circuit, were carried out.

5.3.1 Simplified Equivalent Circuit

In the equivalent circuit of Figure 5.2, the $jZ_x \cot(\alpha/2)$ term may be approximated by a series tuned circuit for frequencies near the resonant value f_o,[65] the compliance, C_M, being given by:

$$C_M = 1/\pi^2 f_o^2 Z_x \qquad (5.1)$$

and the mass, L_M, by:

$$L_M = 1/4\pi^2 f_o^2 C_M \qquad (5.2)$$

Similarly, the $jZ_x \tan(\alpha/2)$ may be approximated by a shunt tuned circuit, the compliance being given by:

$$C_N = \pi^2 C_M/18 \qquad (5.3)$$

and the mass by:

$$L_N = 1/4\pi^2 f_o^2 \, C_N \qquad (5.4)$$

It can be noted that the negative capacitance $C_{E/4} = -C_o/4\phi^2$, lowers the resonant frequency of the series tuned circuit to f_o' where:

$$f_o' = f_o (1 - 4C_M/|C_E|)^{\frac{1}{2}} \qquad (5.5)$$

The transducer circuit thus contains two tuned circuits resonant at f_o and f_o'. As an approximation, for frequencies near resonance, the shunt tuned circuit presents a high impedance and that branch may be regarded as open-circuited. The transducer performance is thus determined by the series resonant branch, and the 'Frequency Constants' tables supplied by the manufacturers give the transducer thickness for this resonant frequency (f_o').

This simple equivalent circuit lends itself readily to measurements. By transferring all the elements to the left-hand side of the ideal transformer in Figure 5.2, an approximate circuit, consisting of a capacitor C_o shunted by a series network L_m, C_m and R_m as shown in Figure 5.10, will be obtained.[77] R_m is seen to represent the sum of the mechanical loss and the radiation resistance.

The admittance of the circuit at a frequency equal to $\omega/2\pi$ is:

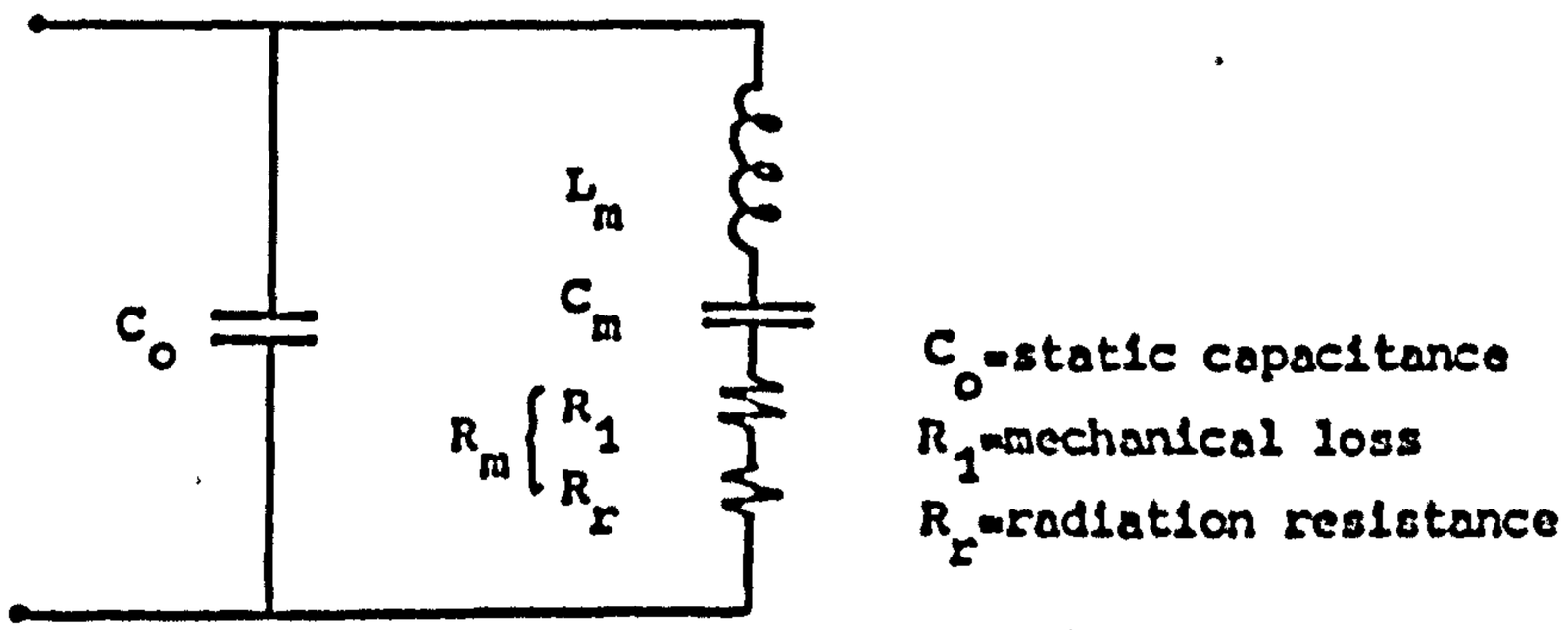

Figure 5.10 Simplified equivalent circuit of transducer

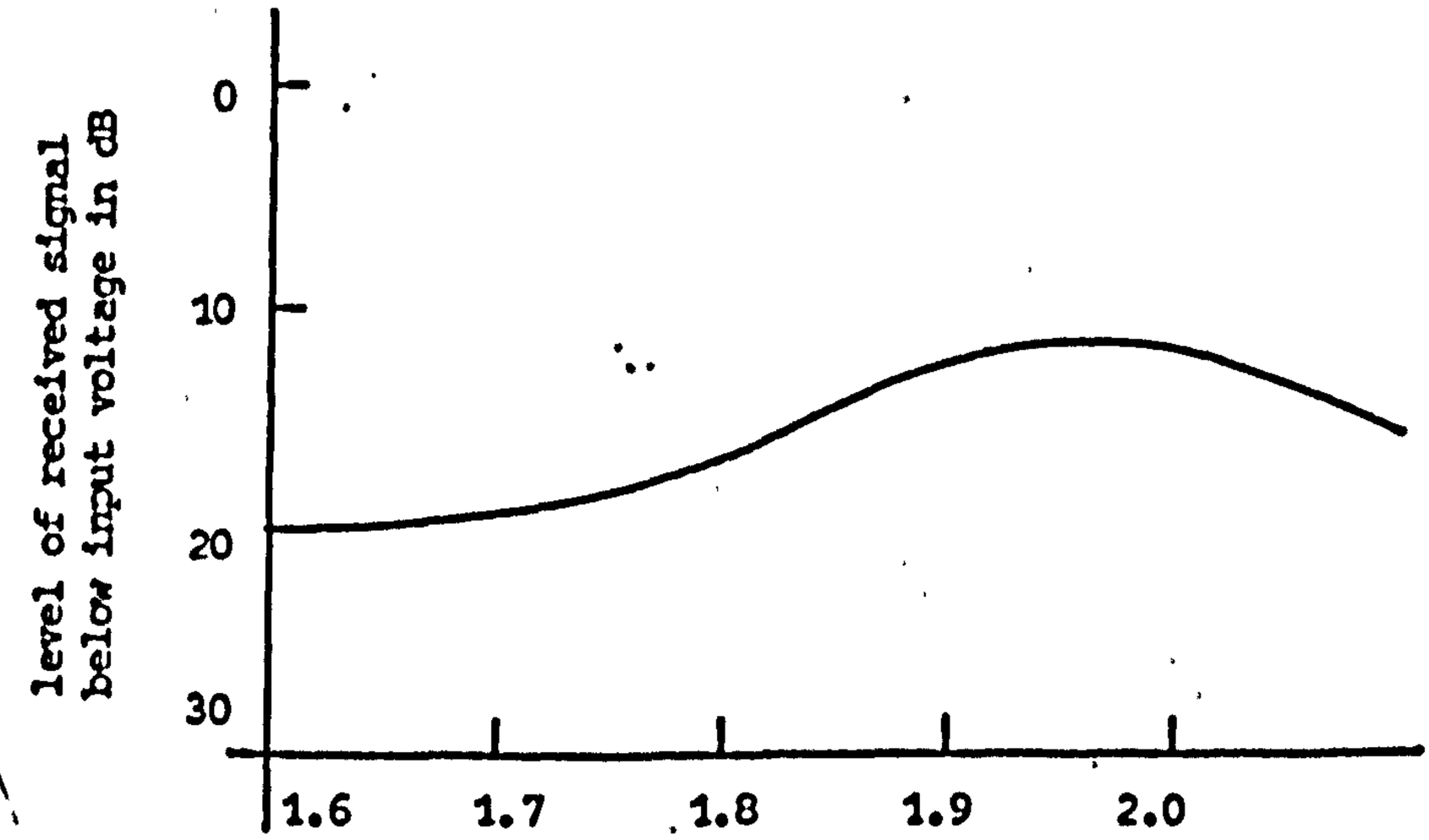

Figure 5.11 Experimental overall frequency response of transducers

$$Y = 1/\{R_m + j\ (\omega L_m - 1/\omega C_m)\} + j\omega C_o \qquad (5.6)$$

The first term represents a circle in the complex plane, and the second term gives the imaginary co-ordinate of its centre. Around the resonant frequencies the second term remains relatively constant and the admittance locus given by the above equation approximates to a circle. From such a plot, the clamped capacitance C_o, the bandwidth and the 'Q' of the transducers can be estimated.

5.3.2 The Circle Diagram[78]

Complex admittance measurements were carried out around the resonant frequencies of the transducers, using an r.f. admittance bridge (Wayne Kerr Type B602) with the transducers first radiating in air (unloaded) and then in water (loaded). The respective complex loci were plotted in Figures 5.12 and 5.13. They were found to be reasonable approximations to circles. For Transducer A, the following data was obtained:

f_r = resonant frequency

= 1.92 MHz

C_o = clamped capacitance

= 663 pF

Δf = 3 dB bandwidth

= the frequency difference between frequencies, f_a and f_b, at which the conductance is half the maximum

= (2.05 - 1.75) MHz = 300 kHz

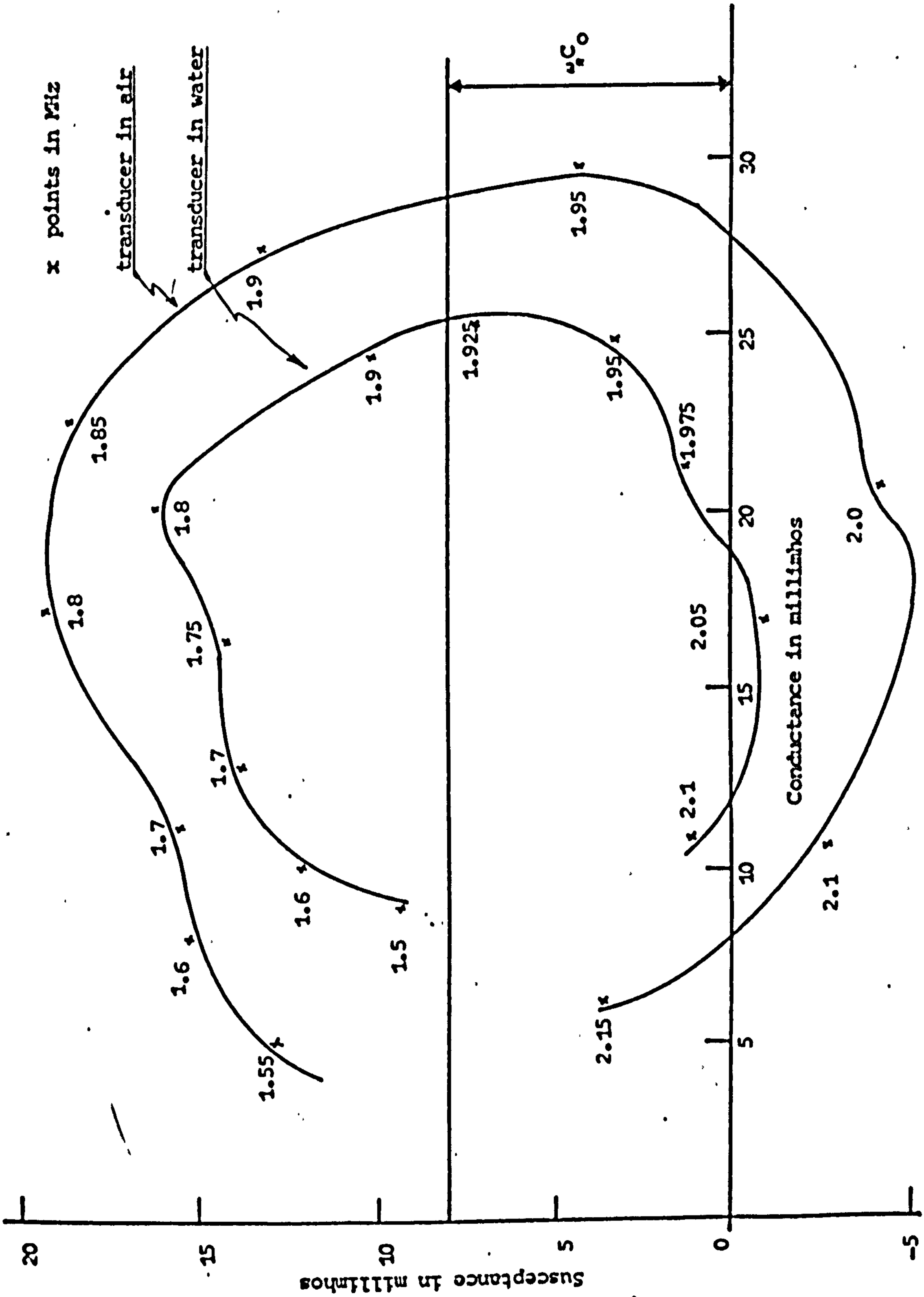

Figure 5.12 Circle diagrams for Transducer A

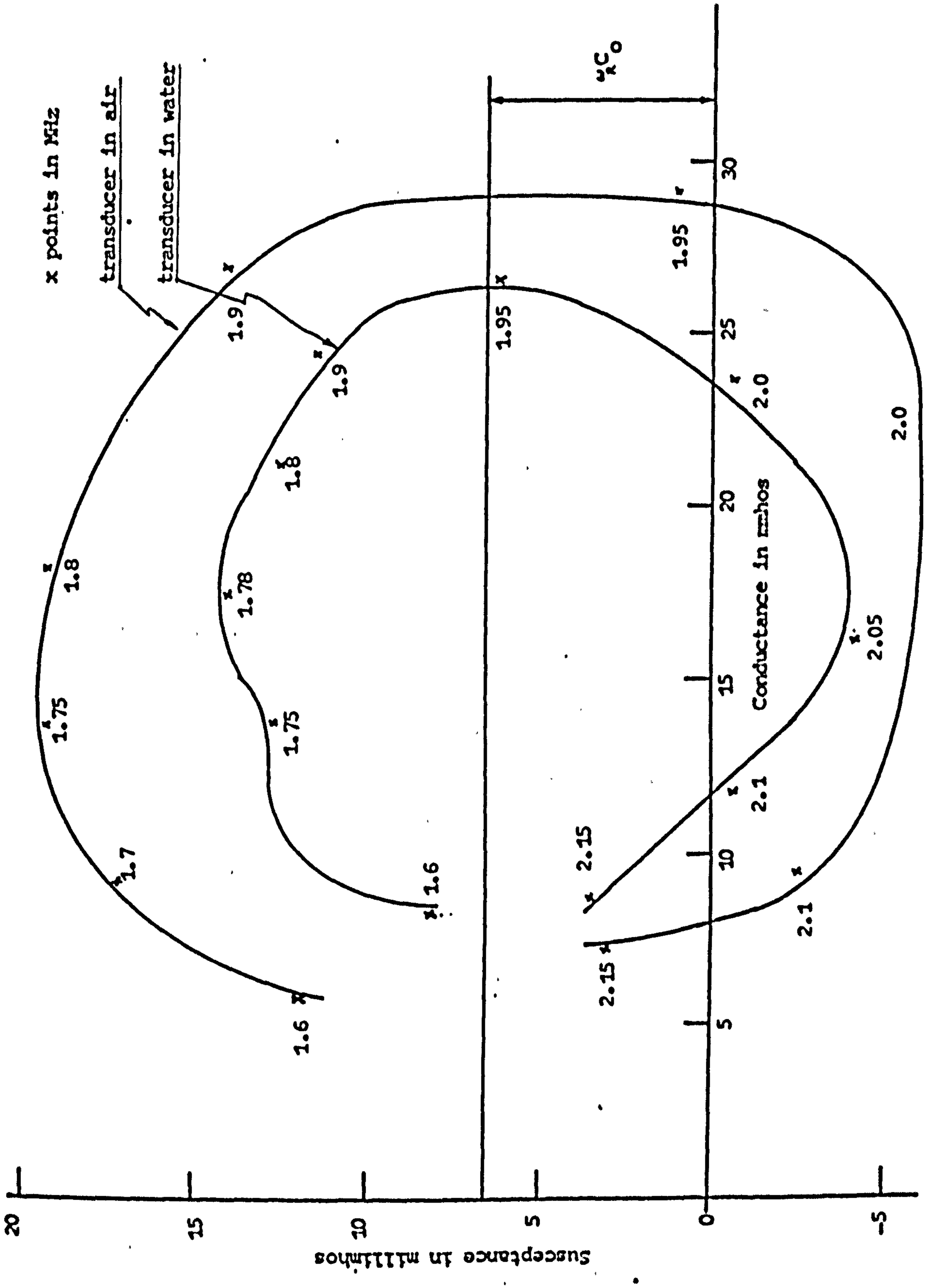

Figure 5.13 Circle diagrams for Transducer B

and Q_{mech} = (resonant frequency)/(3 dB bandwidth)

= 1.92 MHz/0.3 MHz

= 6.4

Transducer B has similar characteristics:

/

f_r = 1.95 MHz

C_o = 570 pF

Δf = (2.06 - 1.78) MHz = 280 kHz

and Q_{mech} = 6.96

The corresponding calculated values are:

C_o = 859 pF (from Table 5.1)

and Q_{mech} = 1.5 (from Response Curve in Figure 5.5b for the case of lead backing).

The Q_{mech} obtained in the practical case, although of a reasonable value, falls far short of the predicted theoretical value. The main reason for this discrepancy might be the non-ideal bonding conditions of the backing medium.

5.3.3 Measured Performance of the Transducers

The transducers were set up in a through-transmission pulse-operation mode inside a water tank with Transducer A as a transmitter and Transducer B as a receiver. Around the resonant frequencies an output of 0.15v p-p was obtained for an input level of 0.6v p-p, representing a loss of 12 dB. The overall frequency response curve was plotted (Figure 5.11). The response has its maximum at 1.95 MHz

and drops slowly away from the resonant frequencies. Over the frequency band of interest it has an appreciable variation in output (8 dB difference). However, since compensation was to be introduced, this response was accepted.

5.4 Beam Pattern of the Transducers

The radiated beam of a transducer can be conveniently described by its beam width and the length of the near field. For a plane circular source vibrating in uniform velocity and phase, the main lobe of the beam can be shown[79] to be confined within $\pm\theta$ where $\sin\theta = 0.61\,\lambda/a$, a being the radius of the piston source and λ the wavelength of sound being propagated.

For the assembled transducer:

$$= \sin^{-1} 0.61 \times (0.83/6)$$

$$= 4.9^{\circ}$$

This value is significant when discussing the lateral resolution of the system.

Due to the finite size of the source, diffraction will occur in regions near to the source (Fresnel Zone).[80] In the case of a disc transducer, where $a >> \lambda$, the near field extends out to a distance that is approximately equal to a^2/λ. Hence, the length of the near field for the transducers is:

$$\text{length of near field} = a^2/\lambda$$

$$= \frac{6^2}{0.83} = 43 \text{ mm}$$

Since within this region there are undesirable interferences, this zone was avoided in the test set-up.

CHAPTER 6

INSTRUMENTATION FOR THE SYSTEM

6.1 General Description

The design of the electronic circuitry necessary for the realisation of the pulse compression system will be given in this Chapter. The basic blocks of the operating system are outlined in Figure 6.1. An output pulse from the master timing unit is integrated into a ramp which is impressed upon the voltage-to-frequency converter to provide the long duration transmitted FM pulse. After being reflected, the echo is received through a separate transducer and fed into the receiving unit where it is compressed by the dispersive delay line. The receiver incorporates phase and amplitude equalisers to compensate for the time delay non-linearities and the non-uniform response of the complete system. By changing the mark/space ratio in the master timing unit and suitably gating the long output pulse, the system could also be made to operate in a short pulse mode. This pulse-echo arrangement provides a basis for comparison.

Since pulse compression is a phase coherent process, it inherently demands precise instrumentation for its implementation. This is evident from the discussion of effects of time delay and amplitude distortions upon the compressed pulse in Section 3.5. In particular, the parameters of the FM generator must properly match the dispersive delay line characteristic. The output pulse was thus designed to have an adjustable duration and its frequency modulation a variable slope. The linearity of the frequency

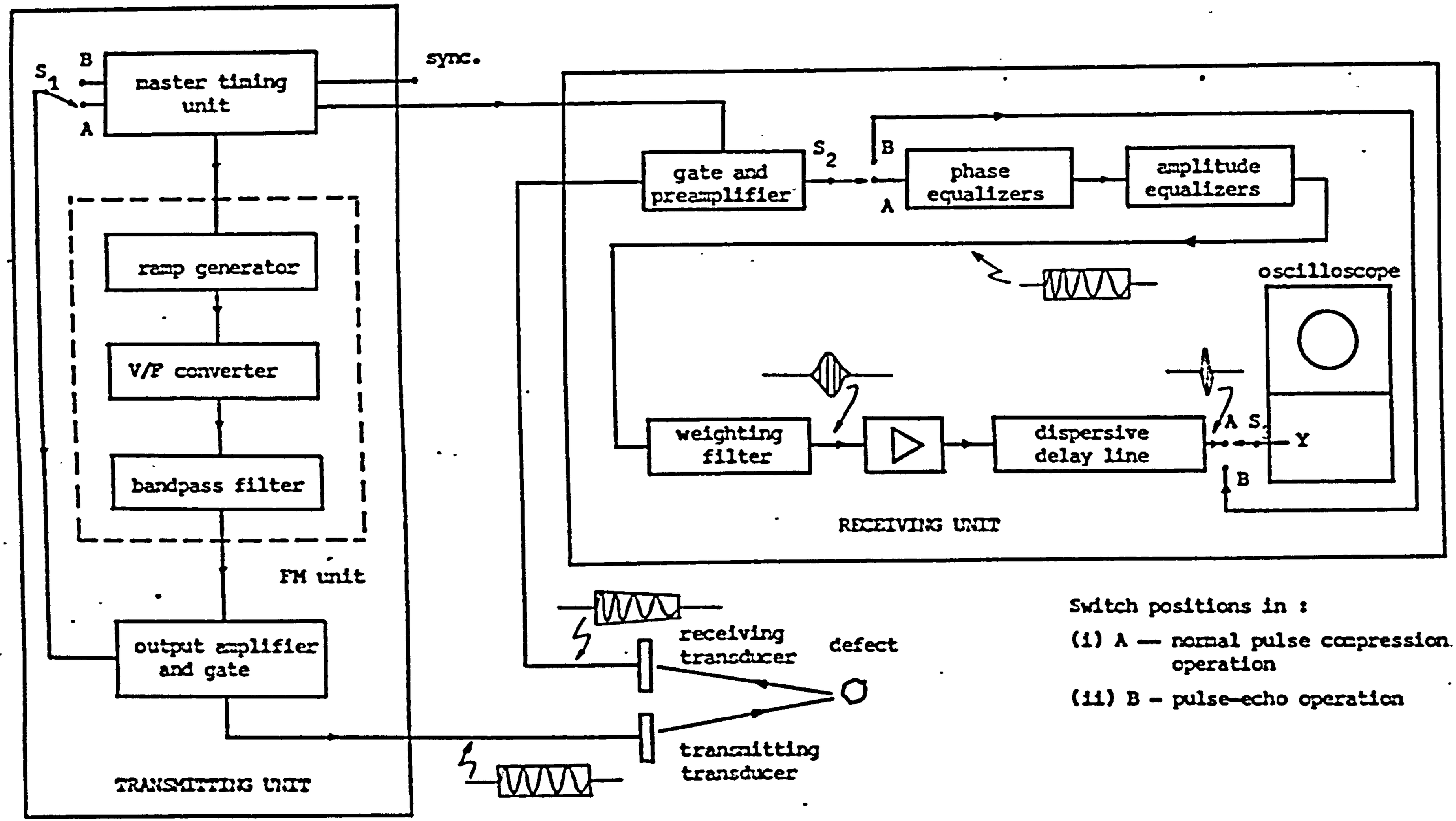

Figure 6.1 Schematic diagram of the pulse compression system

modulation upon the output pulse was also made to be appreciably better than that of the dispersive delay line.

Great care was taken in the fabrication of the circuits. Nearly all circuit boards employ printed circuit techniques and have their power rails decoupled from one another. A separate power rail is allocated to the voltage-to-frequency converter board to minimise the cross-couplings from its high-frequency noise, as well as to maintain the stability (and hence the linearity of the FM) of this unit. The complete system employs convenient plug-in units which provide effective screening.

6.2 The Transmitting Unit

Basically, this consists of a voltage controlled oscillator, a linear ramp, a band-pass filter, amplifiers and various synchronising and gating circuits. Its performance is best summarised through the following data:-

FREQUENCY

Range: 1.6 to 2.1 MHz (adjustable within these limits)

Sweep Rate : variable from 40 kHz/100 µs to 60 kHz/100 µs

OUTPUT

Waveform: Trains of linearly frequency modulated r.f. pulses

Level: A maximum of 6 v p-p into 50 Ω

Impedance: 75 Ω approximately.

FRONT PANEL CONTROLS

Centre frequency: (RV 4)	Sets the carrier frequency of the sweep
Sweep rate: (RV 5)	Acts as a fine sweep rate control around the pre-set value

Pulse width: (RV 2)	Adjusts the duration of the pulse length; variable from 300 μs to 950 μs
Pulse rate: (RV 1)	Varies the pulse train repetition rate from 5 ms to 15 ms
Gain setting: (RV 7)	Varies the r.f. output level continuously
Mode switch S_1:	Shortens the r.f. output into 10 or 20 μs duration when switched to position B

SYNCHRONISATION

Receiver gating:	Provides a delayed pulse. Delay is variable from 400 μs to 10 ms; while length of the pulse is variable from 600 μs to 8 ms
Oscilloscope trigger:	Provides an output pulse train in synchronisation with the transmitter pulses.

6.2.1 Master Timing Unit (Figure 6.2)

This unit provides timing and synchronising pulses for the system. Its various output waveforms are illustrated in Figure 6.3, which shows their timing sequence in relation to the output FM pulse. IC1(MC725) is the master astable formed by cross-coupling two NOR gates. The "ON" and "OFF" times of the astable can be adjusted through RVI and RV2, which serve as the duration and width controls of the output pulse respectively. IC2 (MC799) acts as a buffer and produces two outputs in antiphase (waveforms A and B in Figure 6.3). Pulses in A are fed into the integrator to produce the sawtooth C, and also into the Monostables 1 and 2. The latter circuits provide an output gating waveform D, which is seen to be delayed (by 50 μs) and shortened (by 100 μs) with respect to Waveform A. This gating arrangement ensures that the non-linearities occurring at the beginning and the end of the sawtooth waveform, will be excluded

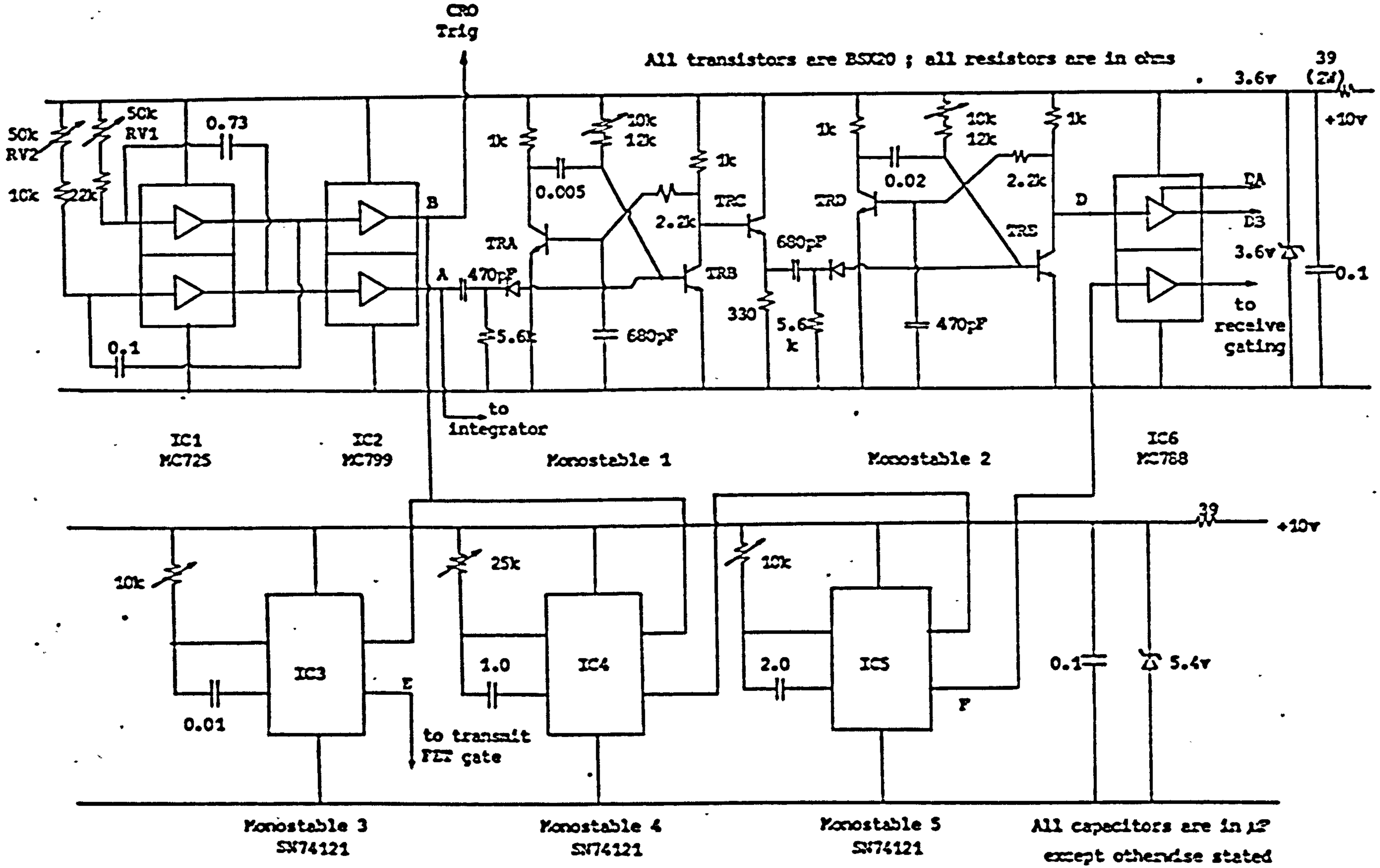

Figure 6.2 Master timing unit

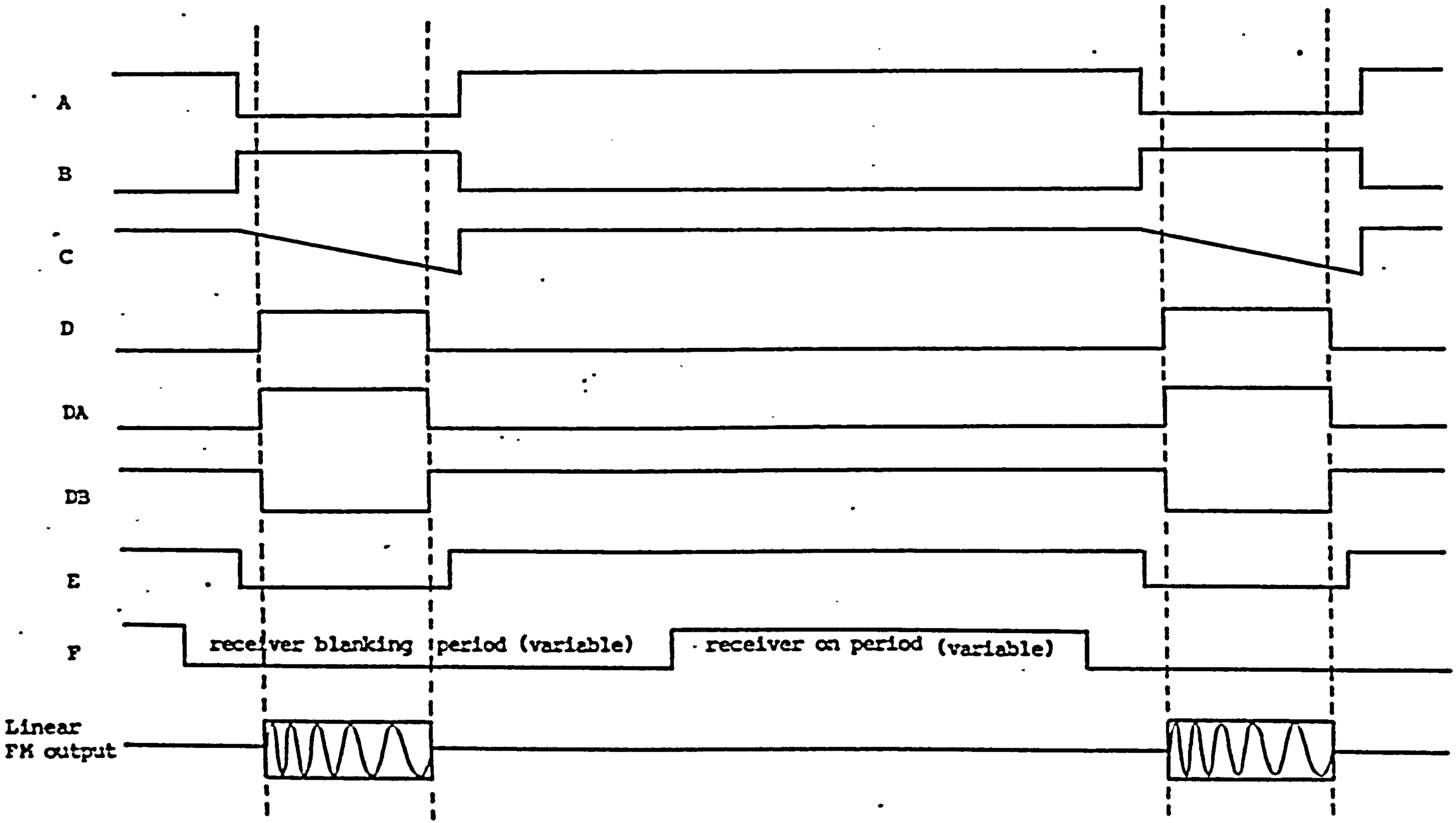

Figure 6.3 Timings of transmitter waveforms in the system

from the output pulse. Pulses in B go to Monostables 3 and 4 as well as to an oscilloscope synchronisation output point. Monostable 3 (SN 74121) produces another gating waveform E, which is used to drive the output series FET switch. Monostables 4 and 5 utilising two SN 74121, generate waveform F which is for receiver gating and is intended to be used to gate off the transmitter voltage when the system is arranged in a pulse-echo single-transducer set-up. Half of IC6 (MC 788) is used to buffer the above waveform; while the other half is utilised to produce two opposite going waveforms (DA and DB) from waveform D.

6.2.2 FM Oscillator

In view of the high linearity required and the relatively wide bandwidth involved, the voltage controlled oscillator utilises a multivibrator type voltage-to-frequency converter. The oscillator can be conveniently described under three headings:

(a) Ramp Generator (Figure 6.4a)

The modulating sawtooth is produced by integrating waveform A with a Miller integrator circuit. The input pulses switch TR1 "ON" and "OFF". When TR1 is "OFF", current from the supply charges up the 0.02 μF capacitor producing the sawtooth. RV3 affects the charging rate and is used as the sawtooth slope control. TR2 and TR3, connected in a Darlington configuration, form an extremely high gain amplifier. Linearity measurements were carried out by using a CR differentiating network (Figure 6.4b) and confirmed that the ramp has good linearity (better than 0.1%). Slight non-linearities were noted to occur at the two extreme ends of the sweep. This is because in the first few tens of microseconds of the sweep, TR2 and

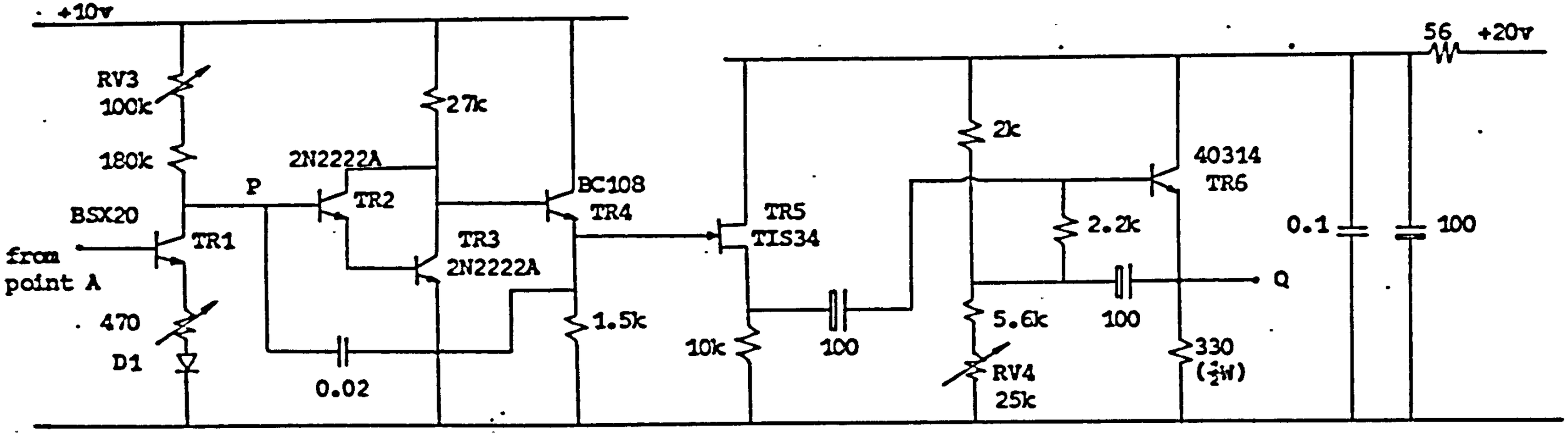

Figure 6.4a Integrator and driver

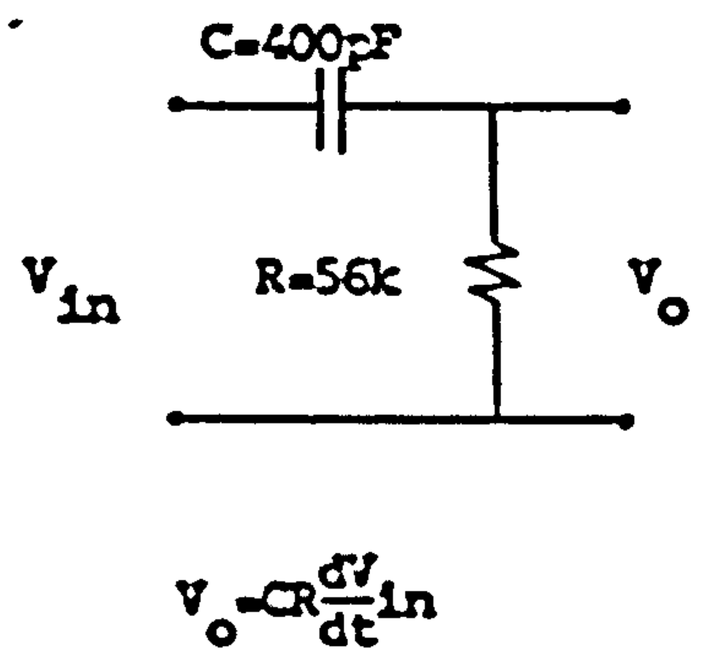

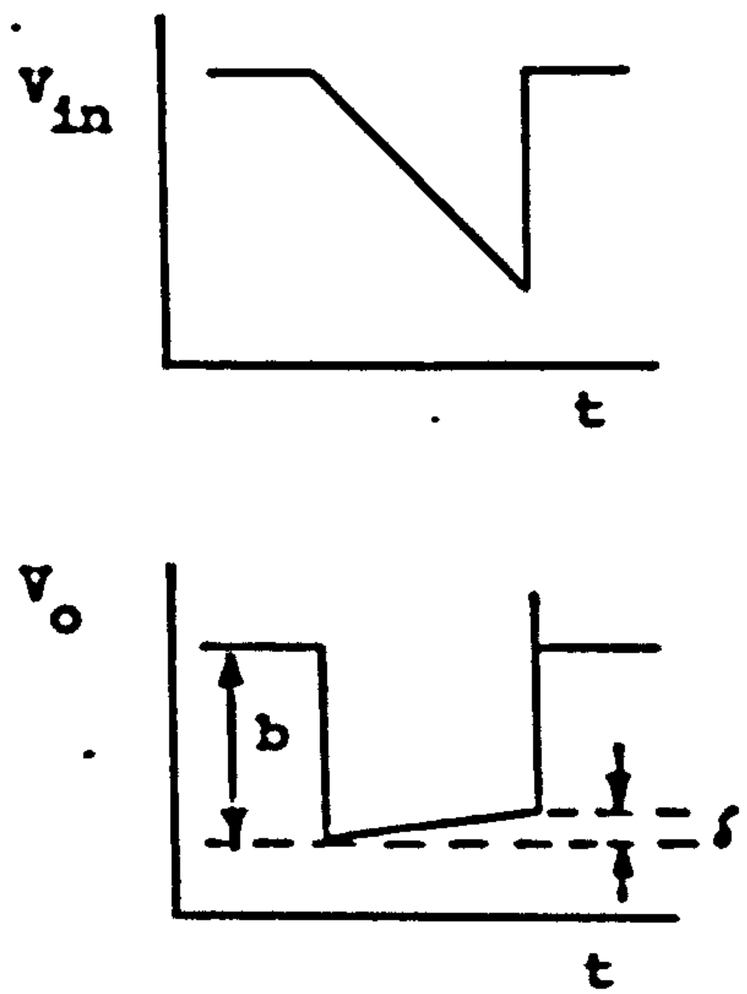

% non-linearity
$= \frac{\delta}{2b}$

Figure 6.4b Non-linearity measurements

TR3 are not yet fully forward biased and the gain of the amplifier is then low; while the tail part of the sweep suffers from the exponential nature of the charging current. The first effect is alleviated by raising the quiescent voltage at point P when TR1 is "ON"; diode D_1 serves this purpose. However, as pointed out earlier, both the initial and tail parts of the sweep are gated out from the output pulse.

The sawtooth is then fed into a driver possessing an input impedance of MΩ or higher. The driver comprises an FET (TR5) of source follower configuration and a bootstrapped emitter follower (TR6). TR6 utilises a higher rated transistor (2N 40314) and meets the current requirements of the voltage-to-frequency converter. RV4 sets the d.c. level of the output sawtooth and functions as a frequency range control.

(b) Voltage-to-frequency Converter (Figure 6.5)[81]

It is essentially a version of the conventional astable multivibrator in which TR8 and TR9 are the main oscillating transistors. To ensure linear charging of the timing capacitors, the two charging resistors are replaced by current sources TR10 and TR11. Transistors TR12 and TR13 are emitter followers for rapidly discharging the timing capacitors, hence extending the upper frequency limit. In order to render the frequency independent of the supply voltage and transistor-parameter variations, the voltage swing of the timing capacitors must be held constant. This is achieved by the use of a Zener diode, ZD1, in connection with the fast silicon diodes D3-D6. From analysis, the frequency of

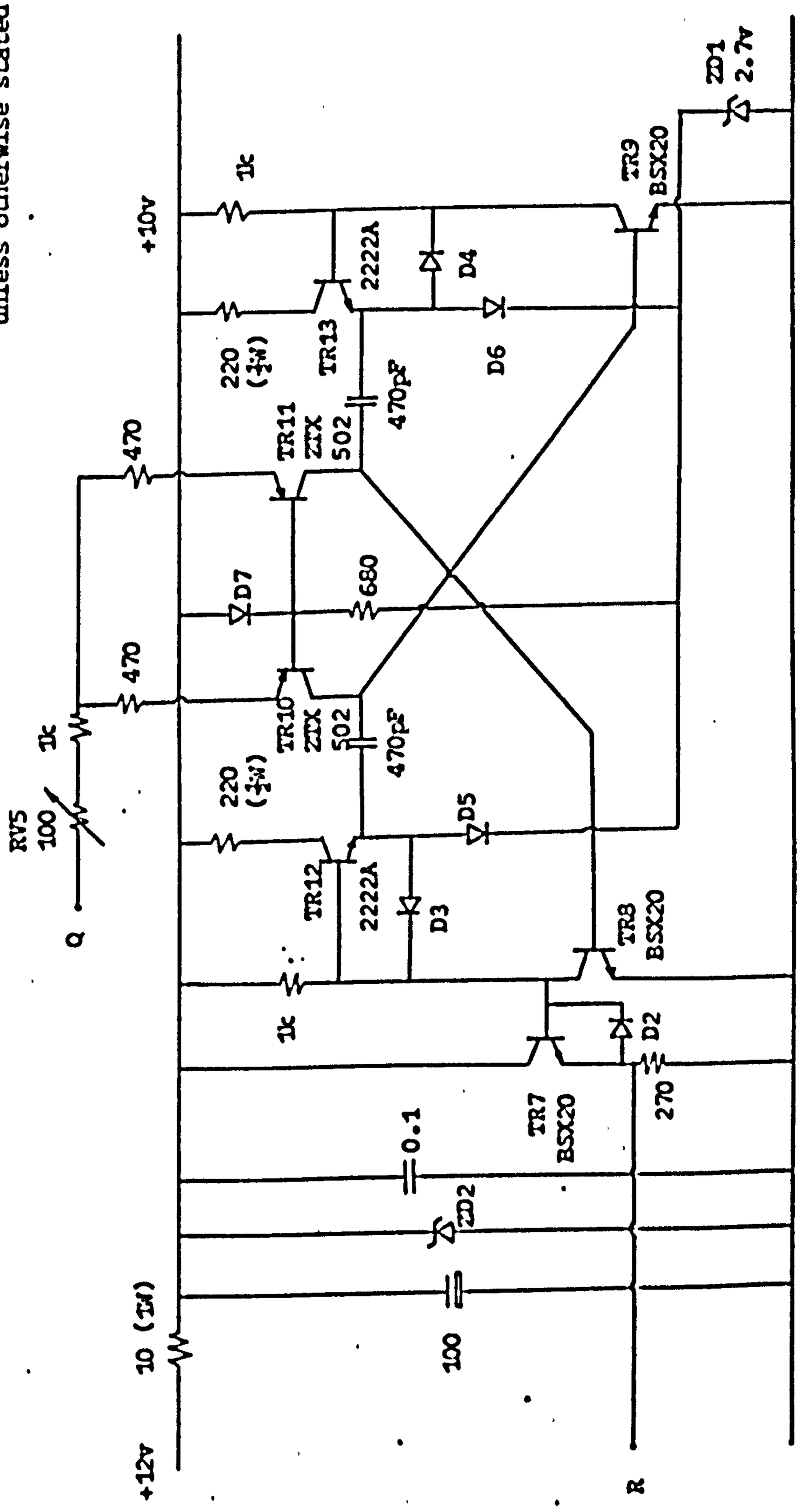

Figure 6.5 Voltage-to-frequency converter

oscillation is given as proportional to the voltage at Q. Thus the sawtooth voltage applied to Q will result in a linear FM output. A small variable resistor RV5 is placed in the charging path and serves as a fine sweep rate control. Calibration curves showing the measured control characteristics of the converter for several settings of RV5, are plotted in Figure 6.6. They demonstrate that the converter is highly linear over the frequency band of interest.

(c) Bandpass Filter (Figure 6.7)

The design of the filter is based upon Skwirzynski's filter data.[82] A Chebyshev response was aimed at with the following specifications:-

D_p = maximum permissible distortion in the passband

= 0.5 dB

D_a = Minimum rejection in the stop band

= 55 dB

$k = \frac{f_p^+ - f_p^-}{f_a^+ - f_a^-}$ = selectivity factor

= 0.725

f_p^+ , f_p^- = edge frequencies defining the transmission bands

= 1.5 to 2.15 MHz

f_a^+ , f_a^- = edge frequencies defining the attenuation band

= 1.4 and 2.31 MHz respectively.

R_1 = input resistance = 50 Ω

R_2 = terminating load resistance = 50 Ω

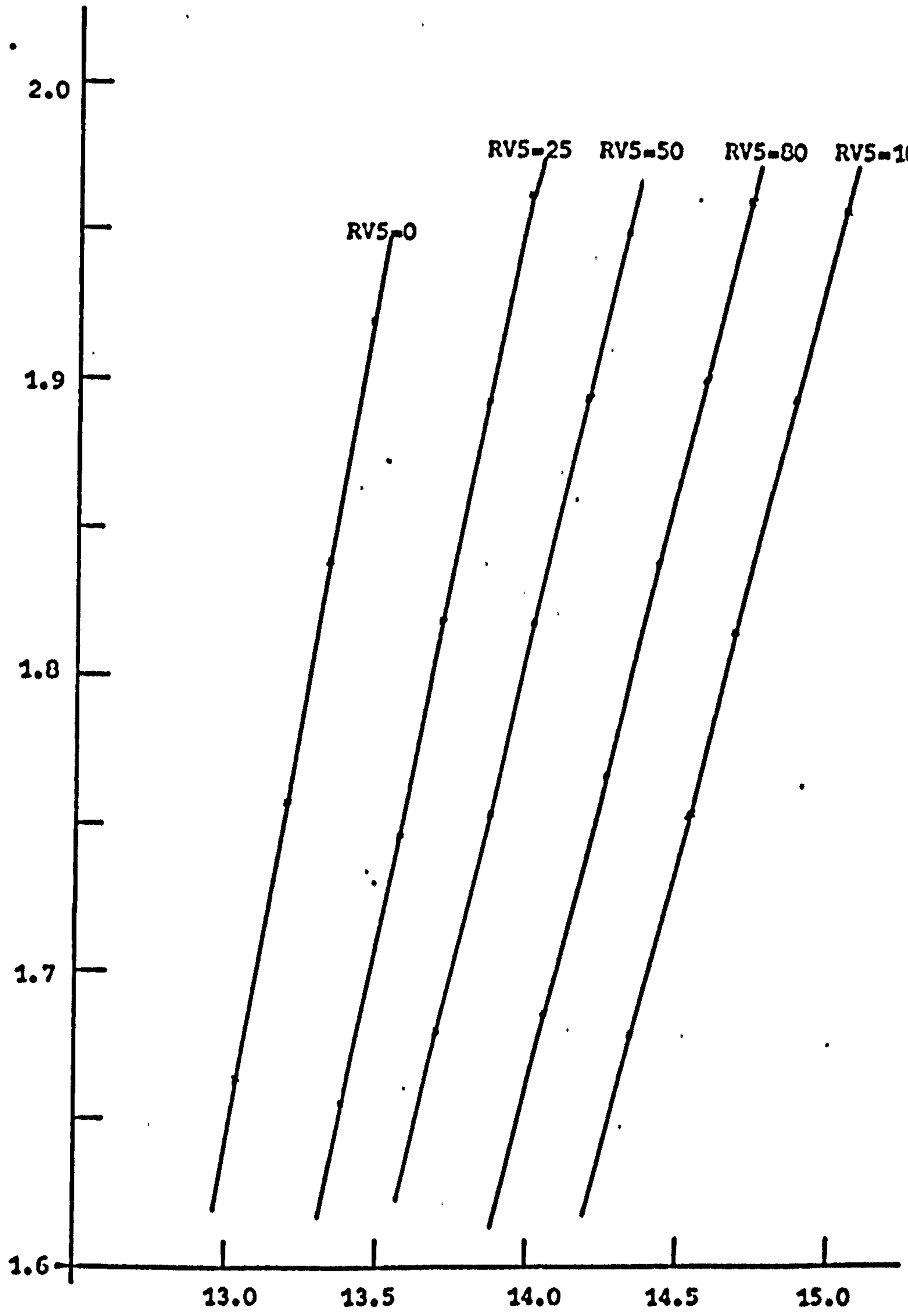

Figure 6.6 Voltage to frequency characteristics for the converter

A bandpass TA symmetrical bar type ladder structure with six branches was decided upon. The corresponding coefficients and hence the element values were calculated from the compiled data. However, the calculated values gave inconveniently small values of inductances and the impedance levels had to be raised to 1 KΩ. The resultant filter is shown in Figure 6.7 and its insertion loss curve in Figure 6.8.

6.2.3 Gating and Pre-amplifier Circuits (Figure 6.9)

The output from the FM oscillator is then fed into a source follower (TR14) before it is gated by a symmetrical six diode gate,[83] which possesses fast switching times. Diodes D8 and D9 are normally "ON", back-biasing the bridge diodes D10-D13 and no transmission of signal through the gate is possible. During transmission period, antiphase pulses from waveforms DA and DB switch diodes D8 and D9 "OFF", leaving the bridge diodes free to conduct. To minimise output spikes during the opening and closing of the gate, control pulses should have equal rise and fall times. For this purpose, the resistor RV6 is made adjustable. This resistor also sets the d.c. level of the gated output. It should be noted that control pulses are derived from waveform D and hence the gate will select the most linear part of the FM signal. Gating is done at this low level stage so that it can be more effective.

Source follower TR15 buffers the gated output and applies it to a wideband video amplifier. The amplifier utilises an MC 15520 connected in a non-inverting mode[84] with a maximum gain of 30 dB. The series resistor RV7 serves as a gain control.

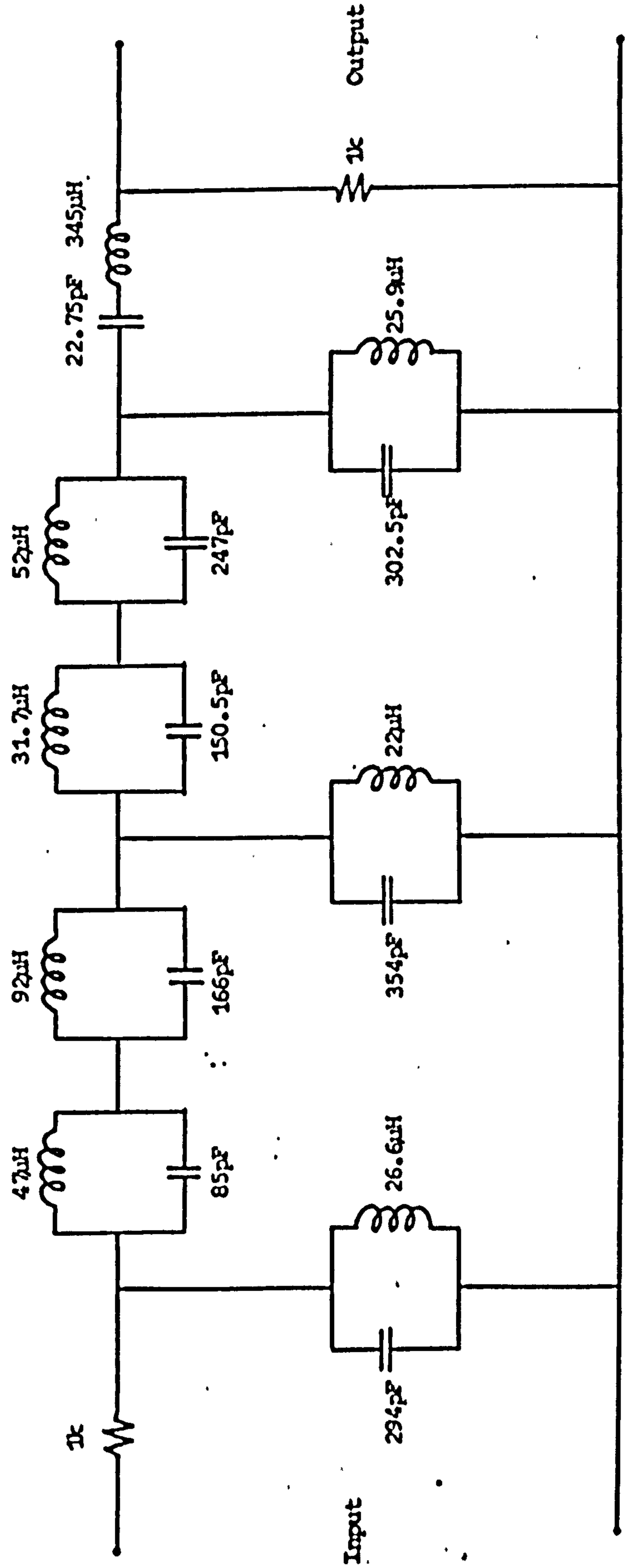

Figure 6.7 Band-pass filter

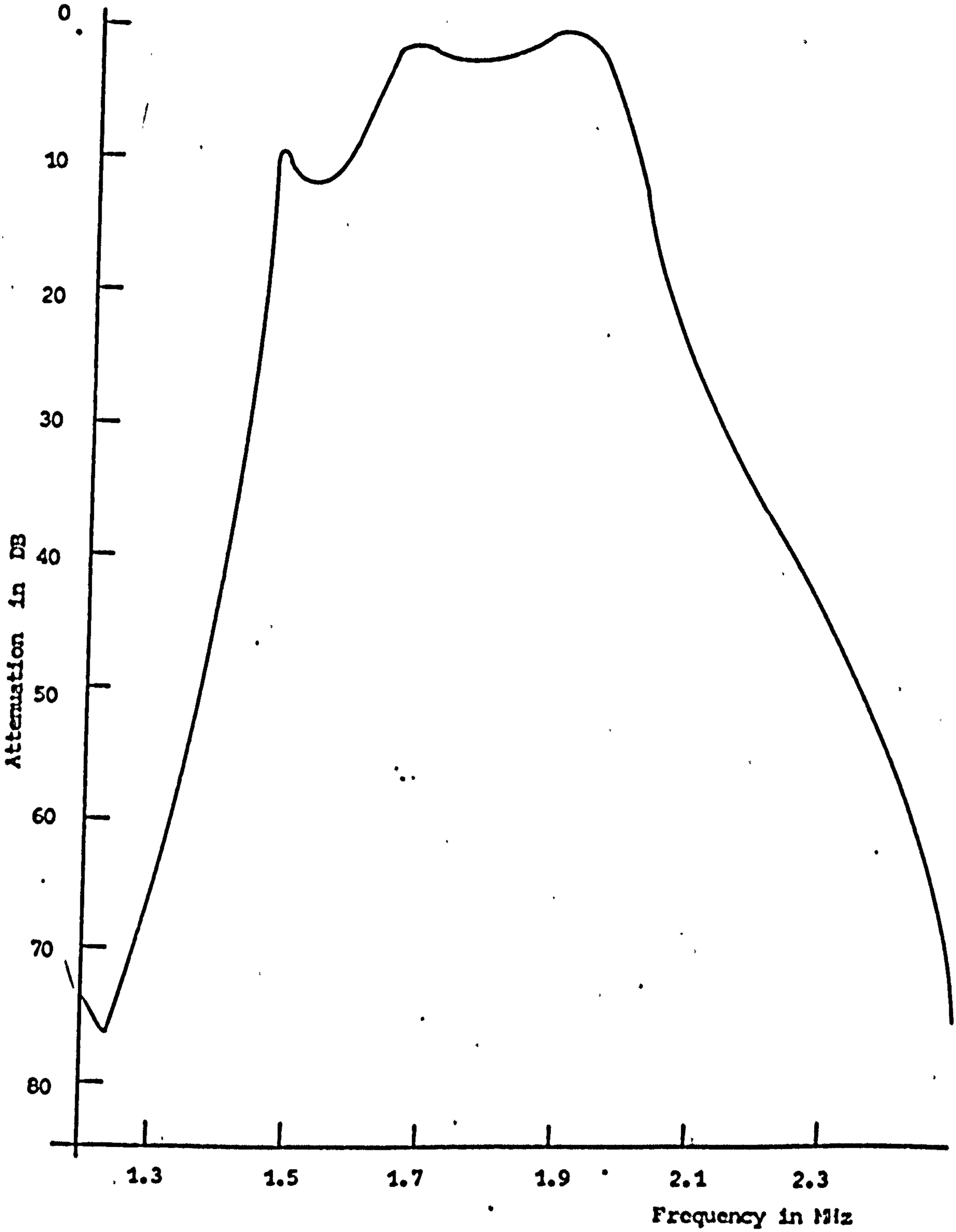

Figure 6.8 Band-pass filter characteristics

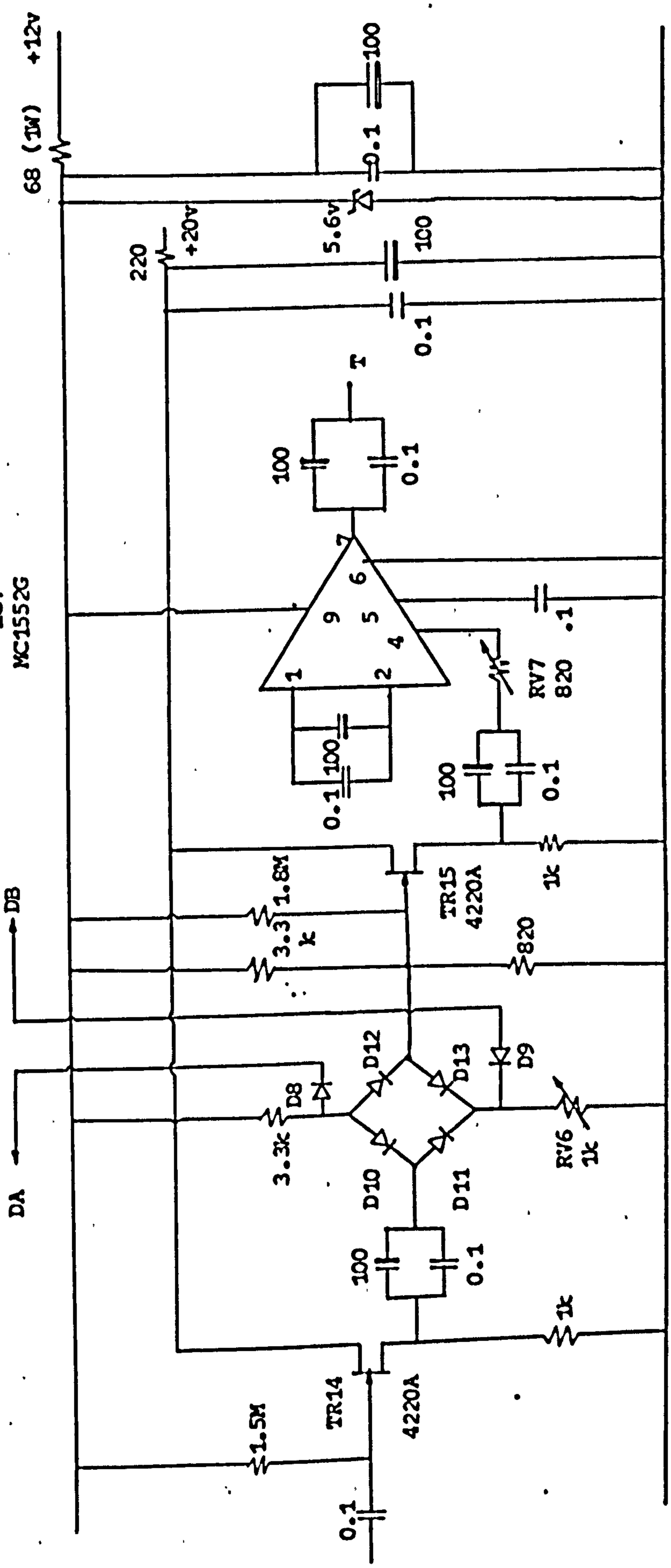

All capacitors are in μF

Figure 6.9 Gate and amplifier circuit

6.2.4 Output Amplifier (Figure 6.10)

To drive the transmitting transducer effectively, a high-current, low output impedance amplifier is desired. In Figure 6.10, TR17 is the driver for the main power transistor TR18 (BD 123), which has a rating of 45W, and is mounted at the back panel of the instrument. To preserve linearity, a Class A mode is employed. Heavy feedback is provided by RV8, giving a stabilised operation. An output current capability of more than 100 mA is afforded by this amplifier. However, the gain of the amplifier is relatively low and has a value of 4.

6.2.5 FET Series Switch (Figure 6.11)

It was noted that the output point of the power amplifier had a noise level of around 20 mV when the transmitter was at its "OFF" period. This was attributed to the coupling of the oscillator and timing unit pulses into the power rails. To overcome this, a series switch was inserted between the power amplifier and the transducer. The switch consists of a high current rating FET MFE 2012 (TR20) and a driver TR19.[85] TR19 is normally biased to fully "ON" by the control waveform, E, applied to its base. Its collector assumes a negative voltage and the FET switch is "OFF". During transmission period, a negative pulse is applied to the base of TR19, whence its collector rises to a positive potential. The FET switch has a positive gate-to-source voltage and is then fully "ON". As the gating waveform E occurs earlier and lasts longer than the output FM pulse, the latter is therefore not affected by the switching transients. For the short pulse mode operation, a much shortened waveform E, obtained by switching in smaller resistors to Monostable 3[86] in the master timing

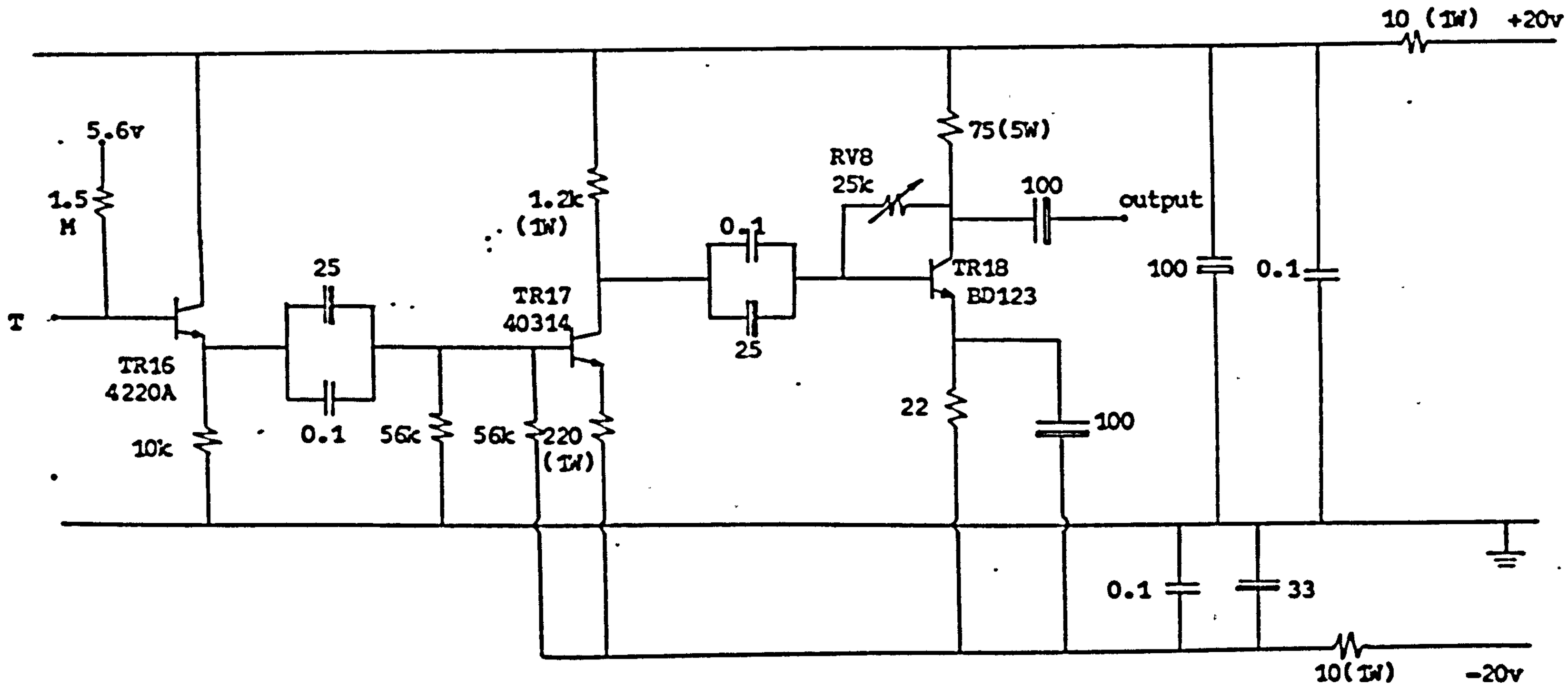

All capacitors in μF

Figure 6.10 Output amplifier

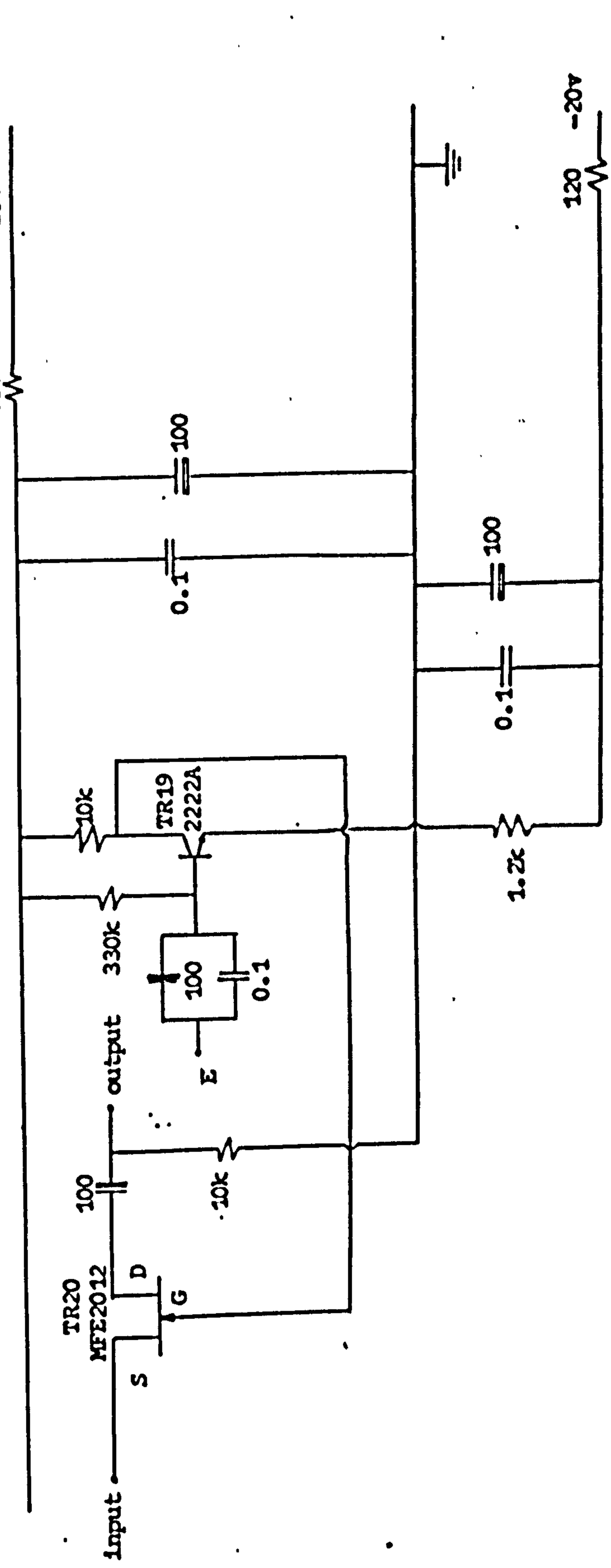

Figure 6.11 Transmitter RF gate

unit, gates the output pulse to the appropriate length.

6.3 The Receiving Unit

This is best described under the following headings:-

6.3.1 Receiver Gate and Pre-amplifier (Figure 6.12)

The receiver gate also employs an FET series switch and is similar in design to the switch in the transmitter unit, except that it utilises a much lower rating FET. Under normal operating conditions, two separate transducers are employed and this gating is unnecessary. A manual switch S_A is thus incorporated to enable the received signal to by-pass the gate. The subsequent pre-amplifier consists of two integrated circuits, IC8 and IC9. IC8 utilises an MC 1510 high frequency differential amplifier connected in a single-ended input mode. Its other input terminal is earthed through a small resistor, giving the amplifier a high common mode rejection. This stage provides a gain of 30. IC9 is a wideband operational amplifier connected in a simple amplifying configuration. It furnishes a maximum gain of only 5, but has a large output swing capability. If large received signals are encountered, IC8 can be switched out of the circuit by operating switch S_B.

6.3.2 Time Delay Equalisers (Figure 6.13)[56]

Six delay equalisers have been introduced to correct the time delay error in the system. They are of constant resistance all-pass, bridged-T networks derived from their corresponding lattice counterparts. Their various peak delay times and their resonant frequencies are given in Figure 6.13. The respective circuit element

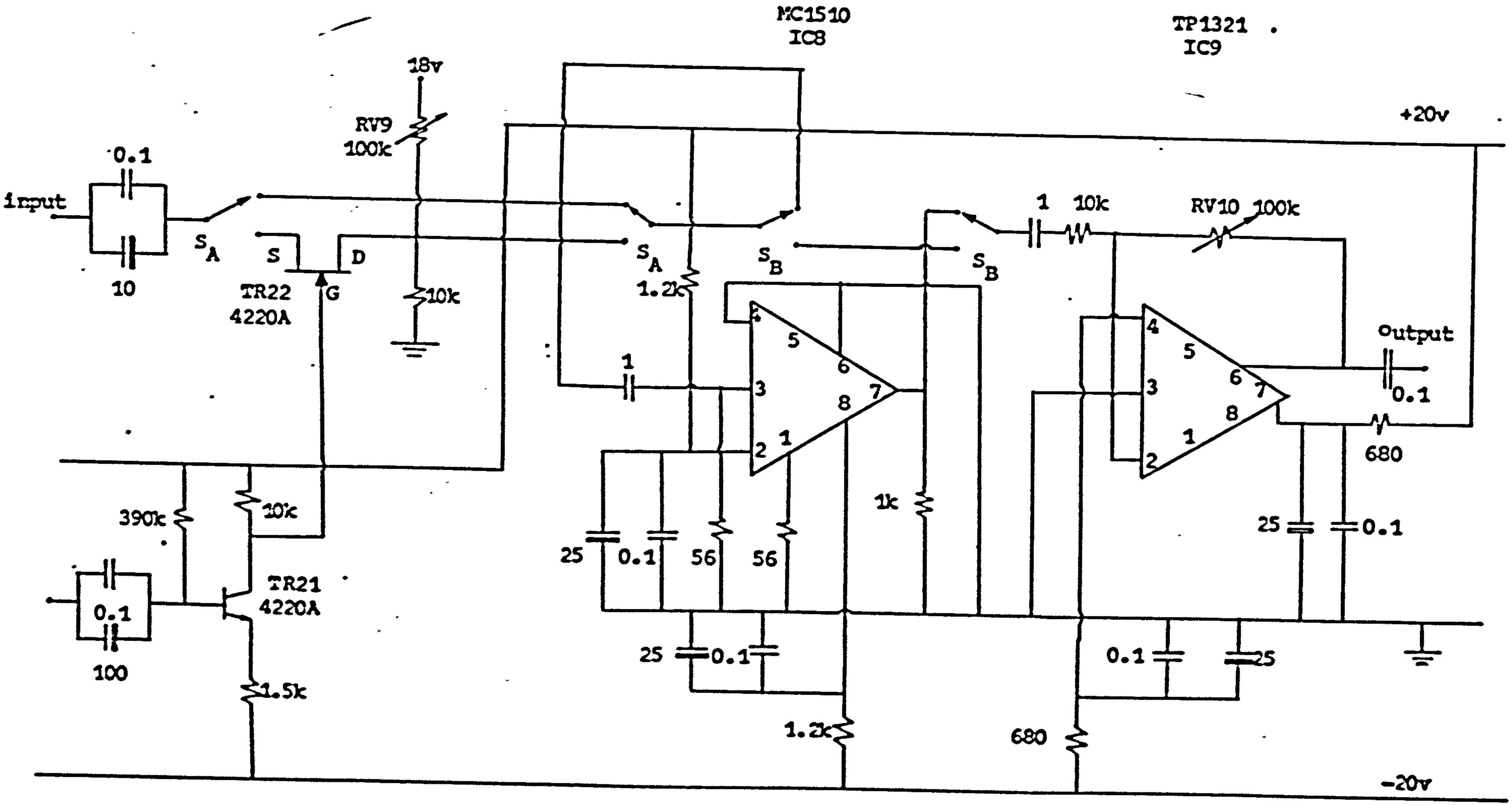

All capacitors in μF

Figure 6.12 Receiver gate and preamplifier

All capacitors in pF and inductors in μH unless otherwise stated

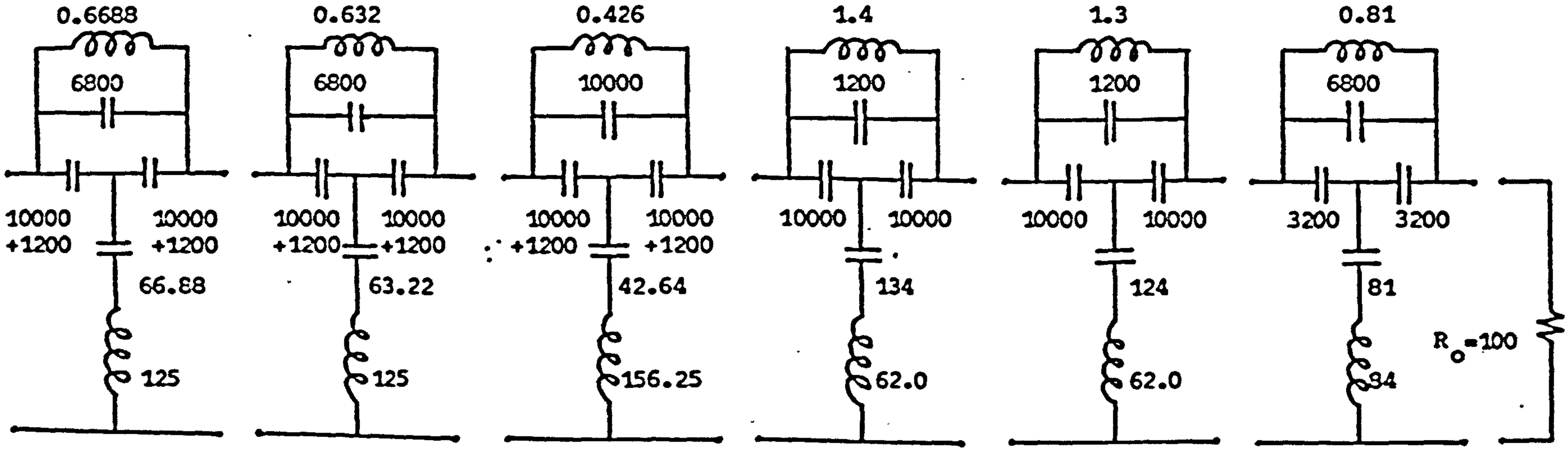

Figure 6.13 Time delay equalizers

values were calculated from Equations D.2 to D.6 in Appendix D.

In order to obtain reasonable values of Q, the inductors were wound with multistranded wires, while polystyrene capacitors were utilised. For the same reason, non-minimum element bridged-T networks were used. Details of equalisation procedure and its associated practical problems are discussed in Chapter 7.

6.3.3 Amplitude Equalisers (Figure 6.14)

To equalise the amplitude response of the system, two amplitude equalisers are included in the receiver. Each of the equalisers consists basically of a parallel tuned L,C and R circuit, driven by a current source. The response of the network can be conveniently expressed in terms of the Q_o of the tuned circuit.[87]

$$\left| \frac{V}{V_o} \right| = \frac{1}{\sqrt{1 + Q_o^2 \left(\frac{f}{f_o} - \frac{f_o}{f} \right)^2}} \qquad (6.1)$$

where V_o is the response at the resonant frequency f_o and $Q_o = \omega_o CR$. Thus, in Figure 6.14, the inductors and capacitors of the tuned circuits are chosen to resonate at frequencies where an increased response is desired. The variable resistors RV12 and RV14 set the Q_o's of the circuits and hence the shapes of the responses. IC 10 and IC 11 are i.f. amplifiers (MC 1550G) with adjustable gains (RV11 and RV13) and provide the required current sources. Source followers TR23, TR24 and TR25 are inter-stage buffers. This equalising unit, together with the previous time-delay equalisers have a net loss of around 15 dB.

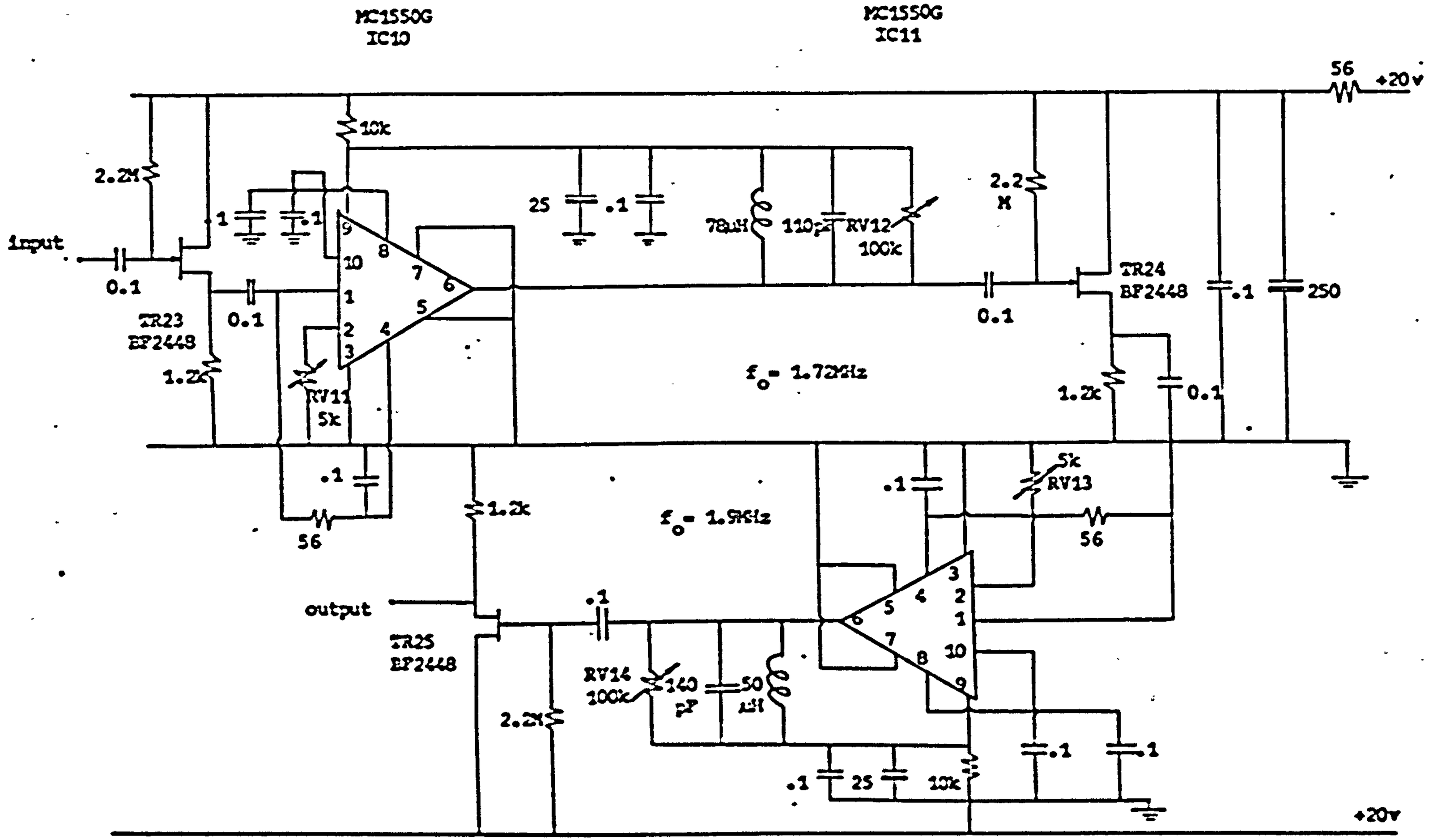

All capacitors in μF unless otherwise stated

Figure 6.14 Amplitude equalisers

6.3.4 Weighting Filter (Figure 6.15)

The equalisers are followed by a Gaussian weighting filter which shapes the output spectrum to reduce sidelobe level to an acceptable value. Equation 3.22 indicates that the heavier the weighting in the spectrum, the more spread out will be the compressed pulse. However, as seen from Equation 3.30, there is a minimum amount of tapering required before a specified level of sidelobes due to truncation effects could be obtained. If a -30 dB truncation level is aimed at, Equation 3.30 shows that a value of 24 dB for D, the attenuation at the edge frequencies, would be sufficient and this was taken as the design figure.

The implementation of this filter presented some difficulties. Initially, the possibility of employing a conventional linear phase (maximally flat delay) filter[88] was investigated. The transfer function of this type of filter may be approximated through the use of Bessel polynomials;[89] the higher the order of Bessel polynomials used, the more constant will be the group delay characteristics for large variations in the frequency response modulus, which then approaches a Gaussian shape. In order to obtain reasonable approximation to a Gaussian shaped response, the order of Bessel polynomials must be at least ten.[90] As a Gaussian filter at band-pass is required, a low-pass to band-pass frequency transformation is necessary. This means that a network having more than ten lossless circuits would have to be employed. Since the Q's of the available inductors were around 80, a realisation of the above lossless network would give a very distorted response. Moreover, the usual low-pass to band-pass transformation gives a frequency response, the modulus of which does not have the necessary symmetry about the band centre,

and the phase of which is no longer linear.[88] In view of these difficulties, this direct approach was abandoned.

The design problem was solved by following Dishal's approach,[91] in which Gaussian magnitude characteristic is approximated and realised through the use of coupled-resonator band-pass circuits with the dissipation of the elements fully taken into account. Furthermore, a tuning and alignment procedure which is essential in the construction of any filter, is available.[92] Since the response shape is Gaussian, the phase characteristic of the filter will be smooth and relatively linear. Its effect on the phase characteristic of the system can easily be compensated.

Two filters were implemented: a 5th order and an 8th order. Since the 8th order, which theoretically approximates the Gaussian response up to the 27 dB point,[91] gave a better performance, it was subsequently employed. The design specifications for it were:

Centre frequency = 1.8 MHz

Unloaded Q of resonators = 100

3 dB down bandwidth = 70.72 kHz

(this corresponds to 24 dB taper at 1.7 and 1.9 MHz respectively)

A loaded-on-both-ends design was used, as the resulting response shape is then less sensitive to element value changes. The nominal circuit values are as shown in Figure 6.15. Plots of relative attenuation and group delay curves are given in Figures 6.16 and 6.17. For comparison, the desired Gaussian characteristic is also plotted in Figure 6.16. Due to the large number of tuned circuits involved, the filter is quite lossy with an attenuation of 26 dB at its centre frequency. Figure 6.18 shows the response of this filter when fed with the linear FM signal from the transmitting unit.

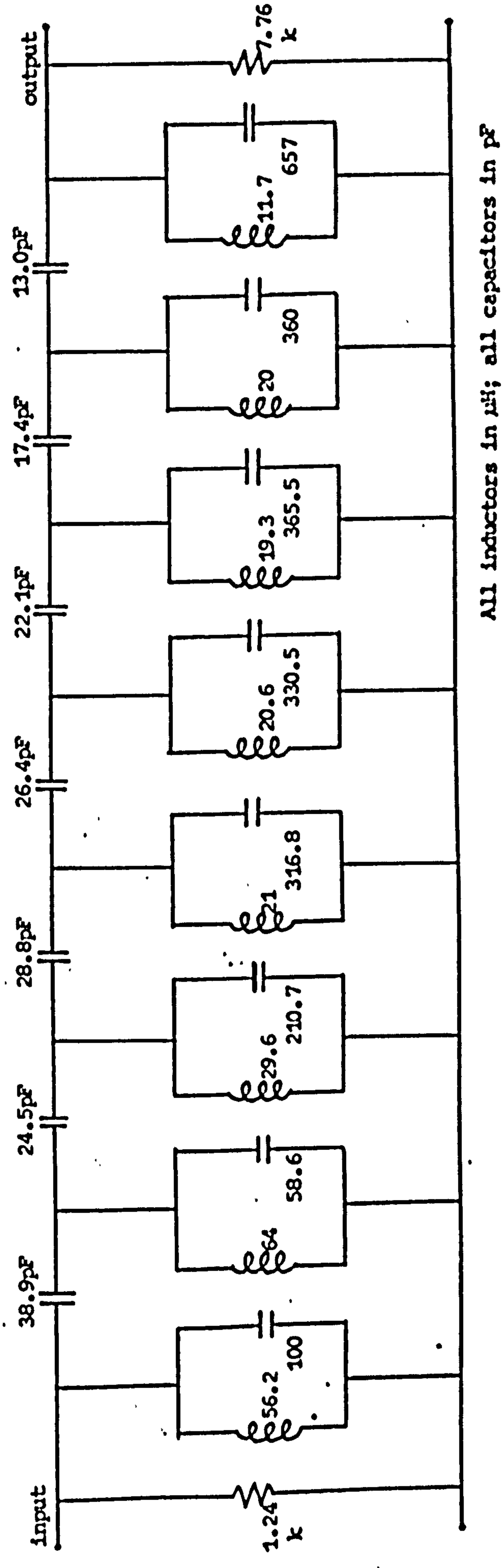

Figure 6.15 Gaussian weighting filter

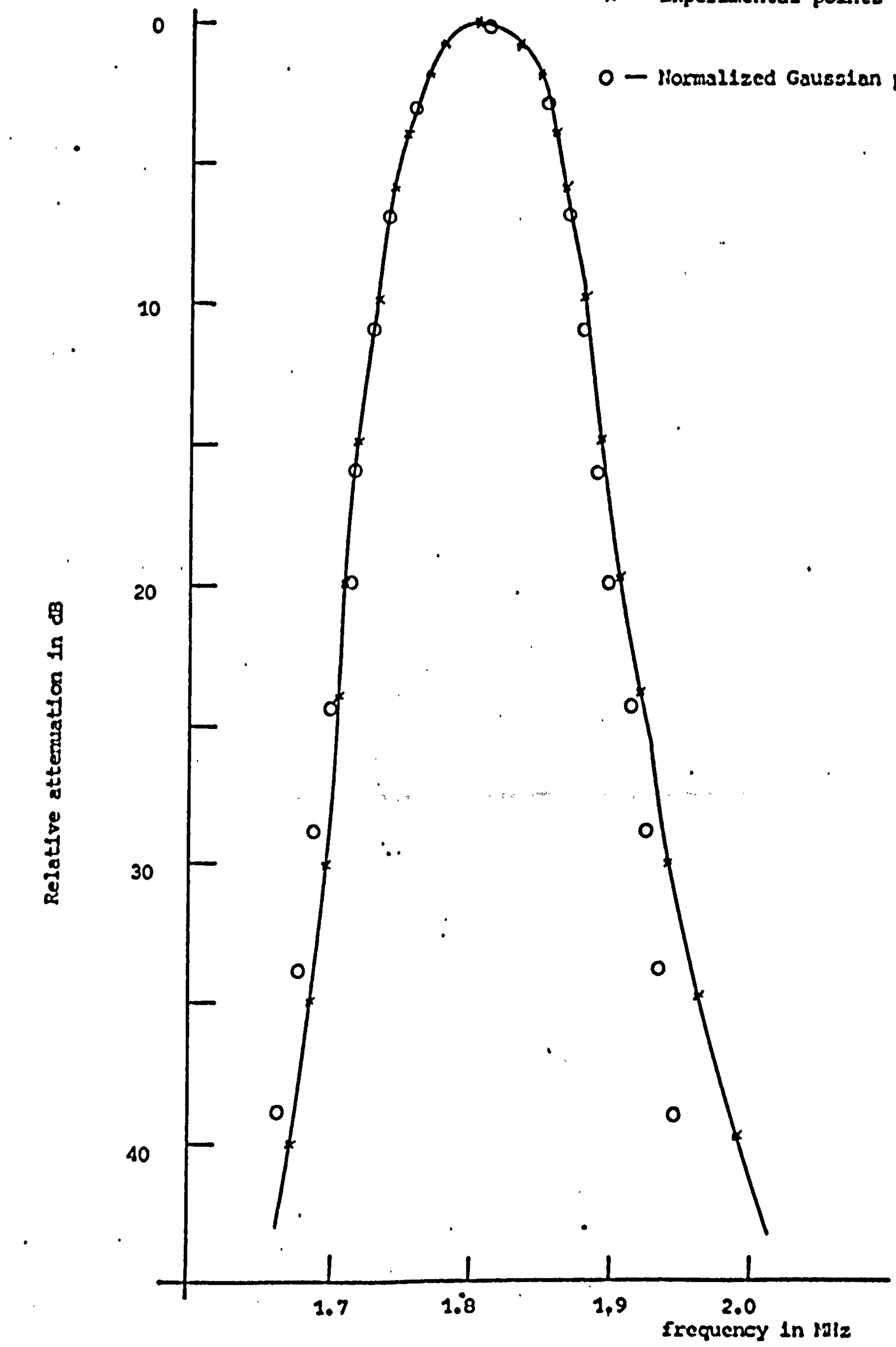

Figure 6.16 Attenuation characteristic of weighting filter

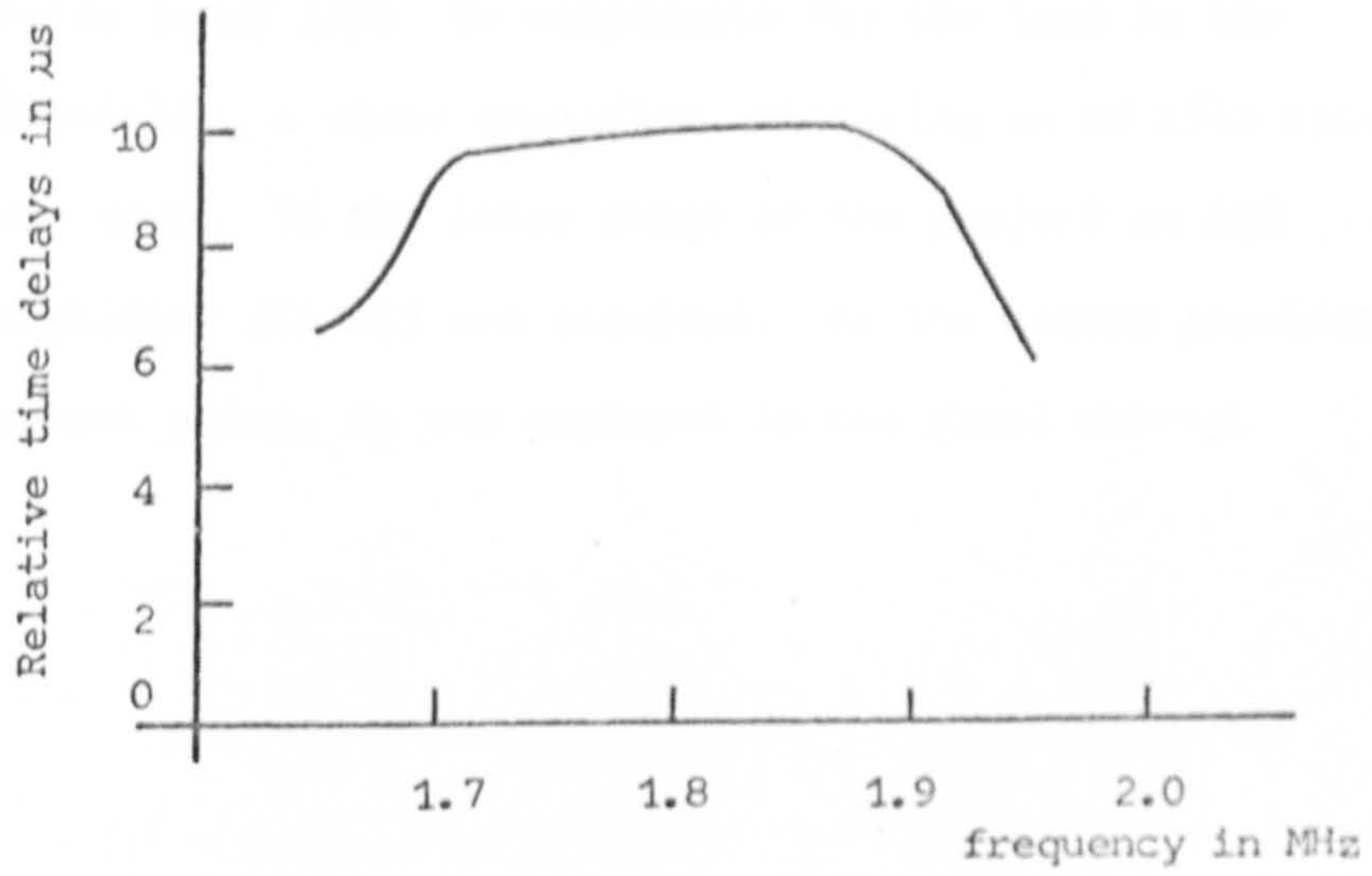

Figure 6.17 Group delay characteristic for the weighting filter

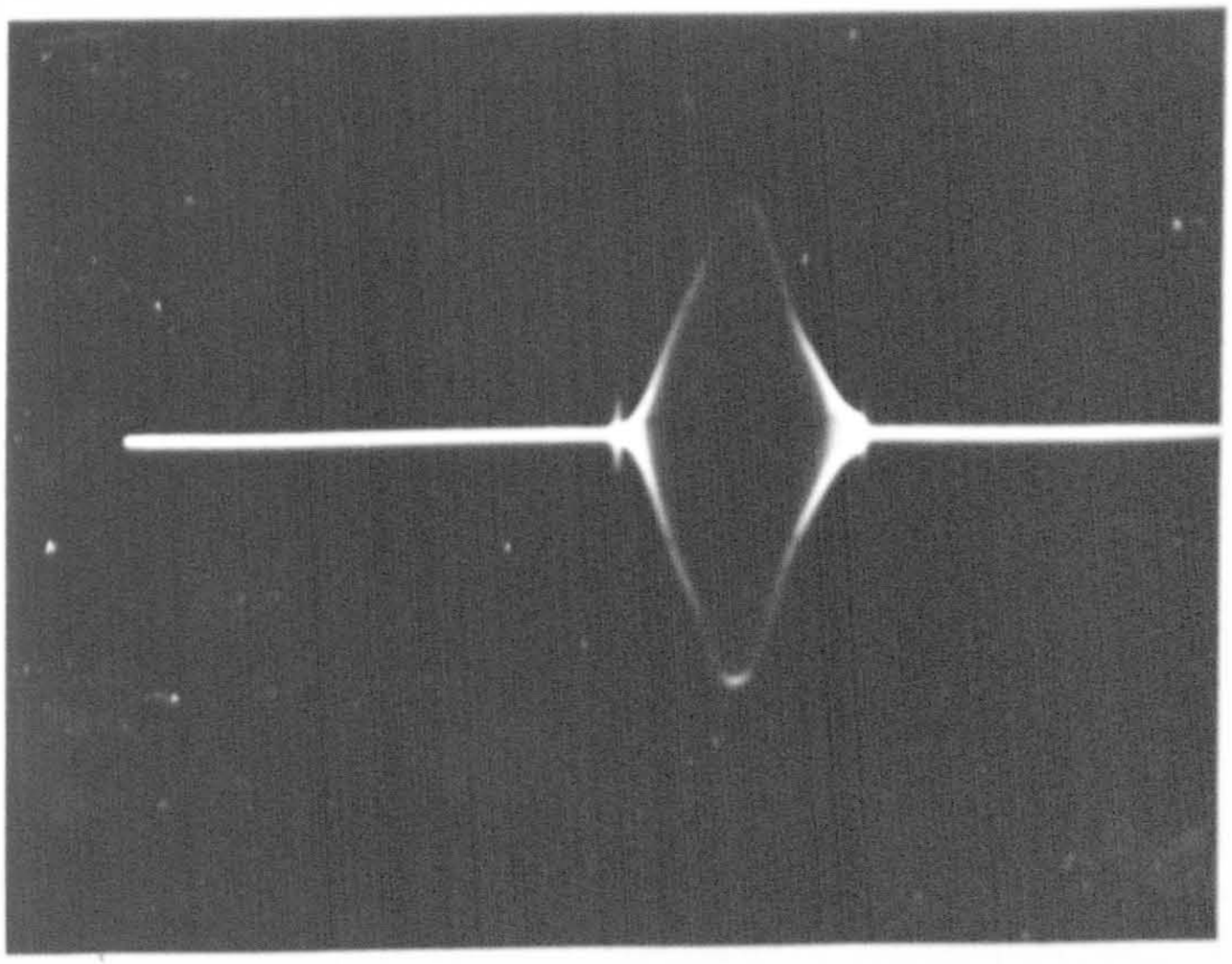

Figure 6.18 Response of weighting filter when fed with linear FM signal from transmitter. Time scale: 200 µs/cm.

6.3.5 Receiver Amplifier

An amplifier is introduced between the weighting filter and the dispersive delay line to compensate for the loss in the system. Initially, a video amplifier, utilising an MC 1510 integrated circuit, was used. In the later stage of the project an AIM wideband amplifier ACA 123 was acquired. As the latter provides a larger output swing, it was employed in the final set-up.

CHAPTER 7

EQUALISATION

Results in Section 3.5 stressed the importance of time delay linearity and overall response flatness in the system. From the measured performance of the delay line and the transducers, it was obvious that equalising circuits had to be introduced.

7.1 Measurement of Time Delay Errors

Before time delay compensation could be proceeded with, a precise measurement of the time delay errors in the delay line, as well as in the whole system, is a prerequisite. From Section 3.5.2 it is noted that the measuring instrument must be capable of measuring time delay of up to 0.1 μs accuracy. As the nominal mean delay in the delay line is of the order of 1 ms, a 0.1 μs accuracy in the delay measurements calls for a precision of 0.01%. Conventional methods which generally involve the calibration of an oscilloscope time base by time markers, fail to give the required accuracy on account of the long nominal delays encountered in the measurements, and a special measuring set-up must be devised.

The pi-point method was first investigated. In this method, the exact frequencies where the phase shifts in the delay device are successive integer multiples of π radians, are measured. The time delay is defined by:

$$t(f) = -\frac{1}{2\pi}\,\frac{dB(f)}{df} \qquad (7.1)$$

where B(f) is the transfer phase characteristic of the device.

If at frequency f_1 the phase shift is $n\pi$ radians and at frequency f_2 the phase shift is $(n+1)\pi$ radians, then the time delay may be approximated as:

$$t(f_{12}) = \frac{1}{2\pi} \quad \frac{(n+1)\pi - (n\pi)}{(f_2 - f_1)}$$

$$= \frac{1}{2(f_2 - f_1)} \qquad (7.2)$$

Since the frequencies f_1 and f_2 may be conveniently determined through Lissajous figure measurements, the simplicity of the method recommends itself. However, in order to measure up to 0.1 μs delay accuracy, Equation 7.2 shows that the difference between f_1 and f_2 must be determined up to seven significant digits, and at the frequencies of interest, (around 1.8 MHz), this implies that readings up to 0.1 Hz must be taken. As such stable oscillators (0.1 ppm) were not available, this approach was abandoned.

The method employed is basically an adaptation of May's method.[93] The set-up is as shown in Figure 7.1. It consists essentially of a stable signal generator, a pulse generator, a low-pass Gaussian filter and a balanced multiplier. The pulse generator delivers a narrow pulse into the low-pass filter and produces a Gaussian envelope, which subsequently modulates the r.f. output of the signal generator to obtain a Gaussian r.f. pulse through the use of the balanced multiplier. Since the output pulse has a Gaussian envelope, it has a defined bandwidth and preserves its shape on passing through the delay line. By applying both the delay line input and

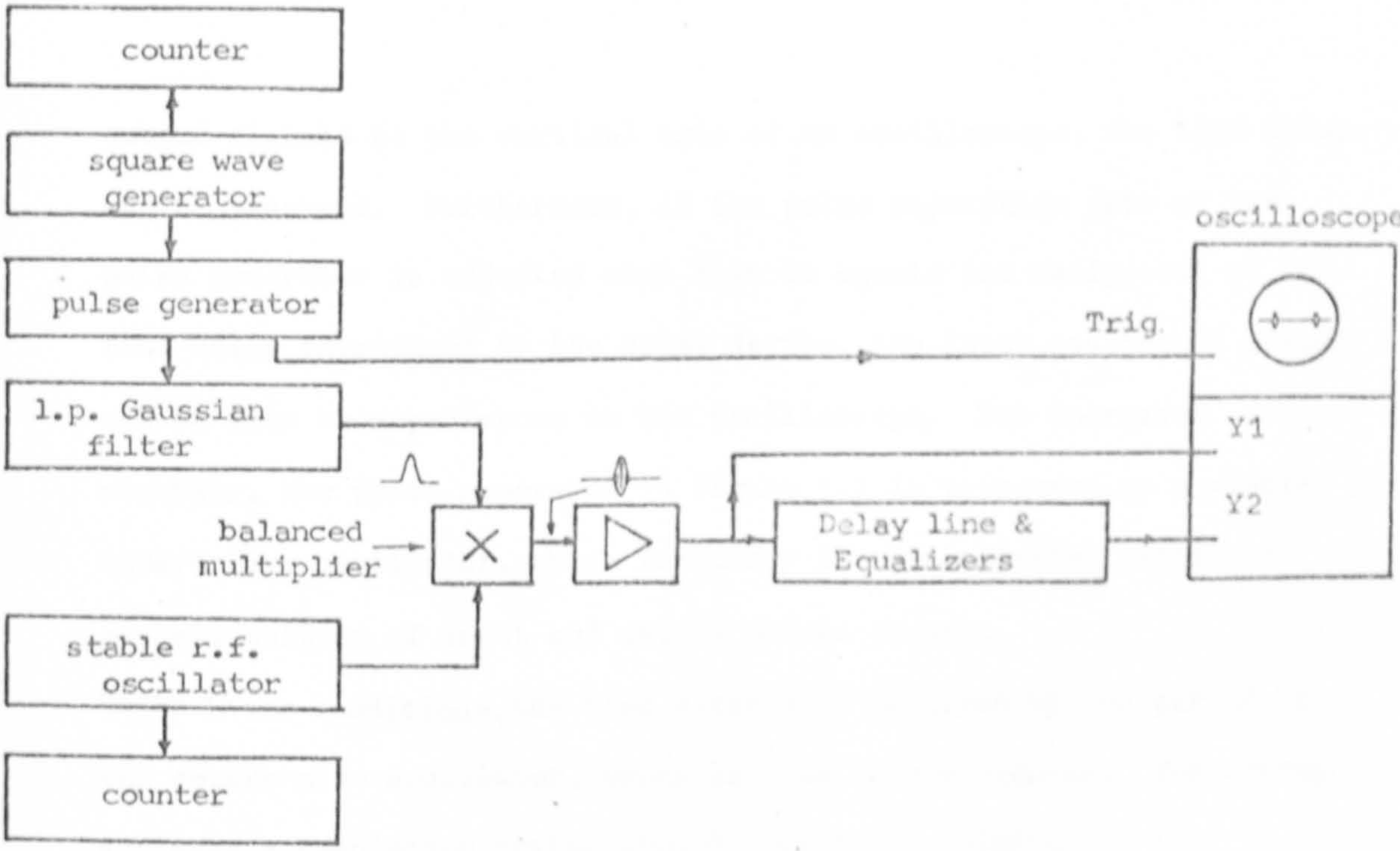

Figure 7.1 Set-up for time delay measurements

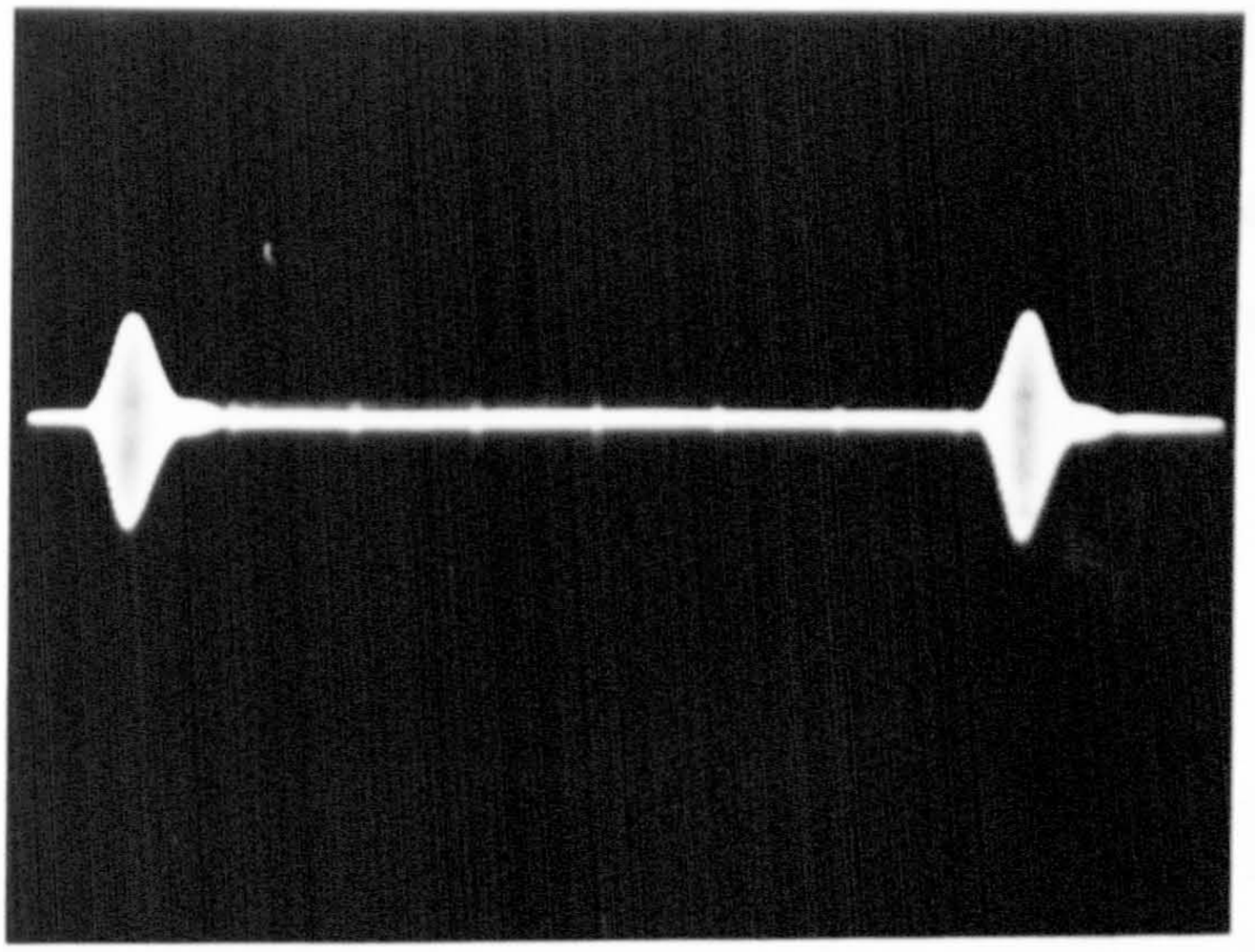

Figure 7.2 Quasi-Gaussian envelope r.f. test pulses

Time scale : 200 µs/cm

output signals to the vertical axis of an oscilloscope, the time delays can be measured. Furthermore, if the pulse repetition rate of the pulse generator is adjusted such that it equals the reciprocal of the time delay introduced by the delay device, the input and output pulses can be made to superimpose on the oscilloscope. For increased accuracy, the pulse generator in Figure 7.1 is triggered by a stable square-wave oscillator, whose frequency is then adjusted until the superimposition of input and output pulses occurs.

Under these conditions, the time delay will be given by the period of the square-wave oscillator, which is read from a counter. The set-up achieves a resolution better than 0.1 μs and is limited by the precision to which the superimposition of input and output pulses can be determined. A picture of the quasi-Gaussian r.f. pulses used is shown in Figure 7.2. Figure 7.3 shows the circuit details of the balanced multiplier which utilises an integrated circuit SG 2402. In Figure 7.4 the circuit elements for the low-pass Gaussian filter are shown. A 5th order low-pass Gaussian filter design having an impulse response of around 200 μs duration was employed. This long envelope pulse ensured that the resultant r.f. pulse would have a bandwidth of less than 10 kHz. Other design parameters for this filter are:

Unloaded Q of inductors = 100

3 dB bandwidth, BW_{3dB} = 2.85 kHz

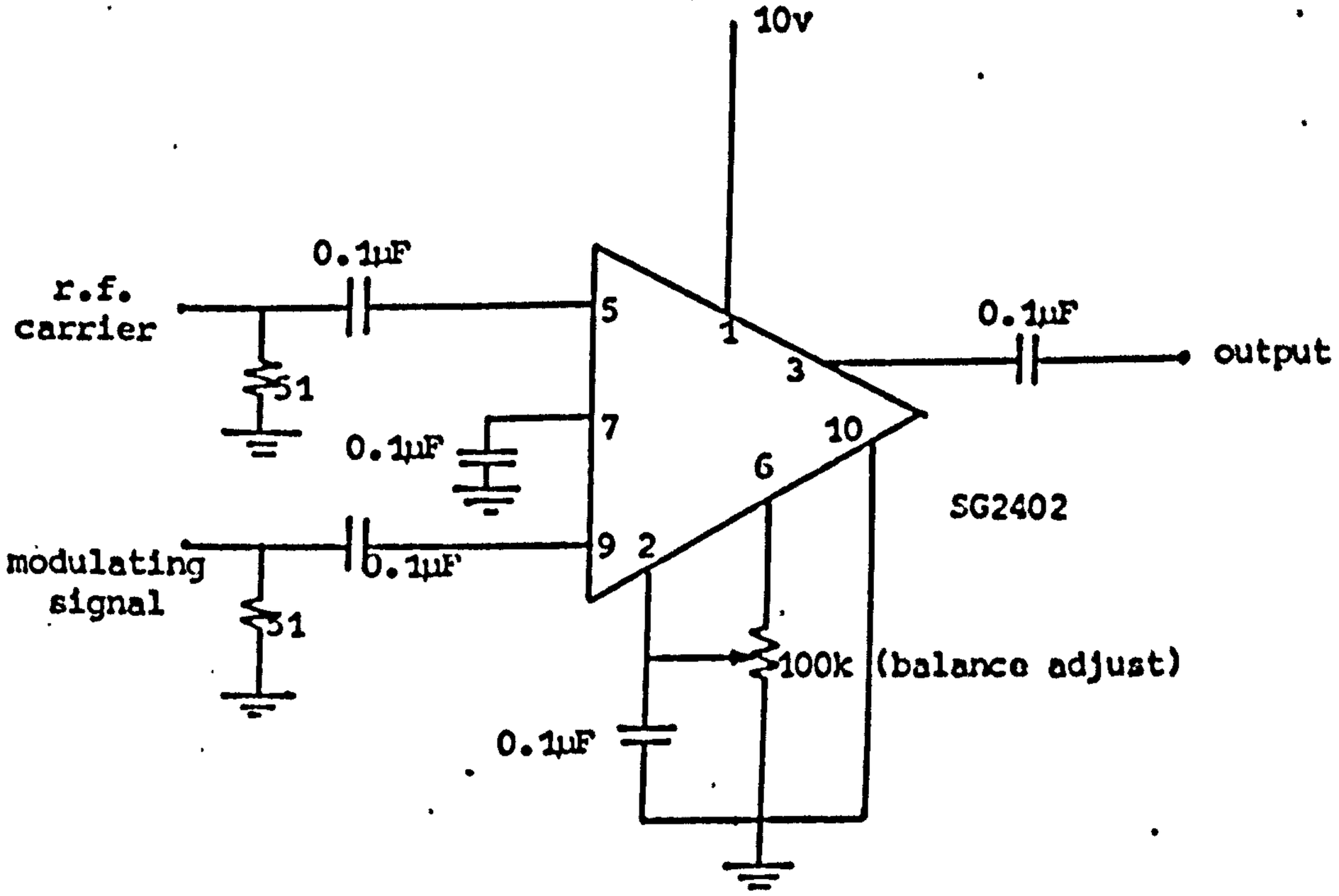

Figure 7.3 Balanced multiplier

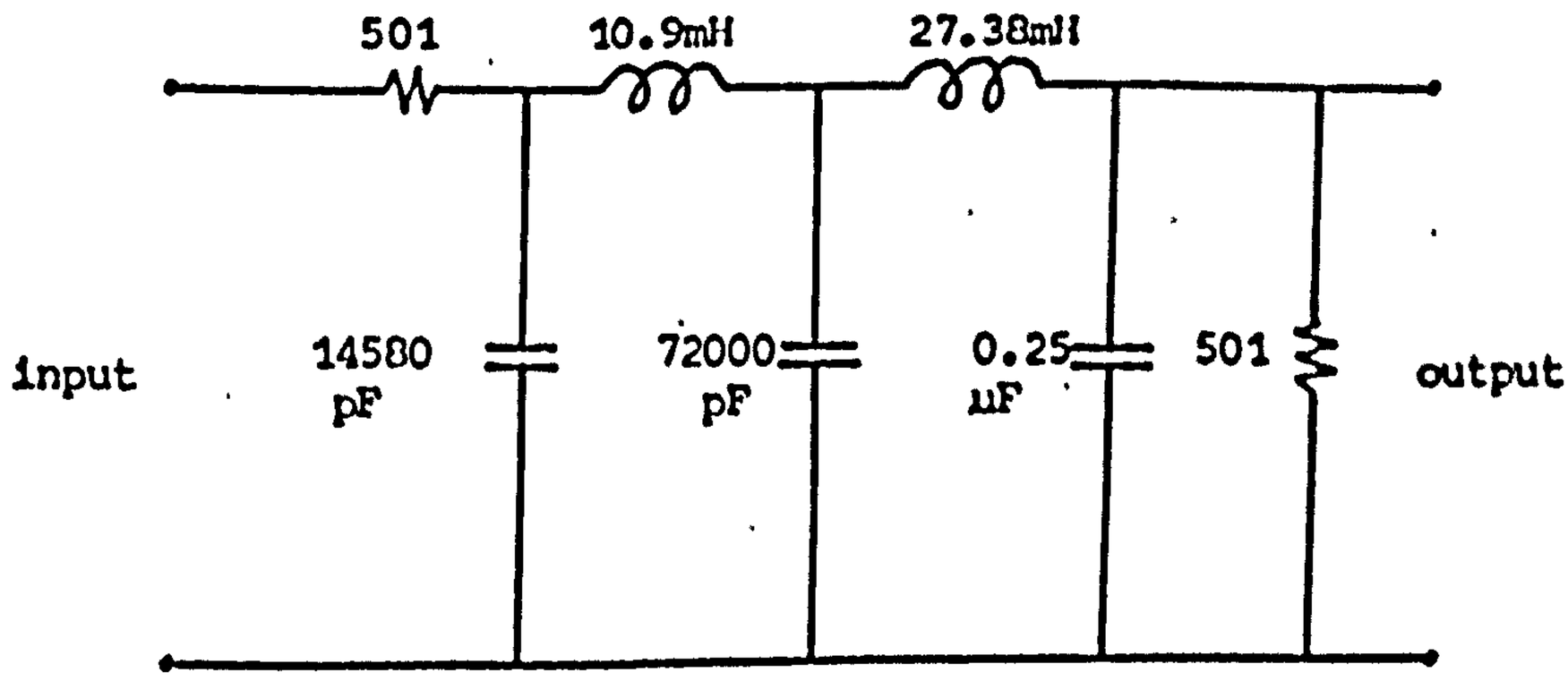

Figure 7.4 5th order Gaussian low-pass filter

7.2 Equalisation Procedure

7.2.1 Design Curves for Equalisers

To facilitate the design of equalisers, design curves for both the time delay and amplitude correcting networks were developed.

As mentioned in Section 6.3.2 all-pass bridged-T networks were employed to correct for the time delay errors. From Equation D.15 in Appendix D, the group time delay for a single bridged-T network is approximately given as:

$$t_d = \frac{2}{\sigma_o} \quad \frac{1}{1 + \left(\frac{\omega - \omega_o}{\sigma_o} \right)^2} \qquad (7.3)$$

The peak delay occurring at $\omega = \omega_o$ is $\frac{2}{\sigma_o}$, and the expression can be plotted for different peak delay values. A set of such delay curves is shown in Figure 7.5. It should be noted that since the peak delay is the only determining parameter in the delay curve, the centre frequency of the design will not affect the shape of the curve once the peak delay has been chosen. These curves provide a basis for combining a number of such curves, staggered at different centre frequencies, to obtain a composite error correcting curve. Once the proper combination of peak delays and their associated frequencies have been set, the components of each bridged-T section can be evaluated from Equations D.2 to D.6 in Appendix D.

Design curves for the amplitude equalisers were also developed. These equalisers consist of tuned amplifiers (Section 6.3.3) with responses given by Equation 6.1. This equation can be plotted for different values of Q_o (Figure 7.6). By inserting a number of these tuned amplifiers having different Q_o's and gains at various frequencies,

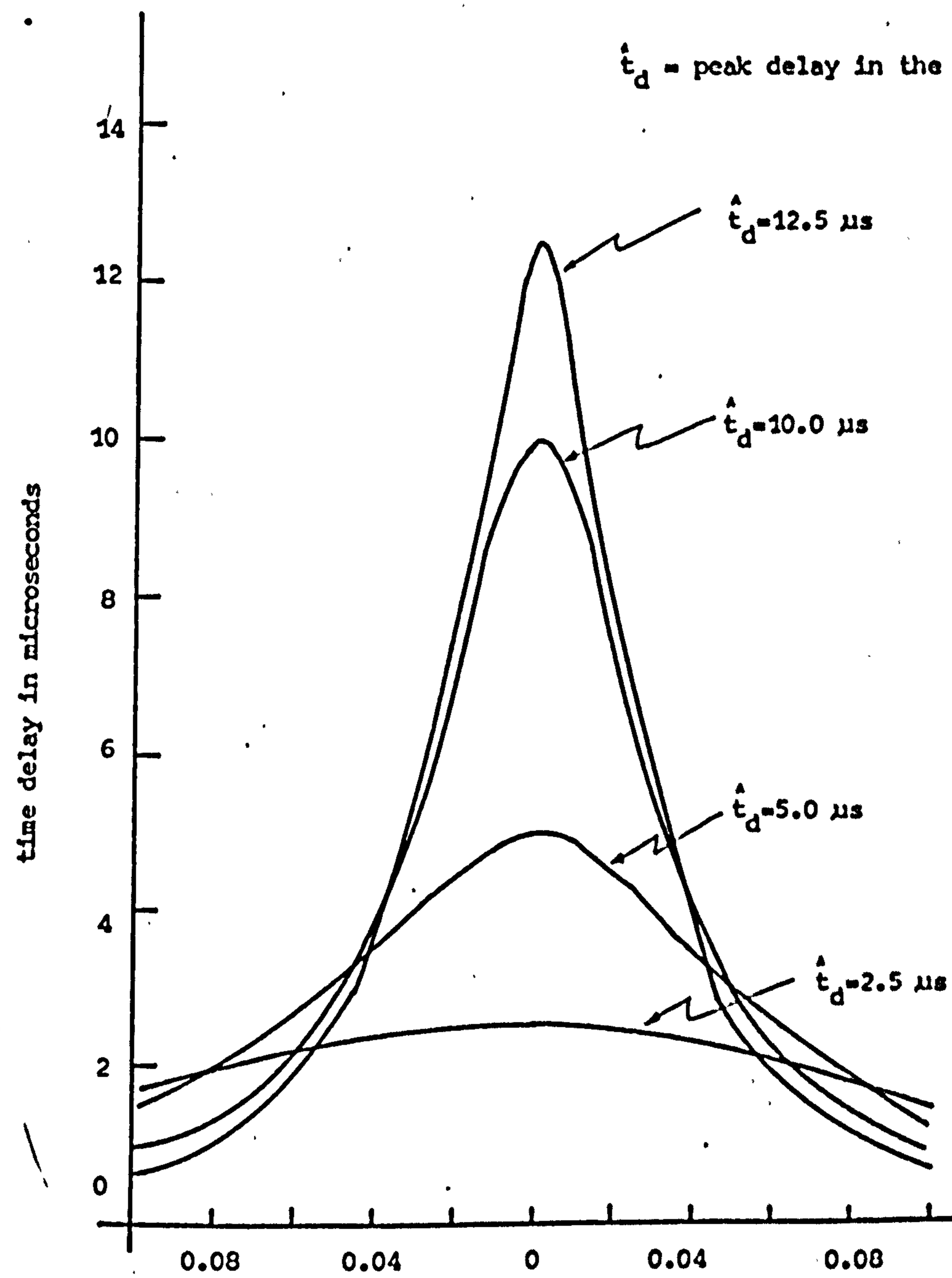

Figure 7.5 Standard time delay curves for bridged-T sections

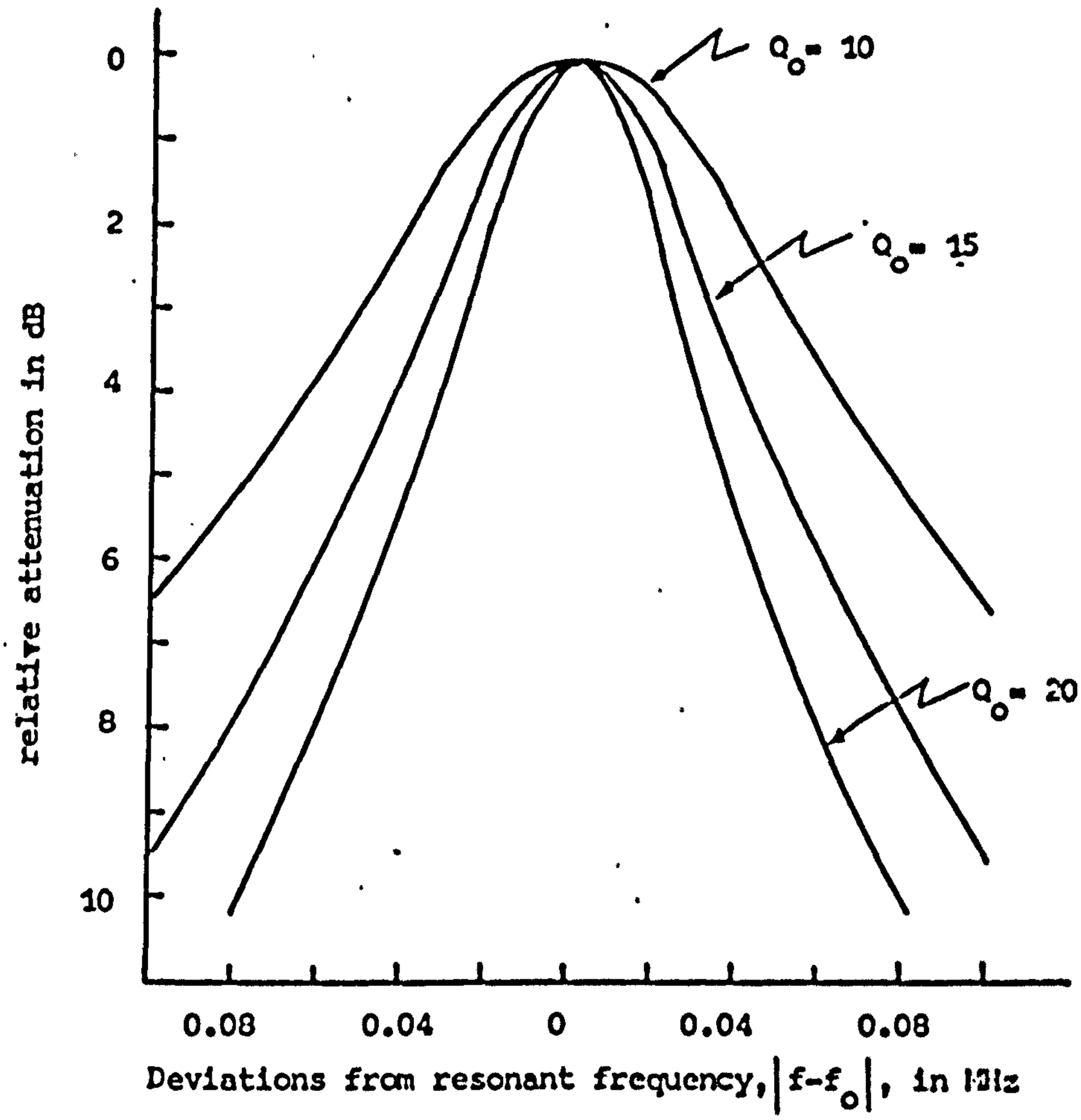

Figure 7.6 Frequency response of tuned circuits

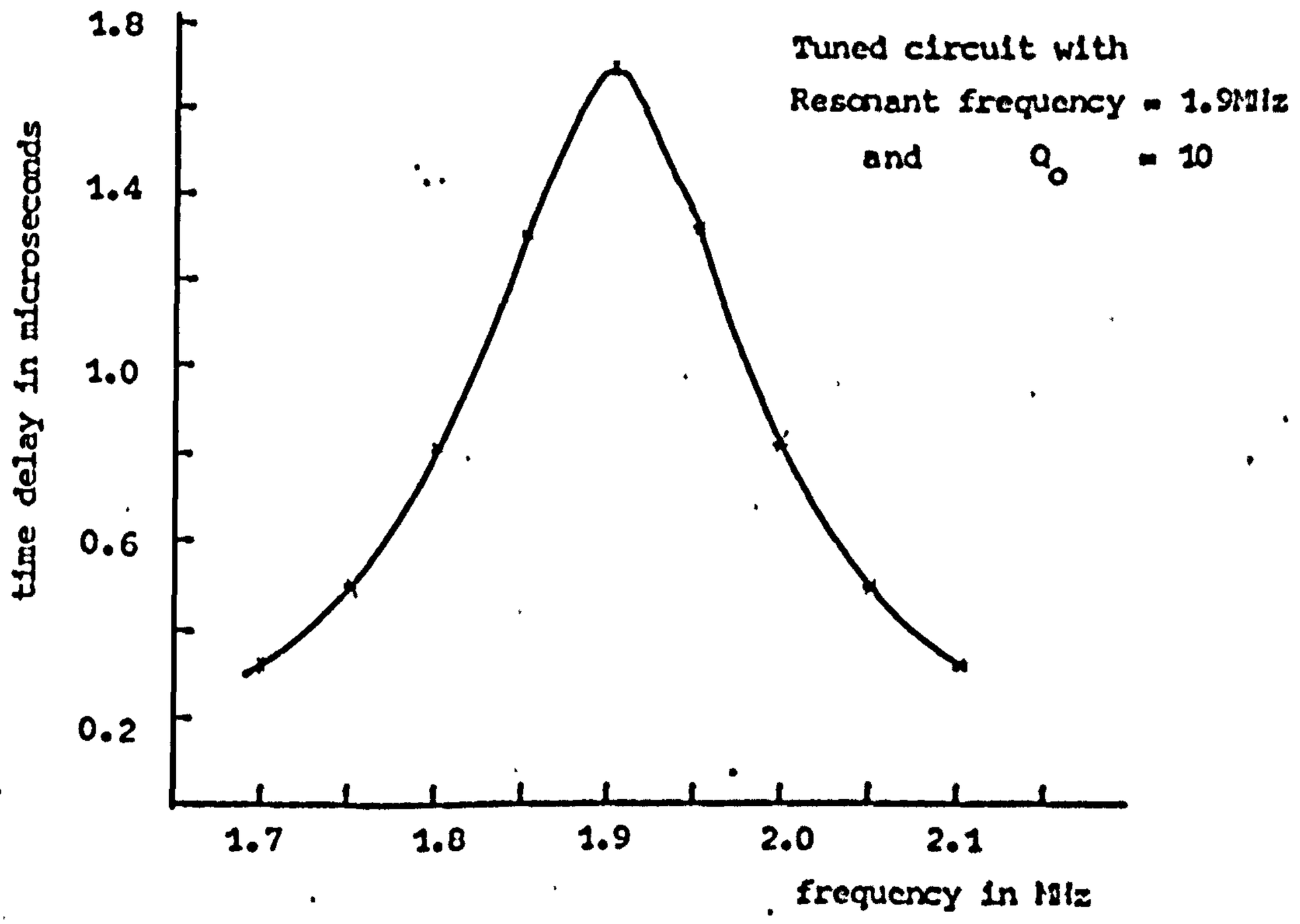

Figure 7.7 Theoretical time delays introduced by one of the amplitude equalizers

compensation in the amplitude response can be effected. However, it must be pointed out that these amplitude correcting networks will influence the delay error curve and will have to be taken into account in the delay error correction procedure. In fact, the group delay introduced by a single amplitude equaliser can be derived, since its phase shift function, B, is:(87)

$$B = \tan^{-1}\left[-Q_o\left(\frac{f}{f_o} - \frac{f_o}{f}\right)\right]$$

$$t_d(f) = -\frac{1}{2\pi}\frac{dB(f)}{df}$$

$$\pm \frac{1}{\pi}\frac{Q_o}{f_o}\cos^2 B \qquad (7.4)$$

Figure 7.7 shows a calculated delay curve for one of the amplitude equalisers employed and illustrates the typical variations in time delays caused by the network.

7.2.2 Steps in Equalisation

The equalisation process can be summarised in the following steps:

(a) A time delay error curve over the frequency band of interest (1.7 - 1.9 MHz) for the dispersive delay line (Figure 7.8) was first established. This was done by obtaining an accurate delay measurement and plotting the difference between the measured delay curve and the least-square-fit linear curve, to the measured delay points.

(b) Delay equalisers were introduced to compensate for these delay errors. A complementary error correction curve was generated (Figure 7.9) from the delay error curve and, utilising the design curves in Figure 7.5, delay equalisers were then designed. It

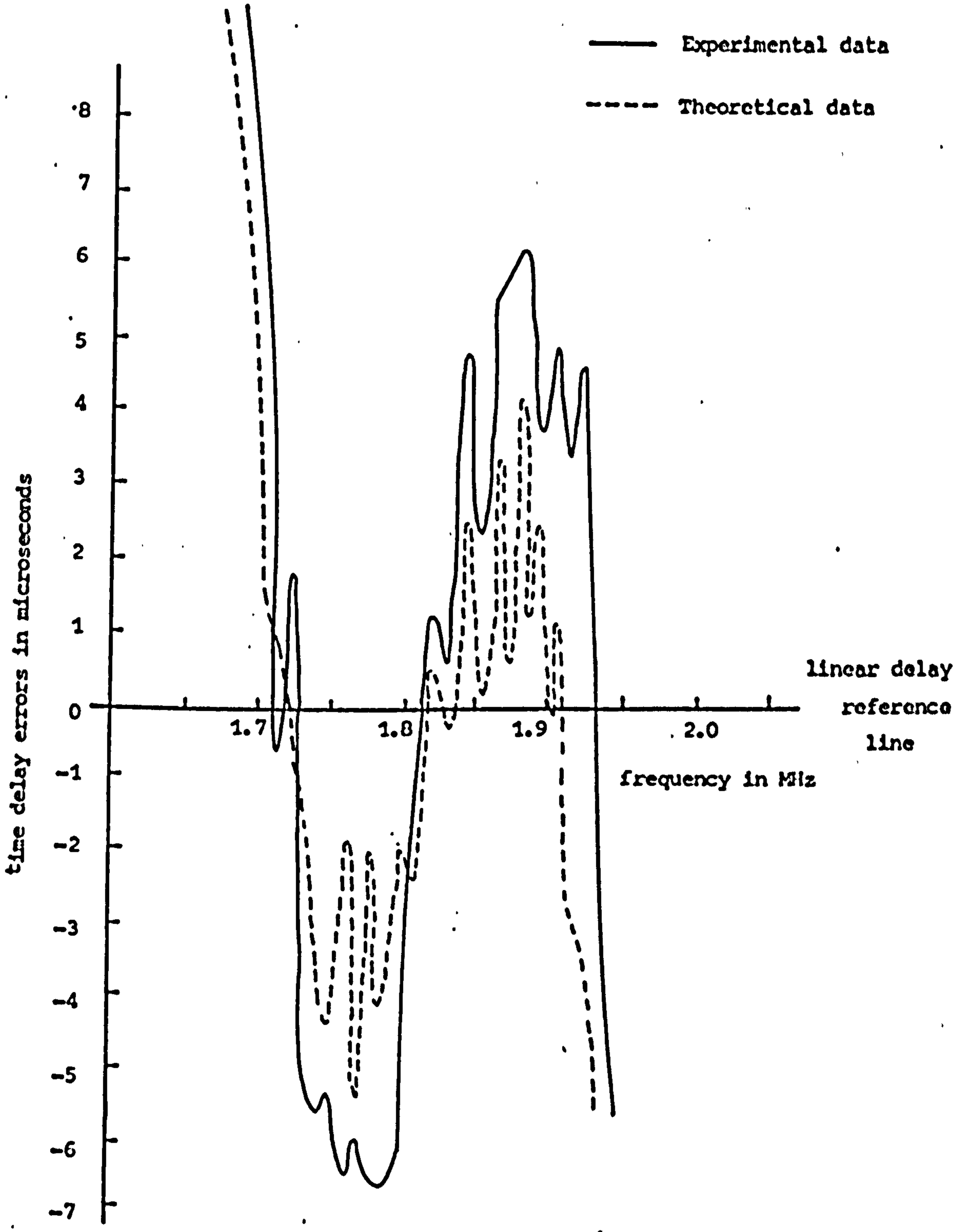

Figure 7.8 Experimental and theoretical time delay error curves for the dispersive delay line

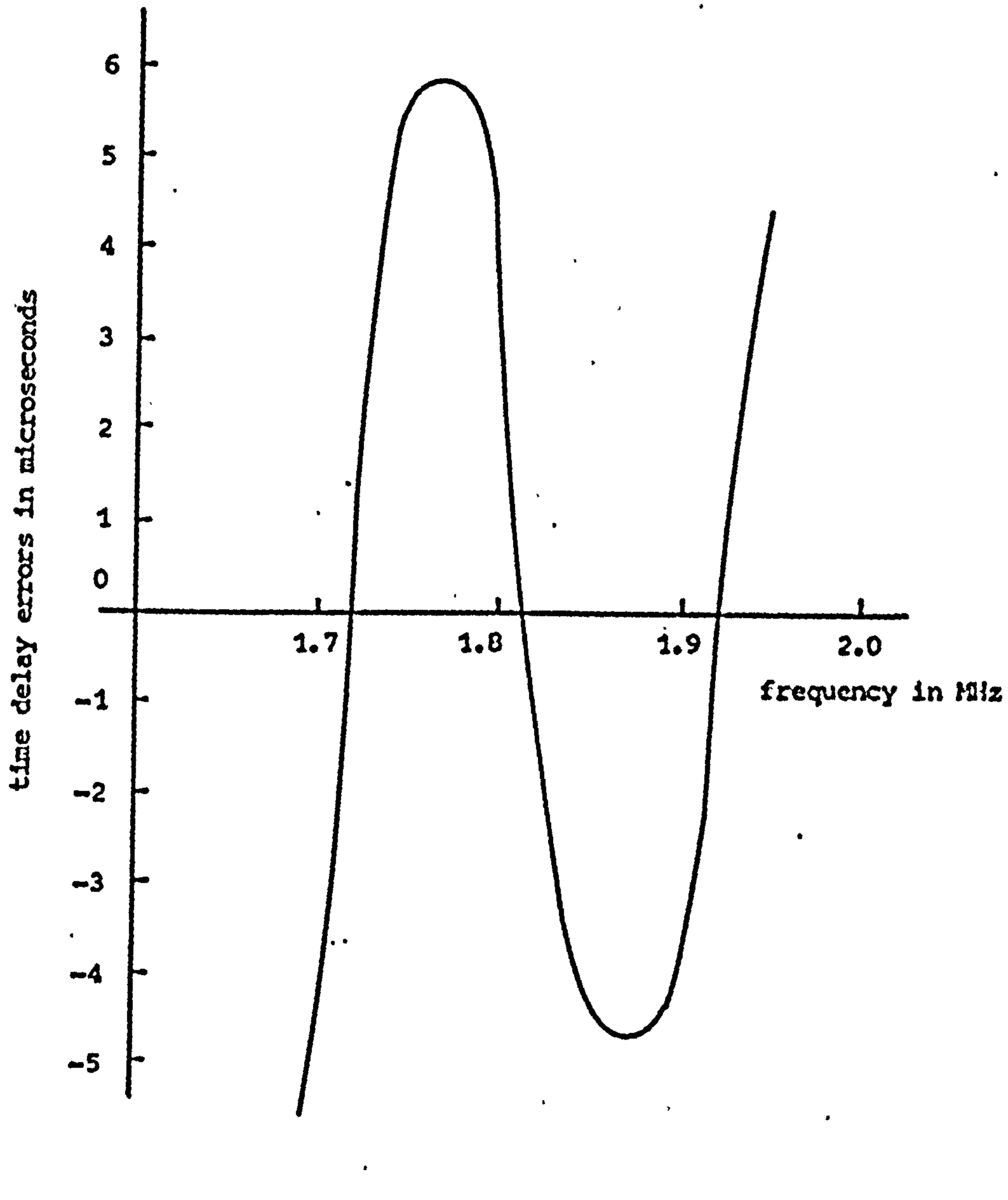

Figure 7.9 Smoothed error correcting curve for the delay line

was found that three bridged-T sections with peak time delays of 10, 10 and 12.5 μs, and centre frequencies at 1.74, 1.79 and 1.95 MHz respectively, would approximate the desired curve. These sections were inserted into the system and properly aligned.

(c) An insertion loss curve for the whole receiving system, including the transducers and the delay equalisers, but excluding the Gaussian filter, was experimentally taken (Figure 7.10). Amplitude equalisers were then designed with the help of the design curves in Figure 7.6. Two amplitude equalisers with Q_o = 15 and 10, and f_o = 1.72 and 1.9 MHz respectively, were found to equalise the response reasonably well.

(d) The time delay equalisation process was repeated, but this time the compensation was extended to the complete receiving system. The resultant error curve was given in Figure 7.11. Three more bridged-T networks with peak delays of 5,5 and 7.5 μs, and design frequencies at 1.745, 1.815 and 1.93 MHz, were then introduced for this compensation.

(e) The whole system (transducers plus the receiver) was re-examined to ascertain that deviations in both time delay and amplitude response characteristics were within acceptable limits. Repeated measurements and adjustments were carried out to obtain an optimum performance. The resulting time delay and insertion loss curves are as shown in Figures 7.12a and 7.12b. The reference linear delay characteristic used in Figure 7.12b has a slope of 2100 μs per MHz.

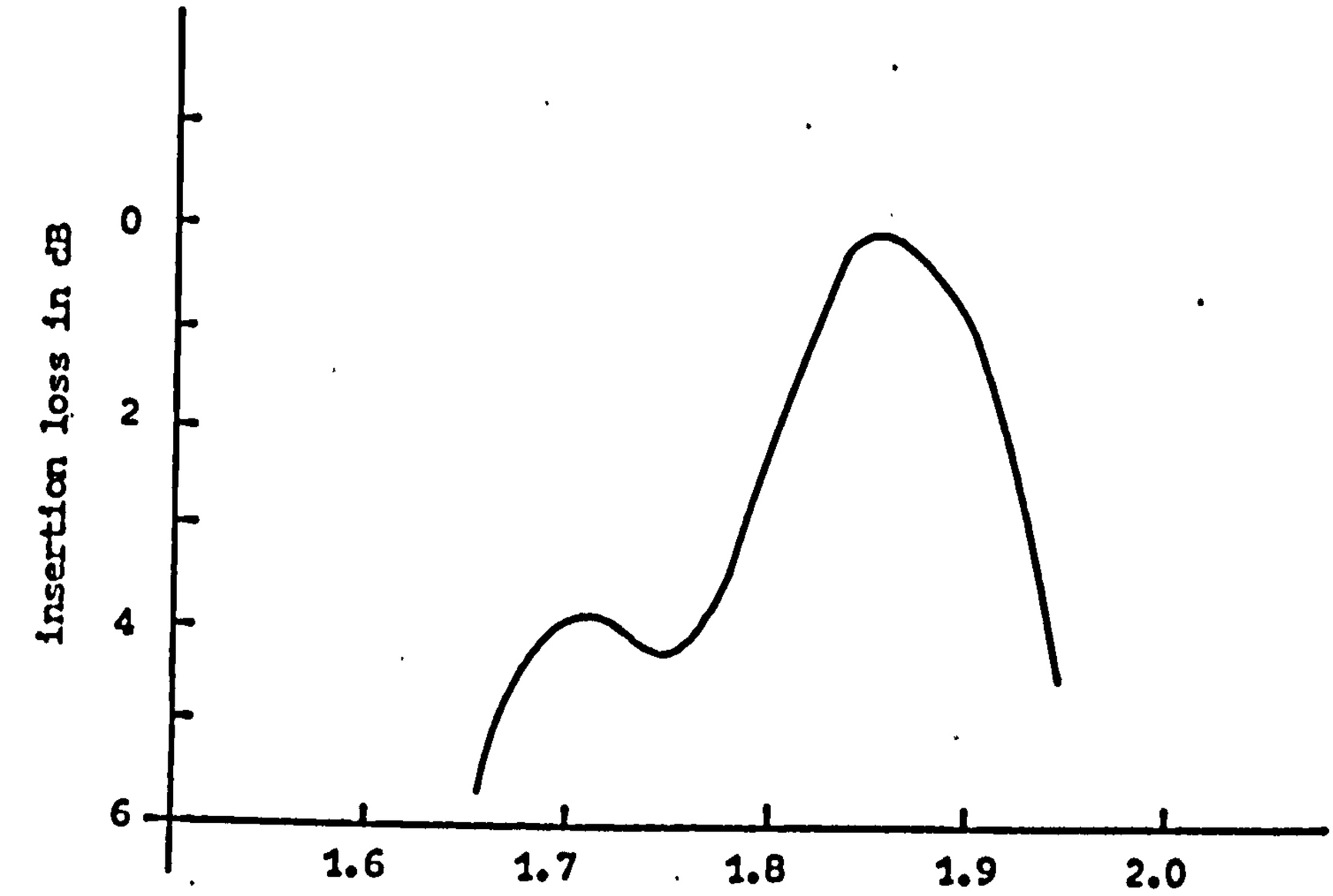

Figure 7.10 Insertion loss curve for the receiving system before amplitude equalization

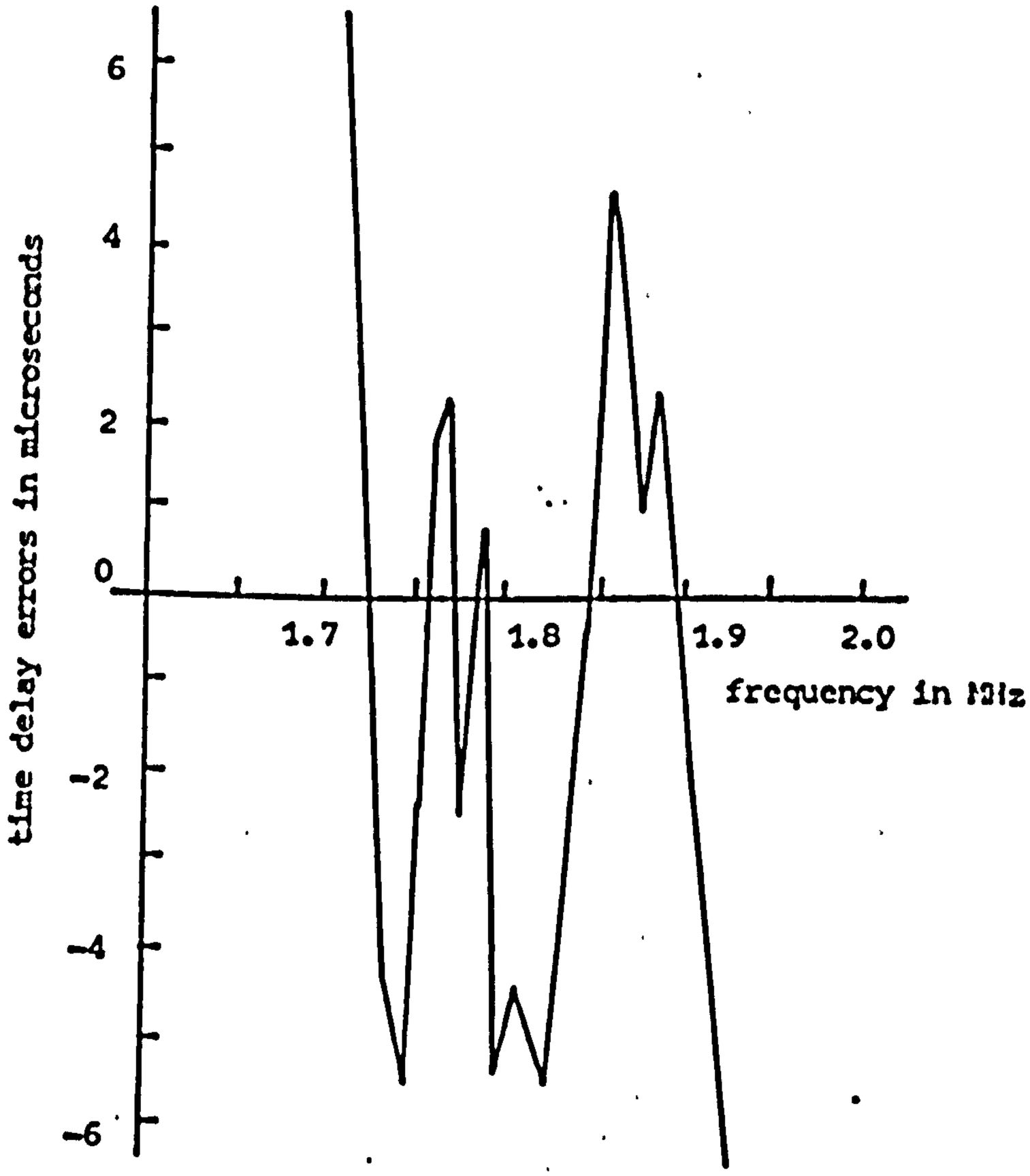

Figure 7.11 An intermediate delay error curve

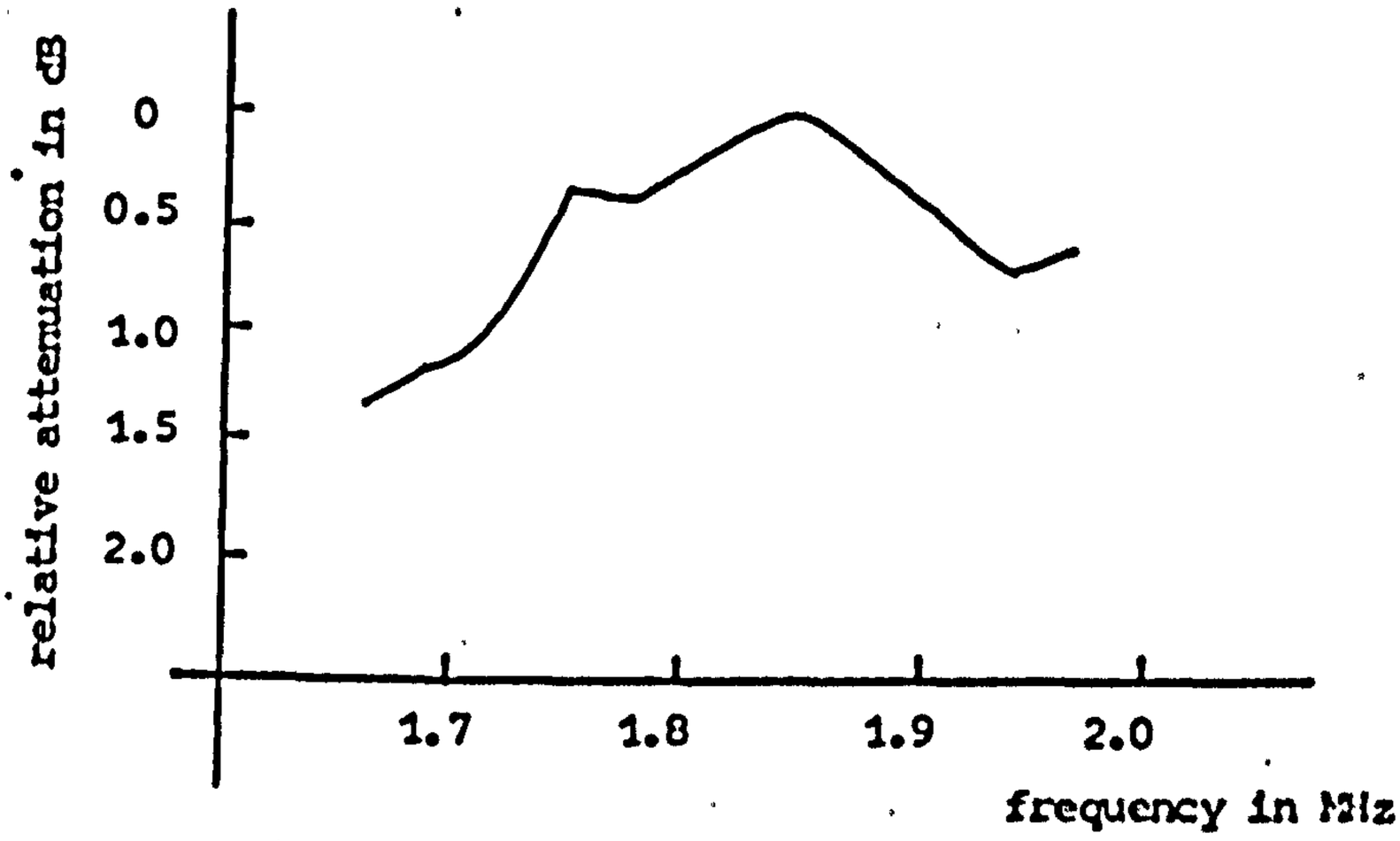

Figure 7.12a Final amplitude response of the system

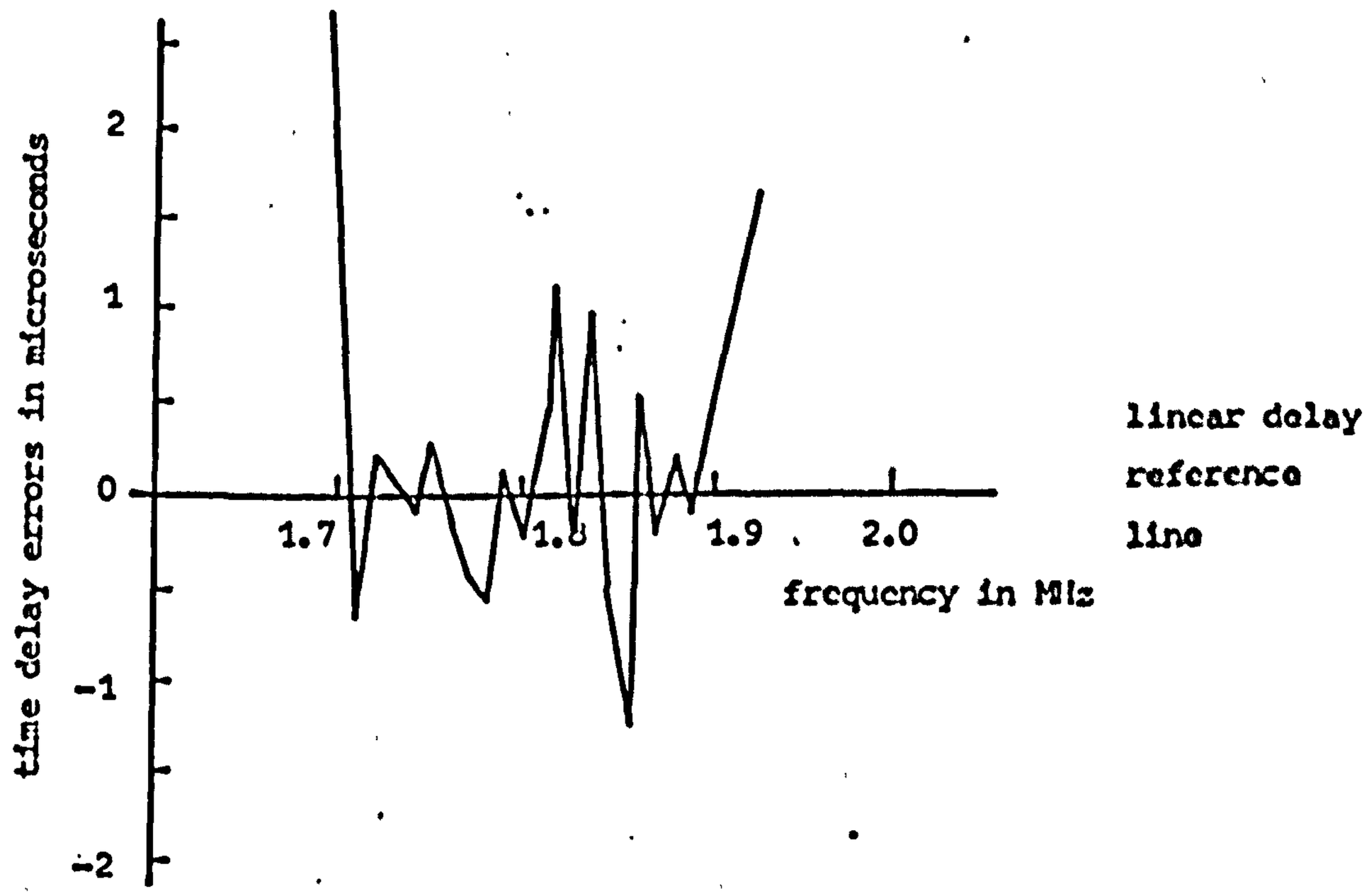

Figure 12b Final delay errors in the system

7.3 Discussions on Equalisation

(a) It is interesting to note that the measured delay error curve for the delay line agreed well with the theoretical error curve obtained from the programming results in Section 4.2.2. For comparison's sake, the latter was also plotted in Figure 7.8.

(b) The approach outlined relies heavily on measurement techniques. In fact, the ultimate limits of the compensation process are set by the precision to which the delay errors, amplitude variations or the component values for the equalisers, can be measured.

(c) An important source of inaccuracies in the compensation process was the implementation of the delay equalisers. Apart from the inexactitude of the design procedure, their realisation was plagued by practical problems. To introduce the required long time delays, large capacitances (12,000 pF) were needed in the bridged-T networks. At the system frequencies, these large capacitors became relatively lossy and gave low Q-factors, (of the order of 50). Consequently, the practical delay equalisers had delay values falling short of the designed ones. Moreover, they exhibited amplitude variations. Fortunately, in the final stage of compensation smaller capacitors, having more reasonable values of Q, could be used in the shorter time delay equalisers, which were then more predictable in performance. This eased the final error correcting procedures considerably.

(d) Theoretically, the required cascade of bridged-T networks could be computed from Equation 7.1 to produce the exact composite error correcting curve. However, on account of the non-ideal behaviour of the available components, this was not done and simple engineering judgements based on the design curves were applied. Similarly, a tuned amplifier as amplitude equaliser was chosen in preference to a conventional constant resistance amplitude correcting network; the tuned amplifier has a response that can be easily adjusted and possesses a more defined time delay characteristic.

(e) The interdependence of the time delay and amplitude responses in the practical equalisers not only increased the tedium in the compensation process, but also rendered it difficult to reduce residual delay errors to extremely low values. Nevertheless, Figures 7.12a and 7.12b demonstrate that a system delay error within ± 1 μs was obtained with a corresponding amplitude response maintained flat to within ± 0.5 dB. It is also seen that the number of cycles of the delay error function had been deliberately kept large. Since the peak phase error, which is the most important parameter in the delay distortion analysis, is inversely related to the error ripple rate, the results obtained satisfied the specifications laid down in Section 3.5.

CHAPTER 8

OPERATION OF THE PULSE COMPRESSION SYSTEM

In this chapter the actual operation of the pulse compression system is demonstrated. Test results using the system are presented.

8.1 Demonstration of Pulse Compression

The system was connected up as illustrated in Figure 6.1, with the transducers immersed in a water tank lined with absorbent material. Initially, a through transmission arrangement was employed. A photograph of the experimental set-up is shown in Figure 8.1.

The transmitter unit was first adjusted to give the correct swept pulse. From Section 7.2.2, the dispersive delay slope of the receiving system is obtained as 2100 μs/MHz. Since an operating bandwidth of 200 kHz is desired, the pulse length was set to 420 μs. A swept rate corresponding to the reciprocal of the dispersive delay slope was then set with a centre frequency at 1.8 MHz. The output spectrum of the FM pulse, when examined on a spectrum analyser (Hewlett Packard 8553), was found to resemble the theoretical plot in Figure 3.2, and this confirmed the proper working of the transmitting unit. In order to effect a perfect match with the receiver, final alignments were made after the complete system had been set up.

Figure 8.2 shows both the received long FM pulse and the corresponding short compressed pulse. The photograph was taken during the preliminary setting-up process and weighting had not been introduced. It can be seen that pulse compression was effected, though the resulting sidelobe levels were excessively large (Figure 8.3). When the complete system was properly set up, these sidelobes were

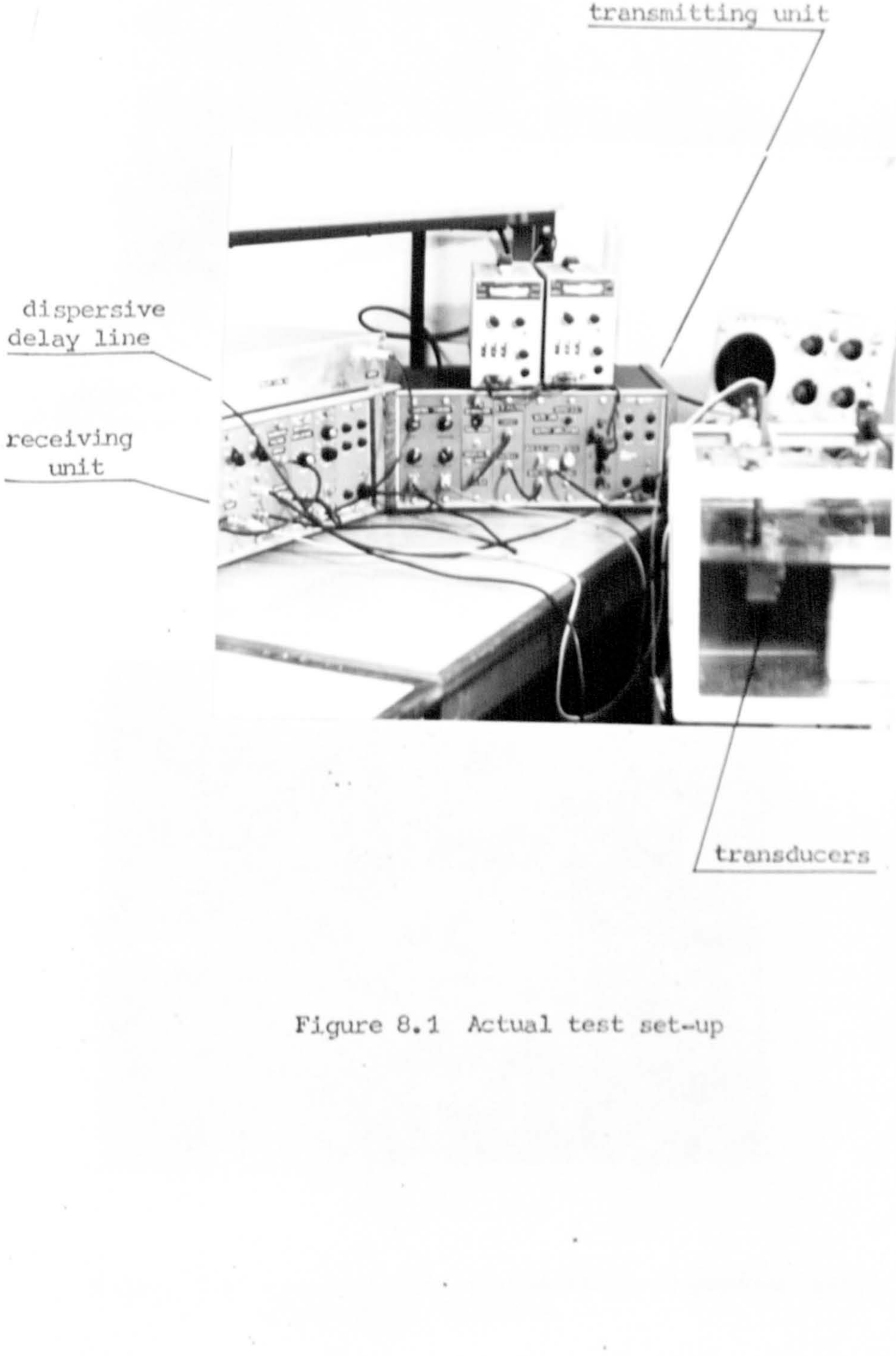

Figure 8.1 Actual test set-up

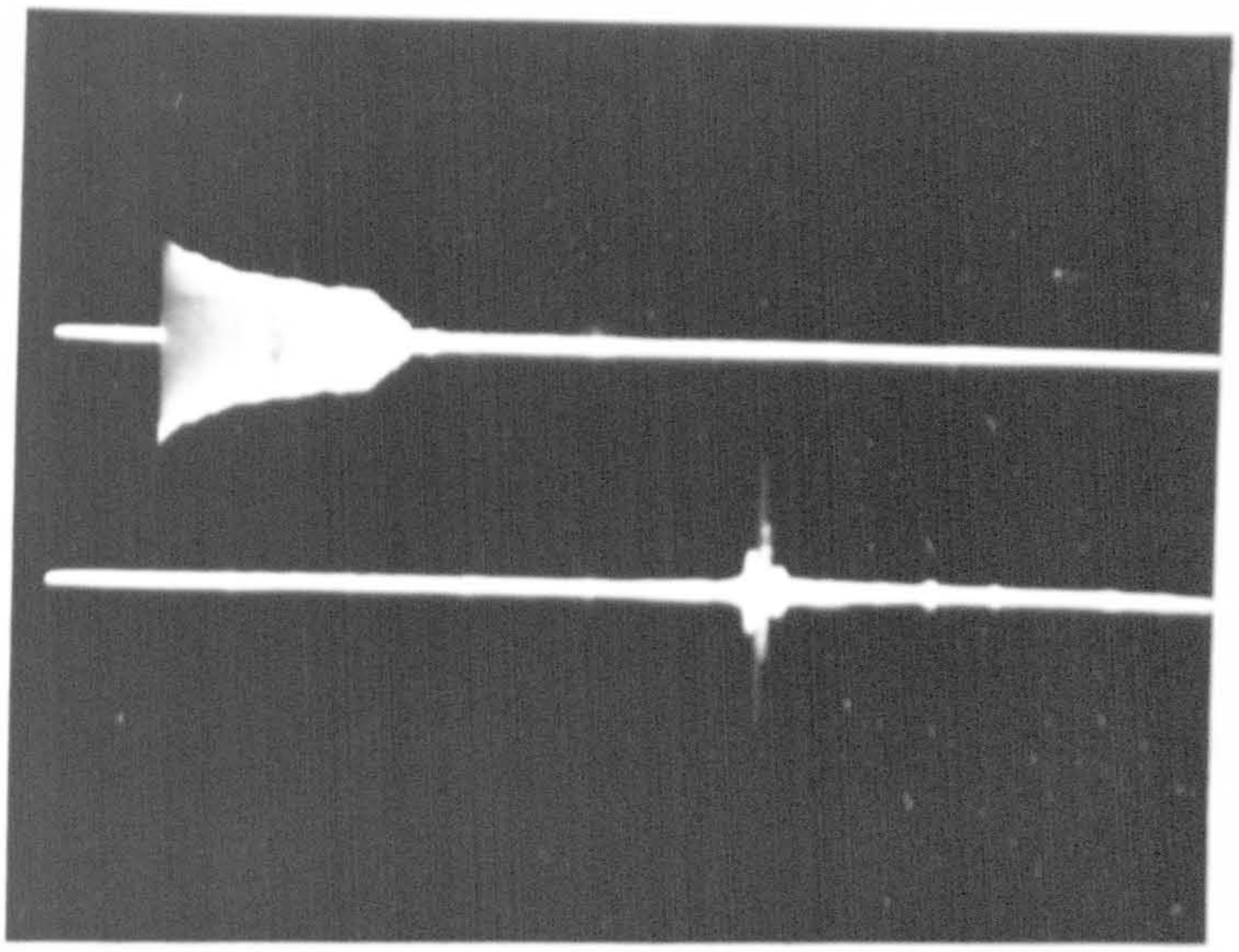

Upper trace shows the long received pulse at the receiving transducer.
Lower trace shows the compressed output pulse. Time scale: 0.2 ms/cm.

Figure 8.2 Demonstration of pulse compression at a preliminary stage of experimentation

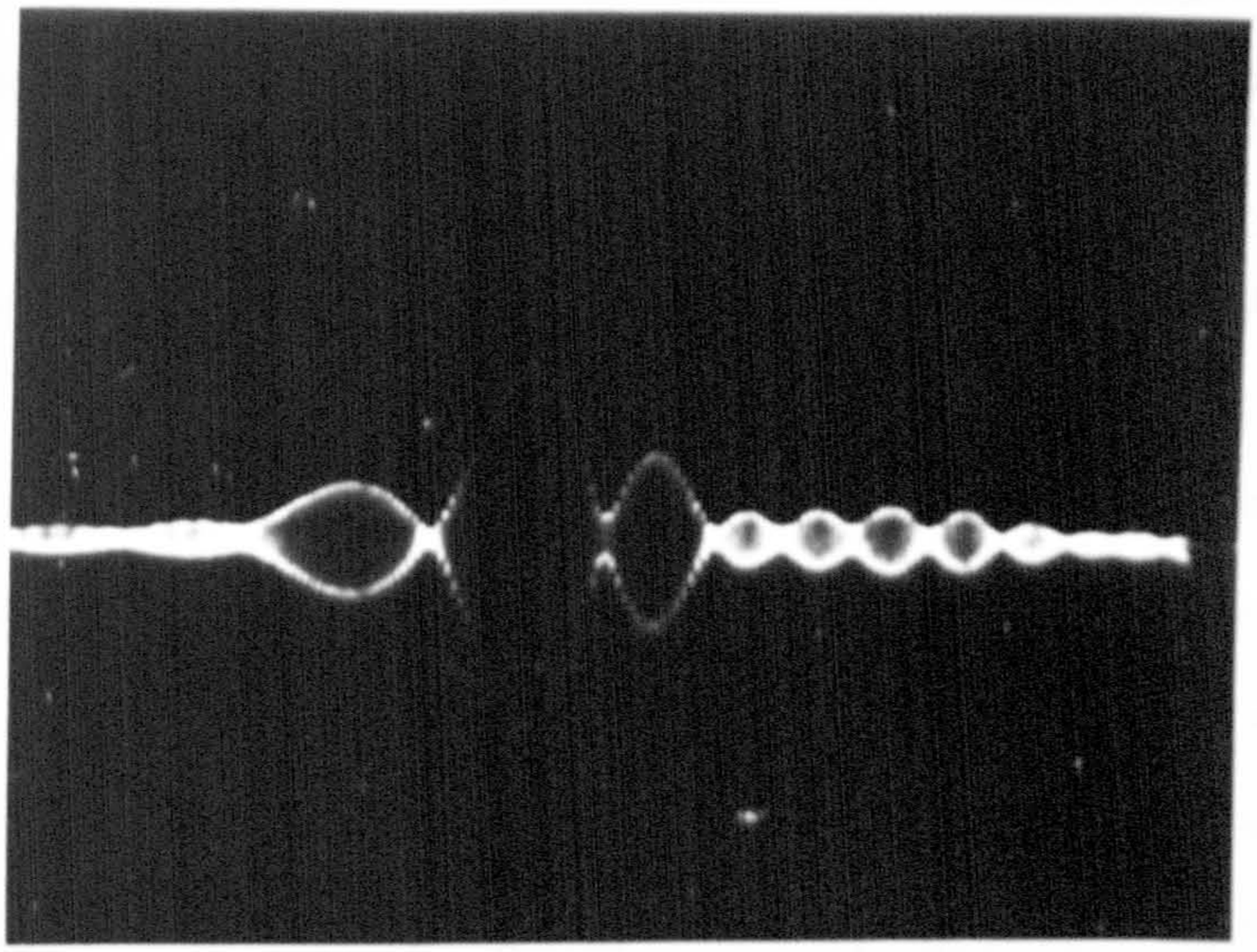

Figure 8.3 Expanded view of the above compressed pulse
Time scale: 10 μs/cm.

duly suppressed. Figure 8.4 shows the final output pulse, where sidelobes are of the order of - 25 dB. A magnified view of the output pulse showing the details of sidelobes is given in Figure 8.5.

8.2 Measurements on the System

(a) System delay

The delay of the compressed pulse was measured to be 1144 μs from the start of the received long pulse. Due to the addition of equalisers and other system blocks, this delay is longer than the centre frequency delay of the dispersive delay line, which is 1133 μs.

(b) Signal-to-noise ratio

The signal-to-noise ratio of the receiving unit was determined with the help of a General Radio type 1383 noise generator (Figure 8.6). Noise from the noise generator was bandlimited to 400 kHz, centred at 1.8 MHz with a band-pass filter and then applied to the transmitting transducer. The level of noise was set at a value of 200 mV, which was at least 20 dB above the noise in the receiving unit. The input swept signal was added to the noise through an attenuator. By adjusting the latter, the signal was made just visible in noise on an oscilloscope. The oscilloscope was then transferred to the output terminals of the receiving unit and the input signal level was attenuated until the output compressed pulse was again just visible in noise. The attenuator reading was found to be 18 dB. Allowing for the fact that the input noise bandwidth was 400 kHz rather than 200 kHz, the improvement in signal-to-noise ratio was then corrected to 15 dB.

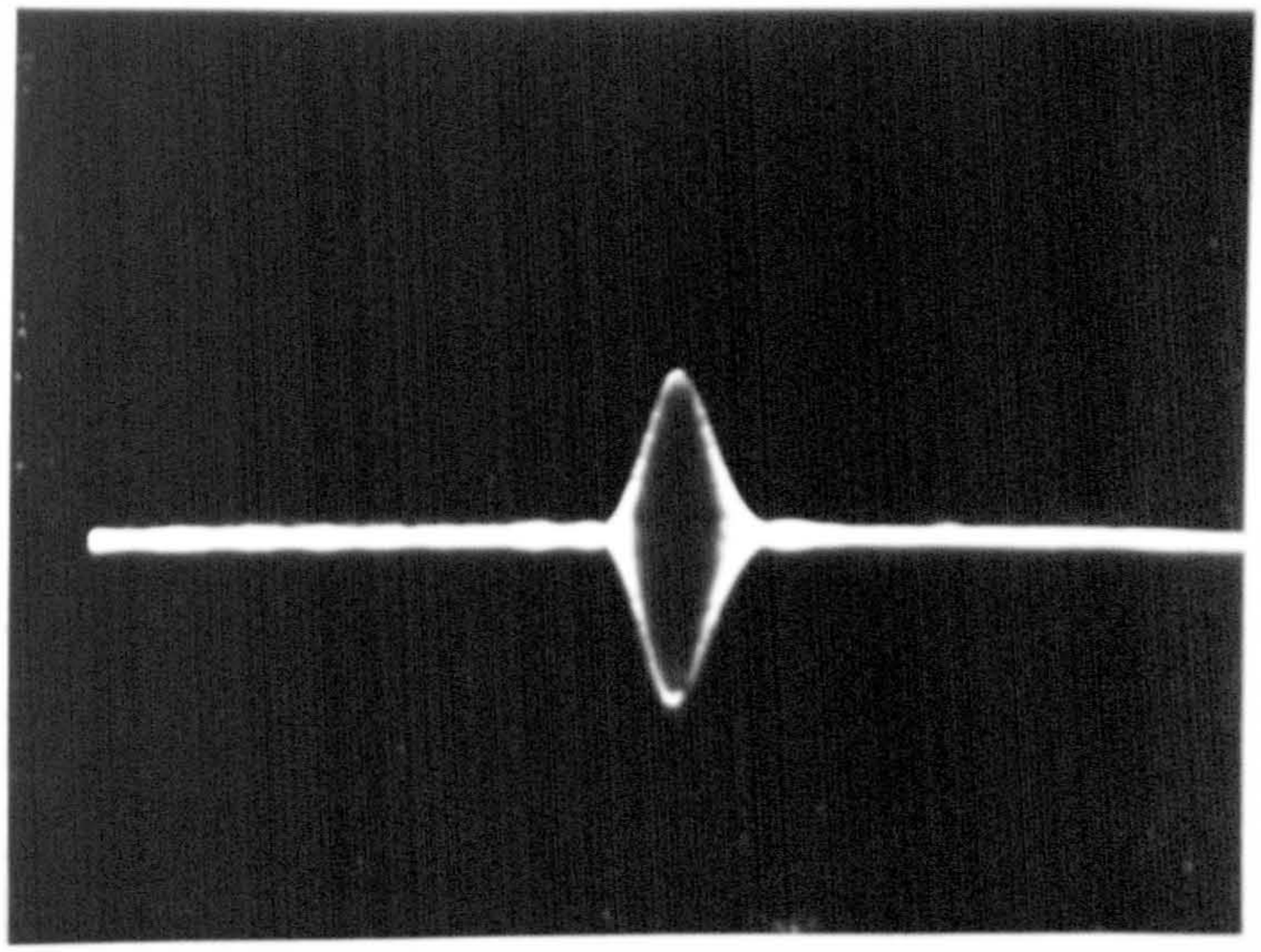

Figure 8.4 The final weighted compressed pulse. Time scale: 20 μs/cm. Vertical scale: 100 mV/cm.

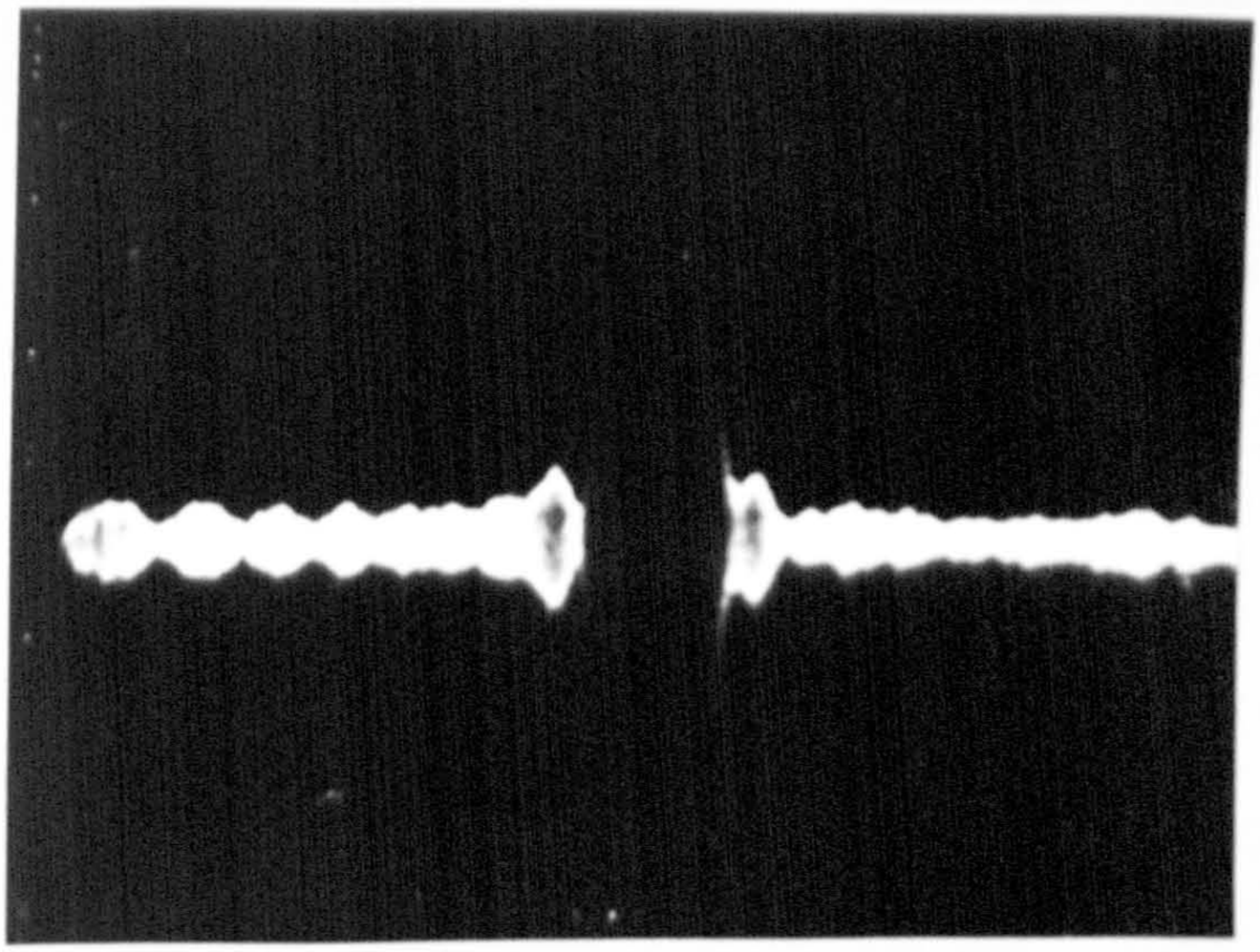

Figure 8.5 Magnified view of the compressed pulse. Time scale: 20 μs/cm. Vertical scale: 10 mV/cm.

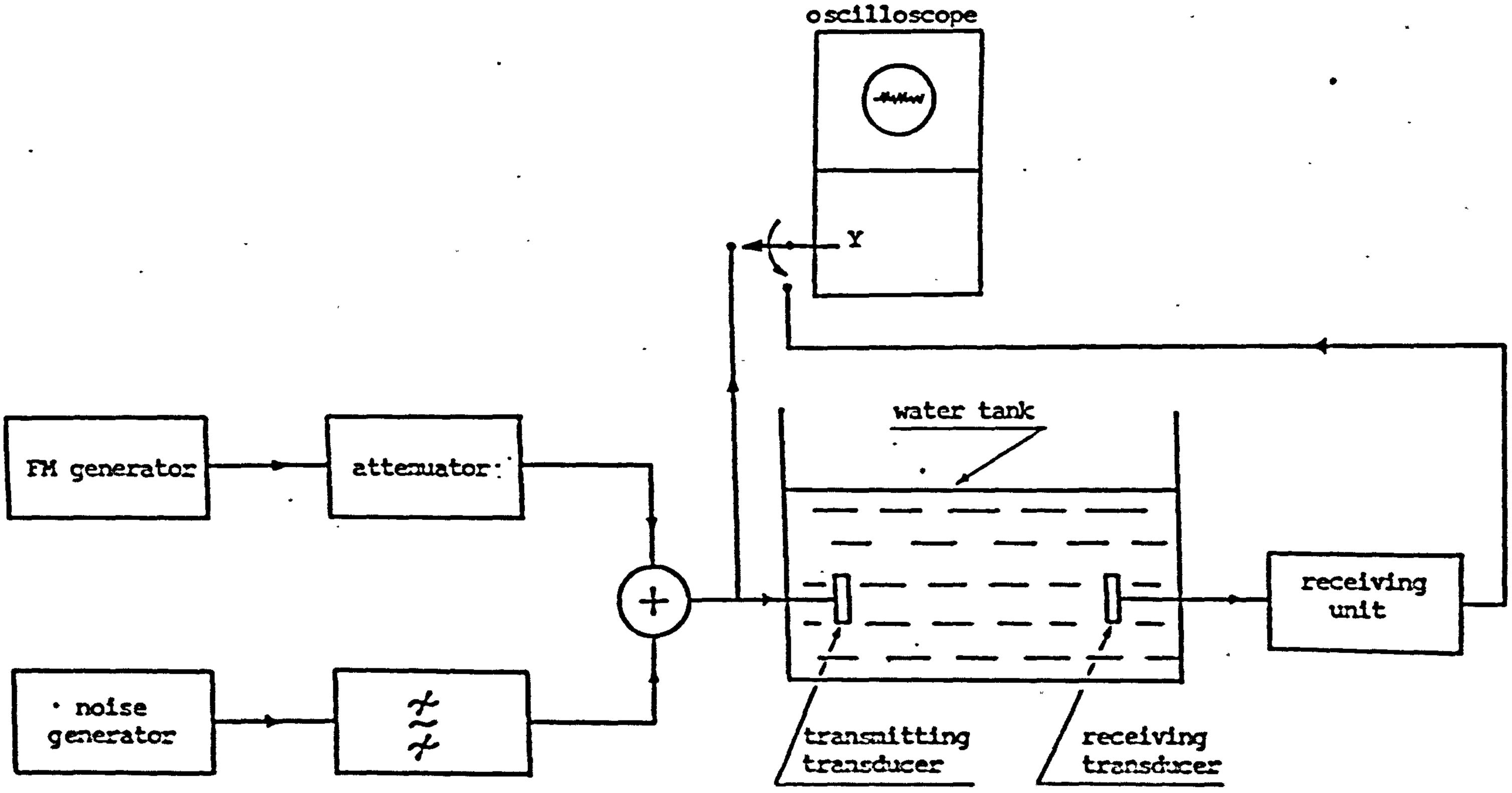

Figure 8.6 Measurement of signal-to-noise ratio improvement

(c) Linearity between input and output levels

The input long pulse/ output compressed pulse curve for the system is shown in Figure 8.7 where the system is seen to be linear up to an output level of about 550 mV p-p.

8.3 Operating System Performance

8.3.1 Detection Capability

The system was set up in a through transmission arrangement. A 30 dB attenuation was introduced in the transmission path by the insertion of a block of lossy material (expanded polystyrene). The long pulse appearing at the receiving transducer was nearly immersed in noise (lower trace, Figure 8.8), but the signal was recovered after compression (upper trace, Figure 8.8). Figure 8.9 compares the deterioration in waveform of the compressed pulse before and after the insertion of the lossy material. The system was then switched over to a 20 μs short pulse mode, and outputs from the pre-amplifier in the receiving unit were monitored. Figure 8.10 illustrates the difference in output waveforms due to the insertion of the lossy material. The noise level was much higher in this case.

The above result was put in more quantitative terms by inserting an attenuator between the transmitting unit and the transmitting transducer. With the system operating in a 20 μs short pulse mode and with the lossy material inserted, the attenuator was adjusted until the output signal was barely visible in noise (lower trace, Figure 8.11). The procedure was repeated with the system in a pulse compression operation (upper trace, Figure 8.11). It was found that an additional 38 dB attenuation on the input signal could be

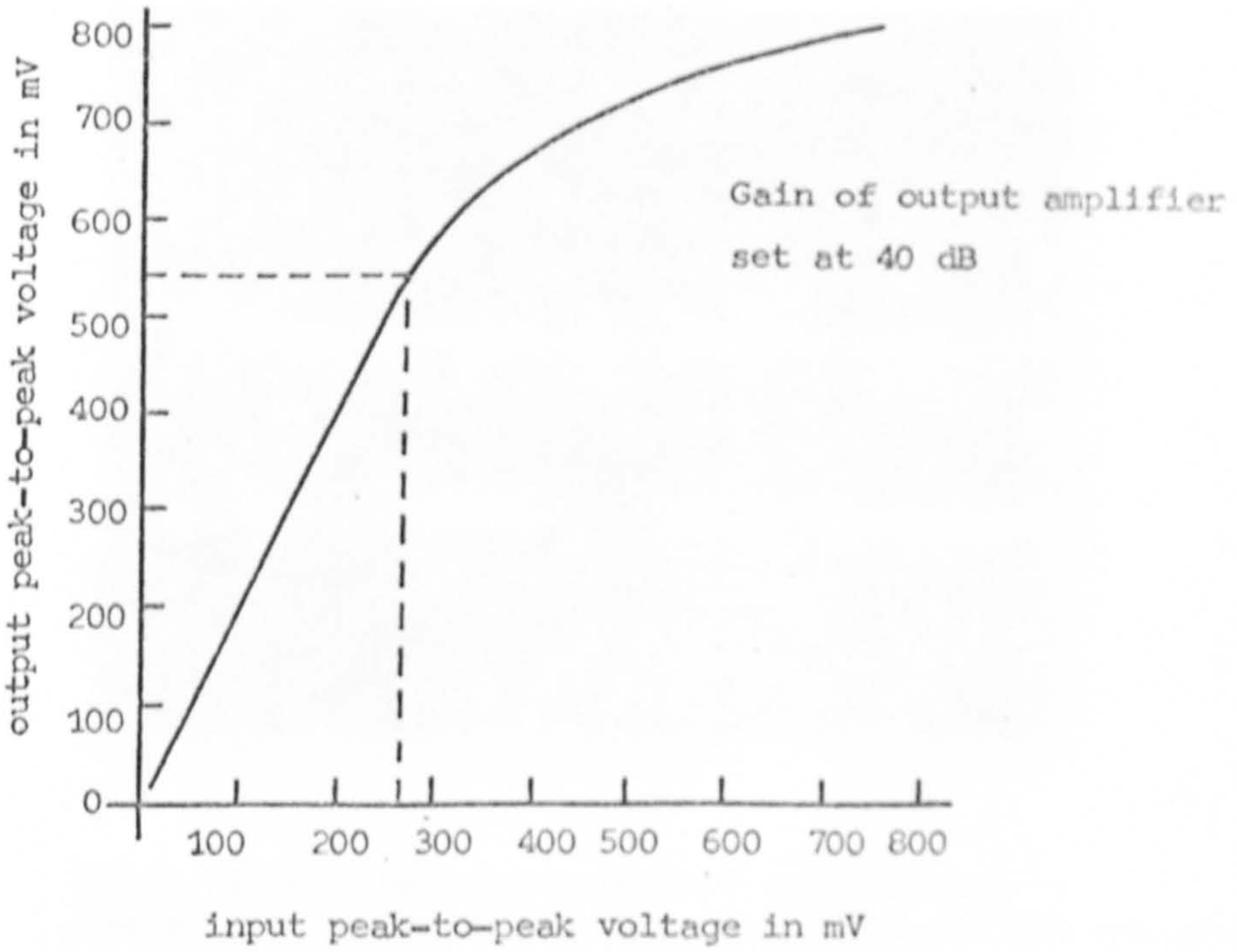

Figure 8.7 System input and output relationship

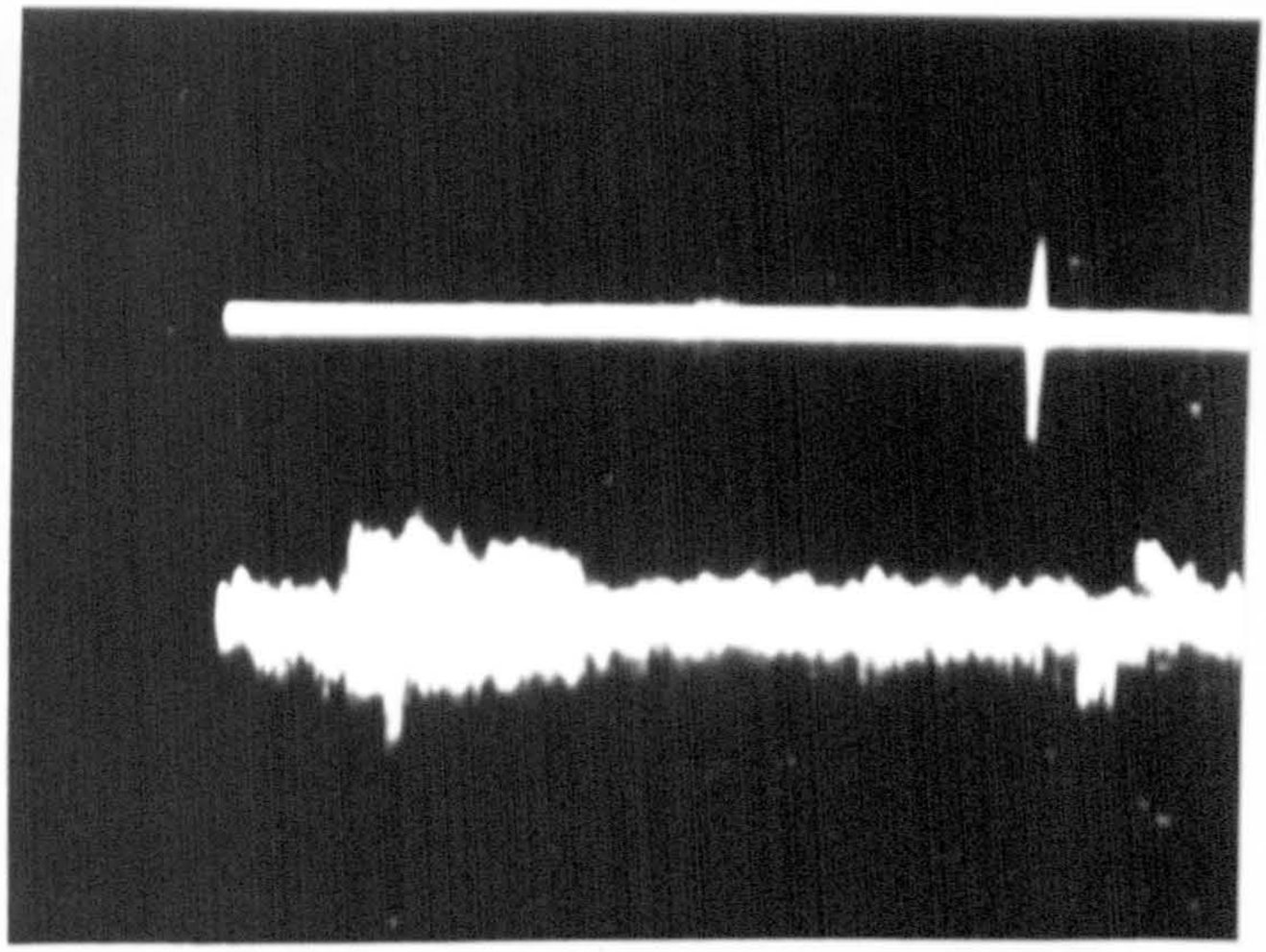

Lower trace shows the noisy input to the system
Upper trace shows the output after compression

Figure 8.8 Illustration of the power of pulse compression.
Time scale: 0.2 ms/cm.

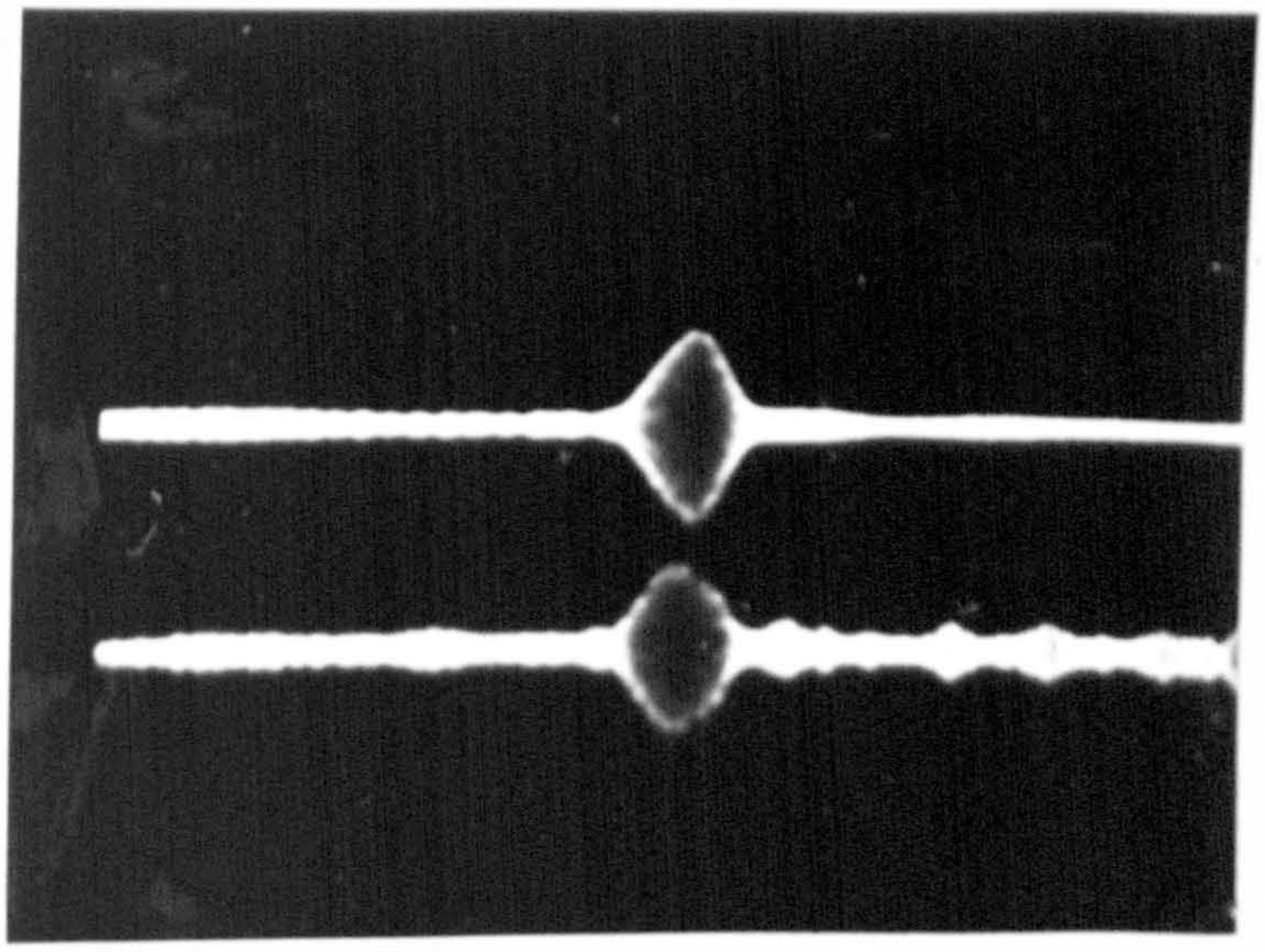

Upper trace shows direct through transmission
Lower trace shows output when lossy material was introduced

Figure 8.9 Degradation in signal-to-noise ratio after insertion of a lossy material when the system operates in a pulse compression mode. Time scale: 20 μs/cm.

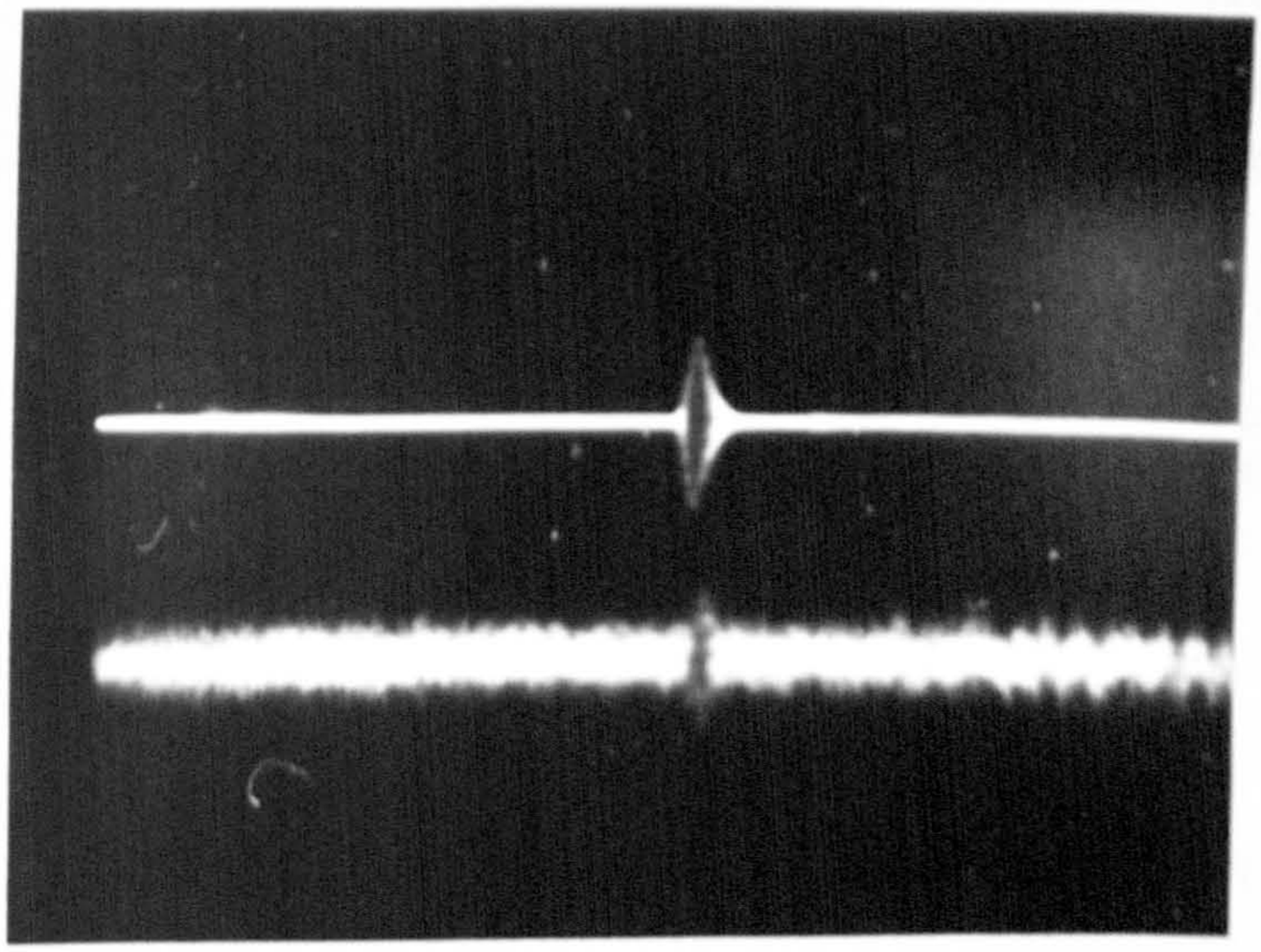

Upper trace shows direct through transmission
Lower trace shows output when lossy material was introduced

Figure 8.10 Degradation in signal-to-noise ratio after insertion of a lossy material when the system operates in a short pulse mode. Time scale: 50 μs/cm.

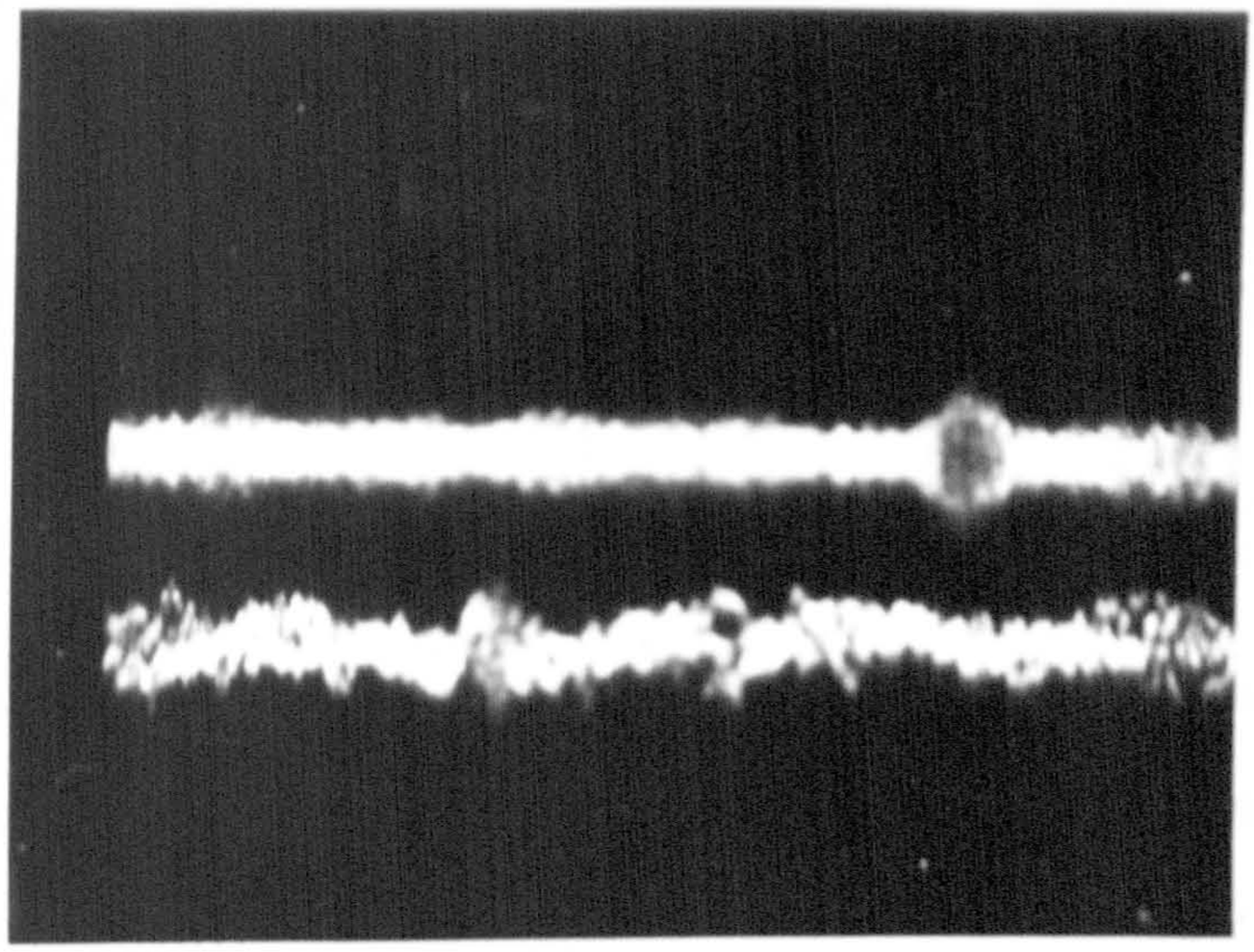

Upper trace shows output from the pulse compression system

Lower trace shows output from conventional short pulse system

Figure 8.11 Conditions under which the output waveforms in the pulse compression and the short pulse system were assumed to have equal S/N. Time scale: 20 us/cm.

tolerated in the latter case.

To demonstrate the operating system in a practical situation, the arrangement in Figure 8.12 was set up. Target A was a composite structure consisting of a 2.8 mm thick rubber sheet bonded to a 2.6 mm thick steel plate. Target B was another steel plate of 2.6 mm in thickness. The transducers were aligned to focus upon the latter. Figure 8.13 shows the compressed output waveforms before (upper trace) and after (lower trace) the insertion of Target B. The presence of Target B was clearly revealed.

8.3.2 Resolution

The resolution capability of the system was assessed with the same arrangement as in Figure 8.12, but using a test jig (Figure 8.14) as the target. A 2 mm thick perspex sheet was mounted in front of the movable reflector in the jig. This arrangement provided two reflectors with a well-defined distance between them, and by adjusting the movable reflector the received pulses could be made to overlap. The upper trace of Figure 8.15 shows the long overlapping reflected signals at the receiver input. After compression, they were seen to be completely resolved into distinct short pulses (lower trace, Figure 8.15). In Figure 8.16 the lower trace shows the output compressed pulses when the reflectors were spaced at 8 mm apart. For comparison, the corresponding output signals when the system was operating in a 20 μs short pulse mode, are also shown (upper trace). The resolution limit for the system was estimated to be 8 μs (12 mm of water path) for targets of nearly equal strength.

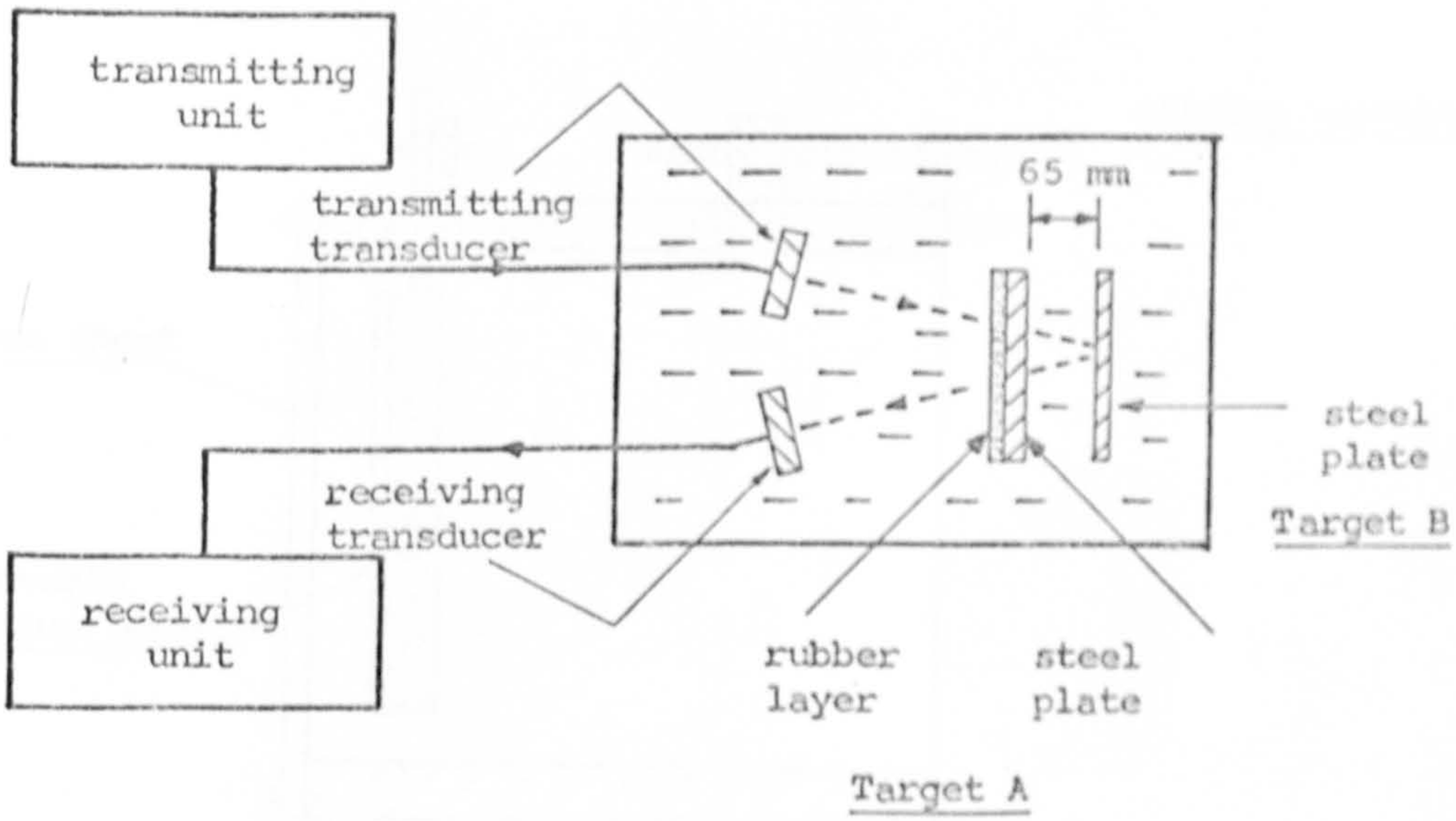

Figure 8.12 Detection capability of the pulse compression system in a practical test set-up

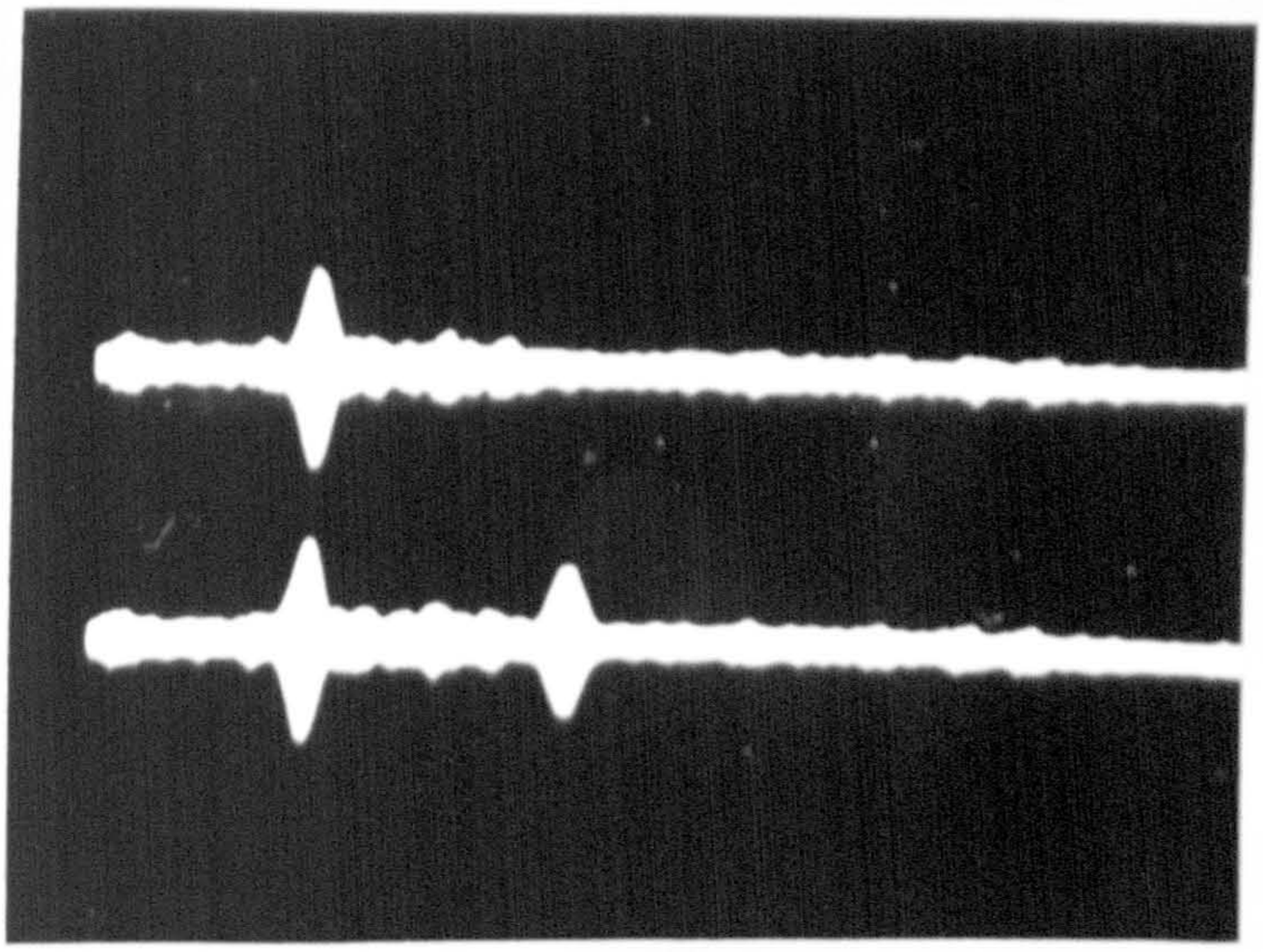

Upper trace: Ouput compressed pulse — echo from target A

Lower trace: An extra pulse appears when target B is inserted

Figure 8.13 Ouput waveforms obtained from the above test set-up.
Time scale: 50 μs/cm.

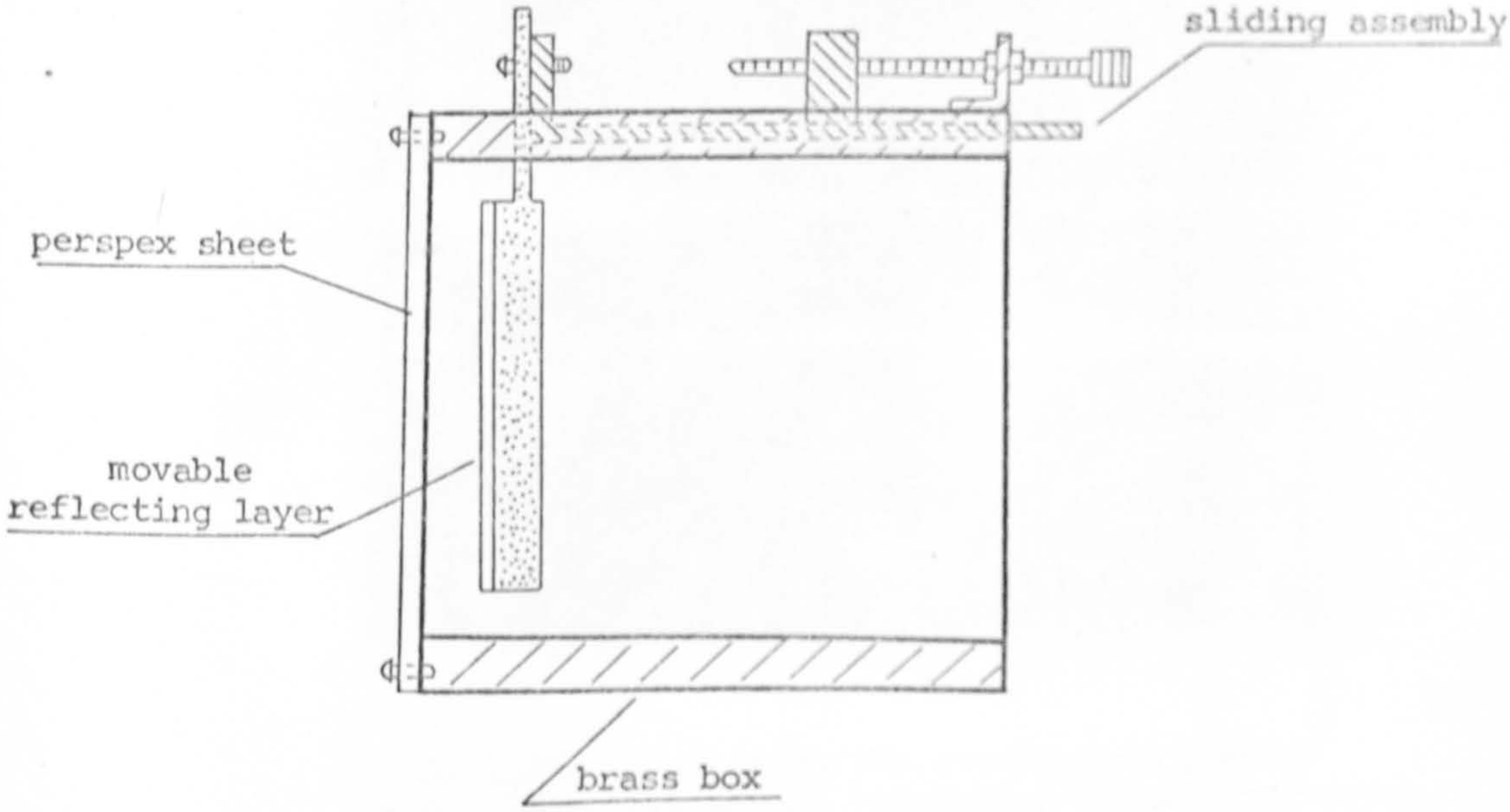

Figure 8.14a Schematic diagram of the test jig

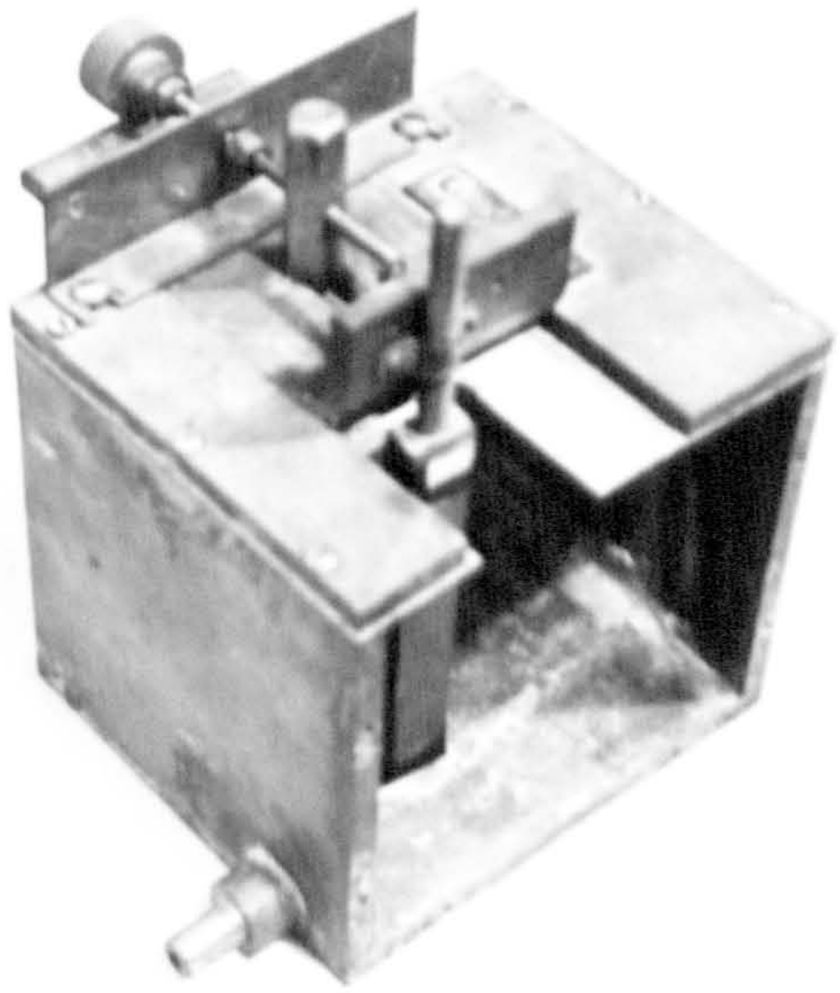

Figure 8.14b Picture of the test jig (with front perspex sheet removed)

Figure 8.14 The test jig

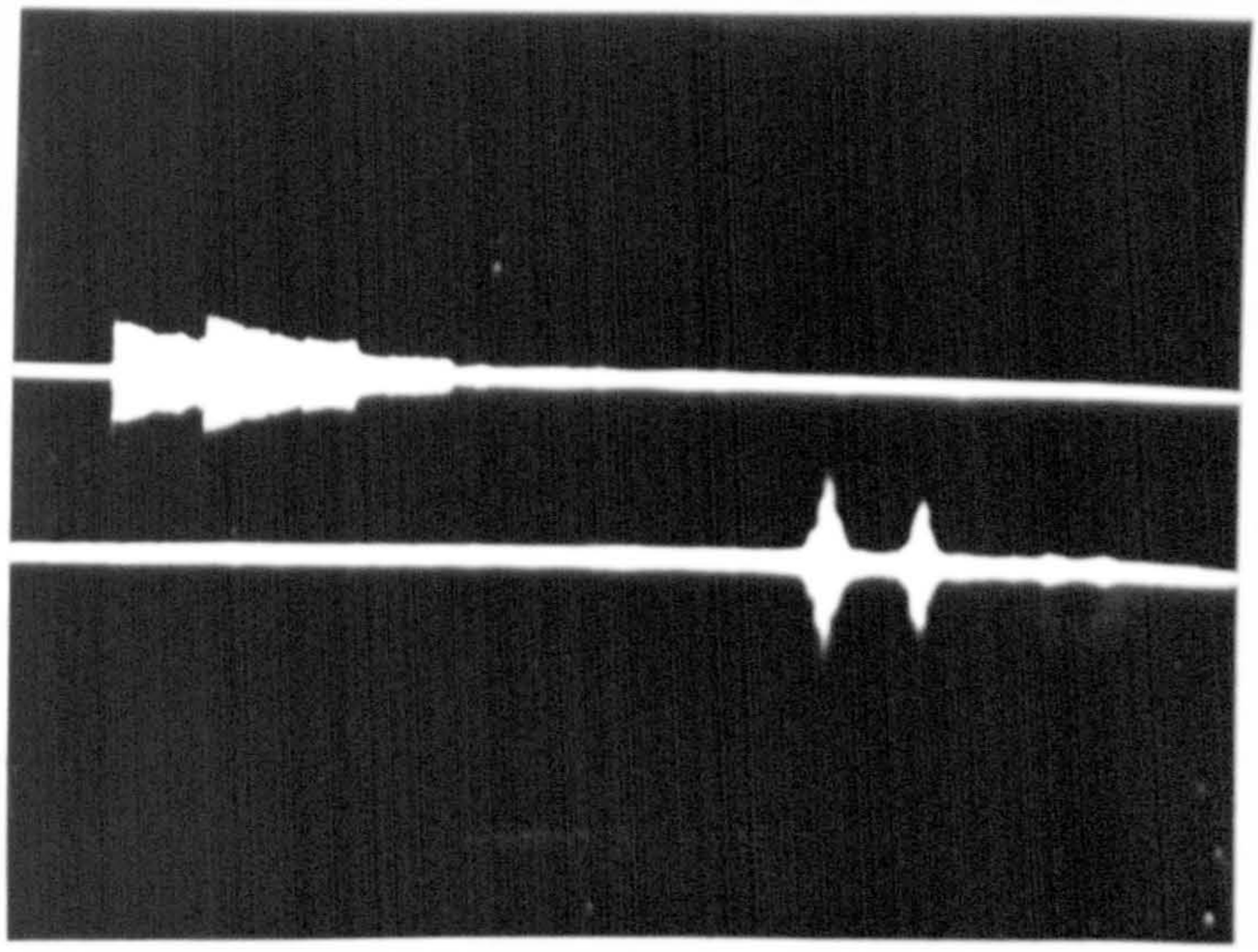

Upper trace illustrates the overlapping inputs
Lower trace illustrates resolution after compression

Figure 8.15 Pulse compression resolution capability

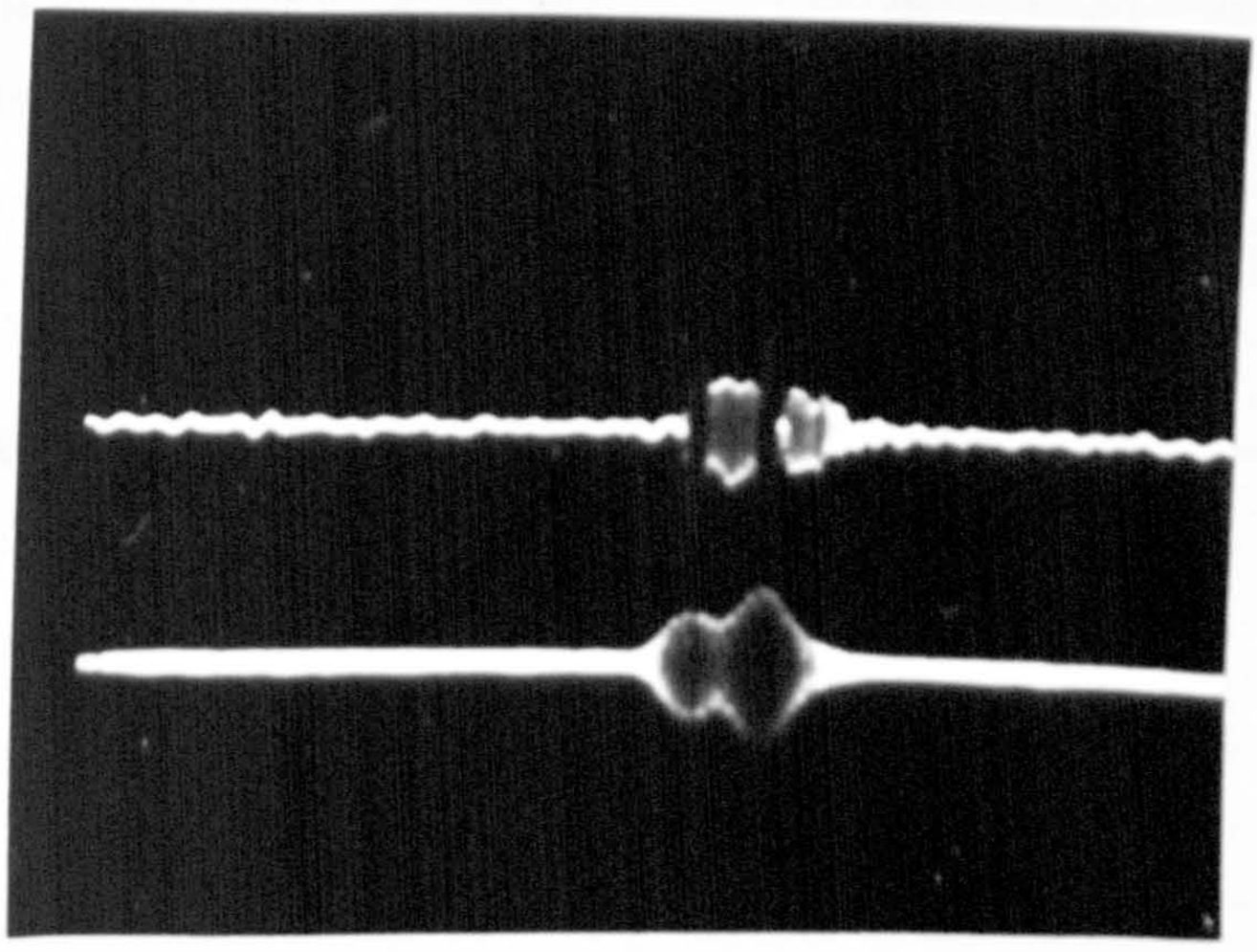

Upper trace shows return signals when the system operates in short pulse mode
Lower trace shows return signals when the system operates in pulse compression mode

Figure 8.16 Minimum resolution limit in the system. Time scale: 20 μs/cm.

8.4 Discussions of Results

(1) It is to be noted that the connection of the various receiver system blocks in Figure 6.1 can be arranged in some other order as well. Weighting or equalisation can be performed after compression. However, since the dispersive delay line maximises the signal-to-noise ratio, it is placed as the final unit in the system.

(2) The envelope of the compressed pulse can be compared to that predicted by theory. Using Equation 3.22 with Δf = 200 kHz and K = 11 (i.e. 24 dB attenuation at band edges), the theoretical envelope can be plotted. Figure 8.17 shows the theoretical plot along with the experimental points. Due to system imperfections, a slight widening in the envelope was obtained in the practical results with the -4 dB points at 8 μs apart. When compared with the ideal unweighted pulse, which has its -4 dB points at 5 μs (1/200 kHz) apart, this represents a weighting broadening factor of 1.6.

(3) The magnified view of the output sidelobe structures in Figure 8.5 illustrates that the distortion sidelobes extend quite a distance on either side of the main pulse. This is a consequence of the ripples in the delay characteristic.

(4) The signal-to-noise ratio improvement due to pulse compression effect was found to be 15 dB. The theoretical figure should be around 18 dB. This low figure was probably due to the difficulties of making threshold comparisons visually and of assessing the input noise bandwidth as well as errors in system parameters. When compared to a conventional wideband short pulse

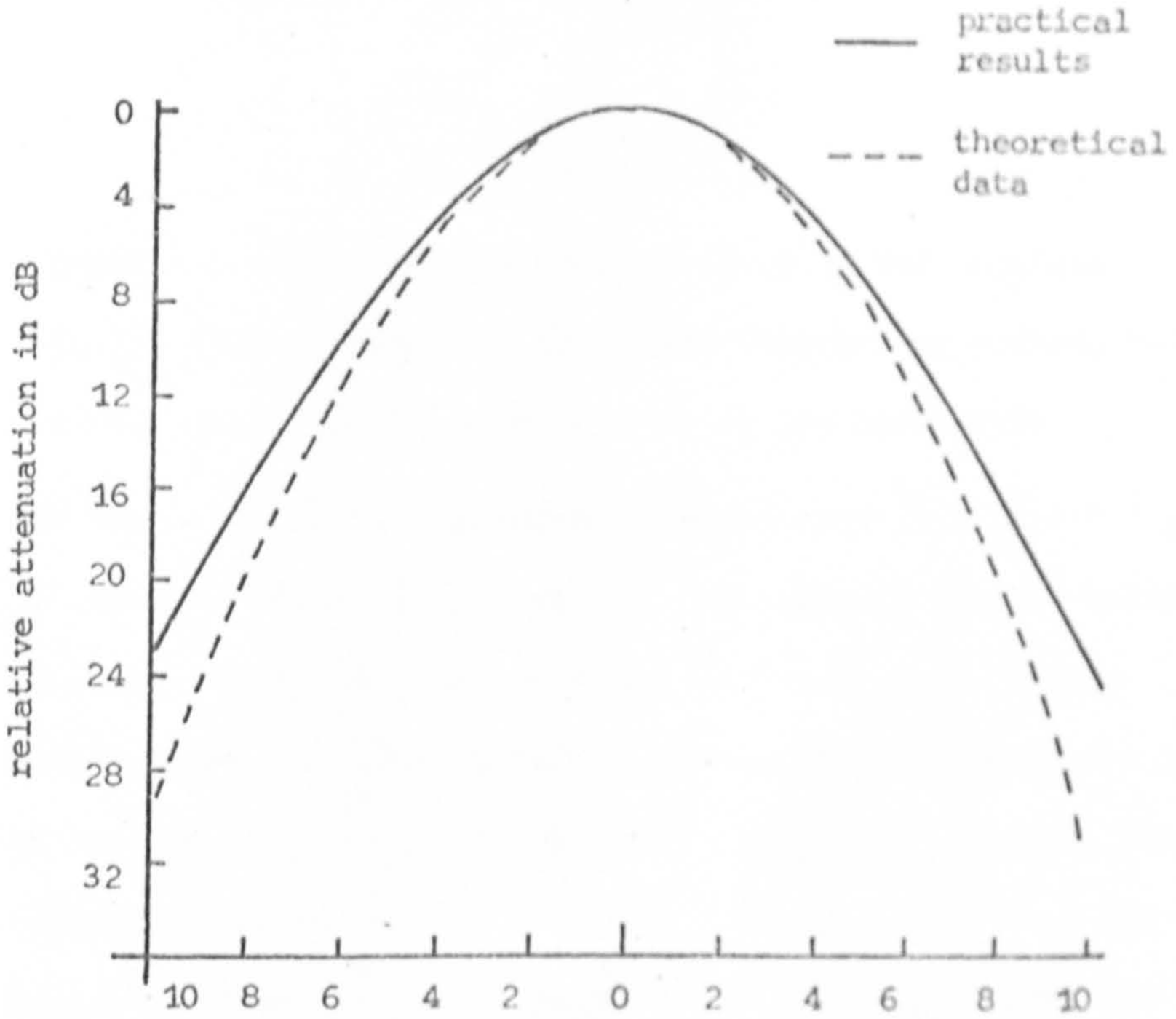

Figure 8.17 Envelope of the compressed pulse

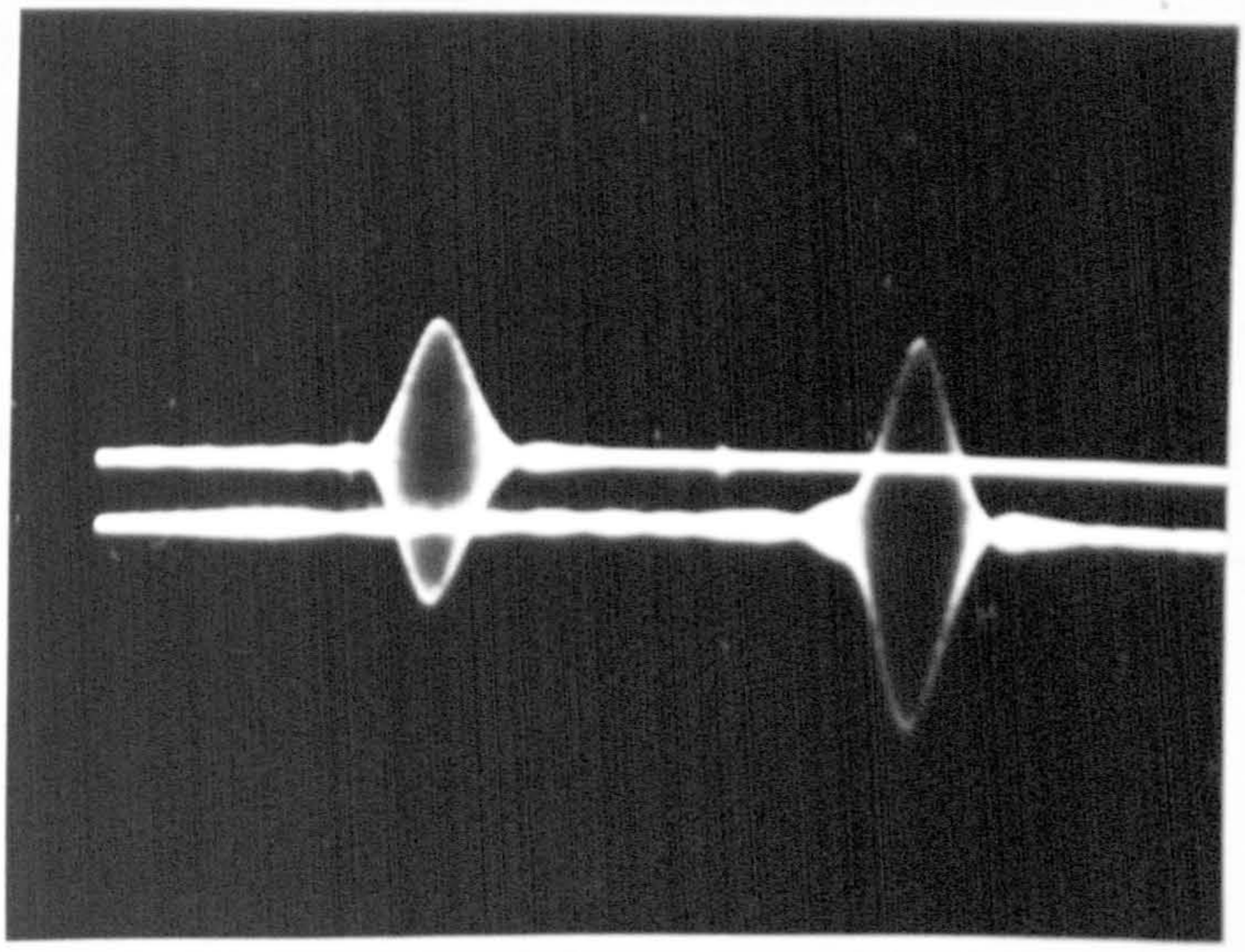

Upper trace shows normal compressed pulse

Lower trace shows output when input exceeds the dynamic range of the system

Figure 8.18 Waveform degradation caused by dynamic range limitation

system, a much larger improvement of 38 dB was obtained. This is to be expected as the pulse compression system, being a bandlimited one, eliminates much of the band noise.

(5) The input and output linearity measurements in Figure 8.7 give the dynamic range of the system. The maximum output before departure from linearity sets in, is 550 mV p-p. If the minimum usable output is taken as twice the minimum noise level at the output terminals, which was measured to be 3 mV, the dynamic range is seen to be 45 dB. The main source of the output noise was found to be the interference pick-ups due to the physical length of the line. .The maximum output was limited by the output swing of the amplifier driving the delay line. Figure 8.18 shows the normal output (upper trace) as well as an output when the amplifier was overdriven (lower trace). It can be seen that spurious sidelobes begin to appear. This is because any non-linearities in the system will always give rise to time-spaced interfering pulse signals at the output, on account of the dispersive nature of the delay line. In this respect, the pulse compression system degrades more rapidly than the conventional short pulse system, once the dynamic range is exceeded.

(6) On the whole, the experimental results are satisfactory. This is because system imperfections which include the linear delay mismatch between transmitter and receiver, the phase modulation error in the transmitter FM output, the stability of the carrier frequency, as well as imperfect Gaussian weighting, will inevitably degrade its performance. It is interesting to

compare the results with those obtained from a dispersive network produced at Marconi Research Laboratory.[94][95] The latter system has a time-bandwidth product of 50 and a range sidelobe of -25 dB, but the dispersive network comprises three panel mounted sub-assemblies, each containing two identical groups of 12 differing filter sections mounted on printed boards within a screening box. Moreover, their performance figure was obtained under laboratory conditions with a linear rectangular FM signal directly fed into the dispersive network. It can be seen that the present results obtained under operating conditions compare favourably with their reported ones.

CHAPTER 9

CONCLUSIONS

From the foregoing theoretical and experimental work, the following concluding remarks may be made:-

(1) Pulse compression does provide a means of operating an ultrasonic pulse echo detection system with long transmitted pulses for increased sensitivity, but without sacrificing resolution. The method is, in fact, a practical implementation of a matched-filter system and possesses a signal-to-noise ratio approaching the theoretical maximum (Section 3.2.2). By virtue of this signal-to-noise enhancement capability, pulse compression may thus be applied to testing situations where peak-power limitations exist or where highly absorbent media are encountered.

(2) An ultrasonic non-destructive testing system using pulse compression was implemented. The system successfully demonstrated pulse compression. The basic characteristics of the system can be summarised as follows:-

Input pulse duration	420 μs
Frequency sweep	decreases linearly from 1.9 to 1.7 MHz
Centre frequency	1.8 MHz
Dispersive bandwidth	200 kHz
Weighting function	Gaussian, with -24 dB at band edges
Output compressed pulse	8 μs at -4 dB points
Sidelobe level	-25 dB

Compression ratio (time bandwidth product) 84

(3) To achieve the long dispersive delay in the system, it was proposed to employ an aluminium strip dispersive delay line. Theoretical and subsequent experimental work confirmed this approach. The constructed delay line demonstrates its compactness as well as its economy.

(4) The final output pulse is of 8 μs duration. This pulse length contains nearly 15 cycles of the carrier frequency and is relatively long for good resolution. However, the bandwidth of the system, which is governed by the delay line's linear dispersive range, sets both a theoretical and a practical limit to the compressed pulse duration. Similarly, the duration of the transmitted pulse can only be extended by increasing the length of the line, provided more equalisation is introduced. In general, the time bandwidth product affords a criterion in assessing a dispersive delay device and is related to the complexity of a system.

(5) As pulse compression relies upon a phase coherence process for its operation, it is highly susceptible to parameter errors. A successful system depends critically on the sweep generator, the weighting function, the compensating network and the overall linearity and stability. The paired-echo analysis expounds this point fully.

(6) The economical aspect of the present implementation must be emphasised. All component inductors, capacitors and resistors used are of standard available values. The PZT transducers are of standard frequency and the aluminium strip line is of a standard commercial gauge. When assessed against the design criteria for a low distortion system, which call for a rigid control of phase and amplitude fidelity, the system performance is seen to be satisfactory.

(7) Certain refinements in system design are possible. Wider bandwidth transducers are obviously desirable. An improved linear delay and greater percentage bandwidth characteristics in the delay line, may be achieved by the use of a stepped thickness delay line.[96] The controlled tapering of its width along the length of the delay line may also effect better spurious mode rejection, as well as a desirable amplitude response.[97] However, to design lines with these properties requires an extremely precise mill-rolling or chemical bath etching process.

(8) The pulse compression method has its limitations. Theoretically, as a linear system is postulated, the technique cannot be applied to situations where any non-linear effects exist, either in the test system or in the medium under test. Its range resolution capabilities are usually slightly inferior to those of a short pulse, because of the fundamental limitations imposed by its sidelobes. This latter shortcoming, together with the practical implementation complexity, must be weighted against any advantage gained from its use.

(9) Despite these limitations, it should be appreciated that the technique does provide a possible solution to the problem of testing highly absorbent materials. Experimental evidence in the previous chapter demonstrates the power of the pulse compression system. Within the dynamic range of the system, a resolution capability nearly equivalent to the reciprocal of system bandwidth is obtained.

(10) To summarise: In this report the basic principles involved in the pulse compression technique were presented and the primary considerations for successful application of the method to a non-destructive testing situation were pointed out. From remarks made in the last paragraph, it can be concluded that as instrumentation and application techniques are perfected, the present method should prove to be a useful solution to some non-destructive testing problems, which the conventional pulse-echo technique fails to solve.

REFERENCES

1 ENSMINGER D — Ultrasonics: The low and high intensity applications
Chapters 6 and 7, Marcel Dekker Inc., New York, 1973.

2 KRAUTKRÄMER J and KRAUTKRÄMER H — Ultrasonic Testing of Materials
Chapter 3, George Allen & Unwin Ltd., London, 1969.

3 GOLODAEV B G — 'Evaluating the Sensitivity of the Mirrow-shadow method of Ultrasonic Inspection'
Zavodskaya Laboratoriya, Vol. 30 No. 8 pp 954-956, August, 1964.

4 SAVAGE F M — 'An Ultrasonic Method of Gauging'
J. of Brit. I R E, 14, pp 436-444 September, 1954.

5 SCHLIEKELMAN R J — 'Non-destructive testing of adhesive-bonded metal structures, Part 2: The Fokker Bond Tester'
Adhesive Age, 7, pp 33-37, June, 1964.

6 LANGE YU V and SHVARTSMAN S M — 'IAD-3 Amplitude-phase Impedance Defectoscope'
Translated from Defektoskopiya No. 5, pp 96-102, September-October, 1971.

7	BOTSCO R J	'NDT of composite structures with the Sonic Resonator' Materials Evaluation, Vol. XXIV, No. 11, pp 617-623, November, 1966.
8	LoPILATO S A and CARTER S W	'Unbonded Detection using Ultrasonic Phase Analysis' Materials Evaluation, Vol. XXIV, No. 17, pp 690-695, December, 1966.
9	SCHROEER R ROWAND R and KAMM H	'The Acoustic Impact Technique - a versatile tool for non-destructive evaluation of aerospace structures and components' Materials Evaluation, Vol. 28, pp 237-243, November, 1970.
10	HARRIS-MADDOX B	'The Ultrasonic Testing of Boost Motors' Ultrasonics, pp 60-64, April-June, 1964.
11	SCHOFIELD B H	'Acoustic Emission from Metals - its detection, characteristics and source' Proc. 4th Symposium on Physics and NDT, S W Research Institute, San Antonio, Texas, 1963.
12	POLLOCK A A	'Acoustic Emission Methods of NDT' Brit. Journal of NDT, Vol. 13, pp 85-89 May, 1971.

13	BIRCHON D DUKES R and TAYLOR J	'Defect, Location and Assessment in Pressure Vessels using stress wave emission techniques' Second International Conference on Pressure Vessel Technology, San Antonio, Texas, October, 1973.
14	COOK E G and VAN VALKENBURG H E	'Surface Waves at Ultrasonic Frequencies' ASTM Bull, TP 127, pp 81-84, May, 1954.
15	HUDGELL R J MORGAN L L and LUMB R F	'NDT Measurement of Depth of Surface-breaking cracks' Brit. J of NDT, Vol. 16, No. 5, pp 144-149 September, 1974.
16	MATVEEV A S and KRAKOVYAK M F	'An Ultrasonic Free-wave Flaw-detection Method for Inspection of thin walled tubes' Translated from Zavodskaya Laboratoriya Vol. 26, No. 11, pp 1235-1238, November, 1960.
17	FREDERICK C L and WORLTON D C	'Ultrasonic Thickness Measurements with Lamb Waves' Non-destructive Testing, pp 51-55, January - February, 1962.
18	ALDRIDGE E E and DAVEY C N	'Recording Ultrasonic Micrometers' in Non-destructive Testing (Ed. H D Egerton) Chapter 6, pp 45-56, Harwell/Oxford 1969.
19	GERICKE O R	'Determination of the Geometry of Hidden Defects by Ultrasonic Pulse Analysis Testing' JASA, Vol. 35; No. 3, pp 364-368, March, 1963.

20 GERICKE O R — 'Defect Determination by Ultrasonic Spectroscopy' J. of Metals, Vol. 18, No. 8, pp 932-937, August, 1966.

21 ADLER, LASZLO and WHALEY H L — 'Interference Effect in a Multifrequency Ultrasonic Pulse Echo and its application to flaw characterisation' JASA, Vol. 51, No. 3 (Part 2), pp 881-887, March, 1972.

22 MORGAN L L — 'The Spectroscopic Determination of Surface Topography by using Acoustic Surface Waves' Acustica, 30 (4), pp 222-228, April, 1974.

23 CURTIS G J — 'Current Ultrasonic Non-destructive Testing Developments in the United Kingdom' IEEE Ultrasonics Symposium Proceedings, pp 691-697, November, 1974.

24 ROZENBERG L D — 'Survey of Methods used for the Visualisation of Ultrasonic Fields' Soviet Physics-Acoustics, 1, pp 105-116, 1955.

25 ALDRIDGE E E — 'Ultrasonic Holography' in Research Techniques in Non-destructive Testing (Ed. R S Sharpe), Chapter 5, Academic Press, London, 1970.

26 HEUTER T F and BOLT R H — Sonics pp 247-249 Wiley & Sons, New York, 1955.

27 BERLINCOURT D A, CURRAN D R and JAFFE H — 'Piezoelectric and Piezomagnetic Materials and their function in Transducers' in Physical Acoustics (Ed. W P Mason), Vol. 1 Part A, Chapter 3, Academic Press, New York, 1964.

28 HÜTTMANN E — 'Verfahren zur Entfernungsmessung' German Patent No. 768,068, filed March, 1940, issued May, 1955.

29 SPROULE D O and HUGHES A J — 'Improvements in and relating to systems operating by means of wave trains' British Patent No. 604,429, filed June, 1944, issued July, 1948.

30 DICKE R H — 'Object Detection System' U S Patent No. 2,624,876, filed September, 1945, issued January, 1953.

31 DARLINGTON S — 'Pulse Transmission' U S Patent No. 2,678,997, filed December, 1949, issued May, 1954.

32 CAUER W A — 'Verfahren zur Nachrichtenübermittlung durch' German Patent No. 892,772, filed December, 1950, issued August, 1953.

33 COOK C E — 'Pulse Compression-key to more efficient radar transmission' Proc. IRE Vol. 48, pp 310-316, March, 1960.

34 KLAUDER J R
PRICE A C
DARLINGTON S and
ALBERSHEIM W J
'The Theory and Design of Chirp Radars'
Bell System Technical Journal, Vol. 39, pp 745-808, July, 1960.

35 OHMAN G P
'Getting High Range Resolution with Pulse Compression Radar'
Electronics, pp 53-57, October, 1960.

36 RAMP H O and
WINGROVE E R
'Principles of Pulse Compression'
IRE Transactions on Military Electronics, pp 109-116, April, 1961.

37 TIBERIO U
'Sul rapporto eco-rumore che è possible consequire nei radar mediante la compressione di impulso'
Alta Frequenza, pp 665-670, September, 1961.

38 LOHRMANN D
'Ein Hilfssatz zur theoretischen und praktischen Behandlung des Cauer'schen Impulskompressions-verfahrens'
Frequenz, pp 156-164, April, 1962.

39 STEWART J L and
WESTERFIELD E C
'A Theory of Active Sonar Detection'
Proc. IRE, pp 872-881, May, 1959.

40. REMLEY W R
'Correlation of Signals having a Linear Delay'. JASA, pp 65-69, January, 1963.

41 GOUPILLAUD P L and
LEE M R
'Some Theoretical Aspects of the VIBROSEIS System, and their practical implications'
Presented at the Annual Meeting of the Society of Exploration Geophysicists, New Orleans, October, 1963.

42 WOODWARD P M — Probability and Information Theory, with Applications to Radar. McGraw Hill, New York, N.Y., 1953.

43 TURIN G L — 'An Introduction to Matched Filters' IRE Transactions on Information Theory, pp 311-329, June, 1960.

44 GABOR D — 'Theory of Communication' Proc. of IEE, Part III, pp 429-457, 1946.

45 ANSTEY N A — 'An Introduction to Correlation Techniques' Data Correlation Division, Seismograph Service (England) Ltd., December, 1963.

46 FARNETT E C; HOWARD T B and STEVENS G H — 'Pulse Compression radar' in Radar Handbook (Ed. M I Skolnik), Chapter 20, McGraw Hill, New York, 1970.

47 BRANDON P S — 'The Design of a Non-linear Pulse Compression System to give a low loss high resolution radar performance' Marconi Review, Vol. XXXVI, No. 188, pp 1-45 First Quarter, 1973.

48 TEMES C L — 'Sidelobe Suppression in A Range-channel Pulse Compression Radar' IRE Transactions on Military Electronics, Mil 4-6, pp 162-169, April, 1962.

49 COOK C E and BERNFIELD M — Radar Signals Academic Press, New York, 1967.

50 CHIN J E and COOK C E — 'The Mathematics of Pulse Compression' Sperry Engineering Review, Vol. 12, pp 11-16, October, 1959.

51 THOR R C — 'A large time-bandwidth product pulse compression technique' IRE Transactions on Military Electronics, Mil-6, pp 169-173, April, 1962.

52 BRANDON P S — 'The Spectra of Linear and Non-linear FM used in Pulse Compression, and the effects on the resultant compressed pulse' Marconi Review, Vol. XXXVI, No. 189, pp 69-92, Second Quarter, 1973.

53 WHEELER H A — 'The Interpretation of Amplitude and Phase Distortion in terms of paired echoes' Proc. IRE, 27, pp 359-385, June, 1939.

54 BURROWS C R — 'Discussion of Paired Echo Distortion Analysis' Proc. IRE (correspondence), 27, pp 384, 1939.

55 MAINES J D and JOHNSTON J N — 'Surface Acoustic Wave Devices and Applications - 2. Pulse Compression Systems' Ultrasonics, pp 211-217, September, 1973.

56 O'MEARA T R — 'The Synthesis of Band-pass, All-pass time Delay Networks with Graphical Approximation Techniques' Hughes Aircraft Co. Research Lab., Malibu, California, Report 114, February, 1962.

57 BRANDON.P S 'The Design Methods for Lump-constant Dispersive Networks suitable for Pulse Compression Radar' Marconi Review, 28, pp 225-253, 1965.

58 MAY J E 'Wire-type Dispersive Ultrasonic Delay Lines' IRE Transactions on Ultrasonic Engineering, Vol. UE-7, pp 44-53, June, 1960.

59 MEEKER T R 'Dispersive Ultrasonic Delay Lines using the First Longitudinal Mode in a Strip' IRE Transactions on Ultrasonic Engineering, Vol. UE-7, pp 53-58, June, 1960.

60 FITCH A H 'A Comparison of Several Dispersive Ultrasonic Delay Lines using Longitudinal and Shear Waves in Strips and Cylinders' IRE International Convention Record, Vol. 8, Part 6, pp 284-292, March, 1960.

61 LAMB H 'On Waves in an Elastic Plate' Proc. Royal Society (London), A 93, pp 114-128, 1917.

62 REDWOOD M Mechanical Waveguides Chapter 5, Pergamon Press, Oxford, 1960.

63 MEEKER T R and MEIZTLER A.H 'Guided Wave Propagation' in Physical Acoustics, Principles and Methods (Ed. W P Mason), Vol. 1, Part A, pp 111-167, Academic Press, New York, 1964.

64 MEEKER T R 'The Application of the Theory of Elastic Waves in Plates to the Design of Ultrasonic Dispersive Delay Lines' IRE International Convention Record, Part 6, pp 327-333, 1961.

65 MASON W P Electromechanical Transducers and Wave Filters pp 399-404, Second Edition, D Van Nostrand Co., Princeton, New Jersey, 1948.

66 TIERSTEN H F 'Thickness Vibrations of Piezoelectric Plates' JASA Vol. 35, No. 1, pp 53-58, January, 1963.

67 MEEKER T R 'Thickness Mode Piezoelectric Transducers' Ultrasonics, Vol. 10, No. 1, pp 26-36, January, 1972.

68 MINDLIN R D and FOX E A 'Vibrations and Waves in Elastic Bars of Rectangular Cross-section' Journal of Appl. Mech, Vol. 27, Transactions of the ASME, pp 152-158, March, 1960.

69 FABIAN E L 'The Design of Rectangular Bar Transducers for Use with Ultrasonic Dispersive Strip Delay Lines' IEEE International Convention Record, Part 9, pp 96-101, 1963.

70 MASON W P — Piezoelectric crystals and their Applications to Ultrasonics. First Edition, D Van Nostrand Co., New York, 1950.

71 BROCKELSBY C F; PALFREEMAN J S and GIBSON R W — Ultrasonic Delay Lines. Iliffe, London, 1963.

72 MEITZLER A H — 'Selective Attenuation of Elastic Wave Motions in Strips of Polycrystalline Metals' JASA, Vol. 34, No. 4, pp 444-453, April, 1962.

73 ALEKSANDROV K S; GUROVITS L S and KAMENSKII E I — 'Effect of an Intermediate Layer on the Frequency Characteristic of Ultrasonic Delay lines' Soviet Physics Acoustics, Vol. 6, No. 2, October-December, 1960.

74 KOSSOFF G — 'The Effects of Backing and Matching on the Performance of Piezoelectric Ceramic Transducers' IEEE Transactions on Sonics and Ultrasonics, Vol. SU-13, No. 1, pp 20-30, March, 1966.

75 NORTON E L — 'Wave Filter' U S Patent No. 1,681,554, August, 1928.

76 VERNITRON LTD., ENGLAND — 'Six Modern Piezoelectric Ceramics' Bulletin 66011/D, March, 1969.

77 BLITZ J — Fundamentals of Ultrasonics
pp 50-55, Second Edition, Butterworths, London, 1967.

78 TUCKER D G and GAZEY B K — Applied Underwater Acoustics
pp 143-159, Pergamon Press, Oxford, 1966.

79 KINSLER L E and FREY A R — Fundamentals of Acoustics
pp 174-187, Second Edition, Wiley, New York, 1962.

80 FREDERICK J R — Ultrasonic Engineering
p 269, Wiley, New York, 1965.

81 SMITH K C and SEDRA A — 'Simple Wideband Linear Voltage-to-Frequency Converter'
Electronic Engineering, pp 140-143, March, 1968.

82 SKWIRSZYNSKE J — Design Theory and Data for Electrical Filters
Van Nostrand, 1965.

83 MILLMAN J and TAUB H — Pulse, Digital and Switching Waveforms
p 646-647, McGraw Hill, New York, 1965.

84 MOTOROLA CO LTD — 'A Wideband Monolithic Video Amplifier'
Motorola Integrated Circuit Application Note AN-404.

85 MOTOROLA CO LTD — 'Field Effect Transistors in Chopper and Analog Switching Circuits'
Motorola Application Note AN-58.

86 TEXAS INSTRUMENTS LTD — 'Application of the SN 74121N TTL Integrated Circuit Monostable'
T I Application Report B 50.

87 I T T CORPORATION — Reference Data for Radio Engineers
Chapter 9, Section 7, Fifth Edition, 1968.

88 WEINBERG LOUIS — Network Analysis and Synthesis
pp 499-507 and pp 536-537
McGraw Hill, New York, 1962.

89 STORCH L — 'Synthesis of Constant-time-delay Ladder Network using Bessel Polynomial'
Proc. IRE, Vol. 42, pp 1666-1675, November, 1954.

90 HENDERSON K W and KANTZ W H — 'Transient Response of Conventional Filters'
IRE Transactions on Circuit Theory, Vol. CT-5, pp 333-347, December 1958.

91 DISHAL M — 'Gaussian Response Filter Design'
Electrical Communication, Vol. 36, No. 1, pp 3-26, 1959.

92 DISHAL M — 'Alignment and Adjustment of Synchronously tuned multiple-resonant-circuit filters'
Electrical Communication, pp 154-164, June, 1952

93 MAY J E — 'Precise Measurement of Time Delay'
IRE International Convention Record, Vol. 6, pp 134-138, 1958.

94 STEWARD K W F — 'A Practical Dispersive Networks System'
The Marconi Review, Vol. XXVIII, No. 159, pp 254-272, 1965.

95 KEALL O E 'Realisation of a dispersive network system'
IEE Conference on 'Delay Devices for Pulse Compression Radar'. Conference Publication No. 20, pp 14-18, 1968.

96 FITCH A H 'Synthesis of Dispersive Delay Characteristics by Thickness Tapering in Ultrasonic Strip Delay Lines'
JASA, 35, pp 709-714, 1963.

97 MEITZLER A H 'Transmission Characteristics of Longitudinal-mode, strip delay lines having asymmetrically tapered widths'
IRE Transactions on Ultrasonic Engineering, Vol. UE-9, pp 30-36, 1962.

98 VAN VALKENBURG M E Network Analysis
pp 263-267, pp 356-357, Prentice-Hall, Englewood Cliffs, N. J., 1955.

99 JAMES M L
SMITH G M and
WOLFORD J C Analog and Digital Computer Methods
Prentice-Hall, Englewood Cliffs, N J, 1964.

APPENDICES

APPENDIX A

MATCHED FILTER RECEPTION FOR LINEAR FM[49]

As a reference for assessment on the performance of a linear FM pulse compression system, it is desirable to compare the output waveform obtained in Section 3.2.1 with that obtained through matched filtering, which represents the optimum receiver design since the process maximizes the output signal-to-noise power ratio.

The frequency response function $H_1(\omega)$ of the matched filter is given by the complex conjugate of the spectrum function $F(\omega)$ of the linear FM signal, i.e.,

$$H_1(\omega) = F^*(\omega) \tag{A.1}$$

Alternatively, the matched filter may be specified through its impulse response which would have the same shape of the time input signal but with the time scale reversed. Hence, from Equation 3.1, the required impulse response is

$$h_1(t) = kf(-t) = k\cos(\omega_o t - \frac{\mu t^2}{2}) \qquad -T/2<t<T/2 \tag{A.2}$$

where k is the matched filter constant and is taken to be $\sqrt{(2\mu)/\pi}$ to give the filter unity gain. (This is done so that results could be compared with those obtained in the dispersive filter case, which has a gain of one).

The matched-filter output signal may be found by using the relation

$$\begin{aligned} y_1(t) &= \int_{-\infty}^{\infty} f(\lambda)\, h(t-\lambda)\, d\lambda \\ &= \sqrt{\frac{2\mu}{\pi}} \int_{-T/2}^{T/2} \cos(\omega_o \lambda + \frac{\mu\lambda^2}{2}) \cos\left[\omega_o(t-\lambda) - \frac{\mu(t-\lambda)^2}{2}\right] d\lambda \end{aligned} \tag{A.3}$$

Since $\cos A \cos B = \frac{1}{2}\left[\cos(A + B) + \cos(A - B)\right]$, the above equation can be written as :

$$Y_1(t) = \frac{1}{2}\sqrt{\frac{2\mu}{\pi}}\int_a^b \cos(\omega_o t + \mu t\lambda - \frac{\mu t^2}{2})\, d\lambda \qquad (A.4)$$

where $a = -\frac{T}{2} + t$, $b = \frac{T}{2}$, for $t > 0$;

$$a = -\frac{T}{2} \text{ , } b = \frac{T}{2} + t \text{ , for } t < 0 \text{ ,}$$

and the high frequency term ($2\omega_o$) has been ignored.

Evaluating for $t > 0$,

$$Y_1(t) = \frac{1}{2}\sqrt{\frac{2\mu}{\pi}}\left\{ \frac{\sin\left[\omega_o t + (\mu t/2)(T - t)\right]}{\mu t} - \frac{\sin\left[\omega_o t - (\mu t/2)(T - t)\right]}{\mu t} \right\}$$

$$= \sqrt{\frac{2\mu}{\pi}}\ \frac{\sin\left[\frac{\mu t}{2}(T - t)\right]}{\mu t}\ \cos\omega_o t \qquad (A.5)$$

Thus, combining with the similar result for $t < 0$, the final expression is :

$$Y_1(t) = \sqrt{\frac{\mu T^2}{2\pi}}\ \frac{\sin\left[\frac{\mu t}{2}(T - |t|)\right]}{\frac{\mu t T}{2}}\ \cos\omega_o t \qquad -T < t < T \qquad (A.6)$$

Putting $\mu T = \Delta\omega = 2\pi\Delta f$,

$$Y_1(t) = \sqrt{T\Delta f}\ \frac{\sin\left[\frac{\mu t}{2}(T - |t|)\right]}{\frac{\mu t T}{2}}\ \cos\omega_o t \qquad -T < t < T \qquad (A.7)$$

The output $Y_1(t)$ given by Equation A.7 is, as expected, also the autocorrelation function for the input signal.

APPENDIX B

COMPUTER PROGRAMS

B.1 Numerical solution of the Lamb wave equation for the first longitudinal mode[99]

The program consists of four segments :

(i) The first segment calculates the phase velocity V for each value of $X = fh/V_s$ by solving the frequency equation.

(ii) The second segment differentiates the phase velocity V with respect to variable X at each pair of V and X.

(iii)The third segment calculates the group velocity and the normalized group delays.

(iv) The fourth segment graphs the results obtained in segments (i),(ii) and (iii).

B.2 Frequency response of transducers with various backings

B1 Numerical solution of the Lamb wave equation for the first longitudinal mode

```
      TRACE 0
      READ FROM (CR)
      MASTER FREON
C        TO SOLVE THE FREQUENCY EQUATION OF THE LONGTITUDINAL MODE WAVE
C     MOTION BY BISECTION METHOD AND FIND THE NORMALISED GROUP DELAY
C
      REAL VP, VS, SIG, X, XINT, XINC, V, VDEL, VINT, VDEL1, EPS, A, B,
     1Q, DR, U, Y
      INTEGER I, NPATH, M, ITER
      DIMENSION X(100), V(100), DR(100), U(100), Y(100)
      WRITE (2,1005)
      READ (1, 1001) VS, SIG, XINT, XINC, M, VINT, VDEL1, EPS
      VP = VS * SQRT (2.0 * (1.0 - SIG) / (1.0 - 2.0 * SIG))
      WRITE (2, 1006) SIG, VS, VP, XINT, XINC, M
C
C     DIVIDE THE RANGE OF X = FREQ * H / VS INTO M INTERVALS
      DO 50 I = 1, M+1, 1
      X(I) = XINT + ((I - 1) * XINC) / 1000.0
C
C     SOLUTION OF THE EQUATION
C     REDUCE IT IN TO ONE UNKNOWN BY SUBSTITUTION OF X
C     NPATH DIFFERENTIATE WETHER V IS FAR OR NEAR THE ROOT
C     ITER COUNTS THE NO OF ITERATIONS FOR EACH SOLUTION
C
      VDEL = VDEL1
      V(I) = VINT
      NPATH = 1
      ITER = 0
      A = F(VS, VP, SIG, X(I), V(I))
   10 B = F(VS, VP, SIG, X(I), V(I)+VDEL)
      ITER = ITER + 1
      IF (ITER .GT. 100) STOP 1
C
C     A * B SHOWS WHETHER THE ROOT LIES BETWEEN V AND V + VDEL OR NOT
      IF (A * B) 30, 30, 20
   20 V(I) = V(I) + VDEL
      A = B
      GO TO (10, 30) NPATH
C
C     FINER INCREMENT OF V(I)
   30 VDEL = VDEL / 2.0
      NPATH = 2
C
C     TO CHECK ACURRACY OF V(I)
      IF (2.0 * VDEL - EPS) 40, 40, 10
   40 WRITE (2, 1007) I, X(I), V(I), VDEL, ITER
   50 CONTINUE
      WRITE (2, 1008)
C
C     FIND THE DERIVATIVES OF THE TABULATED V
C
      WRITE (2, 1009)
      Q = (12.0 * XINC) / 1000.0
      DO 60 I = 1, M-3, 1
C
C     EQUATION FOR THE DERIVATIVE TAKING FIVE CONSECUTIVE POINTS OF V
   60 DR(I) = (-25.0 * V(I) + 48.0 * V(I+1) - 36.0 * V(I+2)
     1+ 16.0 * V(I+3) - 3.0 * V(I+4)) / Q
      DO 70 I = M-2, M+1, 1
```

```
   70 DR(I) = (-25.0 * V(I) + 48.0 * V(I-1) - 36.0 * V(I-2)
     1+ 16.0 * V(I-3) - 3.0 * V(I-4)) * (-1.0) / Q
      C
      C     FIND GROUP VELOCITY AND NORMALISED GROUP DELAY
            DO 80 I = 1, M+1, 1
            U(I) = V(I) / (1.0 - DR(I) * X(I) / V(I))
            Y(I) = VS / U(I)
   80 WRITE (2, 1010) I, V(I), DR(I), U(I), Y(I)
            WRITE (2, 1008)
      C
      C     GRAPHING THE RESULT
      C
            REAL SMAX, SMIN, S, SINC, XMAX, COLUMN, BLANK, DOT, CROSS
            INTEGER GRAPH, J, K
            DIMENSION S(100), COLUMN(101)
      C
      C     READ THE GRAPH SYMBOLS
            READ (1, 1011) BLANK, DOT, CROSS
      C
      C     DETERMINE WHICH GRAPH TO BE DRAWN
            GRAPH = 1
  105 SMAX = 0.0
            SMIN = 1.0E+6
            DO 110 I = 1, M+1, 1
            IF (GRAPH .EQ. 1) S(I) = V(I)
            IF (GRAPH .EQ. 2) S(I) = U(I)
            IF (GRAPH .EQ. 3) S(I) = Y(I)
            IF (S(I) .GT. SMAX) SMAX = S(I)
            IF (S(I) .LT. SMIN) SMIN = S(I)
  110 CONTINUE
      C     COMPUTE VERTICAL AXIS INTERVAL
            SINC = (SMAX - SMIN) / 100.0
            WRITE (2, 1021) GRAPH, SMIN, SMAX, SINC
      C     PRINT VERTICAL AXIS AND INITIAL VALUE OF S
            DO 120 J = 1, 101, 1
  120 COLUMN(J) = DOT
            IF (S(1) .LT. 0.0) STOP 2
            J = 1.5 + (S(1) - SMIN) / SINC
            COLUMN(J) = CROSS
            WRITE (2, 1022) COLUMN
      C     BLANK THE COLUMNS
            DO 130 J = 1, 101, 1
  130 COLUMN(J) = BLANK
      C     PUT A DOT IN COLUMN(1) FOR HORIZONTAL AXIS
            COLUMN(1) = DOT
      C     COMPUTE HORIZONTAL AXIS INTERVAL
            K = (M + 1.0) / 60.0 + 1.0
            DO 140 I = 1+K, M+1, K
            J = 1.5 + (S(I) - SMIN) / SINC
            IF (J .LT. 1) STOP 3
            COLUMN(J) = CROSS
            WRITE (2, 1022) COLUMN
            COLUMN(J) = BLANK
            COLUMN(1) = DOT
  140 CONTINUE
            XMAX = XINT + XINC * M / 1000.0
            WRITE (2, 1023) XINT, XMAX
            WRITE (2, 1008)
            GRAPH = GRAPH + 1
            IF (GRAPH .LE. 3) GO TO 105
```

```
C
 1001 FORMAT (F11.0, 2F10.0, F9.0, I7, 3F11.0)
 1005 FORMAT (1H1//25X, 71HTHE SOLUTION OF THE FREQUENCY EQUATION FOR TH
     1E FIRST LUNGTITUDINAL MUDE)
 1006 FORMAT ((///30X, 30HPOISSONS RATIO                    =  , F8.4 // 30X,
     130HFREE SPACE SHEAR VELOCITY  =  , F8.4, 22H  INS PER MICRO-SECOND
     2// 30X, 30HVELOCITY VP                    =  , F8.4, 22H  INS PER MICR
     30-SECOND/// 47X, 25HTHE INITIAL VALUE OF X IS, F6.2 // 47X,
     421HTHE INCREMENT OF X IS, F5.1, 5H/1000// 47X, 22HTHE NO OF INTERV
     5ALS IS, I5 //// 15X, 4H   I, 5X, 13HX = FREQ*H/VS, 5X, 26HPHASE VE
     6L V INCH/MICRO-SEC, 5X, 10HERROR OF V, 5X, 16HNO OF ITERATIONS//)
 1007 FORMAT (15X, I4, 1PE17.3, 1PE24.5, 1PE23.4, I16)
 1008 FORMAT (/// 38X, 44H********************************************)
 1009 FORMAT (1H1 //// 35X, 49HTHE GROUP VELOCITY AND THE NORMALIZED GRO
     1UP DELAY/// 10X, 1HI, 4X, 15HV INS/MICRO-SEC, 4X, 16HDERIVATIVE DV
     2/DX, 4X, 25HGROUP VEL U INS/MICRO-SEC, 4X, 27HNORMALISED GROUP DEL
     3AY VS/U//)
 1010 FORMAT (8X, I3, 1PE17.5, 1PE20.5, 1PE24.5, 1PE30.5)
 1011 FORMAT (3A1)
 1021 FORMAT (1H1 // 56X, 5HGRAPH, I2 // 22X, 28HTHE RANGE OF VERTICAL A
     1XIS :, 1PE10.3, 3H TO, 1PE10.3, 12H IN STEPS OF, 1PE10.3)
 1022 FORMAT (10X, 101A1)
 1023 FORMAT (// 33X, 30HTHE RANGE OF HORIZONTAL AXIS X, 1PE11.3 , 3H TO
     1, 1PE11.3)
C
      STOP
      END
```

END OF SEGMENT, LENGTH 789, NAME FREQN

```
C     FUNCTION SUBPROGRAM
C
      FUNCTION F(VS, VP, SIG, X1, V1)
      PI = 3.14159625
      C1 = V1 / VS
      C2 = V1 / VP
      R1 = SQRT(ABS(1.0 - 1.0 / C1 ** 2))
      R2 = SQRT(ABS(1.0 - 1.0 / C2 ** 2))
      D1 = (2.0 - C1 ** 2) ** 2
      D2 = 4.0 * C1 * C2 * R1 * R2
      IF (C2 .LT. 1.0) GO TO 205
      F = D1 * SIN(PI * X1 * R1) * COS(PI * X1 * R2)
     1   + D2 * SIN(PI * X1 * R2) * COS(PI * X1 * R1)
      GO TO 215
  205 E1 = 1.0 / SQRT(1.0 -(TANH(PI * X1 * R2)) ** 2)
      IF (C1 .LT. 1.0) GO TO 210
      F = (D1 * SIN(PI * X1 * R1) - D2 * COS(PI * X1 * R1)
     1   * TANH(PI * X1 * R2)) * E1
      GO TO 215
  210 E2 = 1.0 / SQRT(1.0 - (TANH(PI * X1 * R1)) ** 2)
      F = (D1 * TANH(PI * X1 * R1) - D2 * TANH(PI * X1 * R2)) * E1 * E2
  215 RETURN
      END
```

END OF SEGMENT, LENGTH 198, NAME F .

B2 Frequency response of transducers with various backings

```
      TRACE 0
      READ FROM (CR)
      MASTER SIX
C TRANSDUCERS THEORETICAL FREQUENCY RESPONSE
      REAL PHI,CE,ZX,DEV,ZB,ZQ,CO,T1,T2,LT1,LT2,LT3,LO
      COMPLEX COMA,COMB,VI,VM,I1,I2,I3,VN,IA,IB,IC,F2,VO,ZCE,ZCER,ZCEL
      DIMENSION X(200),Y(200)
      PI=3.1416
C READ PARAMETERS
      READ (1,20) PHI,CE,ZX,ZB,ZQ,CO
   20 FORMAT (6F0.0)
C HEADINGS
      WRITE (2,10)
   10 FORMAT (1H ,12HFREQ    RATIO,5X,3HLT1,9X,3HLT2,9X,3HLT3///)
    2 DO 60 K=21,181,2
      DEV=K
      DEV=DEV/100.0
      COMA=CMPLX (2.0*ZB,-(2.0*ZX*COT(PI*DEV/2.0)+2.0/(PI*DEV*2.3*CE)))
      COMB=CMPLX (2.0*ZB, 2.0*ZX*TAN(PI*DEV/2.0))
      VM=CMPLX ((ZQ-ZB)/ZQ,0.0)
      I1=(VM)/(ZQ-ZB)
      I2=(VM)/COMB
      I3=I1+I2
      VI=(I3*COMA)+VM
      ABSVI=CABS(VI)
      T1=1.0/ABSVI
      X(K)=T1
C CALCULATE F2, ASSUMING CO HAS NOT BEEN TUNED OUT
      VO=CMPLX (1.0,0.0)
      ZCE=CMPLX (0.0, (2.0/(PI*DEV*2.3*CE)))
      IA=VO/ZCE
      VN=(IA*COMA)+VO
      IB=VN/COMB
      IC=IA+IB
      F2=IC*(ZQ-ZB)+VN
      ABSF2=CABS(F2)
      T2=1.0/ABSF2
   60 Y(K)=T2
      DO 70 J=21,181,2
      LT1=20.0*ALOG10(X(J)/X(99))
      LT2=20.0*ALOG10(Y(J)/Y(99))
      LT3=LT1+LT2
   70 WRITE (2,80) J,LT1,LT2,LT3
   80 FORMAT (I12,3F12.4)
      STOP
      END


END OF SEGMENT, LENGTH   283, NAME  SIX
```

APPENDIX C

QUOTATION FOR STRIP DISPERSIVE DELAY LINE (TYPE 4201-D)

ANDERSEN LABORATORIES, INC.

1280 Blue Hills Avenue • Bloomfield, Conn. 06002 • (203) 242-0761 • TWX 710-425-2390

University of Hong Kong
Electrical Engineering Department.
Hong Kong

DATE: October 14, 1970

YOUR INQUIRY NO.: letter Dated 28 Sept 70

Attn: Mr. F. K. Lam

OUR QUOTE FILE NO.: 33-11 Dated 10-5-70

Gentlemen:

Thank you for your interest in our products. We are pleased to submit our quotation per your request. Prices are net F. O. B. Bloomfield, Connecticut, U. S. A.

Payment is accepted by Irrecoverable Letter of Credit only which is subject to uniform customs and practice for documentary credits (1962 revision) International Chamber of Commerce Brochure No. 222.

This quotation is valid 60 days from date of issue.

We look forward to the opportunity of serving you.

Sincerely yours,

Christian R Berlit, Manager
International Sales

Delivery 90 to 120 days after receipt of order.

SPECIFICATIONS	PRICE U.S. F.O.B.
Andersen Laboratories, Inc. 4201-D STRIP DISPERSIVE DELAY LINE. Number of lines per set: 1 pair Center Frequency (F_o): 4.95 ±0.05 MHz Center Frequency Stability: -100 ppm/°C Dispersive Bandwidth (ΔF): 210 ±2 KHz Delay Dispersion (ΔD):354 μs (pr.) Center Frequency Delay (D_o): 2056 ± 41 μs (pr.) Center Frequency Delay Stability: ±125 μμm/°C Operating Frequency Delay Stability: +650 ppm/°C Delay Non-Linearity (δD): ±1.8 μs (pr.) Residual Delay Non-Linearity: ±0.15 μs(pr.)	

ANDERSEN LABORATORIES, INC.
1280 Blue Hills Avenue • Bloomfield, Conn. 06002

DATE: October 14, 1970

YOUR INQUIRY NO.: letter Dated 28 Sept 70

OUR QUOTE FILE NO.: 33-11 Dated 10-5-70

PAGE: Two of Two

SPECIFICATIONS (Cont'd)	PRICE U.S. $
Delay Slope: 1680 μs/MHz (pr.) Delay Slope Stability: +250 ppm/°C max. Compression Ratio (C.R.): 74.5 (pr.) Expected Side Lobe Level (weighted): -35 db Insertion Loss (I.L.) (worst point): 40 db Insertion Loss Change (across ▲F): 5 db Insertion Loss Ripple: ±1 db Measuring Systems Impedance: 50Ω Spurious Signals - across ▲F - pulse test method. Nondispersive Spurious (N.S.): -30 db Dispersive Spurious (D.S.): -30 db Triple Travel (T.T.): -30 db Feedthrough (F.T.): -40 db Cross-Talk (C.T.): -30 db Input Resistance: 50 ±10Ω Input Capacitance: ±50 pf Output Resistance: 50 ±10Ω Output Capacitance: ±50 pf Operating Temperature Range: lab.environment Length x Width x Thickness: 10"x10"x5-1/2" Type Mounting: inserts Connector, Signal: BNC Notes: all performance specs per line except as noted PRICE FOR THE QUANTITY OF ONE PIECE:	$ 5,000.00

APPENDIX D

PHASE EQUALIZERS

D.1 Transfer function of a symmetrical lattice[98]

Figure D.1 shows a symmetrical lattice in which both series elements are equal to Z_a and both shunt elements are equal to Z_b, and is terminated in a resistance $R_o = \sqrt{Z_a Z_b}$. R_o is seen to be the characteristic impedance of the network.

The transfer function V_o/V_{in} can be derived by referring to Figure D.2.

$$\frac{V_o}{V_{in}} = \frac{(I_2 - I_1) R_o}{(I_2 + I_1) R_o}$$

$$= \frac{Z_b - Z_a}{Z_b + Z_a + 2R_o}$$

$$= \frac{1 - \sqrt{Z_a/Z_b}}{1 + \sqrt{Z_a/Z_b}} \qquad (D.1)$$

For a second order lattice, Z_a is a parallel combination of L_a and C_a ; while Z_b is a series combination of L_b and C_b (Figure D.3). Let

$$\frac{1}{C_a} = 2\sigma_o R_o \qquad (D.2)$$

and
$$\frac{1}{L_a C_a} = \frac{1}{L_b C_b} = \bar{\omega}_o^2 \qquad (D.3)$$

where $\bar{\omega}_o$ = resonant frequency for both Z_a and Z_b branches.

Then
$$L_a = \frac{2\sigma_o}{\bar{\omega}_o^2} R_o \qquad (D.4)$$

$$L_b = \frac{1}{2\sigma_o} R_o \qquad (D.5)$$

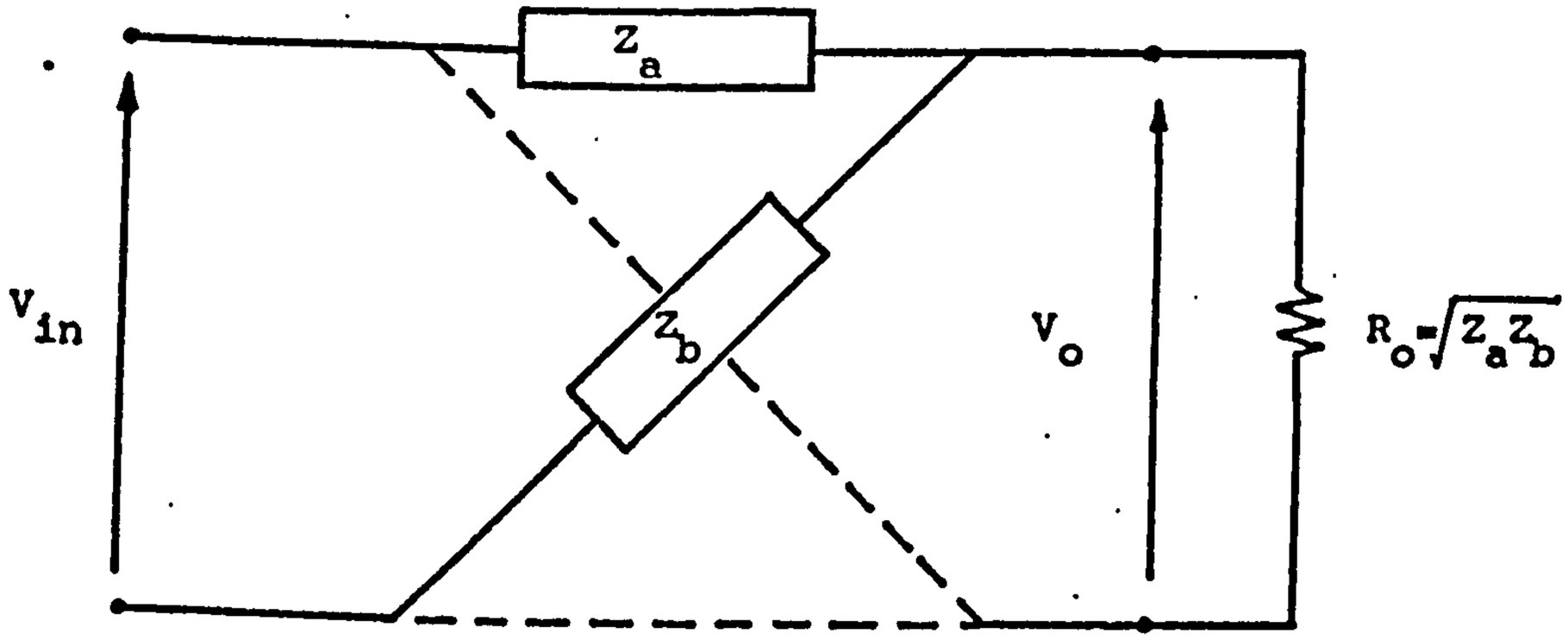

Figure D1 A symmetrical lattice

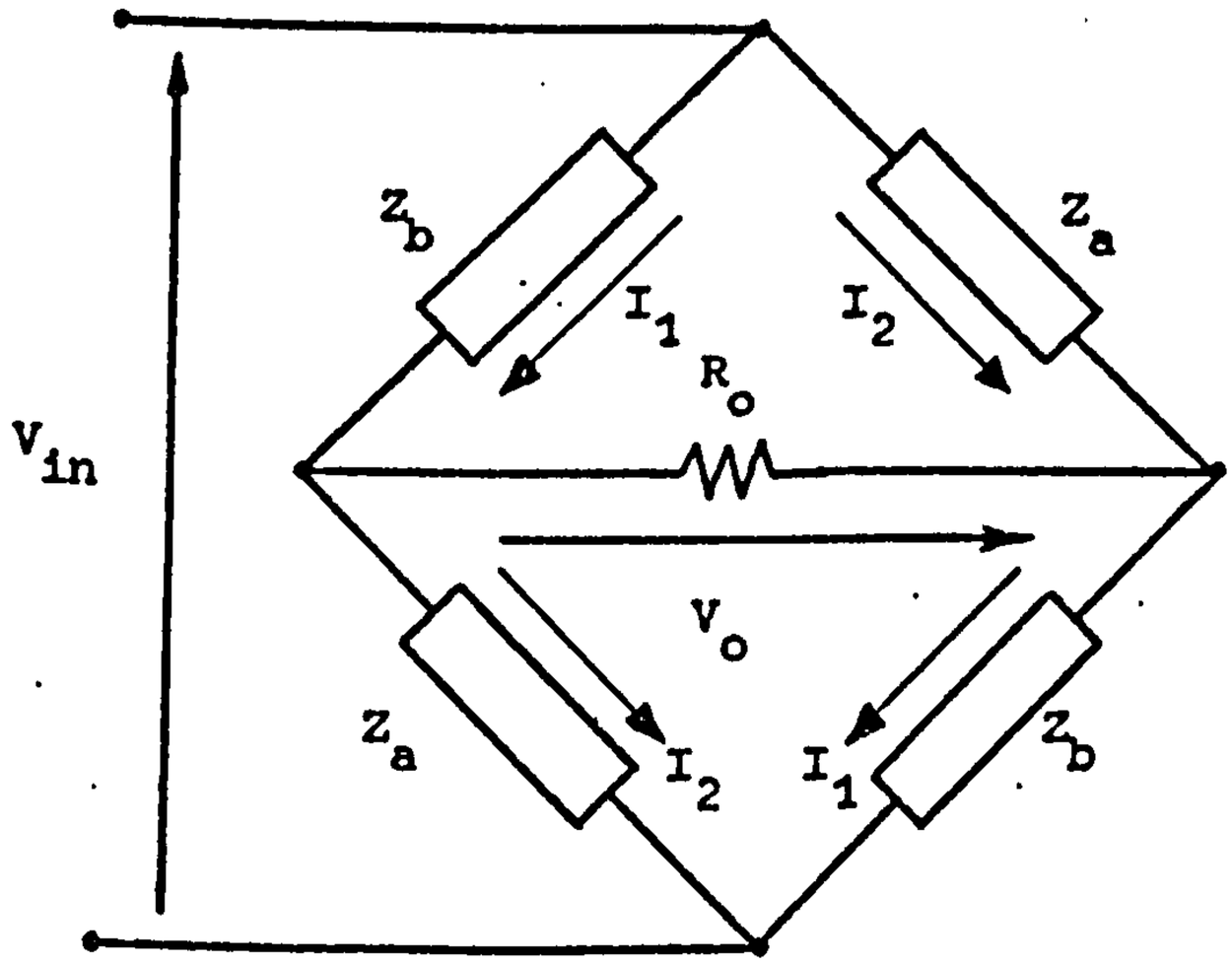

Figure D2 Redrawing of the lattice into a bridge network

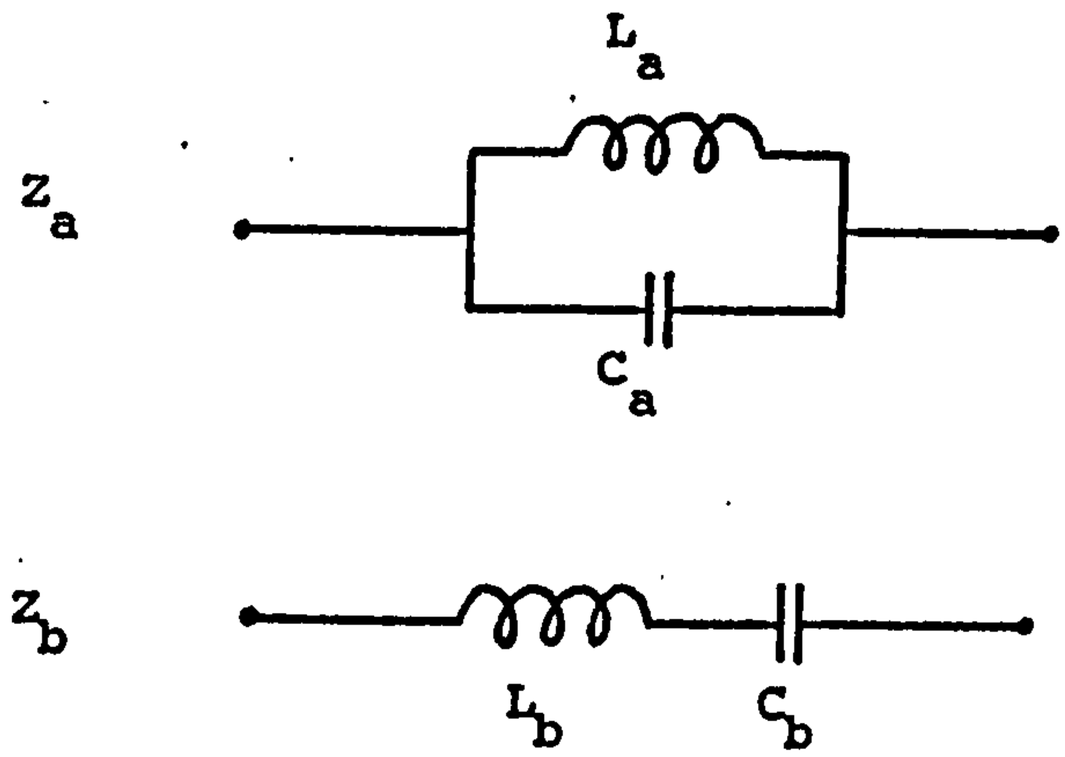

Figure D3 Reactance arms of a second-order lattice

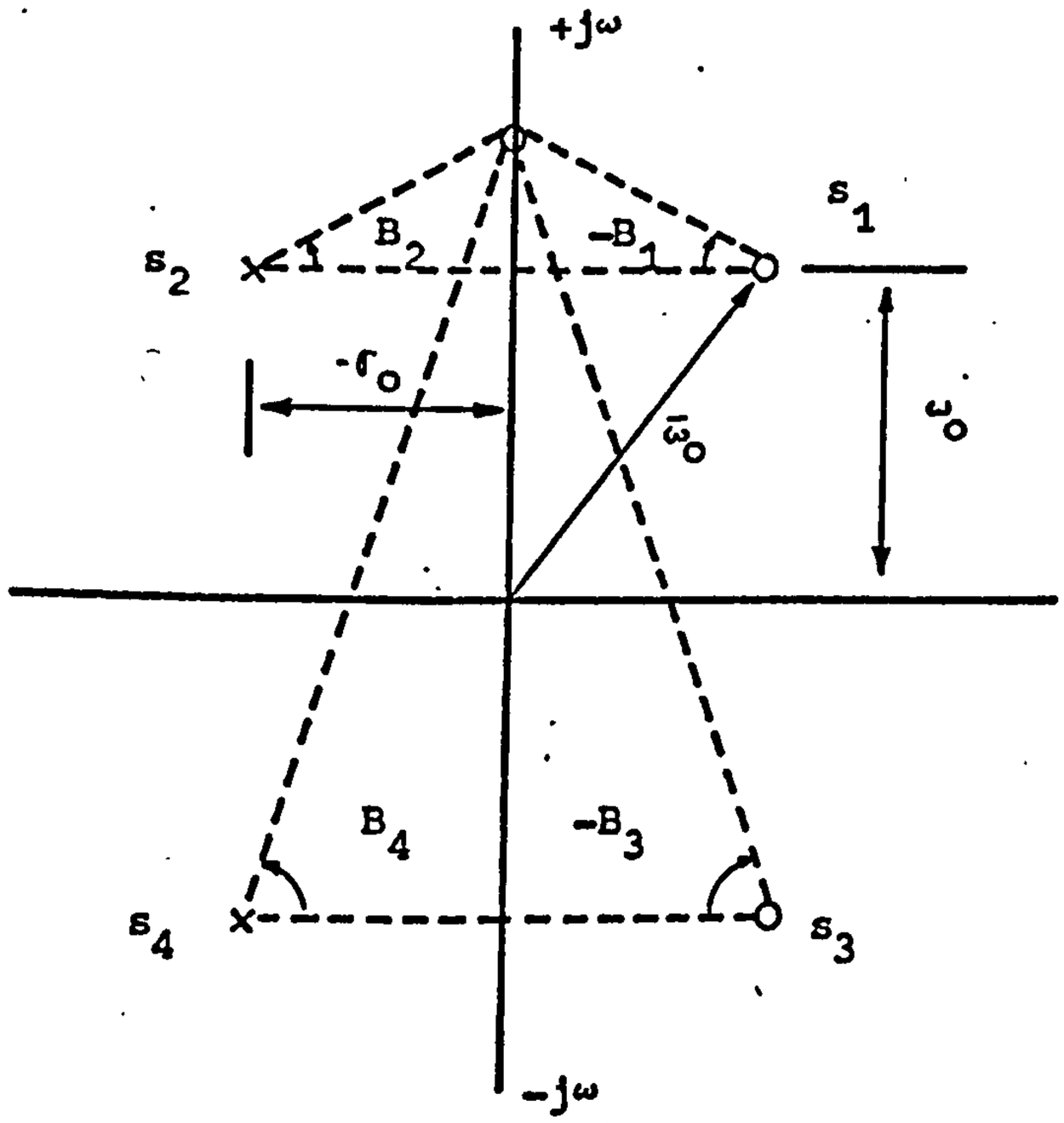

Figure D4 Pole-zero plot of second-order all-pass lattice

$$C_b = \frac{2\sigma_o}{\bar{\omega}_o^2} \frac{1}{R_o} \tag{D.6}$$

$$\sqrt{\frac{Z_a}{Z_b}} = \frac{j\omega 2\sigma_o}{\bar{\omega}_o^2 - \omega^2} = jX \tag{D.7}$$

The transfer function will be

$$\frac{V_o}{V_{in}} = \frac{1 - jX}{1 + jX}$$

$$= \exp (- 2j \tan^{-1} X) \tag{D.8}$$

It has no attenuation and a phase characteristics

$$B = - 2 \tan^{-1} X . \tag{D.9}$$

The group time delay is

$$t_d = - \frac{dB}{d\omega} = \frac{4\sigma_o (\bar{\omega}_o^2 + \omega^2)}{(\bar{\omega}_o^2 - \omega^2)^2 + 4\sigma_o \omega^2} \tag{D.10}$$

D.2 Derivation of approximate group time delay curves[56]

The transfer function can be expressed in the s-plane.

$$H(s) = \frac{V_o}{V_{in}} = \frac{1 - \frac{2s\sigma_o}{\bar{\omega}_o^2 + s^2}}{1 + \frac{2s\sigma_o}{\bar{\omega}_o^2 + s^2}}$$

$$= \frac{(s - s_1) (s - s_3)}{(s - s_2) (s - s_4)} \tag{D.11}$$

where $s_{1,3} = \text{zeros} = \sigma_o \pm \sqrt{(\sigma_o^2 - \bar{\omega}_o^2)}$

$$= \sigma_o \pm j\omega_o$$

$$s_{2,4} = \text{poles} = -\sigma_o + j\omega_o$$

and $$\omega_o^2 = \bar{\omega}_o^2 - \sigma_o^2 \qquad (D.12)$$

From the pole-zero plot of H(s) in Figure D.4, the total phase of the network is given by

$$B = -(2B_2 + 2B_4)$$

$$= -2\left[\tan^{-1}\left(\frac{\omega - \omega_o}{\sigma_o}\right) + \tan^{-1}\left(\frac{\omega + \omega_o}{\sigma_o}\right)\right] \qquad (D.13)$$

With the assumptions that $\omega_o > 3\sigma_o$ and $|\omega_o - \omega| < 0.3\omega_o$ (+ 30% bandwidth), the above equation may be written as

$$B = -2\left[\tan^{-1}\left(\frac{\omega - \omega_o}{\sigma_o}\right) + k_1\omega + C_1\right] \qquad (D.14)$$

where the second term in Equation D.13 has been approximated by a linear function, and k_1 has a small value around the frequencies near to ω_o.

The group time delay then is

$$t_d \doteq \frac{2}{\sigma_o} \frac{1}{1 + (\frac{\omega - \omega_o}{\sigma_o})^2} \qquad (D.15)$$

D.3 Lattice to bridged-T conversion

The symmetrical second-order lattice can be converted into the more practical bridged-T configuration through Bartlett's bisection theorem [99], which states : The lattice equivalent of a symmetrical ladder network has a series arm equal to the impedance of a half of the bisected network measured at the input terminals with the other

terminals short-circuited; the shunt arm is equal to the impedance of the half network with the bisected terminals open. The equivalent networks are shown in Figures D.5 a and D.5 b. Figure D.5 c shows another equivalent but nonminimum element bridged-T network.

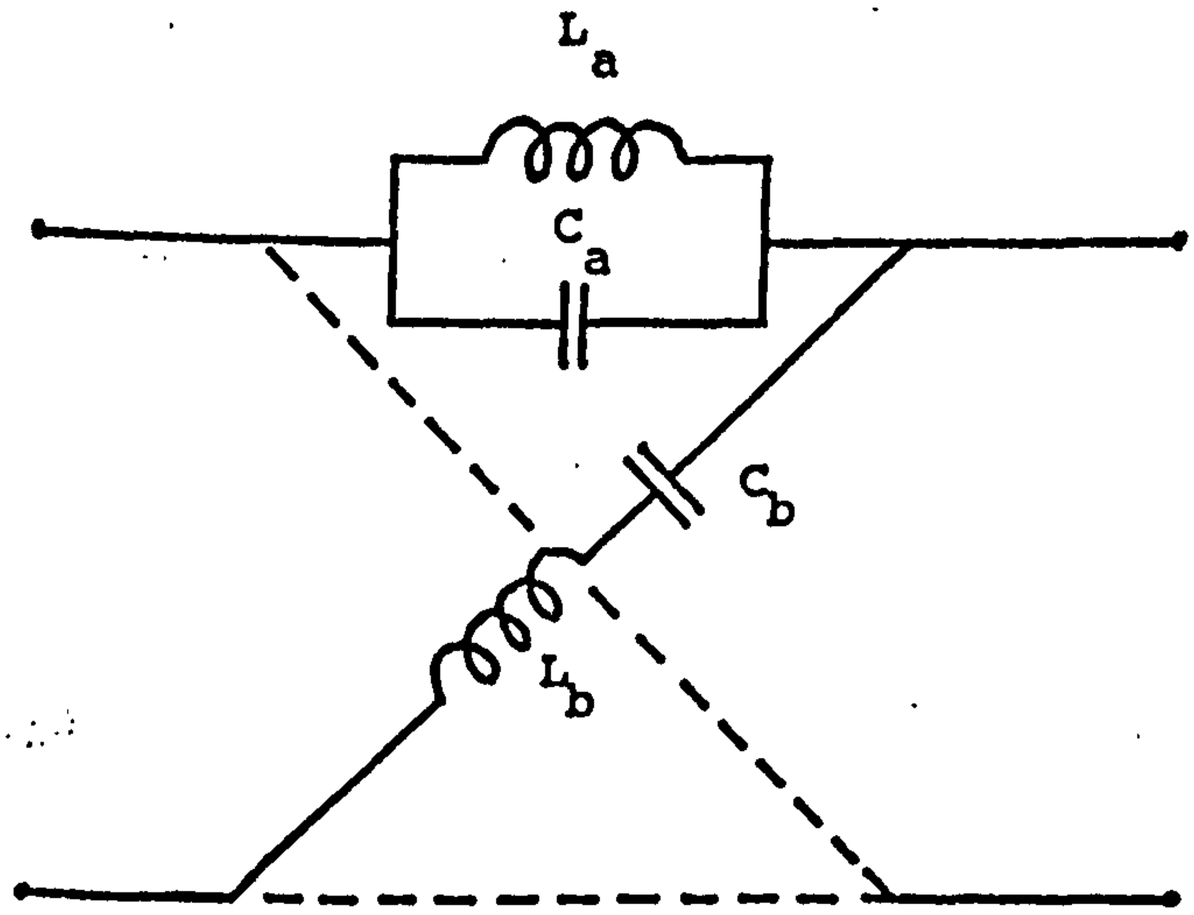

Figure D5a A second-order symmetrical lattice

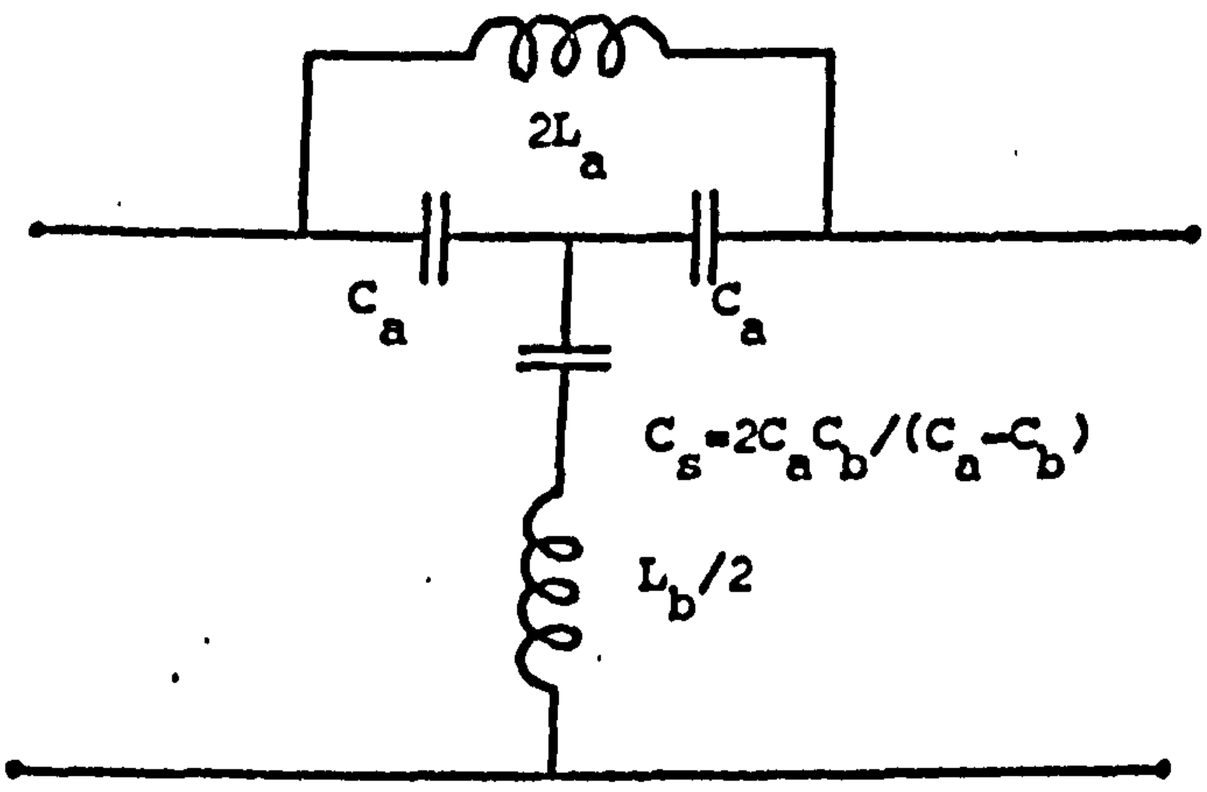

Figure D5b An equivalent minimum element bridged-T

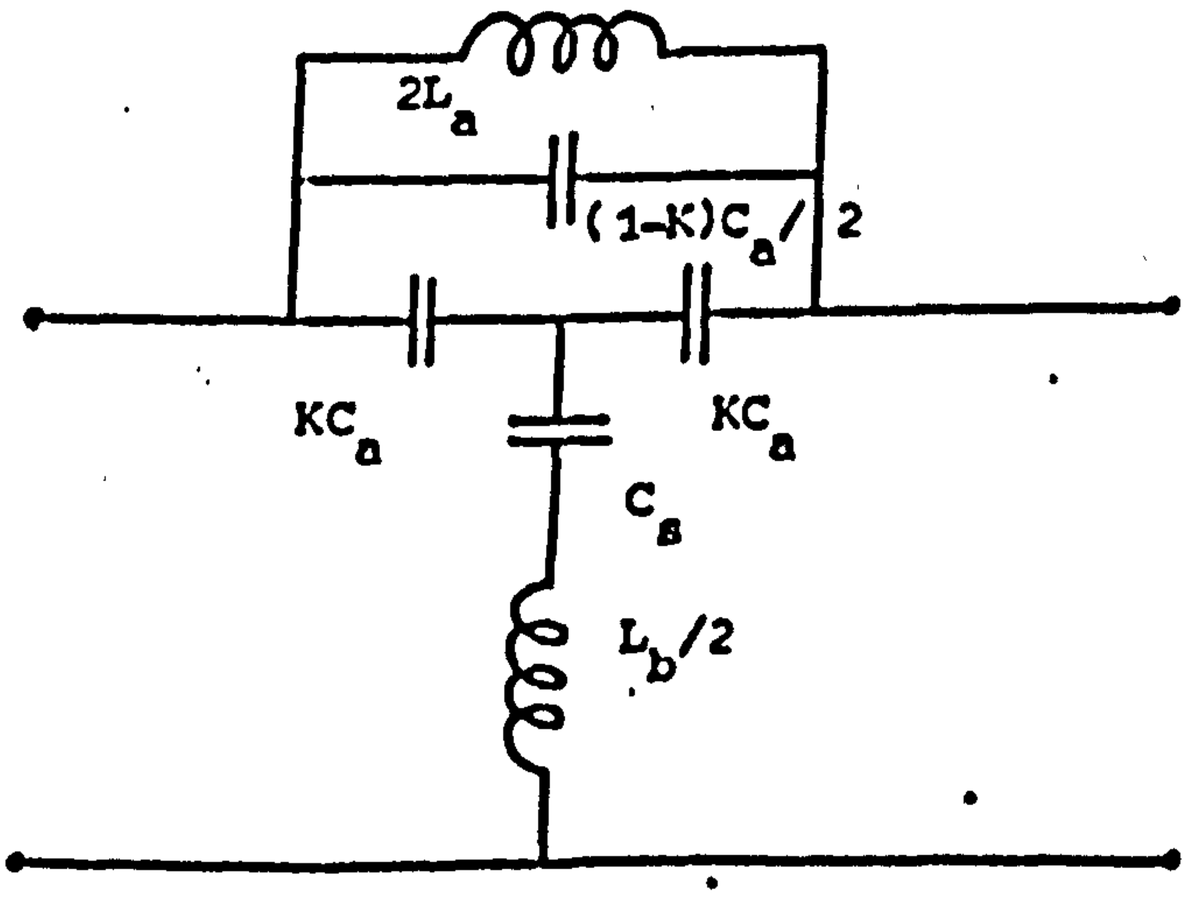

Figure D5c Another equivalent bridged-T but having nonminimum elements